THÈSE POUR OBTENIR LE GRADE DE DOCTEUR
DE L'UNIVERSITÉ DE MONTPELLIER

En Mathématiques et Modélisation

École doctorale : Information, Structures, Systèmes

Unité de recherche : Institut Montpelliérain Alexander Grothendieck

Validation process and clinical impact of a software for virtual simulation for the endovascular treatment of intracranial aneurysms

Présentée par Daniel Eduardo Mantilla
Le 27/09/2022

Sous la direction de Professor Franck Nicoud
et Professor Vincent Costalat

Devant le jury composé de

Franck Nicoud	Professeur, Univ. Montpellier	Directeur
Vincent Costalat	Professeur, CHU Gui de Chauliac, Univ. Montpellier	Co-directeur
Aymeric Rouchaud	Professeur, CHU de Limoges, Univ. René Descartes	Rapporteur
Laurent Spelle	Professeur, Bicêtre Hospital, APHP, Univ. Paris-Saclay	Rapporteur
Paolo Machi	Professeur, HUG - Hôpitaux Universitaires de Genève, Univ. Genéve	Examinateur
Anne Christine Januel	Neuroradiologue interventionnel, CHU, Toulouse, France	Examinatrice
Christophe Chnafa	PhD en Mathématiques et Modélisation, Univ. Montpellier	Examinateur

UNIVERSITÉ DE MONTPELLIER

Contents

Abstract

Intracranial aneurysms (IAs) are defined as a focal dilation or pathological bulge in the arterial walls, which can grow and rupture, generating catastrophic outcomes in patients. Because most unruptured IAs are asymptomatic, their diagnosis is mostly incidental. Currently, there are various therapeutic approaches, however, endovascular management has positioned itself as the management of choice in most cases of ruptured and non-ruptured IA since it has shown less morbidity, fewer hospital stays, and shorter recovery times for patients(1)(2)(4)(5). There are various endovascular devices on the market for the management of IAs, such as flow-diverting stents and intrasaccular devices such as the Woven EndoBridge (WEB), which aim to form intrasaccular thrombosis of the IA (30). The extensive morphological diversity of IAs among patients means that the selection of the intrinsic characteristics of the endovascular device is a complex task that requires high precision. For the above, simulation software are being developed to facilitate this process for health professionals, which has been shown to improve performance, and reduce the presence of errors and surgical time (3).

The validation of medical software consists of confirming with objective evidence that the software complies with its intended uses and consistently satisfies the needs of the user. This process is necessary so that the medical device can be implemented and approved by regulatory entities such as the FDA and the European Commission (37). However, the validation processes of medical software are little or not codified, which does not allow us to objectively judge its applicability and effectiveness. The first objective of this thesis was to describe the validation process used to implement a virtual simulation software in the

endovascular treatment of intracranial aneurysms (Sim&Size^{TM}) and its impact on variables associated with its use such as surgical time, size, and the number of endovascular devices. and potential risks. The second objective of this thesis consists of a first phase in which the validation process of the potential use of 3D printed models of intracranial aneurysms to simulate and select the most appropriate endovascular device is described, evaluating its accuracy in the 3D angiography of the patient and the correspondence between operators. In the second phase, a heterogeneous model was developed by Alain Berod et. al was used to evaluate the computational fluid dynamics (CFD) and the structural mechanics of patients with bifurcation IA treated with the WEB device. Some hemodynamic parameters and indexes of the IA before and after WEB simulation were measured and their relation to complete occlusion was evaluated. The relationships between the geometrical defined parameters of the IA and its relation to the implanted device were also evaluated in order to determine the predictive factors before implantation that favor the chances of the long-term success of the endovascular procedure.

In Chapter 4, forty five patients with intracranial aneurysms treated with flow-diverting stents were included to validate the accuracy of the Sim&Size^{TM} simulation software. To perform the validation, two neurointerventionalist evaluated the differences between the real and simulated PED lengths by overlaying the proximal and distal landing zones of the 2D-DSA images with at least two 3D reconstructions for each case to ensure the quality and reproducibility of the results. The differences were used to assess the concordance between real-life and simulated PED lengths using the Bland-Altman test and calculate cumulative errors in R Core Team (2022).

It was observed that the absolute error in the length of the real-life and simulated stent was less than 5.06 mm in 90% of the simulations, with the difference in length measurement being greater under conditions of significant compression or stretching during stent implantation. Despite these differences, we found the Sim&Size^{TM} simulations to be acceptable for clinical purposes as an agreement of 0.97 (95% CI: 0.94-0.98) was obtained between actual and simulated PED lengths by Sim&Size^{TM}, with most data within two standard deviations of the mean of 0 on the Bland-Altman Plots.

After testing to validate the accuracy of the simulation software, we proceeded to evaluate the change in stent lengths and surgical time caused by their use in the treatment of patients with intracranial aneurysms using flow-diverting stents. For the above, in chapter 6, 197 patients were included, of which in 59 the deployment of the stent was simulated with Sim&Size™. In them, we observed that the stents were 33% shorter on average after the introduction of the Sim&Size™ software in clinical practice. In 2015 the average was 16 mm, in 2016 20 mm, and in 2017 14 mm in length. Regarding the surgical time, we found a reduction of 19.4% (14 minutes) after the acquisition of the simulation software. Because patients treated with PED alone had shorter operative times than those treated with stent and coils (25-40 minutes versus 50-150 minutes), we decided to analyze the two groups separately. We found that the reduction was more pronounced in patients treated with PEDs and coils compared to those using PEDs alone (28% versus 13% reduction in operative time). Therefore, it can be concluded that the software can reduce surgical time by about 34 minutes for interventions that use stents and coils and 8 minutes for interventions that use FD alone.

In Chapter 7, the correlation between occlusion rates and metal surface coverage (MSC) of flow-diverting stents in intracranial aneurysm necks was evaluated using Sim&Size™ simulation software. To make the estimates, two neurointerventionalists were involved, one carrying out the delimitation of the neck of the aneurysm and the other calculating MSC, to increase the objectivity of the estimates. Cristophe Chnafa et al. measured PED and MSC porosity using Expert CT and compared the results with those estimated with Sim&Size™ simulation software to validate MSC measure with the software. To assess the degree of occlusion based on the 3D-DSA of the patients at 6 months and 12 months, a continuous numerical scale ranging from 1 to 4 was defined, with 1 being partial occlusion and 4 being complete occlusion related to time between treatment and angiographic control.

We used Spearman's matching to assess the strength of the match between occlusion rate and MSC at the aneurysm neck, aneurysm greatest diameter length, dome/neck ratio, aneurysm neck diameter, and age and the sex of the patients in R Core Team (2022).

The 3D-DSA of 62 patients treated with PED in two neuroradiology centers was analyzed. The mean MSC at the neck of the aneurysm was 24.0% (SD 11%), with the highest MSC being 60.0% and the lowest at 15.0%. We found no agreement between occlusion rates and

MSC (p-value = 0.122) or any of the other factors assessed (ie, length of largest aneurysm diameter, dome/neck ratio, and aneurysm neck diameter) (p-value > 0.05) according to the Spearman connection. We also found no association between occlusion rates and the age or sex of the patients (p-value > 0.05).

Chapter 8 evaluated the clinical impact of Sim&Size^{TM} simulation software in the treatment of patients with unruptured saccular IAs with flow-diverting stents. For this, a single-center retrospective study was first carried out, followed by a multi-center study in which patients were classified as treated with and without the Sim&Size^{TM} simulation software. In the monocentric study carried out in a center in Bucaramanga, Colombia, of the 73 interventions in 68 patients included, 76.7% were simulated with the Sim&Size^{TM} simulation software and 23.3% were not. Patients treated with Sim&Size^{TM} had shorter stent lengths (16.00 mm vs. 20.00 mm, p-value = 0.001) and shorter surgical time (100.00 min vs. 118.00 min, p-value = 0.496). Additionally, fewer patients in the simulation group required more than one stent (3.6% vs. 17.6% p-value = 0.079). Bleeding complications occurred in 3 patients belonging to the non-simulation group.

Patients treated in Bucaramanga, Colombia, and Montpellier, France were included in the multicenter study. Of the 253 patients included, 56.9% used the Sim&Size^{TM} simulation software and 43.1% were not. The patients treated with the simulation software had shorter stent lengths (15.62 mm versus 17.36 mm, p-value = 0.001). Likewise, fewer simulated patients required the use of two stents (1.39% versus 7.34%, p-value = 0.022). On the other hand, patients without simulation required less use of the balloon (4.59% versus 15.28%, p value= 0.007). In this cohort, 16 complications occurred, seven in the group treated with Sim&Size^{TM} and nine in the group without simulation (4.86% versus 8.26%, p-value = 0.305).

Chapter 9 aims to validate the geometrical accuracy of the 3D models of intracranial aneurysm printed using Stereolithography 3D printing technology comparing to 3D digital subtraction angiography (DSA) of patients' aneurysms. Preplanning 3D-DSA images of five patients with unruptured intracranial aneurysms are included for validation. The DICOM files of the 3D-DSA were transformed into STL files and used the STL to generate 3D

reconstructions of the voxel surface with the Sim&Size^{TM} simulation software. We delimited the aneurysm region, including an expanded part of the proximal and distal vessels. Then, we extended the lumen centerline with the vmtkflowextensions functionality of the VMTK algorithm to allow the plug to the hydraulic circuit. From the processed 3D reconstructions, the 3D printing of the models was made. By the end, we had two 3D reconstructions of the same aneurysm, one from the patient's 3D-DSA and one from the 3D-DSA of the 3D printed model. The two reconstructions were juxtaposed to calculate the deviations at different mesh nodes, finding an overall deviation below 0.21 mm for 80% of the mesh nodes when considering all five aneurysms, indicating that the 3D printed models are accurate.

In collaboration with Alain Berod, the last chapter of this thesis focused on the application of the heterogeneous model based on the marching cubes algorithm to create 3D representations of 27 bifurcated intracranial aneurysms treated with the single-layer WEB device (single-layer (SL); single-layer spherical (SLS)) and with these 3D representations to evaluate how the intrasaccular device affects hemodynamics parameters within aneurysms using CFD calculations. We identified four pre-treatment blood flow patterns (I - IV) within the IA based on the number of vortices within the sac and their stability during the cardiac cycle as a result of the different anatomies of the major arteries. In our cohort, most aneurysms had type I and II flow patterns (37% each). Type II flows were characterized by a high friction zone at the neck bifurcation due to flow separation. Subsequently, we evaluated the impact of WEB on IA hemodynamics, establishing a median value of 30.2% in the apposition ratio (ApR) index to define good apposition to the device wall and using velocity fields averaged over time to visually assess the presence of flow between the IA sac and the WEB border. We found that most cases with adequate wall apposition lacked flow jets near the wall, and malapposition coincided with flow near the wall in 26% of cases. However, 30% of cases did not show a flow jet close to the wall despite poor apposition.

It has been described that the bulge of the WEB is associated with low post/pre Q+ indices due to the effective blockage of flow by the device. To assess the impact of the bulge on flow patterns, we visually classified patients into aneurysms with and without device protrusion. In our cohort, 44% of the cases presented protrusion of the WEB and most of these had a low index, for which the association was confirmed.

When evaluating the possible association between the occlusion status after treatment, the follow-up time, and the patient's age, we found no association between the occlusion and the follow-up time (p-value = 0.600). Regarding the age of the patients, younger patients were more likely to have occlusion failure than older patients (p-value = 0.005). Regarding the association between occlusion status, and anatomical and device-related parameters, we found that large aneurysm volumes (Va) were associated with occlusion failure.

Within the hemodynamic parameters associated with occlusion status, we observed lower treatment entry concentration indices (ICI) before placement of the WEB device (pretreatment) for cases with successful occlusions (p-value = 0.029). Another important finding was that non-occluded cases had lower post-treatment shear rates (SRa) than cases with successful occlusions (p-value = 0.044). Regarding the other hemodynamic metrics, contrary to expectations, we found that cases with occlusion failures had higher pretreatment and posttreatment MATT, suggesting that blood flowing into unoccluded aneurysms had longer residence times. Additionally, we found a lower pre- and post-treatment FN in non-occluded cases, indicating that these cases had less blood flow through the aneurysm neck before and after WEB device placement. However, it should be emphasized that MATT and FN are composite indices, so the hemodynamic (Q+ and Ua) or anatomical (Va) characteristics could influence the result. We were unable to validate these unforeseen associations with the literature as work on the hemodynamics of intracranial aneurysms treated with WEB devices is scarce, making further studies with significant samples essential.

Intracranial aneurysm overview:
epidemiology, risk factors, pathophysiology, classification, symptoms diagnosis, and treatment of intracranial aneurysms

Chapter contents

2.1 Definition

The intracranial aneurysm (IA) is a complex intracranial disease evidenced as a focal dilation or pathological bulging on the artery walls, which can grow and rupture over time. The term aneurysm originally comes from the Greek aneurysma—ana meaning "across" and eurys meaning "broad." (4).

2.2 Epidemiology

According to an autopsy adults series, the unruptured IA prevalence is between 3.2 % and 5 % in the general population (5). However, it is higher for patients with subarachnoid hemorrhage (SAH), a history of autosomal dominant polycystic kidney disease, or an IA family history. Patients of any age can suffer unruptured IA, but this condition is more prevalent in patients older than 50 (6). Regarding gender, the literature presents a 1:1 ratio for women and men suffering from IA, suggesting that women are equally likely as men to suffer from this condition. Still, the International Study of Unruptured Intracranial Aneurysms (ISUIA) reported that women represented 75% of the analyzed IA patients (7)(8). Between 10 % and 30 % of patients present multiple IA, occurring in the same or different places (9). Nearly 85 % of IAs occur in the anterior circulation, in the arteries of the circle of Willis, mainly in the anterior communicating artery (35 %), the internal carotid artery (30 %), and the middle cerebral artery (22 %) (10).

IA rupture leads to SAH. Fortunately, the aneurysm rupture is not predominant, with less than half (50 % - 80 %) of the aneurysm remaining unruptured. The annual IA rupture incidence is low, between 2 and 16 per 100,000 inhabitants and between 0.2 and 2 per 100,000 children (11)(12). However, they account for nearly 0.5 % of the overall deaths (13) and have mortality between 27 % and 44 %. Almost 10 % of patients suffering from IA rupture die before receiving medical attention, and only a third have a satisfactory outcome after treatment (5).

2.3 Risk factors

IA results from genetic, acquired, and local hemodynamic factors interacting with endothelial damage inducers. Among these damage inducers, non-laminar blood flow, arterial

hypertension resulting from pulsatile pressure, and increased shear stress might be the most relevant (14). IA is associated with several risk factors, including modifiable and non-modifiable factors. Hypertension, tobacco smoking, excessive alcohol consumption, and cocaine use are some of the modifiable risk factors. In contrast, age over 30, female sex, and first-degree family history of IA or SAH are non-modifiable.

Other pathologies also seem to increase the IA risk. Among these pathologies, the most known are connective tissue diseases such as Ehlers-Danlos syndrome, neurofibromatosis type 1, autosomal dominant inherited polycystic kidney disease, and congenital cardiovascular malformations such as coarctation of the aorta. Other pathologies include fibromuscular dysplasia, Moyamoya syndrome, pseudoxanthoma elasticum, alfa1 antitrypsin, systemic lupus erythematosus, sickle cell anemia, bacterial endocarditis, fungal infection, tuberous sclerosis, pheochromocytoma, and arteriovenous malformation (14).

The literature about the IA rupture risk is controversial, mainly due to patient cohort discrepancy. The largest meta-analysis by Groving et al. included six prospective cohort studies with 10,272 aneurysms representing 8,382 patients followed for 29,166 patient years. Groving et al. detected six independent risk factors for IA rupture, including patient age, geographic origin, high blood pressure, aneurysm size, aneurysm location, and history of prior rupture of another aneurysm (14). These findings led to the development of the PHASES scoring system, which estimates the 5-year risk of aneurysm rupture.

The PHASES system is limited in not considering several relevant factors (Table 1) (14)(15). For example, PHASES does not consider smoking, first-degree family history of IA or SAH, or irregular IA shape. Also, several studies have demonstrated that geographical origin is influential for IA, but its effect varies from one population to another (Table 1) (14)(15). These variations might influence the 5-year risk of aneurysm rupture PHASES estimates. Therefore, we must be careful when extrapolating the findings of these evaluations.

Risk factor	Change in rupture risk (95% CI)	Evidence level	Geographic region[2]
Patient-related			
Modifiable			

Arterial hypertension	HR 1.4 [1.1; 1.8]	IIa	Europe (incl. Finland), Japan, North America
	HR 1.3 [0.9; 1.9]	IIa	Japan
	HR 7.9 [1.3; 47.4]	IIb	Japan (UIA size <5 mm)
Smoking (active)	RR 2.2 [1.3; 3.6]	IIa	Europe (incl. Finland), Asia (incl. Japan), North America
	HR 3.2 [1.3; 7.6]	IIb	Finland
Alcohol (>150 g/week)	RR 2.2 [1.5; 2.8]	IIa	Europe (incl. Finland), Asia (incl. Japan), North America
Not modifiable			
Age (≥ 70 years)	HR 1.44 [1.05; 1.97]	IIa	Europe (incl. Finland), Japan, North America
Age (<50 years)	HR 5.23 [1.03; 26.52]	IIb	Japan (UIA size <5 mm)
Geographic region			
The USA, Europe except for Finland	Reference	IIa	Europa (inkl. Finnland), Japan, North America
Japan	HR 2.8 [1.8; 4.2]		
Finland	HR 3.6 [2.0; 6.3]		
Prior subarachnoid hemorrhage from another aneurysm	HR 1.4 [0.9; 2.2]	IIa	Europe (incl. Finland), Japan, North America
Female sex	RR 1.6 [1.1; 2.4]	IIa	Europe (except Finland)
Multiple aneurysms	HR 4.9 [1.6; 14.7]	IIb	Japan (UIA size <5 mm)

Family history (≥ 2 first-degree relatives with UIA or SAH)	17-fold elevation	IIb	North America
Aneurysm-related			
Size			
<5.0 mm	Reference	IIa	Europe (incl. Finland), Japan, North America
5.0–6.9 mm	HR 1.1 [0.7; 1.7]		
7.0–9.9 mm	HR 2.4 [1.6; 3.6]		
10.0–19.9 mm	HR 5.7 [3.9; 8.3]		
≥ 20.0 mm	HR 21.3 [13.5; 33.8]		
Localization		IIa	Europe (incl. Finland), Japan, North America
ICA	HR 0.5 [0.3; 0.9]		
MCA	Reference		
ACA incl. AComA	HR 1.7 [0.7; 2.6]		
PCA	HR 1.9 [1.2; 2.9]		
PComA	HR 2.1 [1.4; 3.0]		
Irregular aneurysm shape/lobulation	HR 1.5 [1.0; 2.2]	IIa	Japan
	OR 4.8 [2.7; 8.7]	IIb	Europe
Aneurysm growth >1 mm on serial scans	12-fold	IIIb	USA
Gadolinium uptake in the aneurysm wall	HR 9.2 [2.9; 29.0][1]	IIIb	Europe

Table 1: Patient– and aneurysm-related risk factors for aneurysm rupture according to Etminan et al. (2020), taken from "Unruptured Intracranial Aneurysms—Pathogenesis and Individualized Management." (13)

[1] This value relates to aneurysm instability, i.e., either growth or rupture of the aneurysm.

[2] The significant differences in the risk of rupture depending on geographic region (North America and Europe excluding Finland versus Japan) have the consequence that data from Japan or Finland, for example, are not necessarily applicable to patients in Germany.

The risk factors associated with unruptured IA growth are similar to those mentioned above. However, the ELAPPS score system considers only six factors for estimating the 3-year to 5-year risk of IA growth, including the aneurysm's location, size, shape, and patient's age, geographic origin, and history of previous aneurysm rupture (14).

Backes et al. evaluated the risk factors for IA growth in their meta-analysis, including 4,972 unruptured aneurysms representing 3,990 patients. The authors found that 9 % of the aneurysms grew during 13,987 aneurysm-years of follow-up. The aneurysm growth risk increased with the aneurysm size, with aneurysms > 5mm having a Risk Ratio (RR) of 2.56 (95% CI, 1.93-3.39; I(2)=98%), aneurysms ≥ 7 mm a RR of 2.80 (95% CI, 2.01-3.90; I(2)=96%), and aneurysms ≥ 10 mm a RR of 5.38 (95% CI, 3.76-7.70; I(2)=97%) compared to those < 4mm. Hypertension, smoking, and a history of multiple unruptured aneurysms also increased the risk, having RRs of 1.24 (95% CI, 0.98-1.58; I(2)=40%), 2.03 (95% CI, 1.52-2.71; I(2)=59%) and 2.04 (95% CI, 1.56-2.66; I(2)=90%), respectively. Similarly, women and aneurysms with an irregular shape had higher risks, with RRs of 1.26 (95% CI, 0.97-1.62; I(2)=59%) and 2.32 (95% CI, 1.46-3.68; I(2)=91%), respectively (16).

2.4 Pathophysiology

The IA pathophysiology is still unclear, as its origin is not fully understood. Hemodynamic stress and degenerative changes in the arterial wall are partly responsible for this pathology. Alterations in the blood flow activate inflammatory cascades on the arterial wall and weaken them, compromising the homeostasis between hemodynamic stress and arterial wall integrity. The arterial wall levels of metalloproteinases increase, degrading the endothelial-cell-extracellular matrix and fragmenting the internal elastic lamina (17)(18). The endothelial

damage leads to intimal layer thinning, causing vascular smooth muscle cells to migrate from the middle lamina to the intimal layer. These cells' phenotypes vary due to migration and hemodynamic alterations. They turn them into pro-inflammatory cells, leading to extracellular matrix remodeling. All of the above explains the cuboidal epithelium metaplasia resulting from the exposure of epithelial cells to turbulent flow. It also agrees with the overexpression of prostaglandin E2 and tumor necrosis factor-kB, critical inflammatory mediators in IA formation (17).

Parallel to the endothelial changes, cellular stromal-derived factor (SDF 1) expression also supports IA formation by inducing angiogenesis (17). Mast cells and Lymphocytes also play an essential role in aneurysm formation and progression to rupture (19). Mast cell degranulation induces the expression of reactive oxygen species and metalloproteinases. These events lead to vascular media cells apoptosis and vascular media weakening. On the other hand, lymphocytes secrete metalloproteinases and cytokines that cause vascular remodeling of the aneurysm and perpetuate the inflammatory cascade. These proteins act as chemotactic agents that promote inflammatory cells' migration to the vascular wall (17)(18).

2.5 Classification

IAs fall into different classes according to their morphology, size, pathogenesis, and anatomical location (Table 2) (20).

According to their morphology	
Saccular	A saccular bulge in the arterial wall with a well-defined neck. These aneurysms commonly occur at arterial bifurcations or sharp bends in blood vessels (Figure 1A and Figure 1B)
Fusiform	An elongated, dilated, tortuous, and without defined neck arterial segment. These aneurysms are unrelated to bifurcation sites or angulation (Figure 1C).
Dissecting	A vessel's dilation through a gap results in the perforation of the middle and adventitial layers. Formerly known as pseudoaneurysms.
According to their size	

Small	0-5 mm diameter
Medium	5-10 mm diameter
Big	10–25 mm diameter
Giant	>25 mm diameter

Table 2: Intracranial aneurysm classification, according to their morphology and size.

Saccular aneurysms are the most frequent (Table 2, Figure 1A and Figure 1B), representing 90% of IA. They are also the most commonly associated with morbidity and mortality due to SAH. Several factors are related to saccular aneurysm formation. However, the most relevant is the tunica media and internal elastic lamina degeneration in the intracranial arteries bifurcations, as these regions withstand chronic hemodynamic stress (20).
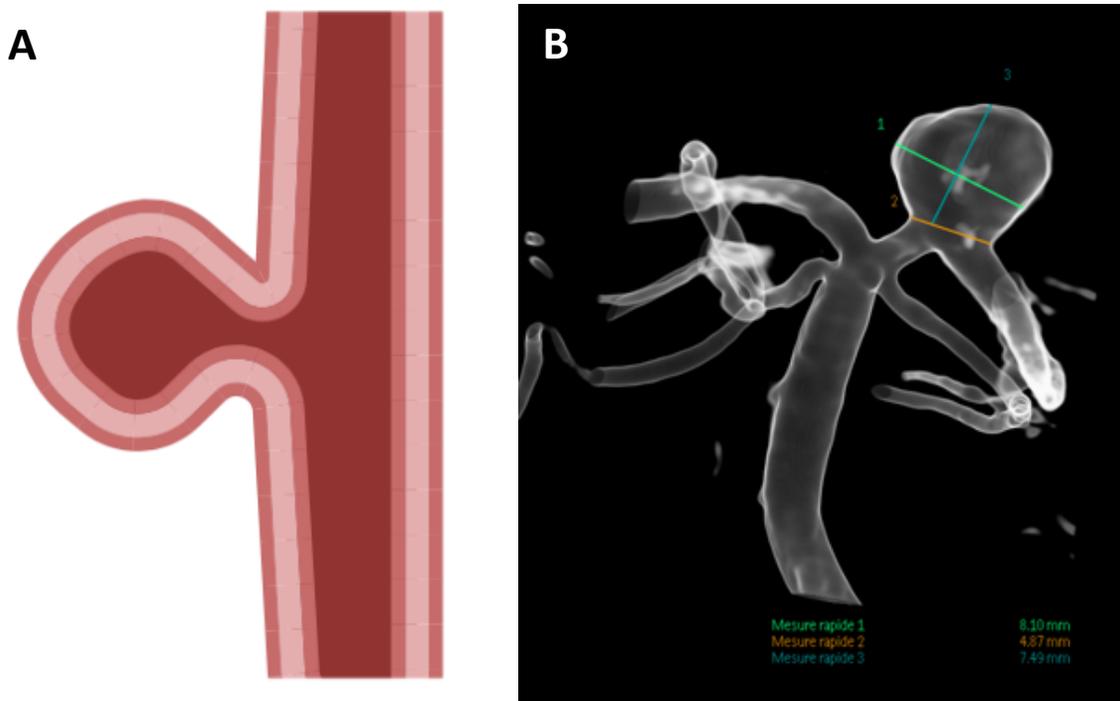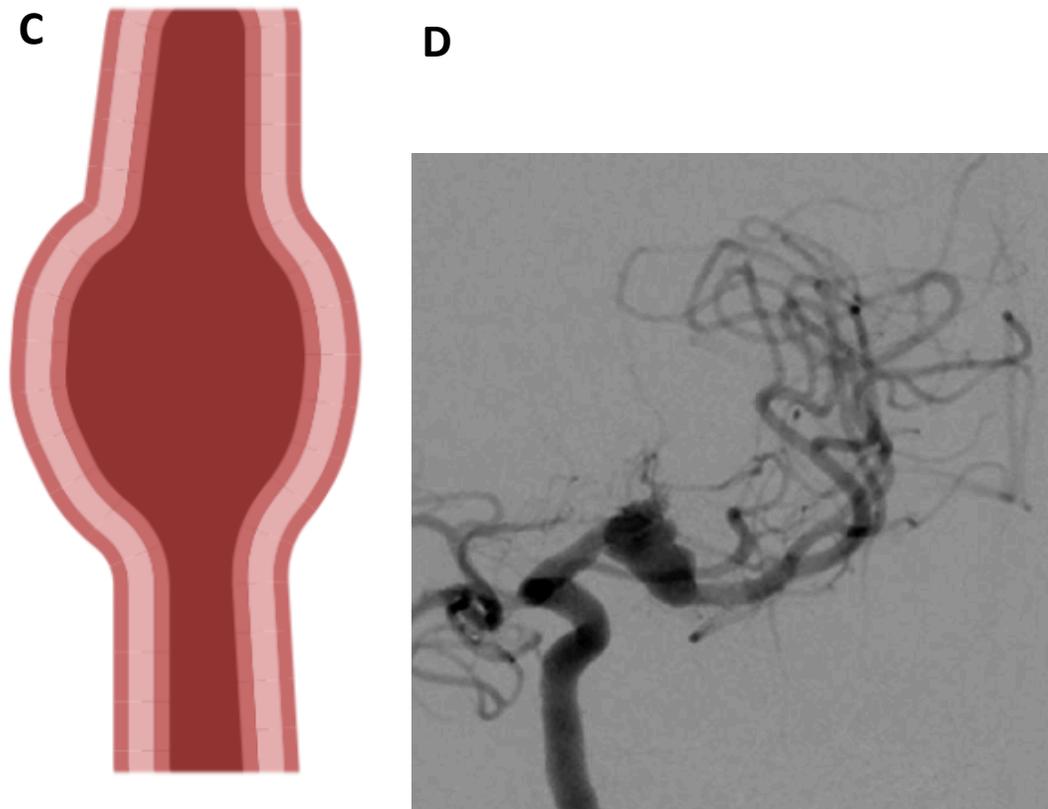
Figure 1: Graphical representation and angiography of the Saccularr (A,B) and Fusiform (C,D) intracranial aneurysms morphologies. Create in Biorender by: Andres Ortiz - Daniela D Vera - Daniel Mantilla

Fusiform aneurysms are associated with atherosclerosis, which damages the tunica media and produces arterial elongation. These aneurysms usually compromise the posterior circulation and have diameters that can reach several centimeters. Unlike saccular aneurysms, they do not have a defined neck (Table 2, Figure 1C and Figure 1D). and are hard to manage by surgical intervention as their blood inflow and outflow are separated. Elongated and tortuous fusiform aneurysms are also referred to as dolichoectasia, from the Greek dolikhós, meaning "long," and ektasis, meaning "distended."

Dissecting aneurysms result from internal or medial elastic lamina tearing. The tearing might come with intramural hemorrhage and causes vessel narrowing or dilation. These vessel modifications lead to a chronic intimal thickening due to tissue granulation, repetitive

intramural hemorrhage, and fragile neovessels rupturing after 14 days (21). Dissecting aneurysms divide into spontaneous or traumatic, depending on their causality. Most are associated with trauma or an underlying vasculopathy, such as fibromuscular dysplasia. However, they can also result from minor trauma such as head-turning, chiropractic manipulation, sneezing, or sports activities, with or without underlying vasculopathy (Figure 2) (21)(22).
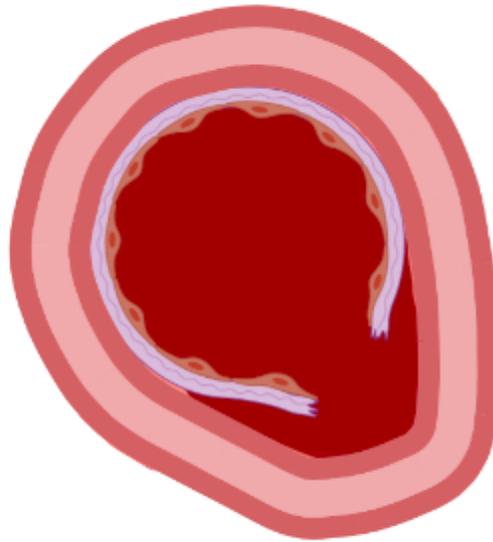
Figure 2: Graphical representation of a dissecting aneurysm. Create in Biorender by: Daniela D Vera - Andres Ortiz - Daniel Mantilla

2.6 Symptoms

Most unruptured IAs are asymptomatic, but some may be symptomatic. The most common symptoms include headache, visual acuity loss, pyramidal tract dysfunction, and facial pain. Cranial neuropathies are also common, especially oculomotor nerve palsy caused by the aneurysm's mass effect or blood leakage. The oculomotor nerve palsy comes with unilateral ptosis, exotropia, and dilated pupil. IA in the basilar artery and superior cerebellar artery can manifest with third cranial nerve palsy. Cavernous aneurysms of the internal carotid artery

can present with third, fourth, and sixth cranial nerve palsies. Finally, aneurysms in the ophthalmic segment of the internal carotid artery can come with visual field defects (23)(24). Most IA diagnoses come upon aneurismal rupture and SAH. The rupture and bleeding occur mainly during non-strenuous activity, rest, or sleep, unlike non-aneurysmal SAH (25). The typical aneurysm-related SAH symptom is the abrupt onset of a localized or generalized headache described as "the worst headache of the patient life." This headache may present with nausea (46.9%), vomiting (61 %), neck pain or stiffness (75 %), photophobia, focal neurological deficit, transient consciousness loss (9%) , or seizures (< 10 %) (26)(27). Several hours after the bleeding, the blood decomposes in the cerebrospinal fluid producing aseptic meningitis. Patients might also present meningismus (28). Regarding prodromal symptoms, 10 % to 43 % of patients report sentinel headaches that occur days or weeks before a significant hemorrhage. Sentinel headache can be caused by various pathologies such as minor aneurysm rupture with low subarachnoid bleeding, bleeding in the aneurysm wall without complete rupture or SAH, and aneurysm wall expansion and stretching (29).

2.7 Diagnosis

Unruptured IA diagnosis relies on brain scanning techniques, including magnetic resonance angiography (MRA), computed tomography angiography (CTA), and digital subtraction angiography (DSA) (27). However, as most unruptured IA are asymptomatic, their diagnosis is usually an incidental finding. Neuro-interventionalists diagnose them on brain images taken to assess other pathologies or following SAH. The angiography selection for the initial IA examination depends on availability, and CTA is generally the first available. CTA has a sensitivity between 77 % and 97 % and a specificity above 87 %. However, its sensitivity falls between 40 % and 91 % for aneurysms smaller than 3 mm. Using a multidetector CTA, the sensitivity and specificity increase above 97 %, and the detection for aneurysms longer than 4 mm improves (30).

MRA has a sensitivity between 74 % and 98 % and a specificity of 100 % for aneurysms of 3 mm or larger. However, similar to CTA, sensitivity decreases to 40 % for aneurysms smaller than 3 mm. MRA does not use ionizing radiation. Therefore, it is helpful for patients with a contraindication or allergy to iodinated contrast medium. However, MRA requires a

longer acquisition time than CTA, making it problematic for anxious or critically ill patients (30).

DSA is considered the gold standard for IA diagnosis. It provides detailed aneurysm anatomy and is the most sensitive for visualizing aneurysms smaller than 3mm and perforating branches. However, DSA is more expensive than CTA and, as it is invasive, can lead to neurological complications (1.0 % - 2.5 %), femoral artery injury (0.1 % - 0.6 %), inguinal hematoma (6.9 % - 10.7 %), and contrast-induced nephropathy (1 % - 2 %) (30).

2.8 Treatment

The literature regarding the treatment of unruptured IA is controversial. The reasons for this controversy are the low IA's natural history understanding and the few randomized clinical trials comparing conservative management and interventional therapy. Neuro-interventionalists base the treatment selection on each patient's life expectancy, hemorrhage risk, and treatment-associated risk. However, several scales are available for assessing the IA rupture risk and helping neuro-interventionalists with treatment selection. Examples of these scales are the PHASES score and the Unruptured Intracranial Aneurysm Treatment Score (UIATS) (30). As previously mentioned, the PHASES score evaluates the 5-year risk of IA rupture. It comes from a pooled analysis of prospective cohort studies conducted in the USA, Canada, the Netherlands, Finland, and Japan. The PHASES score considers risk factors such as age, hypertension, and history of SAH, among others (Table 3) (31).

Criteria	Points
Population	
North American, European (other than Finnish)	0
Japanese	3
Finnish	5
History of hypertension	
No	0
Yes	1

Age	
<70 years	0
≥70 years	1
Aneurysm size	
<7.0 mm	0
7.0–9.9 mm	3
10.0–19.9 mm	6
≥20 mm	10
Earlier SAH from another aneurysm	
No	0
Yes	1
Aneurysm site	
ICA	0
MCA	2
ACA/Pcom/posterior circulation	4

The 5-year absolute risk of aneurysm rupture based on the score:

- ≤2 points: 0.4%
- 3 points: 0.7%
- 4 points: 0.9%
- 5 points: 1.3%
- 6 points: 1.7%
- 7 points: 2.4%
- 8 points: 3.2%
- 9 points: 4.3%
- 10 points: 5.3%
- 11 points: 7.2%
- ≥ 12 points: 17.8%

Table 3: Score PHASES. Posterior circulation includes the vertebral artery, basilar artery, cerebellar arteries, and posterior cerebral artery. ACA: anterior cerebral arteries (including the anterior cerebral artery, anterior communicating artery, and pericallosal artery); ICA:

internal carotid artery; MCA: middle cerebral artery; PcomA: posterior communicating artery; SAH: subarachnoid hemorrhage (31)

UIATS also assesses the IA rupture risk. However, it considers additional IA rupture factors, including treatment-associated complications and psychological aspects, such as fear of aneurysm rupture. UIATS comes from the consensus of 39 aneurysm specialists representing multiple countries and clinical disciplines, i.e., neurosurgery, neuroradiology, neurology, and clinical epidemiology. Thirty additional aneurysm specialists validated the scale (Table 4) (30).

Patient			Favors UIA repair	Favors UIA conservative management
Age (single)	<40 years	4		
	40-60 years	3		
	61-70 years	2		
	71-80 years	1		
	>80 years	0		
Risk factor incidence (multiple)	Previous SAH from a different aneurysm	4		
	Familial intracranial aneurysms or SAH	3		
	Japanese, Finnish, Inuit ethnicity	2		
	Current cigarette smoking	3		
	Hypertension (systolic BP > 140 mm Hg)	2		
	Autosomal-polycystic kidney disease	2		

	Current drug abuse (cocaine, amphetamine)	2		
	Current alcohol abuse	1		
Clinical Symptoms related to UIA (multiple)	Cranial nerve deficit	4		
	Clinical or radiological mass effect	4		
	Thromboembolic events from the aneurysm	3		
	Epilepsy	1		
Other (multiple)	Reduce quality of life due to fear of rupture	2		
	Aneurysm multiplicity	1		
Life expectancy due to chronic and/or malignant Diseases (single)	< 5 years	4		
	5 – 10 years	3		
	>10 years	1		
Comorbid disease (multiple)	Neurocognitive disorder	3		
	Coagulopathies, thrombophilic diseases	2		
	Psychiatric disorder	2		
Aneurysm				
Maximum diameter (single)	< 3.9 mm	0		
	4.0 – 6.9 mm	1		
	7.0 – 12.9 mm	2		
	13.0 – 24.9 mm	3		
	>25 mm	4		
Morphology (multiple)	Irregularity or lobulation	3		
	Size ratio > 3 or aspect ratio > 1.6	1		
Location (single)	BasA bifurcation	5		

	Vertebral/Basilar artery	4		
	AcomA or PcomA	2		
Other (multiple)	Aneurysm growth on serial imaging	4		
	Aneurysm de novo formation on serial imaging	3		
	Contralateral steno occlusive vessel disease	1		
Treatment				
Age-related risk (single)	< 40 years	0		
	41 – 60 years	1		
	61 – 70 years	3		
	71 – 80 years	4		
	>80 years	5		
Aneurysm size-related risk (single)	< 6.0 mm	0		
	6.0 – 10.0 mm	1		
	10.1 – 20.0 mm	3		
	>20 mm	5		
Aneurysm complexity-related risk	High	3		
	Low	0		
Intervention-related risk	Constant*			

*Table 4: UIATS score. *The minimal intervention-related risk is always added as a constant factor (5 points). AcomA = anterior communicating artery; BasA = basilar artery; BP = blood pressure; multiple = multiple selection category; PComA = posterior communicating artery; SAH = subarachnoid hemorrhage; single = single selection category.*

Three types of IA treatment are currently available, conservative management, endovascular treatment, and surgical treatment. Neuro-interventionalists are inclined toward the

endovascular option as it has lower morbidity, fewer hospital stays, and shorter patient recovery times (5).

2.8.1 Surgical treatment

The open surgical treatment, also known as surgical clipping, involves placing a surgical clip through the aneurysm neck or base. This technique excludes the aneurysm from the arterial circulation while preserving the main artery and its adjacent branches. Surgical clipping has a complete aneurysm occlusion rate between 90 % and 95 % and a low recurrence rate in saccular aneurysms. However, it represents a higher risk for patients as it is a more invasive surgery requiring open craniotomy. According to the ISUA study, surgical clipping has one-year morbidity and mortality of 9.8 % and 2.3 %, respectively.

The complications associated with this technique are stroke (6.7 % - 10 %), hemorrhagic complications (2.4 % - 4.1 %), incomplete aneurysm obliteration (5 %), aneurysm recurrence (1.5 %), infection, and seizures (0.1 % for status epilepticus and 9.2 % for any seizure) (7). Patients eligible for surgical clipping include young patients with low surgical risk, patients having aneurysms at the anterior circulation, especially at a superficial location (MCA aneurysms), and those with lesions smaller than 10 mm (30).

Poor surgical clipping outcomes are associated with posterior circulation IAs, such as those located in the superior basilar region. Surgical clipping risk increases with the aneurysm size, with aneurysms smaller than 10 mm having a risk of 4%, aneurysms between 10 mm and 24 mm of 12.1 %, and those above 25 mm of 26.5 %. Patients older than 50 years or with a history of ischemic cerebrovascular disease or symptomatic unruptured aneurysms (i.e., oculomotor nerve palsy) are also at increased risk (30).

2.8.2 Endovascular treatment

The endovascular management of IA emerged in the 1990s. This technique has evolved from aneurysmal sac coil embolization to balloon-assisted and stent-assisted coil embolization. Among these techniques, the former involves a balloon inflated in the main artery, while the latter consists of a stent deployed in the main artery (Figure 3). These more novel techniques stabilize the coils in the aneurysmal sac and facilitate the treatment of wide-neck aneurysms

(> 4 mm) and large and giant aneurysms. The stent in stent-assisted coil embolization prevents the coil from protruding, avoiding thrombus formation and stroke. It also produces hemodynamic changes in the aneurysm due to blood vessel remodeling. These changes decrease the aneurysm recanalization and promote an adequate blood flow in the vessel, guaranteeing stent patency (5).

Flow-diverter stents (FDs) are endovascular devices introduced in 2007 for treating IA, particularly complex IA such as large-sized (giant) and wide-necked aneurysms (5). FDs are self-expanding stents deployed in the main artery for covering the aneurysm neck. They divert the blood flow into the main artery, causing gradual aneurism thrombosis six to 12 months following the treatment (32). Additionally, the inflammatory response, healing, and subsequent endothelial growth resulting from the FD deployment help shrink the aneurysm's size and reconstruct the main artery's lumen while preserving the lateral and perforating branches. FDs have some drawbacks despite their multiple advantages. IA patients treated with FD need dual antiplatelet therapy three to six months before and after the procedure, as they may develop intra-stent thrombosis. They might also present FD treatment complications, including strokes, perianeurysmal edemas, distant and late hemorrhages, and perforator occlusions (30)(32)(33).

The ISUA study showed that IA patients with endovascular treatment had lower morbidity and mortality than those with surgical treatment. Endovascular treated patients had a 6.4 % morbidity and 3.1 % mortality one year following the treatment, despite being older and having larger and posterior circulation aneurysms (7).
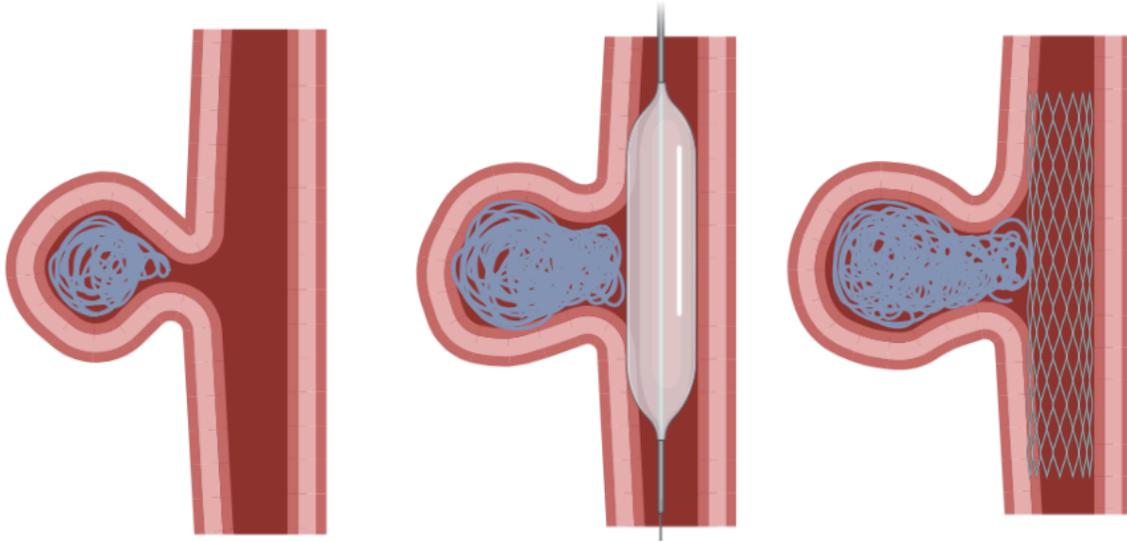
Figure 3: Graphical representation of the intracranial aneurysms endovascular treatment with coil embolization (A), balloon-assisted (B), and stent-assisted (a)coil embolization. Create in Biorender by: Andres Ortiz - Daniela D Vera - Daniel Mantilla

The FD surface has improved to reduce the thrombogenicity risk without compromising the treatment efficacy. The Pipeline Flex with Shield technology (SPED; Medtronic) is a result of these improvements. The SPED contains covalent bonds of phosphorylcholine on its surface, mimicking the exterior of the red-blood-cell membrane and decreasing the thrombosis risk. This device has cumulative mortality and morbidity rates of 2.3 % and 6.8 % per year, respectively. It also has six-month and 18-month adequate occlusion rates of 78.8 % and 90.3 % (34). Other devices resulting from these improvements are the Derivo Embolization Device (DED; Acandis) and the p64MW and p48MW Hydrophilic Polymer Coating (HPC, phenox) flow modulation devices. Li et al. evaluated the SPED and DED safety and efficacy for treating IA in their systematic review and meta-analysis. They analyzed the treatment outcomes of 1,060 IA representing 911 patients and found a technical success of 99.6 %. They also found six-month and 12-month aneurysm occlusion rates of 80.5 % and 85.6 %, respectively, and mortality, morbidity, total ischemia, and severe ischemia rates of 0.7 %, 6.0 %, 6.7 %, and 1.8% (35). Lastly, the Woven EndoBridge, Sequent Medical (WEB device, Aliso Viejo, CA) is another improved version of FD. The

WEB device is placed inside the aneurysm sac and diverts blood flow to the neck, producing intrasaccular thrombosis (30).

2.9 Simulation software

Treating intracranial aneurysms with FD requires adequate planning, which can be challenging for neuro-interventionists when done manually. Automated optimization methods are available for facilitating FD selection and simulating its deployment. Among these methods is the Sim&Size™ simulation software, which is the subject of this study. Specifically, this study includes several chapters evaluating different aspects of using the Sim&Size™ simulation software to select and deploy Pipeline Embolization Devices (PED), a specific FD type.

2.9.1 Sim&Size™ simulation software

The Sim&Size™ simulation software is a virtual simulation software from the Sim&Cure technology company that facilitates the FD selection and deployment. During the planning phase, neuro-interventionists can use patients' 3D-digital subtraction angiography (3D-DSA) images in the Sim&Size™ simulation software to reconstruct their 3D arterial geometries. The software uses these 3D reconstructions to define the microcatheter trajectory in the parent vessel and asks for distal and proximal landing zones, preferably targeting straight-vessel segments. Based on the chosen landing zones, Sim&Size™ simulation software proposes FD dimensions and simulates its deployment.

One advantage of the Sim&Size™ simulation software is that it displays the simulation results as an interactive 3D rendering of the patient's vessels showing the simulated FD. This interactive 3D rendering is helpful because neuro-interventionalists can modify the landing zones and FD dimensions to evaluate their effect on FD behavior. This rendering also includes a color map on the FD surface specifying the degree of FD-vessel wall apposition, which is a piece of critical information for the FD selection. Another advantage of the Sim&Size™ simulation software is that it includes a "push" functionality. This functionality allows the neuro-interventionalist to estimate the amount of 'push' applied during the FD deployment, which is also crucial information for the FD selection.

34

2.9.2 Sim&Size^{TM} simulation software workflow

The Sim&Size^{TM} simulation software is user-friendly and has a simple workflow, making it advantageous for clinical practice. These evaluations used a workflow based on the manufacturer's recommendation. Specifically, patients' 3D-DSA images were exported from the PACS system or workstation into the Sim&Size^{TM} simulation software using a USB memory stick. The software used these images to generate 3D-vessel patient reconstructions, which the neuro-interventionalist validated. Then, the software used the verified 3D reconstructions to determine vessels' centerlines, in which the neuro-interventionalist specified distal and proximal landing zones that target straight-vessel segments. Based on this information, the software simulated the PED deployment and proposed a PED geometry and length, assuring a good apposition and avoiding oversized diameters. The software display the simulation as a 3D interactive rendering of the patient's vessels showing the simulated PED and its apposition level. Multiple PED simulations could be achieved by modifying the PED length or adjusting the landing zones when necessary.

The neuro-interventionalist could use the "push" functionality to force a longitudinal compression during the deployment and increase the FD-vessel wall apposition. During the simulation, the aneurysm and vessel walls were considered rigid and fully constrained. We used the color map provided by the Sim&Size^{TM} simulation software to assess the quality of the PED-vessel wall apposition. Green indicated a complete and red a partial apposition. Parameter adjustments were visualized in real-time in the 3D interactive rendering.

Validation process of medical softwares
Review

Chapter contents

3.1 Introduction

Medical software can help to overcome limitations and create solutions to problems occurring during healthcare. Implementing new drugs, medical devices, and artificial intelligence (IA) software requires validation to confirm the efficacy and safety of these drugs, devices, and software in patients (36).

According to the Food and Drug Administration (FDA) of the United States, software validation is the "confirmation by examination and provision of objective evidence that the software specifications meet the user's needs and intended uses, and that the particular requirements implemented through software can be consistently met." The FDA requires software validation before its approval, and each step of the validation process must be documented, showing that the software complies with the FDA standards. The validation can take place during or after software development (37).

Software validation is critical to ensure software quality and effectiveness. A proper validation guarantees the software's ease of implementation and reliability and reduces failure chances and the need for fixes. It also reduces patient risk, recalls, long-term costs, and liability for creators. Establishing a comprehensive validation method is also critical, as it can reduce the software budget in the long term by lowering the validation costs associated with upgrades and the release of newer versions (37).

Software validation is challenging for software developers as they cannot test the software indefinitely, and estimating the amount of evidence necessary for software validation is challenging. A common strategy is to establish a "confidence level" indicating the requirements and expectations the new software or software version should satisfy, depending on the risk associated with this new release (37).

3.2 4Q Life Cycle Model

The "4Q Life Cycle Model" proposes a software validation methodology used in most validation projects. This methodology comprises four qualifications specifying the stages of the software life cycle that require testing or documenting results. The four qualifications include the Design qualification (DQ), Installation Qualification (IQ), Operational Qualification (OQ), and Performance Qualification (PQ). The DQ, provided by the vendor, outlines design specifications, software requirements, operational specifications, and the vendor's attributes. The IQ establishes the tests for confirming the proper installation of the software considering the vendor's recommendations, the user's requirements, and the guidance of the regulatory entity of the country. The OQ establishes the test for verifying the software's consistent performance when operating within expected conditions. The PQ is the stage that confirms that the software will perform as expected once installed since the previous tests and documentation validate that the software will comply with the requirements for functionality and safety (Figure 4) (37).

Design Qualification
- User requirement specifications
- Functional specifications
- Operational specification
- Vendor qualification

Installation Qualification
- Check arrival as purchased
- Check Installation of hardware and software

Operational Qualification
- Test of key operational functions
- Test of security functions

Performance Qualification
- Test for specified application
- Preventive maintenance
- On-going perfomance tests

Figure 4: 4Q Life Cycle Model (37)

The guide "General Principles of Software Validation; Final Guidance for Industry and FDA Staff" establishes the general principles to consider for software validation, including: (37)

1. Requirements: The software requirements specification must be documented, providing the baseline for the validation process.

2. Defects prevention: The developer must focus on preventing the introduction of errors into the software during its development instead of implementing tests for testing its performance. Error prevention occurs during software development and not

at the end, where the complexity of the software might be a limitation for exhaustive testing.

3. Time and effort: Preparation for software validating should begin early, during design and development planning, to ensure that the software's validation is supported by evidence gathered from planned efforts throughout the software life cycle.

4. Software life cycle: The software life cycle must consider the software validation process. It must include engineering tasks and information for verifying the validation. However, the validation guide does not recommend any particular life cycle model.

5. Plans: The software validation process must be defined and controlled through an established plan specifying the aim and scope of the validation. This plan should include the approach, necessary resources, a schedule, and a list of tasks and work items needed for the validation.

6. Procedures: The procedures specify the actions to follow during the validation process to complete validation activities, tasks, and work items.

7. Validation of the software after a change: A validation analysis must follow any software modification. The validation analysis must evaluate the change impact on the entire software instead of focusing on the part of the software impacted by the change. The developer must use controls and regression tests to demonstrate that the change did not affect the software.

8. Validation coverage: The validation coverage must reflect the software complexity and safety risk.

9. Independence of review: The validation should rely on independent evaluations instead of self-testing when possible, especially in software with significant safety risks. The validation process could include hiring a third party to verify and validate the software. Alternatively, a staff member could be assigned for the validation, but he must be knowledgeable and have no conflict of interest with the software.

10. Flexibility and responsibility: The developer has the flexibility to choose a validation methodology. However, he is responsible for outlining the software validation process and results.

3.3 Classification validation methods

Validation methods can be classified into internal validation, cross-validation, Split-Sample validation, and external validation, depending on who makes the validation or how the data is processed. The internal validation is done by the entity developing the software. It focuses on assuring an expected software performance during its development and not on assessing the performance of the finished software. In contrast, external validation is performed by a third party or someone in the entity developing the software with no conflict of interest. Therefore, it is more objective. It is recommended to complement the internal validation with external validation and compare the results of both evaluations, as the internal validation tends to overestimate the software performance (36).

Internal validation has two subtypes, cross-validation, and split-sample validation (36). Cross-validation is a statistical method for testing models that divides the data into two segments, one used to train and the other to test the model. The k-fold cross-validation (Figure 5) is the simplest form of cross-validation and is helpful for the preliminary evaluations of software performance. The k-fold cross-validation starts by splitting the data into k subsamples, one of which is used for the validation and the remaining (k-1) for training the model. The cross-validation process is repeated k times to obtain the average results of the k cross-validations (36)(38).
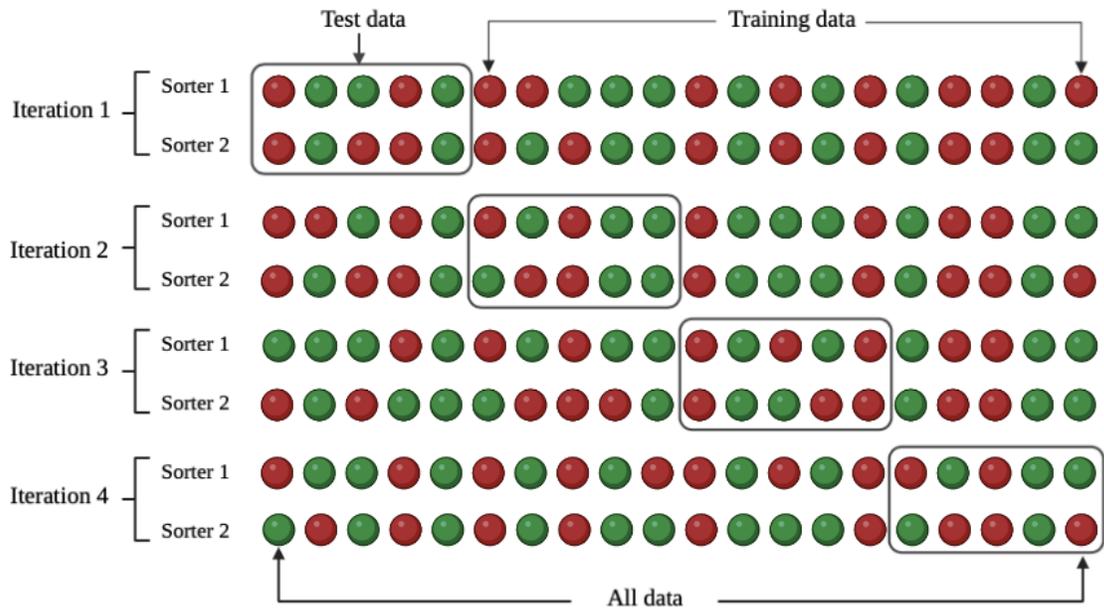
Figure 5: k-fold Cross-validation. Create in BioRender.com by Daniela D Vera – Daniel Mantilla.

The split-sample validation is also a statistical method for testing models that divides the data into three subsets, one used for the training set, the other for tunning, and the other for testing. This method uses the testing subset to evaluate the performance of a trained and tuned model. Subsequently, the data can be stratified depending on the time they were collected or divided randomly. The split-sample validation is the most suitable for internal validation (36)(39).

3.4 Validation of medical softwares

The validation of software intended for medical propose must include an evaluation of the clinical utility of the software. This evaluation should evaluate the effect of the software on patients' outcomes using a randomized clinical trial. However, in cases where the randomized clinical trial is not feasible, a prospective or retrospective observational study adjusted for confounding variables can be used (36). Depending on the country, other technical or sociopolitical factors could be required to validate medical software. Different entities such as the FDA, the European Commission (CE Marking), and medical insurance companies might have additional requirements. For instance, a well-documented validation of the technical performance of the software is a critical validation criterion for software approval.

CE Marking requests a document summarizing all the technical aspects of the medical device or software, including performance tests consequent with the "State of the Art." The "IEC/EN 62304:2006, medical device software – software life cycle processes" is considered state of the art for medical software for the CE Marking. Therefore, all software manufacturing companies must comply with this standard for introducing new medical software in Europe. Medical insurance companies request a validation of the clinical software utility, showing that the medical software improves the patients' outcomes (36).

Validation of the Sim&Size™ simulation for treating patients with intracranial aneurysms using pipeline embolization devices

Chapter contents

4.1 Introduction

The introduction of the Flow Diverter Stent (FD) as an alternative to the stent and coils combination has changed the treatment of intracranial aneurysm (40). Reconstruction of the parent artery with FDs redirects the blood flow, resulting in reduced intra-aneurysmal flow and hemorrhage risk, and increased thrombus formation (41). FDs also lessen secondary aneurysmal growth and rupture (42). Thromboembolic complications, including delayed FD thrombosis and incomplete occlusion, still occur despite the advantages of these devices. These complications might relate to poor FD-arterial wall apposition (43). Decreasing the FD's porosity can increase the flow diversion efficiency inside the aneurysm, which favors thrombotic occlusion. However, it can also increase the risk of post-stenting stenosis in the parent artery (44).

Treating intracranial aneurysms with FDs involves a long and uncertain planning phase as device elongation and contraction are hard to predict. Proper planning is crucial as an inadequate FD-vessel wall apposition increases the risk of thromboembolic complications and in-stent intimal hyperplasia. Considering the patient's anatomy during the planning process influences FD's porosity and metal-surface coverage at the aneurysm neck, which might impact occlusion rates and the intra-procedural confidence of the neuro-interventionalist. Automated optimization methods for simulating FD's behavior based on the patient's anatomy are available. These methods improve interventions' prognosis and treatment outcomes (44). Virtual simulation software such as the Sim&Size^{TM} is among these methods. This software uses patients' pre-therapeutic angiographic data to facilitate FD selection and simulate FD deployment. In this chapter, we aimed to validate the results of the Sim&Size^{TM} simulation software using a cohort of patients treated with FDs for intracranial aneurysms. We also aimed to outline a validation process that can be used before introducing novel virtual simulation software into clinical practice.

4.2 Objective

Validate the accuracy of the Sim&Size^{TM} simulation software in patients treated with flow diverter stent for intracranial aneurysms and describe the protocol used during this validation.

4.3 Materials and methods

4.3.1 Study cohort and DICOM images acquisition

This retrospective monocentric evaluation included data from 116 consecutive patients treated for intracranial aneurysms with FD (Pipeline Embolisation Device (PED)) between July 2009 and January 2014. All therapeutic procedures involved a senior interventional neuroradiologist with experience in stent-placement techniques. Patients' data were collected from a neuroradiology service database, following ethics committee approval and patients' written informed consent.

Patients' 2D and 3D-digital subtraction angiography (3D-DSA) images were acquired on a Philips Allura Xper FD20/20 biplane neuro X-ray system (Philips Healthcare, DA Best, The Netherlands). Sixty-five patients had noninformative 3D-DSA images and were excluded from the evaluations. Other six patients were also excluded as they were associated with telescopic implantation, previously implanted laser-cut stents, overstretched devices, and coils artifacts.

3D-DSA images of the remaining 45 patients were used to reconstruct parent artery morphology and simulate PED deployment using the Sim&Size^{TM} simulations software.

The results of the Sim&Size^{TM} simulation, including PED position and length, were compared with those of the 2D-DSA images (real-life) (Figure 6). Two neuro-interventionalists from the Montpellier Department of neuroradiology carried out all the imaging processes and analysis to ensure two independent evaluations. These neuro-interventionalists were selected for their experience interpreting 3D-DSA images.
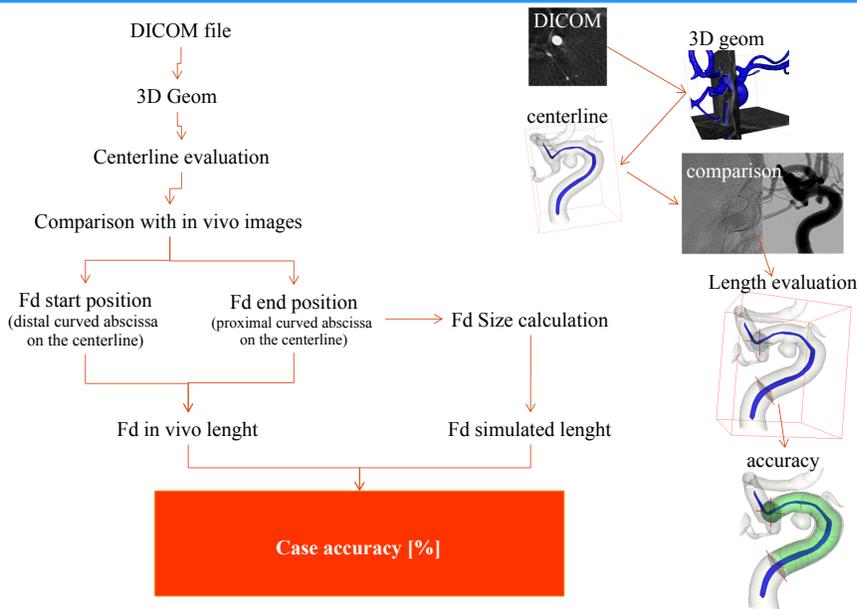
Figure 6. Block diagram showing the process used to validate the lengths of the Sim&Size^TM simulated Pipeline Embolisation Devices..

4.3.2 Sim&Size^TM simulation software and Sim&Size^TM simulation software workflow

The Sim&Size^TM simulation software and the simulation software workflow were described in the corresponding sections.

4.3.3 Validation of the FDsize simulation

Differences between real-life and simulated PED lengths were evaluated by overlapping the proximal and distal landing zones of the 2D-DSA images with those of the 3D reconstructions. The differences were used to assess the concordance between real-life and simulated PED lengths using the Bland-Altman test and calculate cumulative errors in R Core Team (2022). R: A language and environment for statistical computing. R Foundation for Statistical Computing, Vienna, Austria. URL https://www.R-project.org/. Two neuro-interventionalist and at least two 3D reconstructions were involved in the validations to ensure the quality and reproducibility of the results. 3D reconstructions were favored when the viewing direction coincided with the working incidence of the 2D-DSA.

4.4 Results

4.4.1 Patients cohort

The patient's cohort consisted of 116 patients treated with PED for intracranial aneurysms, but only 51 patients (44 %) had informative 3D-DSA. Out of these patients, one had telescopic implantation, three had previously implanted laser-cut stent, one had overstretched device, and one had coils artifacts. These patients were excluded from the evaluations, resulting in 45 patients (39 %) included in the validation process Sim&Size^{TM} simulation software.

4.4.2 Validation of the FDsize simulation

Simulated PED lengths ranged between 12 and 25 mm (mean 17.5 mm). We found a PED elongation of 44.5 % in 89.5 % of the simulations when comparing the unconstrained length at their resting state with the in-vivo measurements after PED placement.

The absolute error between the real-life and Sim&Size^{TM} simulated PED lengths was below 5.06 mm in 90 % of the simulations (Figure 7). However, we noticed increased differences between measurements in PED deployed under significant compression or stretching constraints (Figure 8).

Despite these differences, we found that the Sim&Size^{TM} simulations were acceptable for clinical purposes. We found a concordance of 0.97 (95% CI 0.94-0.98) between real-life PED lengths and those simulated by the Sim&Size^{TM} simulation software (Figure 9), with most of the data lying within two standard deviations of the mean of 0 in the Bland-Altman plots (Figure 10). The accuracy of the Sim&Size^{TM} simulation was 90 % in 86 % of the cases, with an average positioning error of 6%. Only one simulation overestimated the stent length giving a length error of 27 %. The more extended stent size might come from excessive pushing forces applied during the device implantation at the endovascular surgery not considered during our initial validation process.

The 90 % of cases have
an absolute error
minor than 5.06 mm
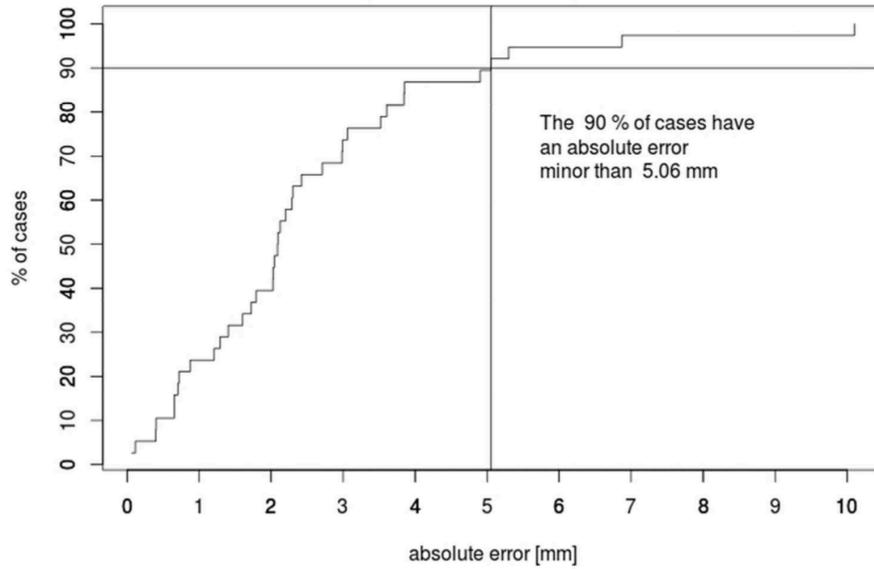
Figure 7. Cumulative frequency of the absolute errors for the lengths of the Pipeline Embolisation Devices simulated with Sim&Size^{TM} simulation software

Figure 8. Representative images showing the high compression of a the Pipeline Embolisation (PED). Images show the mismatch between the Sim&Size^{TM} simulated (A) and real-life (B and C) PED. 84x27 (300 x 300 DPI)

ID: 9   PIPELINE 4.00 / 20

FdSize	Image	error
24.6	24.1	-1.7%

A   B   C
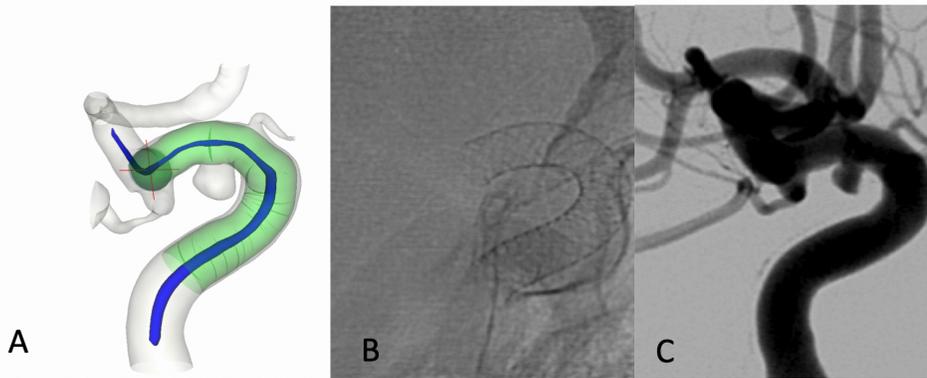
Figure 9. Representative image showing a good correlation between the Sim&Size^{TM} simulated (A) and real-life (B and C) PED. The error for this patient was 1.7 %.
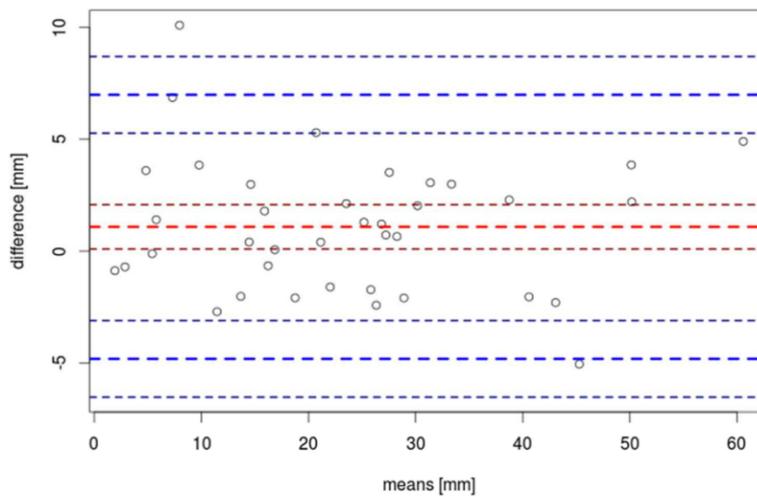
Figure 10. Bland-Altman plots showing the standard deviation of the mean for the lengths of the Pipeline Embolization Devices simulated with the Sim&Size^TM simulation software. 63x46 (300 x 300 DPI)

4.5 Discussion

FDs have been an option for treating intracranial aneurysms in clinical practice since the developing of these devices. They have a dense and fine strut network, which increases the complexity of their meshing (40). Selecting a size for these devices is challenging as their length changes after implantation (45). However, virtual simulation software has been developed to facilitate the FDs' size selection and deployment. We showed that the Sim&Size^TM simulation software provided PED lengths that coincided with real-life ones while simulating PED mechanical and geometrical features in 45 patients.

In clinical practice, virtual simulation software is a valuable tool for treating intracranial aneurysms with FD as it increases the accuracy during the FD design. This software can increase aneurysm occlusion rates and decrease leakage at the aneurysm by assuring a better FD-vessel wall apposition. It can also reduce patients' exposure to metal by decreasing FD length.

Virtual simulation software must be validated before being introduced into clinical practice. However, protocols have not been adequately established for this software validation despite its utility. A possibility to overcome this lack of protocols is to use methods developed for medical devices, including usability engineering and usability validation tests. Usability is defined as the "extent to which a product can be used by specified users to achieve specified goals with effectiveness, efficiency, and satisfaction in a specified context of use" (ISO 9241-11 1998). In particular, the Human Factors and Usability engineering strategy facilitates the medical devices' design and testing process (46). This strategy reduces errors, time, and mental effort associated with medical device design(3).

In healthcare, increasing numbers of public guidance documents have incorporated usability engineering to establish efficient operational procedures. For instance, the FDA outlines three essential steps in the design of medical devices that reduce use-related hazards (47):

- Identify use-related and unanticipated use-related hazards using an analytical process, such as heuristic analysis.
- Develop and apply strategies to mitigate use-related hazards.
- Use Human Factors validation testing to demonstrate the device's safety and effectiveness, either by simulated or clinical validation testing (2).

In this chapter, we proposed a process to assess the validate the PED lengths estimated by the Sim&Size™ simulation software. Our validation process involved two neuro-interventionalists comparing PED distal and proximal landing zones between real-life and Sim&Size™ simulated PED. Our validation process showed that pushing forces during PED deployment affected the device length and reduced the accuracy of the Sim&Size™ simulations. Consequently, we modified the Sim&Size™ simulation software workflow to include the effect of these forces.

Introducing virtual simulation software such as the Sim&Size™ simulation software into clinical practice after the proper validation would improve the treatment of intracranial aneurysm with FD. It will facilitate the planning process and help in the FD selection. Consequently, this software could improve aneurysmal occlusion rates and decrease thromboembolic complications. The Sim&Size™ simulation process also has pedagogic values as it could accelerate the learning curve and promote confidence for young neuro-interventionalist. Therefore, educational programs could benefit from including this software in their curriculums to encourage the usage of FD.

4.6 Conclusion
We proposed a process for validating virtual simulation software before its introduction into the clinical practice for treating intracranial aneurysm with FD. Using this process, we proved the utility of the Sim&Size™ simulation software for estimating PED lengths. Our results showed a good concordance between simulated and real-life PED lengths. These findings

demonstrated that using our validation process and introducing the Sim&Size^{TM} simulation software into clinical practice can improve the treatment of intracranial aneurysms with FD.

5.

Causes, complications, and potential damages associated with a wrong manipulation of the Sim&Size^{TM} simulation software

Chapter contents

5.1 Introduction

The literature has identified flaws in some of the methodologies used for studying medical devices (48). Many of these methods focus on analyzing the coarse device outcome, disregarding the analysis of the user-device interaction or the cognitive process associated with this interaction. Task completion is a performance indicator that reveals information about the user-device interaction, including erroneous or less than optimal device operation and near misses (2). Proper use of medical software is critical for achieving good outcomes in medical practice. Any deviation from the optimal use of software results in non-optimal outcomes, even when the user corrects the misuse (49).

Flow Diverter Stents (FDs) are a standard endovascular treatment for intracranial aneurysms (50). Selecting a proper FD size and position is critical for a good outcome, as the wrong choices increase the surgical intervention time and patient risk. Neuro-interventionalists can use standard manual procedures to select the FD size and position. However, these means do not necessarily result in good choices. Alternatively, neuro-interventionalists can use the Sim&Size^{TM} simulation software to help them during the FD selection and deployment.

The neuro-interventionalist clinical experience with the Sim&Size^{TM} simulation software is critical for achieving good outcomes. We believe that the software does not increase the surgical intervention risk. However, misusing the software might. Misusing and not using the Sim&Size^{TM} simulation software might have equal chances of selecting an incorrect FD size and position. This chapter aimed to analyze and describe potential risks associated with using the Sim&Size^{TM} simulation software for treating intracranial aneurysms with FD. This chapter also aimed to train users to detect possible software pitfalls, risk causes, and solutions.

Distinguishing between the treatment-related and software-related risks is essential. Endovascular treatment of intracranial aneurysms has intrinsic risks associated with embolic or hemorrhagic complications. A meta-analysis of 29 studies that included 1654 intracranial aneurysms treated in 1451 patients reported a treatment-related morbidity of 4.0 %, (95% confidence interval (CI) 3.0-6.0) and treatment-related mortality of 5.0 %, (95% CI 4.0-7.0)(13). Some treatment-related risks include inefficacious treatment due to lack of aneurysm occlusion, long general-anesthesia time, thrombogenic risk related to the FD, and

medium and long-term risk of thrombogenic complications due to the FD. Inadequate FD sizing may influence the treatment outcome. For example, inappropriate FD sizing can increase the thrombotic risk (51).

The Sim&Size™ simulation software is supposed to decrease the FD sizing-related complications. However, some risks might arise from the software misusing or malfunctioning. The neuro-interventionalist experience can help to mitigate this risk by verifying the software results. The neuro-interventionalist should be able to change the FD reference or its position in the patient's vessel when necessary. However, these changes also have an associated risk as they might increase the surgical intervention time, reduce the treatment effectiveness, or require an additional FD.

Several factors are relevant for achieving good results with the Sim&Size™ simulation software. For example, the software uses 3D-digital subtraction angiography (3D-DSA) to simulate the patient's parent artery and aneurysm. A non-optimal 3D-DSA may interfere with the simulation. Therefore, the quality of the 3D-DSA is critical, and the neuro-interventionalist must verify it. We list other factors and common mistakes neuro-interventionalists must consider when working with the Sim&Size™ simulation software, as they can be error sources.

5.2 Critical points causing the selection of a non-optimal FD size when using Sim&Size™ simulation software

1. Using a 3D-DSA image from a different patient for the Sim&Size™ simulation. This error can occur while choosing the DICOM file, as the neuro-interventionalists could select the file above or below the patient's file in the list of files.

2. Using an older 3D-DSA image for the Sim&Size™ simulation. This error can occur when the neuro-interventionalist does not pay attention to the image acquisition date and could influence the FD sizing.

3. Using an image series other than a 3D rotational DSA image series for the Sim&Size™ simulation. This error prevents the simulation from working and can occur when the neuro-interventionalist does not notice that he is using a different image type.

4. Working in a different view plane in the operating room than that visualized in the navigation console of the Sim&Size™ simulation software. Under this scenario, the neuro-interventionalist would look at the patient's vessels from a different angle and might select distal and proximal landing zones different from those specified by the software.

5. Implanting an FD reference different from the one used for the Sim&Size™ simulation. This error occurs during the FD selection and results from the neuro-interventionalist selecting a different FD size or type than that proposed by the software.

6. Skipping the 3D reconstruction adjustment during the Sim&Size™ simulation. Skipping the adjustment is critical, as the neuro-interventionalist verifies the artery walls and aneurysms limits in this step. This error can occur when the neuro-interventionalist is in a rush and press the next button during the arterial 3D reconstruction skipping the adjustment.

7. Falling short while delimiting the region of interest. This error can occur when the neuro-interventionalist selects an area that does not account for the FD deformation. This error can result in a proximal landing zone falling out of the region of interest and wasting time in the operating room.

8. Wasting time during the Sim&Size™ simulation. This error can occur when the neuro-interventionalist has no expertise in Sim&Size™ simulation software and wastes time in the operating room during the Sim&Size™ simulation.

9. Mistaking the distal and proximal landing zones.

10. Misinterpreting the extent of the FD-vessel wall apposition. This error can occur when the neuro-interventionalist does not understand the color scale used by the Sim&Size™ simulation software to indicate the quality of the FD-vessel wall apposition.

11. Mistaking the inlet and outlet while defining the center lines. This error can occur when the neuro-interventionalist is confused about the arrows indicating the arterial inlet and selects the outlet instead.

12. Choosing the wrong threshold value during the 3D reconstruction adjustment. This error can occur when the neuro-interventionalist selects an inadequate threshold value to perform the 3D reconstruction of the region of interest.

5.3 Hazardous situations related to the Sim&Size^{TM} simulation software

The endovascular treatment of intracranial aneurysms has benefited from the introduction of FD, particularly the treatment of petrous to supraclinoid internal carotid aneurysms. Problems and complications, such as ischemic events and distal hemorrhage, arising during FD deployment remain a concern despite the high efficacy of these devices (52). A proper FD-vessel wall apposition is essential for reducing the blood flow into the aneurysm. This reduction eventually leads to blood flow stagnation and aneurysm obliteration while preventing endoleaks (53).

No guidelines exist for managing an inadequate FD-vessel wall apposition. However, the neuro-interventionalist should always check for FD malposition while facing a poor apposition. Unexpected changes may occur in the FD configuration or position following its implantation (54). The FD malposition may be the result of a poor FD size selection. For example, the first case reported for a delayed FD migration was for an intracranial Pipeline Embolization Device (PED). The PED suffered a proximal migration, with the distal landing zone of the PED projected inside the aneurysm. The migration was over 1 centimeter and was related to FD foreshortening. An accurate FD sizing may have prevented this undesirable phenomenon (54)(55).

A poorly positioned FD has been considered a technical complication of endovascular procedures that can lead to delayed life-threatening aneurysm rupture or ischemic events (53). For example, one of our patients with an ophthalmic segment carotid aneurysm required a second treatment due to a delayed PED distal shortening (Figure 11).
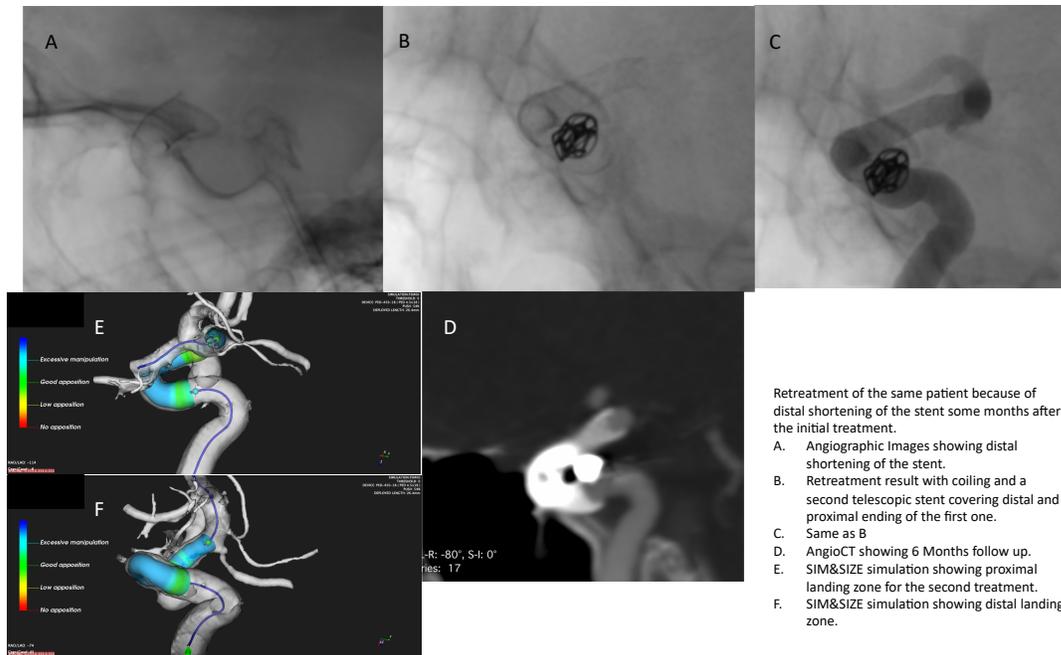
Retreatment of the same patient because of distal shortening of the stent some months after the initial treatment.
A. Angiographic Images showing distal shortening of the stent.
B. Retreatment result with coiling and a second telescopic stent covering distal and proximal ending of the first one.
C. Same as B
D. AngioCT showing 6 Months follow up.
E. SIM&SIZE simulation showing proximal landing zone for the second treatment.
F. SIM&SIZE simulation showing distal landing zone.

Figure 11. Representative images of an ophthalmic segment carotid aneurysm that had a delayed PED distal shortening and required a second treatment. A) Angiographic image showing the PED distal shortening. B) and C) Angiographic images showing the results from the second intervention with the coiling and second telescopic stent covering the distal and proximal endings of the first PED. D) AngioCT showing the six-month follow-up. E) Results from the Sim&Size^{TM} simulation showing the second treatment's proximal landing zone. F) Results from the Sim&Size^{TM} simulation showing the second treatment's distal landing zone. The stent used in the second treatment covered the distal and proximal endings of the first stent.

5.4 Dangerous situations and possible consequences of deploying an FD with a non-optimal size

Selecting a proper FD size is crucial for achieving adequated FD position and FD-vessel wall apposition. Some indications of a non-optimal FD size include:

- The FD has an oversized diameter.
- The FD has an undersized diameter (diameter undercut).
- The FD is too short (over-cutting the length).
- The FD is too long (length undercut).

During the Sim&Size™ simulation, the neuro-interventionalist selects a distal landing zone indicating the FD deployment starting point. Hence, a too long or too short FD length results from the erroneous calculation of the FD proximal landing zone. This incorrect calculation can result from the Sim&Size™ simulation software misuse or malfunction. We have mentioned critical points that can result in a non-optimal FD size selection when using Sim&Size™ simulation software. We will describe different dangerous situations and the possible consequences of deploying an FD with a non-optimal size. Also, we will discuss the actions that the neuro-interventionalist should take to mitigate the adverse outcomes and the possible consequences of these actions.

5.5 Vessel wall damage

An FD with an oversized diameter can cause micro-lacerations on the parent artery wall during deployment. These micro-lacerations induce repair mechanisms associated with excessive endothelial tissue development, which leads to intimal hyperplasia. The neuro-interventionalist can also cause micro-lacerations on the arterial wall trying to manipulate an FD with an undersized diameter.

Several techniques are available for adjusting the FD during deployment, including manipulating the FD with J- shaped, pigtail-shaped, or S-shaped guidewires. The neuro-interventionalist must be careful while operating the guidewire to avoid extending it between the FD and the parent artery wall or the subintimal. Using the microcatheter inside the FD is an alternative to guidewires. However, the neuro-interventionalist must avoid damaging the device's cut edge while manipulating the microcatheter. An intermediate catheter might also be beneficial, especially in the cavernous segment of the internal carotid artery. Another alternative is performing an angioplasty with a compliant balloon in cases where the FD is not fully open. However, the angioplasty must be inside the FD to avoid damaging the artery. When artery wall damage occurs close to the FD, using a second FD with the telescopic technique can be useful (53).

5.6 Metal Surface Coverage reduction

The literature shows that the FD geometry affects the Metal Surface Coverage (MSC) and emphasizes the adverse effects of FD oversizing. A study assessing the impact of the PED

nominal diameter on the MSC considering the recipient artery diameter demonstrated this negative effect (56). These evaluations showed that overlapping FD nominal and parent artery diameters increased MSC. On the contrary, FD nominal diameters wider than the parent artery reduced the MSC (Figure 12). The MSC reductions may result from the FD deformation at the oversized, which decreases the blood flow diversion and compromise the treatment outcome.

The literature suggests that achieving an optimal MSC is crucial for an adequate diversion of the blood flow at the aneurysm neck and endothelialization. Even a modest FD oversizing can affect the MSC and reduce endothelialization (57). However, using an undersized FD to accomplish a better MSC must be avoided. The Sim&Size^{TM} simulation software can predict the MSC at the aneurysm neck, and one chapter of this thesis will address this simulation.
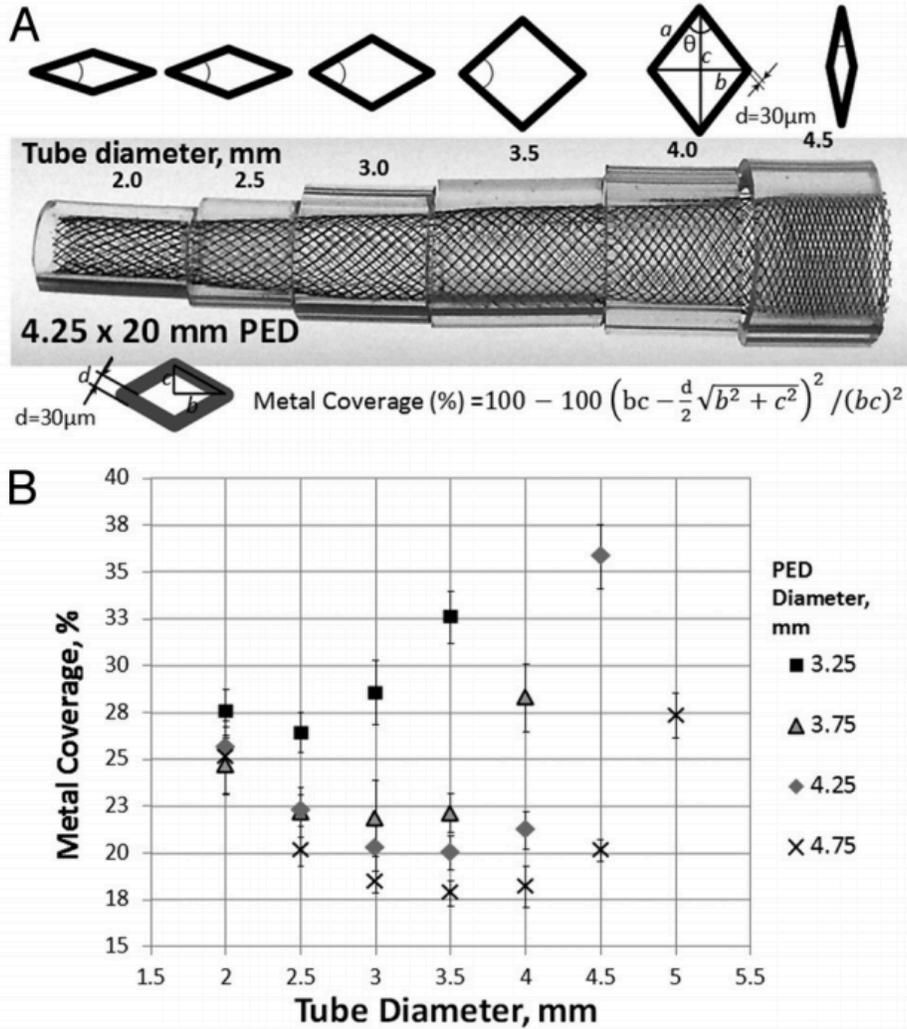
Figure 12. Effects of the Pipeline Embolization Device (PED) nominal diameter on the Metal Surface Cover (MSC). A) Representative image of a 4.25 x 20 m PED inserted into plastic tubes of 0.5-mm incremental diameters showing the variations in the MSC degree. Shown are the schematical configuration of cells (top) and the formula used for the MSC calculations, which uses the long and short rhombus diagonals and the strand diameter (30-um) (bottom). B) Scatterplot showing the MSC (metal coverage,%) for various PED nominal and "parent artery" diameter combinations. Taken from Shapiro et al. http://dx.doi.org/10.3174/ajnr.A3902

61

5.7 Wrong FD-vessel wall apposition

A wrong FD-vessel wall apposition at the proximal FD landing zone may arise during deployments in which the FD lands in an unexpected position. A poorly positioned FD can create non-desired stagnation zones between the FD and the artery. Therefore, the neuro-interventionalist observes a discontinuous apposition, especially at the proximal FD ending. An unnecessarily long FD with an undersized diameter aggravates this situation as achieving the intended FD position becomes more difficult. This situation can induce thrombus formation, increasing the risk of stroke secondary to embolic complications. It may also cause a life-threatening aneurysm rupture or FD migration (53). A wrong FD-vessel wall apposition resulting from the improper FD placement often occurs when the proximal landing zone does not align with the one proposed by the Sim&Size^{TM} simulation. Pushing forces during FD deployment may be responsible for the lack of concordance between the real-life and simulated proximal FD landing zone. The neuro-interventionalist can manipulate the FD to solve this position problem, using a balloon or a microcatheter angioplasty when necessary. However, the neuro-interventionalist might need to change the FD, mainly in cases with a complete lack of apposition. Changing the FD increases the risk for the patient by adding time and maneuvers to the surgical intervention.

5.8 Bad apposition at the aneurysm neck area

The endothelialization of the aneurysm neck is the final goal of FD endothelialization. A wrong FD-vessel wall apposition at the aneurysm neck prevents achieving this goal. This situation may occur during the deployment of an FD with a diameter smaller than the parent artery at the aneurysm neck. The FD might fail to prevent the blood flow into the aneurysm or a future recanalization event. This event compromises the treatment efficiency and delays the aneurysm healing in the best-case scenario. However, it can cause treatment failure, making a second treatment necessary.

Coverage of an arterial branch origin and long-term artery occlusion: FD elongation is more critical than initially considered during the Sim&Size^{TM} simulation. An FD longer than expected may cover an unintended arterial branch, causing endothelial and neointimal tissue

development at the FD segment covering the artery's origin. Endothelialization at the aneurysm neck is desirable. However, this phenomenon at the bifurcation may cause a progressive occlusion of the arterial branch. This progressive occlusion can result in long-term artery occlusion or acute thrombosis next to the origin of the arterial branch.

The gravity of the artery closure depends on the occlusion severity and speed. For example, slow and progressive artery occlusion allows the formation of collateral arteries capable of bypassing the obstruction site and irrigating the compromised area. Here, the arterial network has enough time to compensate for the occlusion without consequences for the cerebral parenchyma or clinical manifestation. However, in the case of sudden occlusion, ischemia can happen (58)(59).

The neuro-interventionalist can solve an unintended coverage of an arterial branch by manipulating or changing the FD. Both cases are undesirable, as they increase the surgical time and the associated thrombogenic risk.

5.9 Partial coverage of the aneurysm neck

An FD that is too short might fail to cover the aneurysm neck, compromising the treatment outcome. Unexpected proximal end shortening or distal end migration might be the cause of a FD that is too short (52), and an FD with an undersized diameter seems to facilitate this situation. The neuro-interventionist can solve this problem changing the FD or using a second FD in a telescopic configuration. However, either solution increases the surgical intervention time and may induce a thrombogenic event.

5.10 Aberrant FD size

The Sim&Size^{TM} simulation aims to decrease the chances of deploying an FD with a non-optimal size. However, the Sim&Size^{TM} simulation software might recommend an FD that is too short or too long. Nevertheless, an improper FD size can also happen when the FD system is unstable, increasing the chance of distal end shortening. Either way, the neuro-interventionalist must change the FD to complete the intervention (Figure 13).
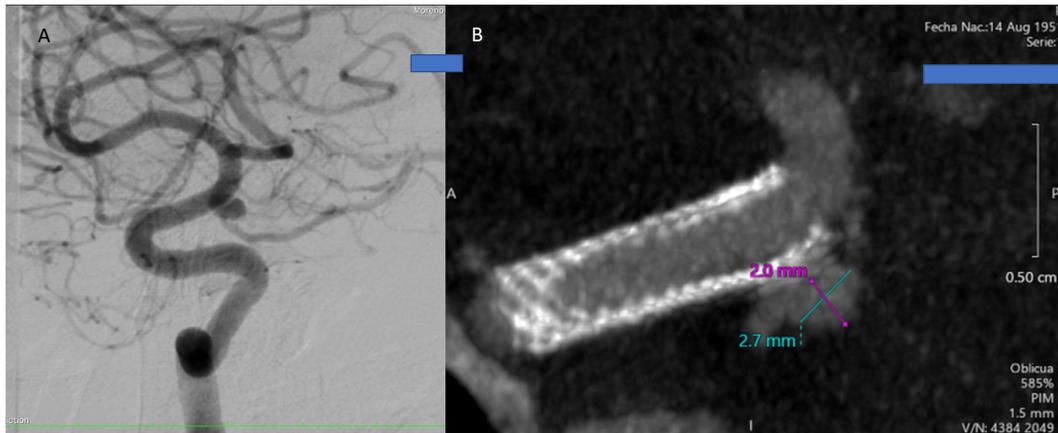
Limit distal possition of a FDs. Close to the neck of
the aneurysm.
A: DSA
B: Low Contrast CT

Figure 13. Representative images of an FD deployment with a limited distal position at the aneurysm neck. A) Angiographic image showing the parent artery. B) Low Contrast CT showing the poor aneurysm neck coverage.

5.11 Acute thrombosis

Acute arterial thrombosis is a complication secondary to a thrombogenic phenomenon. Wrong FD-vessel wall apposition, long surgical interventions, or unintended arterial branch coverages lead to this complication. We clarify that we are referring to a partial and not complete arterial branch occlusion, considering that the FD is a mesh that allows the passage of a slow blood flow. Therefore, the unintended arterial branch coverage does not increase the short-term risk of acute thrombosis. In the short term, the blood continues passing through the FD mesh until the new endothelial tissue obstructs the FD. However, the unintended arterial branch coverage increases the thrombogenic risk at the entry point of the compromised arterial branch. Thrombosis at this point is dangerous as it can cause ischemia. Several studies have addressed the unintended coverage of arterial branches showing satisfactory outcomes in most cases (58). The basilar artery is the exception showing an increased risk when unintendedly covered (60).

The neuro-interventionist always tries to prevent arterial branch coverage. However, the unintended cover occurs now and then. The risk of a bad outcome is low under this scenario and does not associate with the Sim&Size™ simulation software. However, using the software can lead to unintended arterial branch coverage in cases where the proximal landing zone is in the wrong position due to an incorrect simulation. In such cases, the Sim&Size™ simulation could increase the thrombogenic risk.

A meta-analysis evaluating 1152 supraclinoid carotid branches showed that the OphtA occlusion and associated symptoms rates were 5.9% (95 CI% = 3.1-8.6%) and 0.8% (95% CI = 0.1-1.4%), respectively. The PcomA showed a higher occlusion rate (20.7%, 95% CI = 8.9-32.4%) (incidence rate = 19.5% per patient-year), but all the cases were asymptomatic. AchorA was occluded in 1% (95% CI = 0.3-2.4%) of cases, with nearly 1% (95% CI = 0.4-2.3%) of transient neurological symptoms (incidence rate = 0.96% per patient-year). Arteries arising from the aneurysm showed a higher odds of arterial patency at a 94% confidence level (OR = 2.94, p-value = 0.06). Demographic factors and multiple stents were not associated with a higher risk of arterial impairment, and 94.5% of patients with arterial occlusion showed adequate collateral circulation (58).

Symptomatic occlusion of the supraclinoid carotid branches due to the shortening of an adequately placed FD is rare. Therefore, the Sim&Size™ simulation software represents an advantage for treating these arteries.

5.12 Damages resulting from deploying an FD with a non-optimal size

Intimal hyperplasia, decreased treatment effectiveness, longer surgical intervention time, and increased thrombogenic risk are potential damages of deploying an FD with a non-optimal size. Here, we discuss these possible damages.

5.12.1 Intimal hyperplasia

An FD in the artery causes increased endothelial tissue development compared to routine wound healing. This phenomenon development is known as intimal hyperplasia and is usually transitory and regressive, occurring in the first year following the FD implantation (58). However, intimal hyperplasia can continue, leading to a reduction of the arterial diameter and hemodynamic repercussions.

The intimal hyperplasia causes are not fully understood and are currently a research subject. However, undersized and oversized FDs might partially be responsible for this phenomenon. A wrong FD-vessel wall apposition resulting from a smaller than necessary FD may promote thrombosis in the space between the FD and vessel wall leading to endothelial tissue development at the FD contact site. On the other hand, a more extensive than necessary FD will induce excessive endothelial tissue development (Figure 14).

A: Initial treatment with coils and FDs.
B: 12 Months follow-up showing severe intimal hyperplasia of the stent.
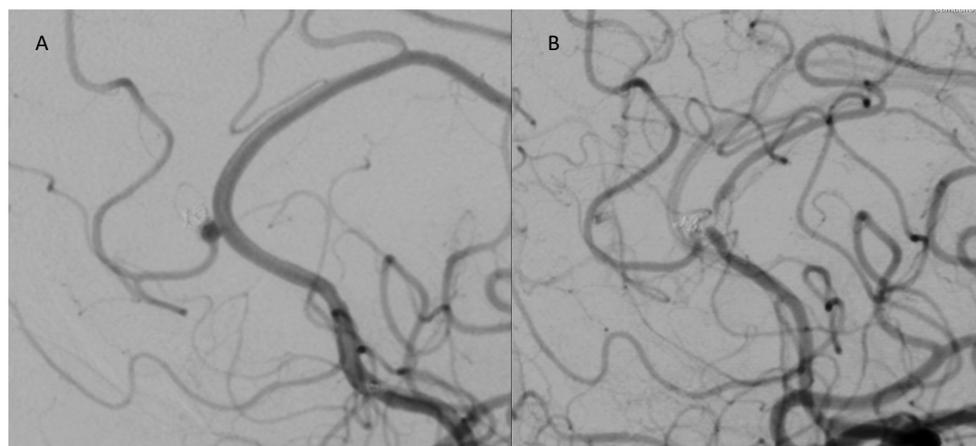
Case showing a patient with a pericallosal aneurysm treated with coils and Flow diverter stent.

Figure 14. Representative images of an FD deployment resulting in intimal hyperplasia. A) Angiographic image showing the aneurysm in the parent artery treated with coils and FD. B) Angiographic image showing the 12-month follow-up in which the several intimal hyperplasias of the FD is evidenced.

5.12.2 Decreased treatment effectiveness

FD promotes aneurysm healing by different means, including blood flow redirection. An FD placed next to the aneurysm neck will redirect the blood to the artery distality, reducing the intrasaccular blood flow. This flow reduction causes stasis within the sac and thrombosis. Another manner FD promotes aneurysm healing is through endothelialization. FD can support the endothelialization and neointimal tissue formation next to the neck of the aneurysm, which also reduces the intrasaccular blood flow (61). Predicting the treatment

effectiveness and possible causes for success or failure is difficult as biological factors specific to the patient and the antiplatelet medication administered to the patient influence treatment outcomes.

The literature reports high intracranial aneurysm occlusion rates. The PUFS study found that the percentage of aneurysms having no residual filling was 74 % after six months and 95 % after one year following the FD treatment (62). However, the five-year follow-up showed that some aneurysms were not wholly cured despite 95 % of patients having a complete occlusion. The study highlighted some important considerations about the long-term aneurysm occlusion: 1. An indeterminate latency period occurs between FD placement and aneurysms occlusion, 2. The placement of an additional FD increases the MSC and the aneurysms occlusion chance, and 3. Some aneurysms never occlude. Aneurysm persistence after treatment is generally considered a treatment failure. However, it is relevant to remember that the blood flow redirection confers protection against aneurysm rupture, even in cases where the aneurysm persists (63).

Placing a second FD in a telescopic configuration might improve the treatment effectiveness, especially in cases where the FD does not fully cover the aneurysm neck. This situation can arise when the FD position does not coincide with the one provided by the Sim&Size™ simulation. The downside of using a second FD is that it increases the metal exposure for patients.

An oversized FD can also reduce the treatment effectiveness. The wires of an FD with a large diameter will adapt to fit the parent artery geometry modifying the MSC and the mesh density at the aneurysm neck. This situation can result in ineffective treatment as the reconfiguration reduces the FD capacity to redirect the flow properly. Also, it reduces the support for endothelial and neointimal tissue formation at the aneurysm neck, compromising the aneurysm occlusion and the treatment outcome. Similarly, an FD with an undersized diameter will compromise the treatment effectiveness. However, under this scenario, the reduced treatment efficacy results from the faulty adhesion of the FD to the parent artery wall. The FD also fails to redirect the blood flow properly and does not provide enough support for endothelial and neointimal tissue formation.

5.12.3 Increased surgical intervention time and thrombogenic risk

Several situations increase the surgical intervention time, and we have explained those resulting from deploying an FD with a non-optimal size. Long surgical interventions are associated with increased risks for the patient. Also, long interventions are taxing for the neuro-interventionist, resulting in an increased risk of human failure. The neuro-interventionalist should make an effort to keep surgical interventions short, reducing the Patients' exposure to foreign bodies such as surgical instruments and the microcatheter as much as possible. Science these elements increase the thrombogenic risk for patients.

5.13 Overview chart of dangerous phenomena, dangerous situations, and damages resulting from deploying an FD with a non-optimal size

We generated an overview chart showing the association between the causes (dangerous phenomena), complications (dangerous situation), and consequences (damages) resulting from deploying an FD with a non-optimal size due to a wrong manipulation of the Sim&Size™ simulation software (Figure 15, Figure 16). Green arrows show hazardous situations that have an acceptable risk. These situations mainly result from deploying an FD with a mildly oversized or undersized diameter and might be missed as the resolution of the medical images is too low to show the anomalies. On the other hand, red arrows point to dangerous situations with too high risks. These situations are associated with FD that are too long, too short, or have a severely undersized diameter. They result in anomalies evident in the medical images, and the neuro-interventionalist must take action to mitigate their damage. Yellow arrows represent the alternative situations that arise from neuro-interventionalists acting to minimize the damage (Figure 15, Figure 16).

The Sim&Size™ simulation software aims to assist neuro-interventionalists during the FD selection and deployment. However, the neuro-interventionalist is responsible for selecting and deploying the FD. He must rely on his experience and good sense and consider each patient's specific conditions during these processes.
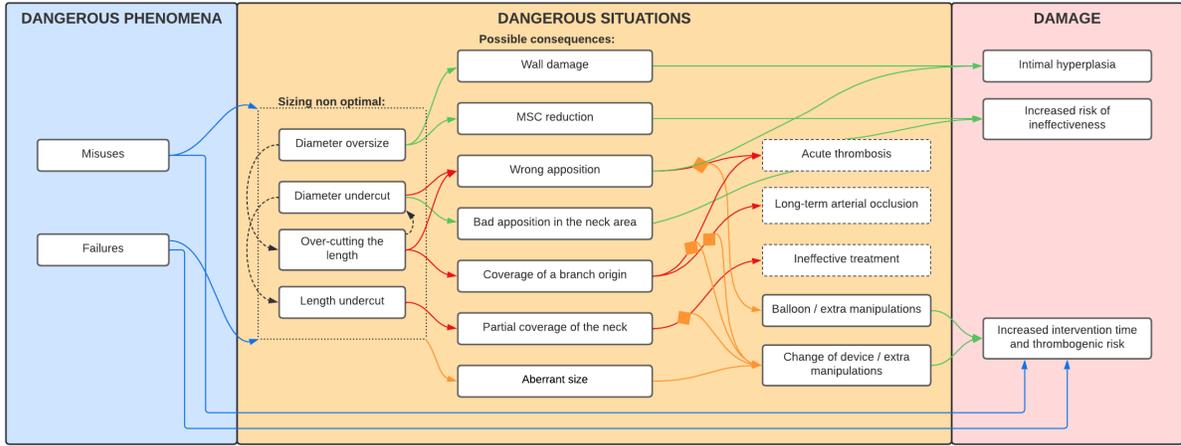
Figure 16. Non-optimal sizing of a FDs and its possible consequences.

Figure 15. Overview chart showing the association between the causes (dangerous phenomena), complications (dangerous situation), and potential damages (damages) resulting from deploying a non-optimal FD reference due to a wrong manipulation of the Sim&Size^{TM} simulation software
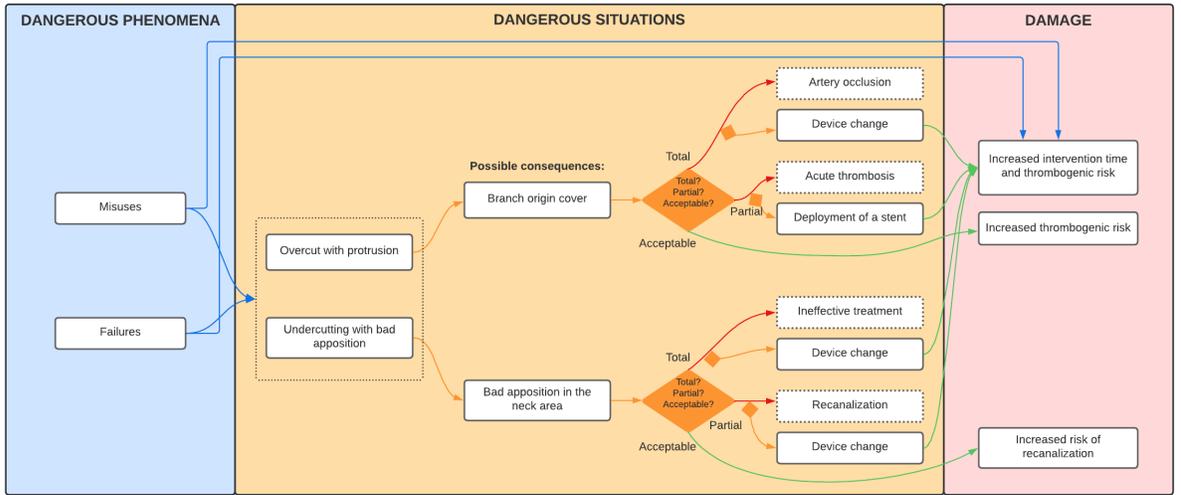
Figure 16. Non-optimal sizing of a FDs and its possible consequences.

Changes in device length and surgical times following the introduction of the Sim&Size™ simulation software in treating patients with intracranial aneurysms using pipeline embolization devices

Chapter contents

6.1 Introduction

Flow diverter stents are common endovascular treatment of sidewall intracranial aneurysms (50). Due to their low porosity and high pore density, FDs reduce the flow into the aneurysm sac, promoting intra-aneurysm thrombosis while keeping the adjacent arterial perforators unblocked. Endothelization occurs on the stent's inner surface within months, forming a new blood flow conduit that bypasses the obliterated aneurysm(64).

Defining a proper FD position during deployment is challenging. Manufacturers provide tables, including cylindrical deployment details. However, this information is often insufficient as it does not consider the vessel's shape and diameter variability of patients(65). Preliminary evaluations addressing this issue have shown that virtual simulation software can help during braided stents' positioning (65). The Sim&Size™ simulation software is an example of such simulation software. This software has been available in our service since 2017 in our clinical practice, and neuro-interventionalists have used it to select the best FD considering patients' vascular anatomy. For instance, we have used it during the treatment of intracranial aneurysms with FD (Pipeline Embolization Devices (PED)) to determine the best device's diameter and length for each patient. However, we ignore whether the Sim&Size™ simulation software has improved the PED selection as expected. This chapter aimed to compare the PED lengths and surgical times before and after introducing the Sim&Size™ simulation software into our daily practice.

6.2 Objective

To assess the change in stent lengths and surgical time caused by the introduction of the Sim&Size™ simulation software into the treatment of patients with intracranial aneurysms using Pipeline Embolization Devices.

6.3 Materials and methods

6.3.1 Study cohort and DICOM images acquisition

These retrospective monocentric evaluations used the data of 196 patients treated with PED for intracranial aneurysms between July 2015 and January 2017. During 2015 any case was performed without simulation software, during 2016 some cases were done using the

software and during 2017 all cases were done using the simulation software. The data was extracted from a neuroradiology service database, following ethics committee approval and patients' written informed consent. The treatment of 59 patients included the Sim&Size^{TM} simulation, as these patients entered our service after the software arrival and certification (2017). The surgical time was taken from the first injection to make the 3D-DSA until the last angiography series of the surgery. For the length of the stent, the length reported by the manufacturer of the device used was taken into account. Finally, we compared the differences in PED length and surgical time between these patients and those treated before the Sim&Size^{TM} simulation software arrival using R Core Team (2022). R: A language and environment for statistical computing. R Foundation for Statistical Computing, Vienna, Austria. URL https://www.R-project.org/.

6.3.2 Sim&Size^{TM} simulation software and Sim&Size^{TM} simulation software workflow

The Sim&Size^{TM} simulation software and the simulation software workflow were described in chapter 2, in the corresponding sections.

6.4 Results

We treated 197 patients with intracranial aneurysms using PED between 2015 and 2017. The mean age was 57 years for these patients, and most (86 %) were females. We simulated the PED deployment using the Sim&Size^{TM} simulation software during the treatment of 59 of these patients.

6.4.1 Changes in Pipeline Embolization Devices lengths

The PED lengths changed between years (Figure 17). Whereas most devices were between 16 mm and 20 mm long in 2015 and 2016, they were between 12 mm and 14 mm long in 2017. PEDs were 33 % shorter on average following the introduction of the Sim&Size^{TM} software into our clinical practice. A possible explanation for these length reductions is that the Sim&Size^{TM} simulation software allowed us to simulate the PED- parent artery wall apposition and predict the PED proximal ending. The software also allowed us to project the PED end into a straight vessel segment. The additional information provided by the software

encouraged us to select shorter stents without compromising the porosity at the aneurysm neck.
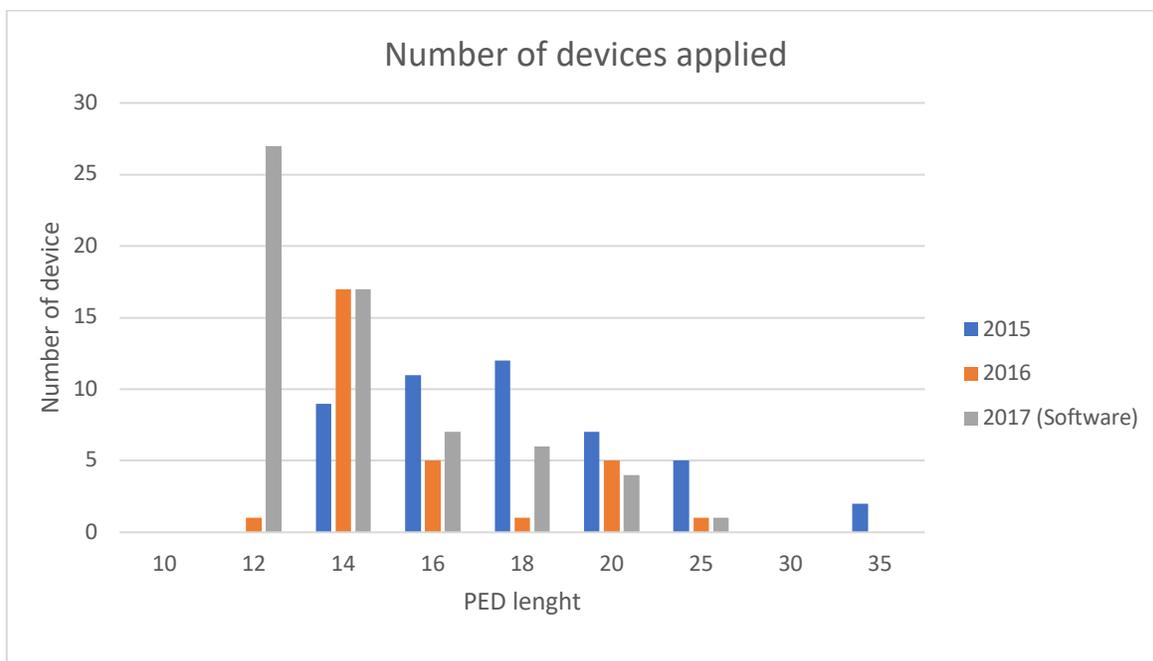
Figure 17. Length distribution for the Pipeline Embolization Devices used for treating patients with intracranial aneurysms between 2015 and 2017. Only the treatments in 2017 used the Sim&Size^TM software.

6.4.2 Changes in surgical time

The surgical interventions lasted one hour and 12 minutes on average in 2015. These interventions were longer than those performed after the Sim&Size^TM simulation software introduction into our service (2017). These interventions lasted 58 minutes on average, showing a reduction of 19.4 % (14 minutes) in surgical time following the software acquisition. The Sim&Size^TM simulation software might not fully explain the drop in surgical time; other factors might also be responsible. For instance, using coils in surgical interventions seems to have also impacted the surgical times.

PED and coils were used in 21 % of patients in 2015 compared with 18 % in 2017. Most interventions using PED and coils lasted between 50 min and two hours and 30 minutes, while those using only PED lasted between 25 min and one hour and 40 minutes regardless

of the year (Figure 18). Therefore, we decided to analyze the changes in surgical times for interventions using PED and coils apart from those using only PED. Interventions using the Sim&Size™ software had shorter surgical times regardless of coils (Figure 19). However, the reduction was more pronounced (28 % surgical time reductions) (Figure 19 A) for interventions using PED and coils compared with those using only PED (13 % surgical time reductions) (Figure 19 B). These results suggest that the software can reduce the surgical time by close to 34 minutes for interventions using PED and coils (Figure 19 A).

Histogram of intervention time
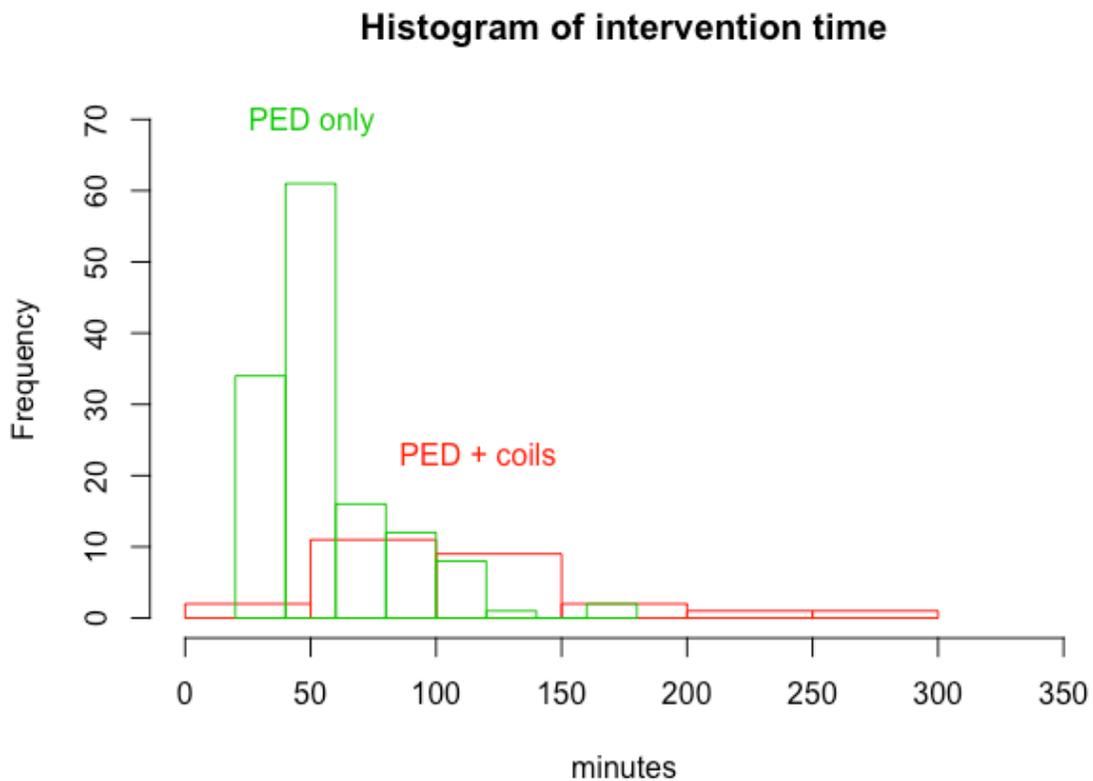
Figure 18. Surgical time distribution for patients treated for intracranial aneurysms using Pipeline Embolization Devices without and with coils between 2015 and 2017.
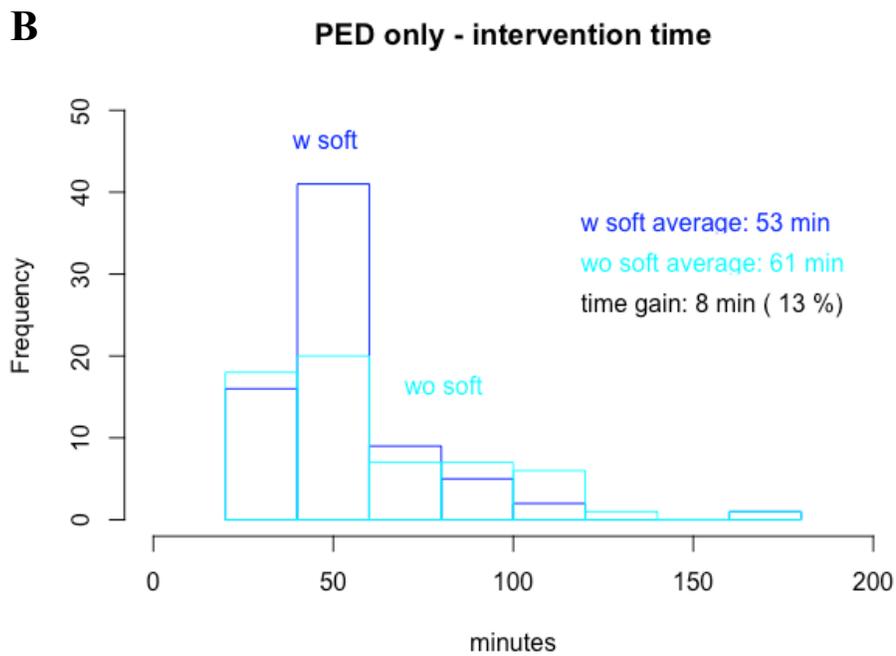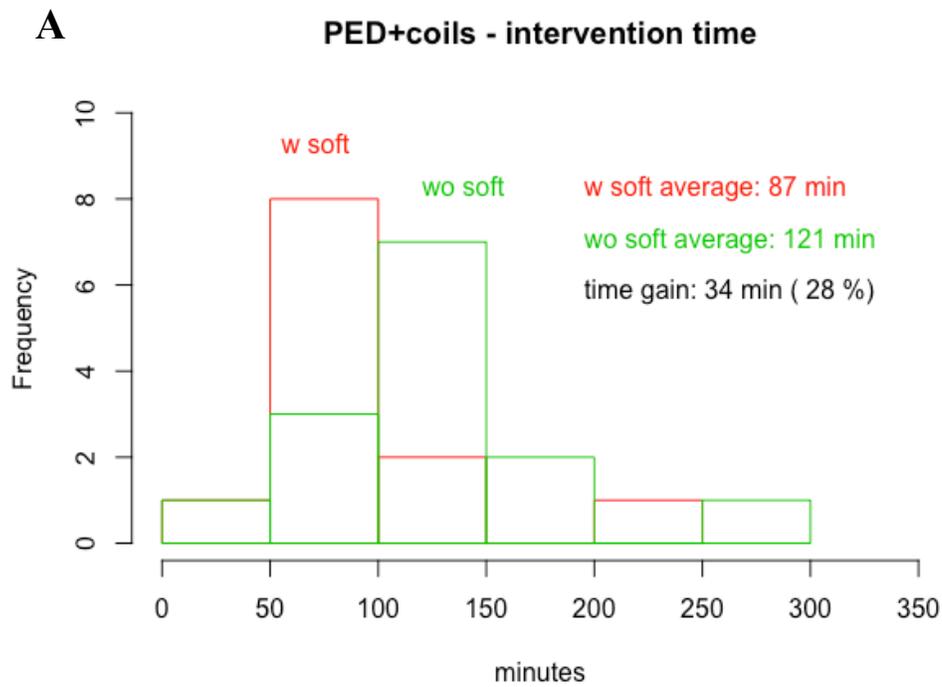
Figure 19. Effect of the Sim&Size^{TM} software on the surgical time distribution for patients treated for intracranial aneurysms using Pipeline Embolization Devices (PED) with (A) and without coils (B) between 2015 and 2017.

Another possible factor impacting surgical times is the aneurysm location. However, most of our intervention compromised the Internal carotid artery (ICA). Only a few cases were associated with the middle carotid artery (MCA) and Anterior Communicating Artery (AComA) (Figure 20). Therefore, we decided to exclude the effect of the aneurysm location on surgical time from our analyses.

The benefit of introducing the Sim&Size™ simulation software into our clinical practice seems evident in terms of surgical time. However, this benefit is secondary to using the software to facilitate PED size selection. The PED size looks to achieve a proper PED-vessel wall apposition and ideally has a proximal ending in a straight artery segment, which reduces the risk of needing a second PED.
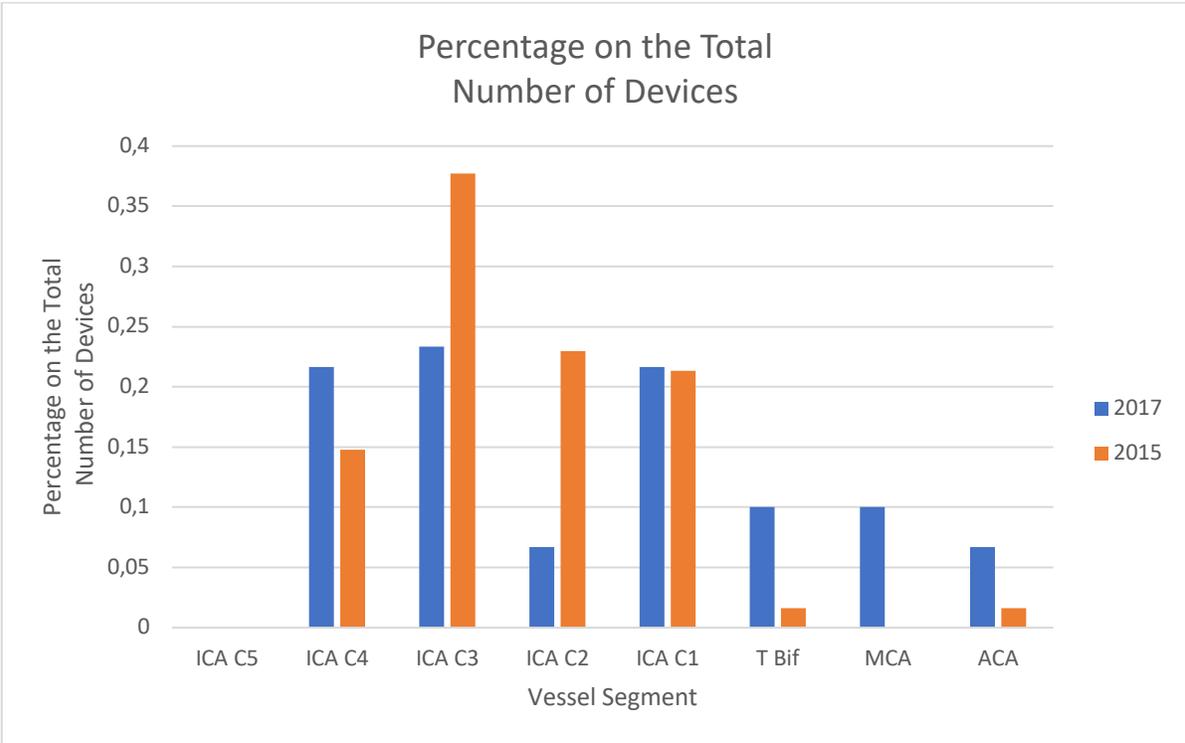
Figure 20. The frequency of the arterial segment compromised in patients with intracranial aneurysms treated using Pipeline Embolization Devices between 2015 and 2017. ICA represents the Internal carotid artery, T Bif, MCA the middle carotid artery and AComA the Anterior Communicating Artery.

6.5 Discussion

FD emerged as an option for treating complex intracranial aneurysms, including wide-necked or fusiform aneurysms, and this complexity comes with several challenges (64). FD size selection is among these challenges as the FD must cover the aneurysm neck. By covering the aneurysm neck, the FD alters the hemodynamics and induces thrombosis within the sac, stopping its growth, preventing its rupture, and likely leading to its complete resorption (66). However, functional arterial branches such as the ophthalmic artery and anterior choroidal must also remain uncovered, as covering them can result in complications for the patient (58).

Virtual simulation software is becoming popular in some medical centers as they allow to overcome challenges associated with FD size selection (65). However, FDs are difficult to simulate due to their dense and fine strut networks (67). Despite this complexity, we showed that using the Sim&Size™ simulation software for selecting PED lengths and diameters can facilitate a proper PED-vessel wall apposition. In theory, this good apposition would result in an increased FD embolization.

Densely packed FD filaments across the aneurysm orifice are desired for minimizing the inflow and keeping perforators open in parent vessels (68). However, our results showed that reducing FD porosity might be secondary to a good FD size selection. We found that shorter PEDs with optimized diameters and proximal endings in a straight artery segment did not compromise the aneurysm's neck coverage. These shorter PEDs still permitted a good PED-vessel wall apposition and did not increase the risk of embolic complications. Foreshortening can affect the FD positioning after its release from the microcatheter. Therefore, achieving the desired FD position or predicting the final position is challenging. Pushing forces are fundamental for predicting the maximal FD shortening in large aneurysm necks, as they influence the FD shortening during deployment. The Sim&Size™ simulation software accounts for the effect of the pushing forces in the FD simulation (Figure 21).

The introduction of the Sim&Size™ simulation software into our medical practice coincided with decreased surgical times. These observations suggest that using the software can reduce the time required for surgical interventions. These time reductions are relevant as shorter surgical times in neurointerventional procedures have been associated with fewer complications and reduced patient exposure to radiation . Time reductions were more

pronounced in interventions using PED and coils, which is relevant as these interventions were also the longest ones. Our findings of interventions using FD and coils having longer surgical times than those using only FD are not novel. They are in line with the intrePED study, which compared surgical times of interventions using PED with and without coils and found that those using coils were longer (135.8 ± 63.9 min vs. 96.7 ± 46.2 min; $P < 0.0001$). These surgical procedures also resulted in higher neurological morbidity (12.5% vs. 7.8%; $P = .13$) (43).
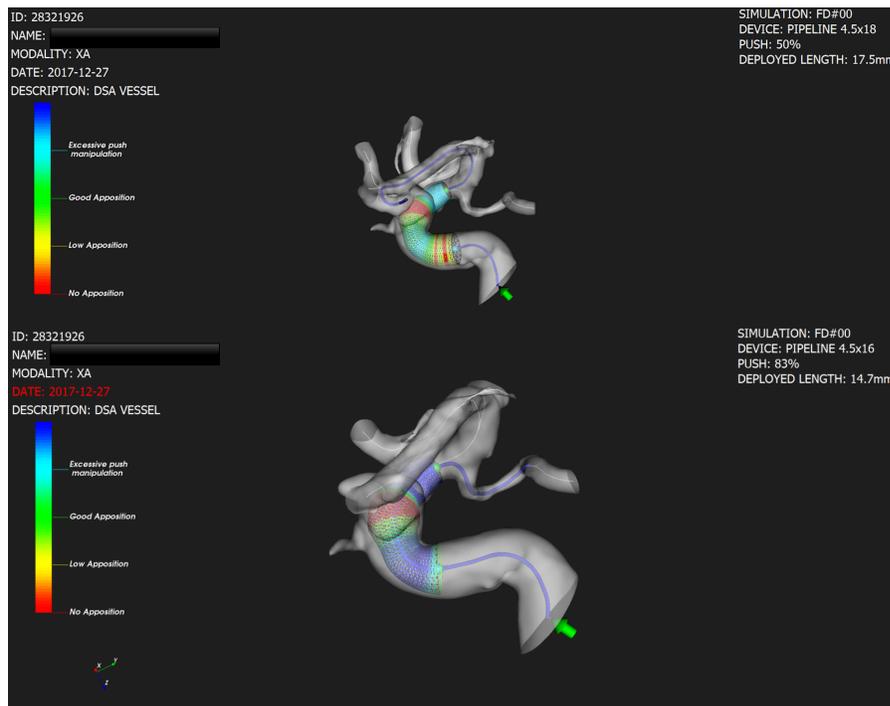
Figure 21: Sim&Size^{TM} simulation showing the effect of pushing forces and flow diverter stent (FD) geometry on the FD-vessel wall apposition. The upper panel shows the simulation of a 4.5x18 mm FD with 50% pushing forces (the real length in this anatomy is 17.5 mm). The lower panel shows the simulation of a 4.5x16 mm FD with 83 % pushing forces (the real length in this anatomy is 14.7 mm). The colors represent the extent of the-vessel wall apposition

6.6 Conclusion

Surgical interventions using the Sim&Size^{TM} simulation software for treating intracranial aneurysms with PED reduced device lengths and surgical times. The reductions in surgical times were more pronounced in interventions using PED and coils. Therefore, we believe that introducing the Sim&Size^{TM} simulation software into our service has optimized the treatment of patients with intracranial aneurysms.

Chapter

7.

Evaluation of the correlation between occlusion rates and surface metal coverage at the aneurysm neck of flow diverter stents used in the treatment of patients with intracranial aneurysms

Chapter contents

7.1 Introduction

The ultimate goal of the treatment for intracranial aneurysms is to reconstruct the vessel wall and correct the hemodynamic disturbance. A Flow Diverter Stent (FD) is a device placed in the parent artery to reduce blood flow into the aneurysm sac and promote stagnation, gradual thrombosis, and neointimal remodeling. It aims to limit the blood flow to the side branches and perforators (69).

Several factors, including parent vessel anatomy, aneurysm anatomy, and FD characteristics, influence the FD hemodynamic capacity, therefore, its efficacy (63). Among the FD characteristics, Pore Density (PD), Surface Metal Coverage (MSC), and the number of wires are relevant for determining the extent of blood flow diversion. A study proposed a new parameter, the Pressure Reduction Coefficient (PRC), to unify all the FD characteristics affecting the hemodynamic capacity. The authors suggested that the PRC was a consequence of the overall FD design as they found no correlation between PRC and individual parameters (i.e., PD, SMC, and the number of wires) (70).

Comparison between FD should consider at least one of the parameters influencing the FD hemodynamic capacity. Evaluations using mice with elastase-induced aneurysms as models showed that the FD porosity (related to MSC) and PD affected the treatment outcome. They found that FDs with a 70 % porosity and 18 pores/mm3 were better in occluding aneurysms after six months of the treatment than FDs with a 70 % porosity and 12 pores/mm3 or with a 65 % porosity and 14 pores/mm3 (71)(72). Similar evaluations assessing the effect of FD hemodynamic related factors on aneurysm occlusion rates in humans are impossible. An alternative for these evaluations is to use virtual simulation software.

Novel virtual simulation software is becoming available for simulating the treatment of intracranial aneurysms with FD. This software looks to increase the treatment efficacy and safety while reducing surgical intervention time and its associated risks (65). We believe that SMC at the aneurysm neck is relevant for selecting an FD as it likely affects the efficacy of the treatment. Therefore, this chapter aimed to use the Sim&Size^{TM} simulation software to evaluate the correlations between the MSC at the aneurysm neck and the occlusion rates.

7.2 Objective

To evaluate the correlation between occlusion rates and Surface Metal Coverage at the aneurysm neck of Flow Diverter Stents used in the treatment of patients with intracranial aneurysms using the Sim&Size™ simulation software.

7.3 Material and Methods

This retrospective evaluation included data from 62 patients treated for intracranial aneurysms with FD (Pipeline Embolisation Device (PED)) between July 2009 and January 2014. All therapeutic procedures involved a senior interventional neuroradiologist with experience in stent-placement techniques. Patients' data came from the database of two neuroradiology services, the FOSCAL clinic in Bucaramanga, Colombia, and the CHU Gui de Chauliac Hospital in Montpellier, France. The ethics committees' approval and patients' written informed consent were obtained before the evaluations. The data included the 3D digital subtraction angiography (DSA) images we used for the Sim&Size™ simulation. We used the PED sizes and distal and proximal landing zones used during the treatments to simulate the same device, using the Sim&Size™ simulation software workflow specified before (Chapter 2).

We visually delimited the aneurysm neck in the 3D reconstructions of the Sim&Size™ simulations and used the color scale showing the extent of FD-vessel wall apposition to estimate the MSC at this region (Figure 22, Figure 23). These estimations involved two neuro-interventionalists, one carrying the aneurysm neck delimitation and the other the MSC estimation, to increase the estimations' objectivity. We validate the MSC estimations with low contrast CT acquired after patients' treatment. Cristophe Chnafa et al. measured the PED porosity and MSC using Expert CT and compared the results with those estimated with the Sim&Size™ simulation software. We found a good concordance between the two methods (publication on work).

We defined a continuous numerical scale ranging from 1 to 4 for assessing the occlusion grade, with 1 being partial occlusion and 4 complete-occlusion. We used this scale for estimating from the patients' 3D-DSA the status of aneurysm occlusion for the first (6 months) and last follow-ups (12 months) or the follow-up registering complete aneurysm

occlusion. The 12 and 24-month follow-ups were extrapolated using the last follow-up when necessary. We used the MSC estimates to calculate the occlusion rate for each patient using the eq 1.
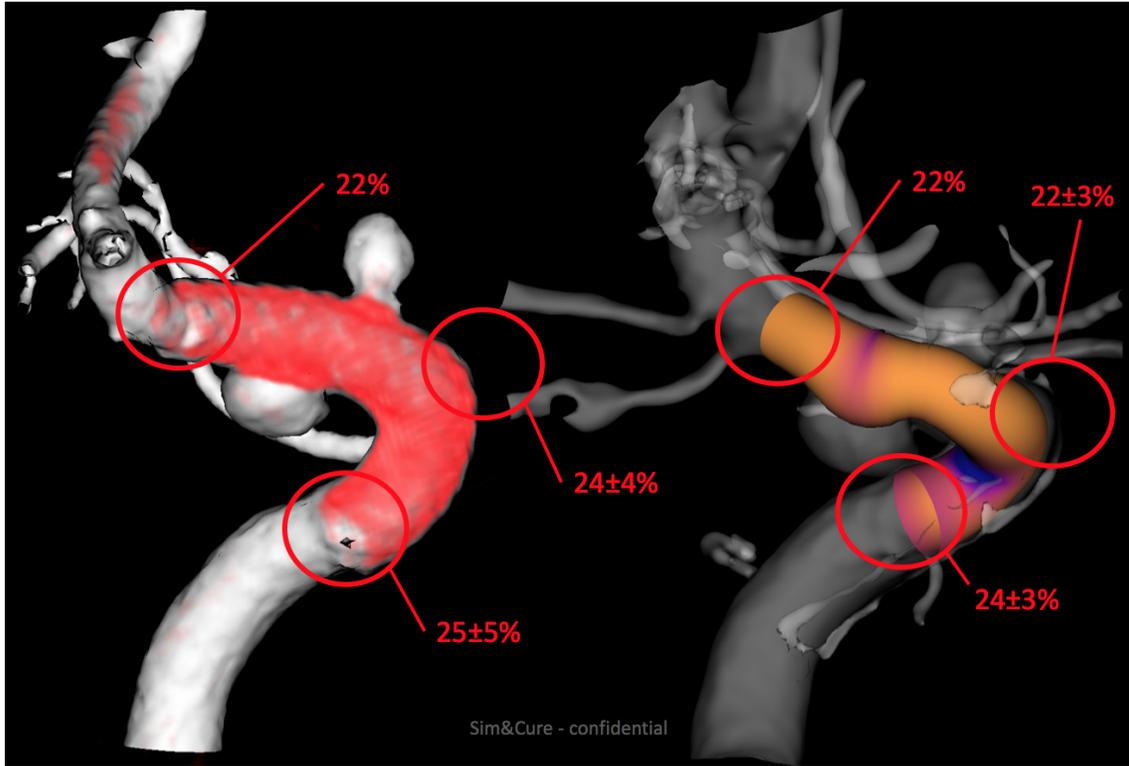
Figure 22
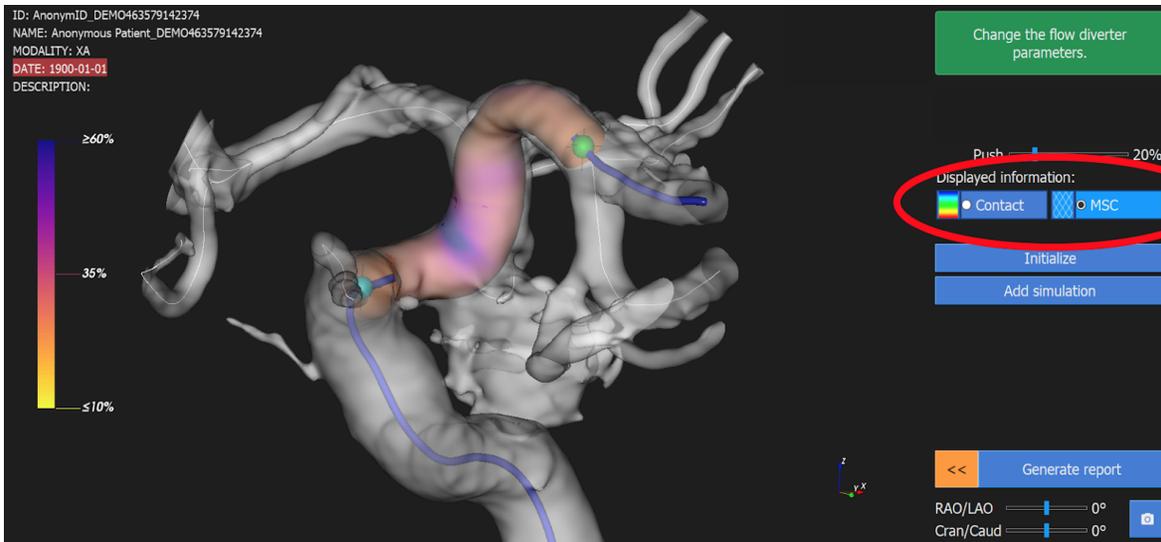
Figure 23

We used the Spearman correlation to evaluated the correlation's strength between occlusion rate and the MSC at the aneurysm neck, the length of the largest aneurysm diameter, the dome/neck ratio, the aneurysm neck diameter, and the patients' age and gender in R Core Team (2022). R: A language and environment for statistical computing. R Foundation for Statistical Computing, Vienna, Austria. URL https://www.R-project.org/.

7.4 Results

We analyzed the 3D-DSA of 62 patients treated for intracranial aneurysms with PED in two neuroradiology centers for these evaluations. Most patients (75.8 %) were female and had a mean age of 57.69 years (SD 13.11). 15.5% of patients were smokers, and 26.7% had hypertension. Regarding the aneurysm characteristics, the average transverse diameter was 3.99 mm (SD 0.81), the mean diameter/neck ratio was 1.56 (SD 0.60), and the mean aneurysm's neck diameter was 5.04mm (SD 2.29).

The mean MSC at the aneurysm neck was 24.0% (SD 11%) according to our estimations, with the highest MSC being 60.0 % and the lowest 15.0 %. Half of the patients had MSC at the aneurysm neck below 17.0 % (Figure 24). We found no correlation between the occlusion rates and the MSC (p-value = 0.122) (Figure 25, Table 5) or any of the other factors evaluated

(i.e., length of the largest aneurysm diameter, the dome/neck ratio, and the aneurysm neck diameter) (p-value > 0.05) according to the Spearman correlation (Table 5). We also found no association between the occlusion rates and the patients' age or gender (p-value > 0.05) (Table 5).

Variable	Coefficient	P
age(years)	-0,0002985	0,912
Sex (male)	-0,0253309	0,756
Average size aneurysm	0,0053115	0,462
diamaterneck	0,0019067	0,974
Neck aneurysm	0,0082744	0,59
Diameter	-0,0352588	0,415
MSC average	0,0530347	0,868

Table 5: Spearman's rank correlation coefficients showing the streinght of the correlation between Occlusion rates and the patients, aneurysm, and Pipeline Embolization Devices characteristics
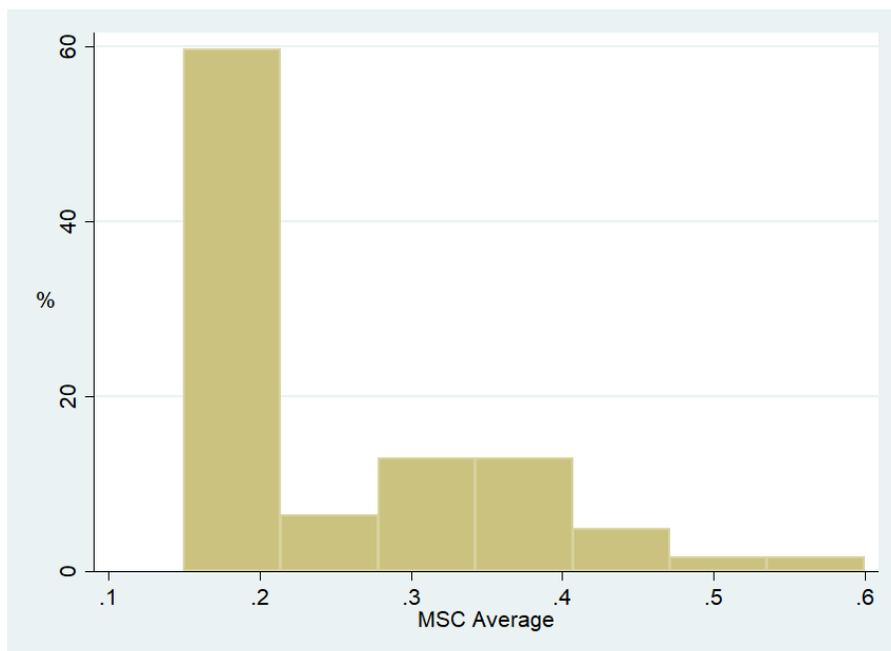
Figure 24: The distribution of the Surface Metal Coverage at the aneurism neck for the Pipeline Embolization Devices used for treating patients with intracranial aneurysms
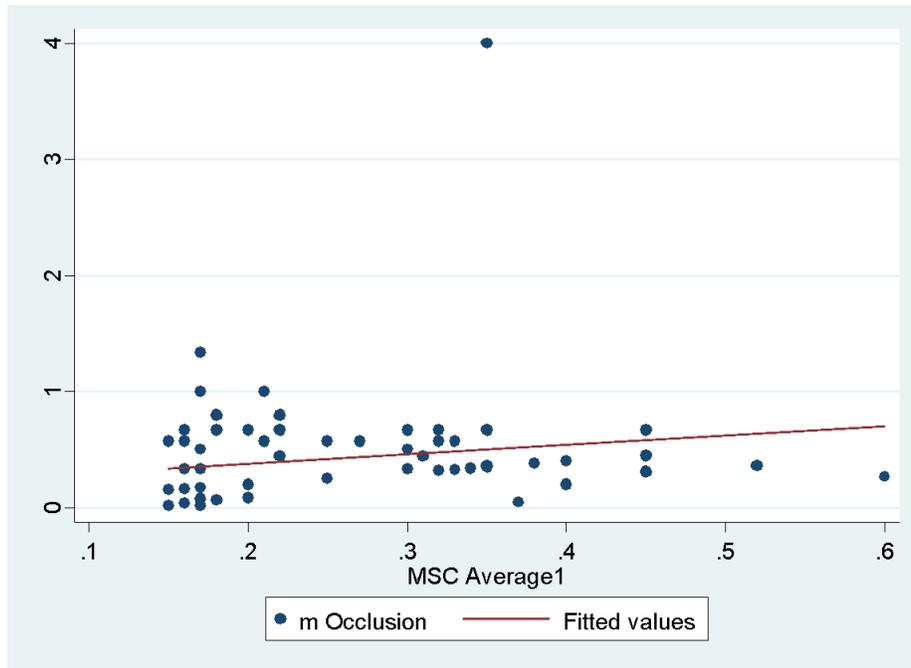
Figure 25: Correlation between aneurysm occlusion rates and the Surface Metal Coverage at the aneurysm neck of Pipeline Embolization Devices used for treating patients with intracranial aneurysms

7.5 Discussion

The intracranial aneurysm treatment aims to reconstruct the vessel wall and correct the hemodynamic disturbance, which can be accomplice by placing an FD in the parent artery (69). The MSC at the aneurysm neck accomplished by the FD may influence these changes. Previous evaluations using mice with elastase-induced aneurysms showed that the FD porosity and PD affected the occlusion rates (71)(72), and PD inversely correlates with MSC. MSC and PD values are difficult to predict or estimate in vivo due to vessel diameter modifications and pushing forces during deployment. Deploying an FD with a non-optimal size may lead to substantial heterogeneity in MSC and PD as the FD transitions between constrained to unconstrained states, even under the circumstances of modest oversizing. Still, the deployment technique might help to mitigate some of these heterogeneity resulting from a poor FD size selection.

We do not fully understood the clinical repercussions of deploying a poorly sized FD in terms of Intra-aneurysmal flow-dynamics modifications that may reduce the treatment efficacy.

However, several reports are available for sporadic events of delayed mass effect and aneurysm rupture following the treatment of large aneurysms with FD. These adverse events show the need for understanding how deploying a poorly sized FD influences the hemodynamic conditions in the aneurysm (57)(73). In vivo evaluations for assessing the factors affecting MSC or PD in humans are not feasible. Hence, virtual simulation software such as the Sim&Size^{TM} software becomes a compelling alternative for these evaluations. We demonstrated that the Sim&Size^{TM} simulation software is useful for estimating the MSC at the aneurysm neck. These estimations are reayble as they considered the patient's anatomy, FD mechanical features, and deployment pushing forces.

We found no clear link between the MSC at the aneurysm neck and the aneurysm occlusion rate for our patients, suggesting that an elevated MSC does not necessarily imply a higher probability of aneurysm occlusion. Therefore, increasing the MSC to decrease the blood flow into the aneurysm and favor the endothelialization process might be unnecessary as low MSC can result in reasonable occlusion rates. However, we must declare that we evidence heterogeneous MSC at the aneurysm neck during our evaluation. The relevance of the MSC homogeneity at the aneurysm neck should not overlook. A homogeneous surface exerts higher hydraulic resistance forces than a heterogeneous surface, decreasing the crossing flow to a greater extent. This parameter might be as crucial as the mean MSC in defining the FD hemodynamic capacity. The heterogeneity observed during our evaluations might partly be responsible for the lack of correlation between MSC at the aneurysm neck and the aneurysm occlusion rate.

MSC, PD, and the number of wires are FD's characteristics that impact its capacity to divert blood flow. Therefore, using a single parameter to compare FD is not recommended. The proposers of the Pressure Reduction Coefficient (PRC) thought that this parameter could be used as an alternative that unifies all the FD characteristics affecting its hemodynamic capacity. However, the utility of this parameter is questionable as it does not correlate with the MSC or PD of the FD (70), and no methods are currently available for its estimation in clinical practice. The possibility of estimating the MSC with the Sim&Size^{TM} simulation software is advantageous and should not be underestimated. Neuro-interventionalists can modify the FD sizes and assess in situ the effect of these changes on the MSC.

Our evaluation did not assess the effect of the number of wires on the aneurysm occlusion rates, as we kept constant the number of wires. One study using rabbits to compare two FDs, one with 48 wires and one with 72 wires, showed that the 72-wires FD presented a time-dependent endothelial cell growth over its surface while the 48-wires FD did not. This endothelial cell growth resulted in a complete or near-complete occlusion when the aneurysm neck diameter was below 4.2 mm (61). Our evaluations also did not assessed the effect of smoking or history of hypertension. Despite the literature showing that these risk factors can influence the MSC and the aneurysm occlusion rates by interfering with the thrombotic process and affecting the flow dynamics inside the aneurysms. Further evaluations assessing the effect of these parameters might be beneficial.

To increase the treatment efficacy and safety is the goal of virtual simulation software currently developed for the treatment of intracranial aneurysm with FD (65). However, this software can also be used to evaluate how several FD characteristics, including MSC at the aneurysm neck, influence the capacity of the device to correct hemodynamic disturbances. We recommend using this software to understand better how the FD adapts to the patient's arteries and how the patient's artery geometry and FD characteristics might affect the MSC at the aneurysm neck. We also recommend testing the hypothesis that a threshold MSC at the aneurysm neck may be sufficient for achieving reasonable aneurysms occlusion rates.

7.6 Conclusion

We found no correlation between the MSC at the aneurysm neck and the aneurysm occlusion rate, for MSC between 15 % and 60%. However, we recommend further assessing this correlation using a larger sample size. We also recommend testing whether an MSC at the aneurysm neck threshold exists that must be achieved to accomplish reasonable aneurysms occlusion rates.

Clinical impact of Sim&Size™ simulation software in the treatment of patients with intracranial aneurysms using pipeline embolization devices

Chapter contents

8.1 Introduction

The prevalence of intracranial aneurysms varies between 0.5 % and 7.0 %, depending on the population. This condition is associated with several risk factors, including smoking, high blood pressure, a family history of a cerebral aneurysm, and genetic alterations such as autosomal dominant polycystic kidney disease. Multiple endocrine neoplasia type I, hereditary hemorrhagic telangiectasia, Ehlers-Danlos syndrome, Marfan syndrome, and neurofibromatosis type I also seem to increase the risk of unruptured cerebral aneurysms but to a lesser extent. Women and older persons also appear more vulnerable to this condition (74)(6).

Open surgery can prevent the rupture of intracranial aneurysms, and neuro-interventionalist use it in patients with large or giant aneurysms in the middle cerebral artery. A less restrictive treatment alternative is endovascular therapy (75)(76). This therapy involves various techniques, including embolization with coils, balloon-assisted coils, stent-assisted coils, and Flow Diverter Stents (FD). Out of these techniques, FD reconstruction of the parent artery appears effective and safe (34)(36). Among FD, Pipeline Embolization Devices (PEDs) stimulate endothelial growth and disrupt the aneurysm's blood flow, causing thrombosis. PEDs are mainly used for aneurysms with complex morphology or in cases where other alternatives are unavailable. The implementation of FD as an endovascular technique is relatively recent. The FDA approved PED for treating giant, wide-necked aneurysms located between the petrous segment and the pituitary of the internal carotid artery in 2011 (75)(77).

Proper stent size is essential for treatment safety. Long stents make difficult stent implantation, increasing the stroke risk. On the other hand, short stents may fail to cover the aneurysm neck. Stents with small diameters complicate unfolding due to lack of anchorage and might result in incomplete aneurysm coverage (78). Stent malposition is associated with increased device migration risk, delayed aneurysm rupture, and stroke (79). Selecting the proper stent size is challenging due to the tortuous and irregular nature of cerebral arteries. Neuro-interventionalists can select the stent size manually, using 3D digital subtraction angiography (3D-DSA). Alternatively, they can use virtual simulation software developed

for this purpose. Among this software, the Sim&Size™ simulation software (Sim&Cure, Grabels, France) simulates PED (Medtronic) behavior considering the patient's vessel.

Several centers have successfully used the Sim&Size™ simulation software for treating intracranial aneurysms. This software provides confidence to neuro-interventionalists when choosing the FD size by simulating patients' anatomy. Simulation software such as the Sim&Size™ is expected to increase the stent size accuracy and reduce complications. This retrospective evaluation assessed the clinical impact of the Sim&Size™ simulation software on the endovascular treatment of unruptured saccular intracranial aneurysms with PED. Precisely, it determined the effect of the software on stent size, surgical time, number of stents used, and whether using the simulation software associated with fewer complications.

8.2 Methodology

This study is a retrospective analytical evaluation of patients treated with PED (Flex and Flex with SHIELD) for unruptured intracerebral aneurysms consisting of two parts. The first part is a monocentric evaluation including patients treated in Bucaramanga, Colombia, between June 1, 2014, and December 31, 2019, in the FOSCAL clinic. This evaluation was approved by the institution's medical ethics committee (FOSCAL clinic), but informed consent was waived as the study's observational nature generated minimal risk to participants. The Sim&Size™ simulation software was used for all patients joining the center after the software acquisition in December 2017. Patients entering before this date were not simulated.

The second part of this study is a multicentric evaluation including the aforementioned Colombian patients and patients treated in Montpellier, France, between January 1, 2015, and December 31, 2017, in the CHU Gui de Chauliac Hospital. Both evaluations excluded patients with ruptured intracranial aneurysms and morphologies other than saccular.

The study evaluated changes in the stent dimensions, surgical time, number of stents used, and complications following the introduction of the Sim&Size™ simulation software into clinical practice. The data came from patients' medical records and included demographic information and comorbidities (age, sex, history of chronic arterial hypertension, history of smoking, and aneurysm in the family). The variables evaluated were aneurysm morphology,

size and location, previous treatment of the aneurysm, the diameter and length of the stent, and the number of stents used. They also included surgical and follow-up times, intraoperative complications, aneurysms occlusion rates, and 30-days and 12-month post-procedure outcomes. We defined surgical time as the time between puncture and the end of anesthesia. The complications considered were thromboembolic, hemorrhagic, and vascular access complications, sudden stent shortening, and the need to adjust the stent position due to suboptimal size. The 3D angiography provided the size, location, and number of aneurysms.

The center relied on four neuro-interventionalists for the patient's treatment, and each procedure involved at least two of them. Neuro-interventionalists had at least five years of experience in the endovascular treatment of intracranial aneurysms. Also, they had performed treatments with flow-diverter stents on at least ten occasions before the study evaluation period.

8.2.1 Stent deployment technique

All patients were started on acetylsalicylic acid (ASA) (100 mg per day) and clopidogrel (75 mg per day) 10 days prior to surgery. The antiplatelet response was assessed 48 h before the procedure whit the VerifyNow® test, considering an optimal value between 60 and 200 PRU. Patients with low responses (i.e., PRU > 200) received 180 mg of oral ticagrelor the day before the procedure and 90 mg every 12 hours for the following six months. Patients with high responses (i.e., PRU < 60) received 75 mg or 37.5 mg of oral clopidogrel every 48 hours or 72 hours. A second VerifyNow® test was performed in high-responder patients seven days following the procedure.

The Seldinger technique was used for the 3D-DSA by puncturing the femoral artery under Doppler ultrasound guidance with an 18G argon angiographic needle. The Destination 6Fr catheter was raised. Then, unfractionated heparin was subministrated at a dosage of 50 IU per kilogram. The activated coagulation time was measured, and the Navien 6Fr intermediate catheter was placed in the petrous segment of the internal carotid artery (ICA). Patients were under general anesthesia during the procedure, and all cases used Marksman™ microcatheter for PED stent implantation.

8.2.2 Stent manual sizing

Distal and proximal target landing zones were selected from a straight segment of the main vessel by the consensus of two neuro-interventionalists during the manual stent sizing to ensure a good wall apposition. 2D-DSA parent artery measurements at the proximal target landing zone were used to determine implant diameter. Then, the operators predicted possible areas of stent elongation, particularly proximal to the aneurysm, and possible foreshortening. These predictions were based on the length of the aneurysm neck and the operators' experience. The stent length was estimated considering the parent vessel centerline measured between the distal and proximal target landing zones using the 3D-DSA reconstruction of the Angio suite. All these measurements contributed to the choice of stent diameter and length.

8.2.3 Stent sizing with the simulation software

The commercially available, CE-marked, and FDA-approved Sim&Size™ simulation software (version 1.2) was used to determine the stent size and simulate the stent behavior according to the manufacturer's specification. This software reconstructs the 3D arterial geometry on a local computer using 3D-DSA acquisition data and predicts the movement of endovascular devices such as PED. The accuracy of the reconstruction can be optimized by the neuro-interventionalist when necessary. The software defines the microcatheter trajectory in the parent vessel and allows the neuro-interventionalist to set the distal and proximal landing zones, targeting straight-vessel segments. Then, it determines the optimal flow-device dimensions and simulates its deployment within the chosen landing zones. The software shows the degree of wall apposition in the interface, which appears as an interactive color scale along the stent. The effect of different landing zones and device dimensions on the device behavior can be evaluated using the Sim&Size™ simulation software. Also, the amount of 'push' applied during the deployment of the device can be estimated in real-time (Figure 26).
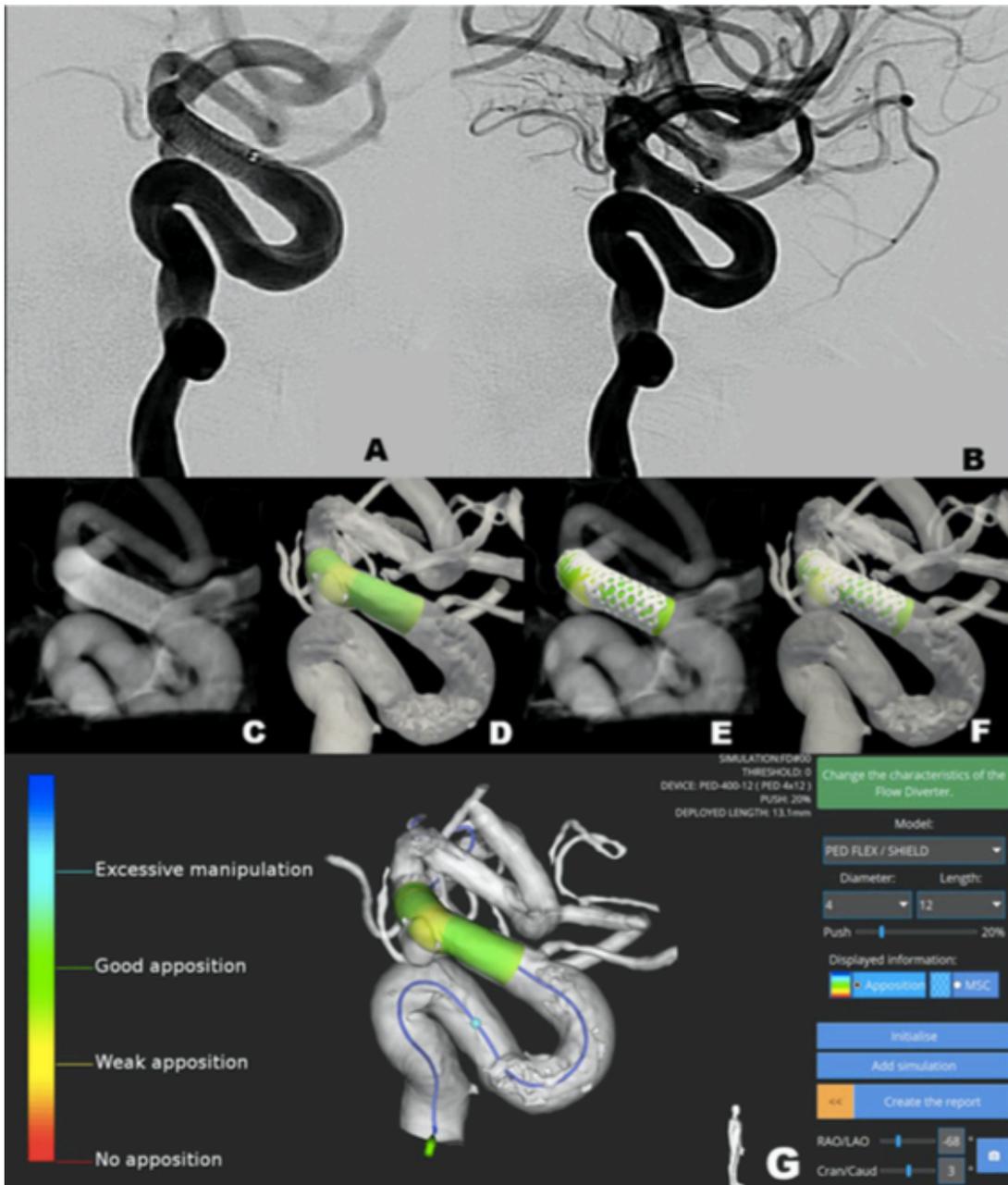
Figure 26: Representative images of a Sim&Size^TM simulation for a patient with an anterior choroidal aneurysm. A: Projection of the aneurysm after Pipeline Embolization Device (PED) deployment. B: Lateral projection of the aneurysm showing the PED proximal landing zone. C: Low contrast CTA showing the PED wall apposition and proximal landing zone. D: Sim&Size^TM simulation indicating the proximal endings of the PED, giving a good vessel wall apposition (Green). E and F: Simulated PED superposed on the Low Contrast CTA

8.2.4 Statistical analysis

Patients' demographic, clinical, and background characteristics were analyzed using descriptive statistics. The categorical variables were reported as counts and percentages, and continuous variables as median and interquartile ranges (IQR). The student t-test was used to evaluate differences between the two groups of patients (i.e., with Sim&Size^{TM} simulation and without simulation) for the continuous variables following normal probability distribution. The Mann-Whitney test was used for non-parametric continuous variables and Fisher's exact test for categorical variables. The normality of continuous variables was assessed using the Kolmogorov-Smirnov test.

A multivariate analysis was used to assess the simultaneous predicting capacity of variables to differentiate between the two groups of patients (i.e., with Sim&Size^{TM} simulation and without simulation). Specifically, A binary logistic regression was modeled using the binomial family. The model included variables showing differences between the two groups of patients in the bivariate analysis with a confidence level of at least 92% (p-value < 0.080). These variables were aneurysm size, number of stents used, hemorrhagic complications, stent length, and occlusion occurrence. We also included stent diameter and surgical time in the model, as we considered them essential predictors. Model simplification was performed with a stepwise model selection by AIC using the R package MASS (version 7.3–13) (80).

The effect of the aneurism localization-patient group interaction on stent diameter and diameter was evaluated using a two-way ANOVA and a generalized linear model with the Poisson family. This analysis only considered aneurysms localized in the ophthalmologic segment of the left ICA, the posterior communicating segment of the right ICA, the cavernous segment of the left ICA, and the left ICA, as both patient groups included patients with aneurysms in these sites. All the analyses used a confidence level of 95% and the R package Stats (version 4.0.4) unless otherwise stated, and the data was visualized using the R package Ggplot2 (version 3.3.3) (81).

8.3 Results

8.3.1 Results for the monocentric evaluation

For the monocentric evaluation, the cohort comprised 75 patients with cerebral aneurysms treated using PED between June 1, 2014, and December 31, 2019, in Bucaramanga, Colombia. Our evaluations excluded seven of these patients, as three had fusiform aneurysms, two had dissections, one had a blister-like aneurysm, and one had a ruptured aneurysm.

The number of interventions performed was 73 for the 68 remaining patients. In the interventions, 64 dealt with single aneurysms, seven with two aneurysms embolized in the same procedure, and two with three aneurysms treated simultaneously using the same device. Most patients required one intervention. Five patients were the exception requiring two interventions, with four having two aneurysms treated in separate interventions and one having the same aneurysm treated twice.

Most patients were women (86.3%), and the most prevalent comorbidities were high blood pressure (42.5%), followed by smoking (13.7%). The median age of patients was 64.00 (IQR 50.00–73.00). Table 6 summarizes the characteristics of the patients.

Population Characteristics	Univariate analysis (n=73)	Bivariate analysis		P-value
		Without Simulation (n=17)	With Simulation (n=56)	
Median age (IQR)	64.00 (50.00-73.00)	62.00 (54.00-75.00)	64.00 (49.00-72.25)	0.684
Female sex (n (%))	63 (86.3)	17 (100.0)	46 (82.1)	0.104
High blood pressure (n (%))	31 (42.5)	7 (41.2)	24 (42.9)	1.00
First degree relative with cerebral aneurysm (n (%))	8 (11.00)	1 (5.9)	7 (12.5)	0.672
Smoking (n (%))	10 (13.7)	3 (17.6)	7 (12.5)	0.690
Median aneurysm size mm (IQR)	6.00 (5.00-9.00)	8.00 (6.00-19.00)	6.00 (4.50-7.25)	0.019
Localization (n(%)):				
ICA ophthalmic segment	41 (56.2)	13 (76.5)	28 (50.0)	0.055
ICA posterior communicating segment	19 (26.0)	1 (5.9)	18 (32.1)	

ICA choroidal segment	4 (5.5)	0 (0)	4 (7.1)	
ICA cavernous segment	4 (5.5)	1 (5.9)	3 (5.4)	
ICA	2 (2.7)	1 (5.9)	1 (1.8)	
Middle cerebral artery	1 (1.4)	1 (5.9)	0 (0)	
Anterior cerebral artery A3	2 (2.7)	0 (0)	2 (3.6)	
Previous treatment (n (%))	12 (16.4)	1 (5.9)	11 (19.6)	0.272
Adjunctive coils (n (%))	15 (20.5)	4 (23.5)	11 (19.6)	0.739
Aneurysm number (n (%))				0.810
1	64 (87.7)	15 (88.2)	49 (87.5)	
2	7 (9.6)	2 (11.8)	5 (8.9)	
3	2 (2.7)	0 (0)	2 (3.6)	
Median follow-up time (month)(IQR)	15 (12-25)	20.5 (9.8-28.8)	15 (12-25)	0.471

Table 6: Demographic and clinical characteristics of the patients treated in Bucaramanga, Colombia, with endovascular interventions using Pipeline Embolization Devices for intracranial aneurysms. ICA: Internal carotid artery.

8.3.1.1 Aneurysm characteristics

Most patients (56.2%) had multiple aneurysms, with 34 belonging to the group with Sim&Size™ simulation and seven to the group without simulation. Most of the aneurysms were in the ICA. Three were the exception, including two in the anterior cerebral artery and one in the middle cerebral artery. The aneurysm greatest diameter had a median of 6.00 mm (IQR 5.00–9.00), with the lowest value of 2.00 mm and the largest of 40.00 mm.

8.3.1.2 Intervention and device

Fifty-six of the 73 interventions (76.7%) included the Sim&Size™ simulation software, while the remaining 17 (23.3%) did not. Only the second intervention of patients requiring two interventions used the Sim&Size™ simulation, resulting in successful occlusion for all the cases (Table 7).

Surgical time had a median of 105.00 min (IQR 88.75–130.00), with the shortest procedure lasting 55.00 min and the longest 205.00 min. One of the patients in the group with Sim&Size™ simulation had no record of surgical time. The median stent length was 16.00

mm (IQR 12.00–20.00), with the shortest stent being 12.00 mm long and the longest 35.00 mm. The median stent diameter was 4.00 mm (IQR 3.50–4.31), with the narrowest being 2.50 mm and the widest 5.00 mm.

Patients in the group with Sim&Size™ simulation had shorter stent lengths than those in the non-simulated group (16.00 mm vs. 20.00 mm p-value = 0.001), and a lower proportion of them required more than one stent (3.6% vs. 17.6% p-value = 0.079). The surgical times also tended to be shorter in these patients (100.00 min vs. 118.00 min), but this result was not statistically supported (p-value = 0.496) (Table 7).

Outcomes	Univariate analysis	Bivariate analysis		P-value
		Without Simulation (n=17)	With Simulation (n=56)	
Median surgical time (min) (IQR)	105.00 (88.75-130.00)	118.00 (90.00-140.00)	100.00 (85.00-125.00)	0.496
Median stent diameter (mm)(IQR)	4.00 (3.50-4.25)	3.75 (3.00-4.00)	4.00 (3.50-4.31)	0.112
Median stent length (mm)(IQR)	16.00 (12.00-20.00)	20.00 (20.00-20.00)	16.00 (12.00-20.00)	**0.001**
Two stent used (n(%))	5 (6.8)	3 (17.6)	2 (3.6)	**0.079**
Two stent implanted (n(%))	4 (5.5)	2 (11.8)	2 (3.6)	0.230
Stent Shortening (n(%))	2 (2.7)	1 (5.9)	1 (1.8)	0.414
Occlusion (n (%)):				
Complete	48 (76.2)	8 (57.1)	40 (81.6)	**0.078**
Partial	15 (20.5)	6 (35.3)	9 (16.1)	
Hemorrhagic complications (n (%))	3 (4.1)	3 (17.6)	0 (0)	**0.009**
Vascular access hemorrhage (n (%))	4 (5.5)	1 (5.9)	3 (5.4)	1.000

Table 7: Outcomes of the patients treated in Bucaramanga, Colombia, with endovascular interventions using Pipeline Embolization Devices for intracranial aneurysms.

Only one stent implantation failed due to technical failure of the device. This failure occurred in one patient belonging to the group without stimulation. Four patients needed two stents to

cover the neck of the aneurysm, one of them belonging to the group with Sim&Size^{TM} simulation. Two patients suffered from stent shortening, with one belonging to the group with Sim&Size^{TM} simulation and one to the non-simulated group.

8.3.1.3 Follow-up and aneurysm occlusion

Sixty-three (86.3%) of the 73 interventions had follow-up imaging, with 53 using 2D-DSA and 10 MRI. Out of these 63 interventions, 48 (65.8%) had complete occlusion and 15 (20.5%) incomplete occlusions, with a median clinical follow-up of 15.00 months (IQR 12.00– 25.00). Only 47.1% of patients in the group without simulation had complete occlusion, with a median follow-up was 20.50 months (Table 7). On the other hand, 71.4% of patients in the group with Sim&Size^{TM} simulation had complete occlusion, with a median follow-up of 15.00 months.

8.3.1.4 Complications

Complications included three intracranial hemorrhagic complications, all in patients in the group without simulation. One of these complications occurred during surgery and was secondary to an aneurysm rupture. This patient was treated using PED and coils, and the rupture happened during coiling. The other two occurred after the surgical procedure, one in the immediate postoperative period and the other in the following 30 days. In both cases, intraparenchymal hemorrhage happened without the involvement of the previously treated aneurysm. The Fisher grade for the hemorrhages was Fisher III for the former and Fisher IV for the latter. The latter also had an initial PRU of 128. Still, this value might be misleading as the clopidogrel responses change over time, and the PRU was not evaluated during the hemorrhage. Hemorrhagic complications related to femoral vascular access occurred in four patients, three in the group with Sim&Size^{TM} simulation and one in the group without simulation. No neurological sequelae secondary to complications were observed during the 30-day follow-up.

Four patients in the group with Sim&Size^{TM} simulation (6.3%) presented stent-related complications before the 12-month follow-up. One of these patients suffered a stroke occlusion of the right anterior choroidal artery six weeks after stent placement. This patient

also had non-optimal stent apposition at the anterior choroidal artery origin and a VerifyNow of 181 PRU, close to the upper limit of the test. Regarding the other patients with stent-related complications, one patient suffered from left-monocular hemianopsia, and another from visual acuity decreases. The last patient experienced a 70.0% in-stent stenosis at the 12-month follow-up. The mortality percentage for the study was 0% at the 12-month follow-up.

8.3.1.5 Multivariate analysis

The multivariate analysis corroborated the bivariate analysis to some extent. Patients presenting shorter stents (log odds = −0.21, Std. Error = 0.74, p = 0.003) but with increased diameter (log odds = 2.19, Std. Error = 0.07, p = 0.003) were more likely to come from the group with Sim&Size™ simulation. Aneurysm size, number of stents used, hemorrhagic complications, occlusion occurrence, and surgical time gave no information about whether the patient underwent the Sim&Size™ simulation (p-value > 0.050).

8.3.1.6 Aneurysm site association with stent size

Different aneurysm sites were associated with differences in stent diameter. For instance, we saw the narrowest diameters in patients treated for an aneurism in the posterior communicating segment of the right ICA (Figure 27A). However, the patient group (i.e., patients with Sim&Size™ simulation and without simulation) did not influence this association (p-value = 0.425), and the association was loose (p-value = 0.066).

Different aneurysm sites were also associated with varying lengths of stents (Figure 27B), and using the Sim&Size™ simulation software seemed to influence this association (p-value = 0.010). For instance, patients in the group with Sim&Size™ simulation had shorter stents than those without simulation for most aneurysm sites. Still, the opposite occurred for patients with an aneurism in the left ICA (Figure 27B).
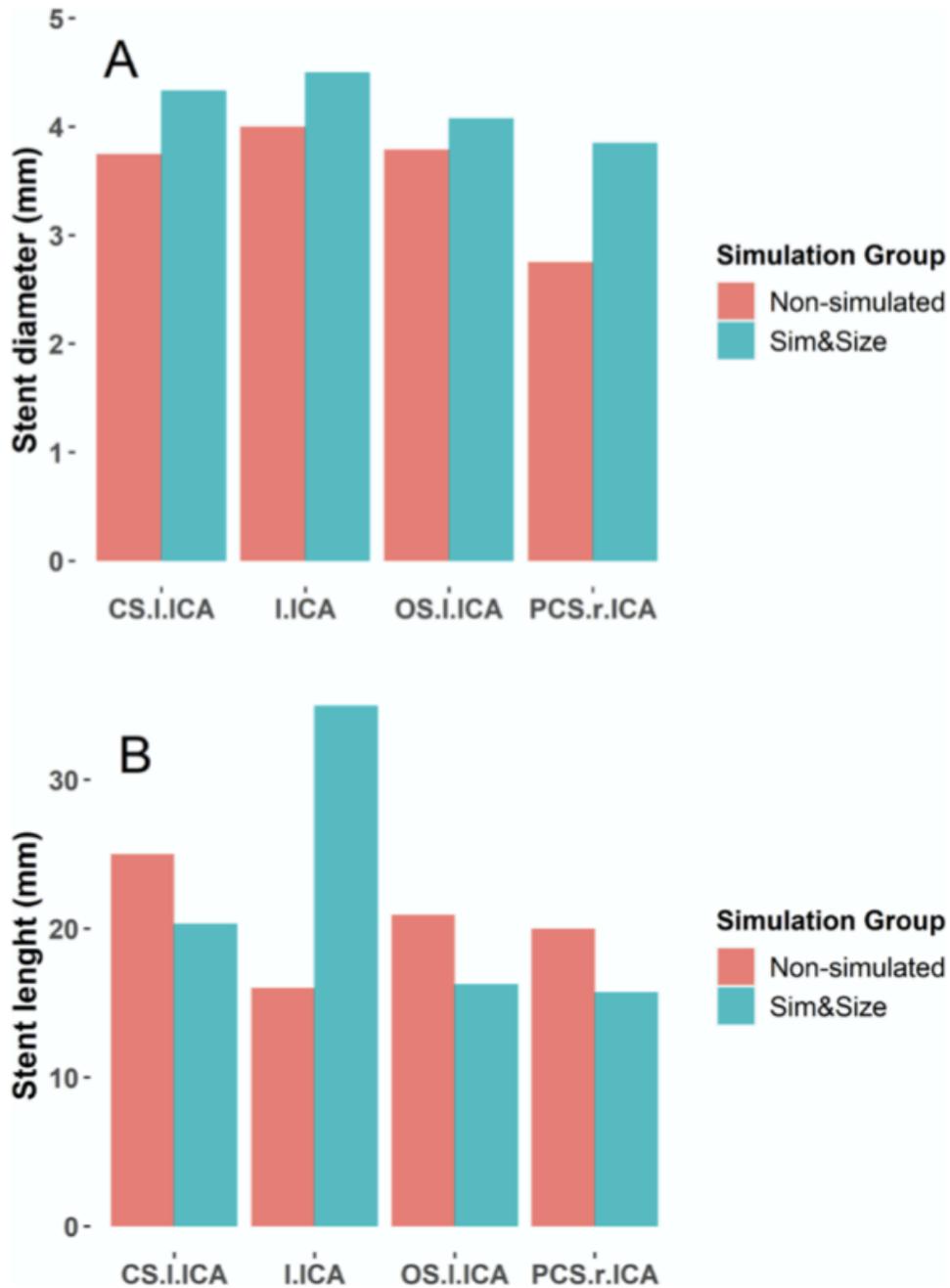
Figure 27: Dimensions of the Pipeline Embolization Devices used in Bucaramanga, Colombia, in the endovascular treatment of patients with intracranial aneurysms according to the aneurism localization. Shown are the mean stent diameter (A) and length (B) of the patients treated with and without the Sim&Size^{TM} simulation. CS.l.ICA denotes cavernous segment of the left internal carotid artery (ICA), l.ICA left ICA, OS.l.ICA ophthalmologic segment of the left ICA and PCS.r.ICA posterior communicating segment of the right ICA.

8.3.2 Results for the multicenter evaluation

The multicentric cohort included 253 patients with cerebral aneurysms treated using PED. These 253 patients comprised the 75 treated in Bucaramanga, Colombia aforementioned, and 178 treated between January 1, 2015, and December 31, 2017, in Montpellier, France. Our evaluation excluded 16 of these patients, including the seven Colombian patients excluded from the monocentric evaluation and nine from the French cohort, which had multiple Pipeline constructs planned for giant or fusiform aneurysms.

Most patients were women (83.8%), and their median age was 57.48 (IQR 55.84-59.12). The most prevalent comorbidities were high blood pressure (37.9%), followed by smoking (36.0%), hyperlipidemia (22.1%), and diabetes (7.1%) (Table 8).

8.3.2.1 Aneurysm characteristics

For the multicenter cohort, the median aneurysm size was 8.11 mm (IQR 7.33-8.88), and most patients had large vessel occlusion (88.1%). The majority of the aneurysms were on the left side (53.4%) and were located in the ICA paraclinoid segment (56.8%), followed by ICA (15.2%) and ICA posterior communicating segment (14.8%) (Table 8).

Population Characteristics	Univariate analysis (n=253)	Bivariate analysis		P-value
		Without Simulation (n=109)	With Simulation (n=144)	
Median age*	57.48 (55.84- 59.12)	57.63 (55.21-60.04)	57.37 (55.12-59.62)	0.878
Female sex (n (%))	212 (83.79)	91 (83.49)	121 (84.03)	1.000
High blood pressure (n (%))	96 (37.94)	41 (37.61)	55 (38.19)	1.000
Diabetes (n (%))	18 (7.11)	7 (6.42)	11 (7.64)	0.808
Hyperlipidemia (n (%))	56 (22.13)	22 (20.18)	34 (23.61)	0.544
Smoking (n (%))	91 (35.97)	41 (37.61)	50 (34.72)	0.692
Median aneurysm size (mm)*	8.11 (7.33- 8.88)	9.22 (7.76-10.68)	7.26 (6.48-8.05)	0.013
Localization (n(%)):				
ICA paraclinoid segment	142 (56.80)	60 (55.05)	82 (58.16)	0.054
ICA	38 (15.20)	21 (19.27)	17 (12.06)	
ICA posterior communicating segment	37 (14.80)	10 (9.17)	27 (19.15)	
Middle cerebral artery	13 (5.20)	9 (8.26)	4 (2.84)	
Vertebral or PICA artery	3 (1.20)	2 (1.83)	1 (0.71)	

Anterior communicating artery	3 (1.20)	2 (1.83)	1 (0.71)	
Anterior cerebral artery	14 (5.60)	5 (4.59)	9 (6.38)	
Large vessel oclussion (ICA, vertebral, Basilar)	223 (88.14)	93 (85.32)	130 (90.28)	
Left side (n (%))	135 (53.36)	60 (55.05)	75 (52.08)	0.703

Table 8: Demographic and clinical characteristics of the patients treated in Bucaramanga, Colombia, and Montpellier, France, with endovascular interventions using Pipeline Embolization Devices for intracranial aneurysms. ICA: Internal carotid artery

8.3.2.2 Intervention and device

For the multicenter cohort, the median stent diameter was 3.82 mm (IQR 3.74–3.0-), and the median stent length was 16.37 mm (IQR 15.85-16.89). Forty-six patients (18.2%) had coils in their treatments, and 27 (10.7%) had Balloon. Ten patients (4.0%) required more than one PED, and 46 (18.2%) required corrective intervention (Table 9). The records of this cohort did not include surgical time.

One-hundred forty-four of the 253 patients (56.9%) included the Sim&Size™ simulation software, while the remaining 109 (43.1%) did not. Patients in the group with Sim&Size™ simulation had shorter stents than those without simulation (15.62 mm vs. 17.36 mm p-value= 0.001). Also, a lower proportion of these patients required more than one stent (1.4% vs. 7.3% p-value=0.022), and a greater proportion required a balloon (15.3% vs. 4.6% p-value=0.007). The remaining analyzed variables were undistinctive (p-value>0.05) between the two groups of patients (i.e., with Sim&Size™ simulation and without simulation) (Table 9).

8.3.2.3 Complications

The multicenter cohort reported 16 complications, seven in the group with Sim&Size™ simulation and nine in the group without simulation. We referred to seven of these complications in the results of the monocentric evaluation, including three vascular access hemorrhages in the group with Sim&Size™ simulation, and in the group without simulation, three hemorrhagic complications and one vascular access hemorrhage.

103

Five of the remaining nine complications occurred in patients in the group without simulation. These complications included two minor intraparenchymal hematomas, likely resulting from perforator artery ruptures, like those caused by the stent guidewire.

One of these intraparenchymal hematomas was accompanied by a modest subarachnoid hemorrhage. The remaining three complications included two minor strokes (i.e., diffusion-positive spots in the lenticular nucleus and corona radiata) with mild loss of motor skills, which were wholly regressed, and one post-procedure subarachnoid hemorrhage, similar to those resulting from arterial stretching,

The remaining four complications occurred in the group with Sim&Size™ simulation. Three of these complications included a partial embolic occlusion in the right central sulcus artery (Rolandic artery), resulting in a partially resolved hemiparesis, a minor stroke with a transient leg deficit, and an asymptomatic internal carotid artery dissection. The database included the fourth complication for the group with Sim&Size™ simulation, but the clinical record was unavailable for this patient. All complications were resolved without sequelae. The exception was the partial embolic occlusion, in which leg weakness persisted after discharge (Table 9).

Outcomes	Univariate analysis (n=253)	Bivariate analysis		
		Without Simulation (n=109)	With Simulation (n=144)	P-value
Median stent diameter (mm)*	3.82 (3.74- 3.90)	3.81 (3.69-3.94)	3.82 (3.72-3.92)	0.902
Median stent lenght (mm)*	16.37 (15.85-16.89)	17.36 (16.68-18.04)	15.62 (14.88-16.36)	**0.001**
Two stent used for insufficient neck coverage (n(%))	10 (3.95)	8 (7.34)	2 (1.39)	**0.022**
Coils used (n(%))	46 (18.18)	21 (19.27)	25 (17.36)	0.743
Balloon used (n(%))	27 (10.67)	5 (4.59)	22 (15.28)	**0.007**
Corrective intervention needed (n(%))	46 (18.18)	21 (19.27)	25 (17.36)	0.743
Complications	16 (6.32)	9 (8.26)	7 (4.86)	0.305

Table 9: Outcomes of the patients treated in Bucaramanga, Colombia, and Montpellier, France, with endovascular interventions using Pipeline Embolization Devices for intracranial aneurysms..

8.4 Discussion

Endovascular treatment with FD is a safe and effective alternative for intracranial aneurysms (82). However, selecting the stent dimensions is challenging due to the patient's anatomy and the stent's conformation. Neuro-interventionalists can use virtual simulation software such as the Sim&Size™ simulation software to simplify this selection. Yet, few studies have evaluated the intraoperative and clinical impact of the Sim&Size™ simulation software.

We saw more treatments that included the Sim&Size™ simulation software in our patients' cohort, especially in the Colombian cohort. Nearly two-thirds of the interventions in Colombia used the software. This higher number results from the technique's continuous evolution and the neuro-interventionalists' confidence in the simulation software. Also, it is in line with the constant improvement of the FOSCAL clinic, which is a benchmark for its region. Treatments that included the Sim&Size™ simulation came following the Sim&Size™ simulation software acquisition, meaning they are also the most recent. It is crucial to consider that the experience gained by the neuro-interventionalists teams in this technique might have influenced our results to some extent.

8.4.1 Surgical time

Patients treated using the Sim&Size™ simulation software in Bucaramanga, Colombia, tended to have shorter surgical interventions (median surgical time 100 min (IQR 85–125) versus 118 min (IQR 90 −140)). Despite the lack of statistical support (p-value = 0.496), this tendency observed in the Colombian cohort toward shorter times is relevant as it may represent a lower risk for patients. These observations align with a similar evaluation by Piergallini et al. study (83), in which the authors found shorter surgical times for patients treated using the Sim&Size™ simulation software (46 min vs. 52 min p-value = 0.002). The differences between Piergallini et al. surgical times and ours come from the criteria used by the study to define this time. The surgical time in our study was the period between the femoral puncture and the femoral sheath removal, including catheterization. In comparison, Piergallini et al. measured surgical time from the catheter positioning in the internal carotid or vertebral artery to the end of the procedure (83).

Other studies have shown that shorter neurointerventions result in lower complication rates (84). Shorter times lead to more procedures per angiosuite and lower patient radiation exposure (85). Our evaluations did not include the radiation dosage or fluoroscopy time of patients, and further studies are required to determine whether using the Sim&Size^{TM} simulation decreases the patients' radiation exposure. Shorter neurointerventions are also associated with lower rates of ischemic events (84). Reducing surgical time in the operating room is critical, and the Sim&Size^{TM} simulation software likely reduces these times, leading to fewer complications and lower radiation doses. Therefore, we stress the need to evaluate further the effect of Sim&Size^{TM} simulation software on surgical time.

8.4.2 The size of the Pipeline Embolization Device

During the simulation, the Sim&Size^{TM} simulation software predicts the proximal landing zone based on the patient's artery anatomy and the stent's dimensions provided by the neuro-interventionalist. The software tries to set a landing zone in a straight segment of the parent artery. A straight proximal landing zone facilitates the stent-artery surface apposition. A good apposition improves the endothelialization process and decreases leaks (86). The neuro-interventionalist can achieve a desired proximal landing zone by modulating the stent dimensions during the Sim&Size^{TM} simulation. In this manner, the software helps the neuro-interventionalist determine the proper stent size for each patient.

We found that using the Sim&Size^{TM} simulation software resulted in shorter stents. We evidenced these shorter stents in our monocentric (16 mm (IQR 12–20) v.s 20 mm (IQR 20–20) p-value = 0.001) and multicentric (15.62 mm (IQR 14.88–16.36) v.s 17.36 mm (IQR 16.68–18.04) p-value = 0.001) evaluation. These stent length reductions align with other studies, although these other studies found less pronounced reductions (83). Using shorter stents is beneficial as it decreases the chances of covering arterial branches originating from the parent artery. It also reduces the amount of metal inside the parent artery, which results

in good appositions with the vessel wall. A proper apposition promotes endothelization and lowers intimal hyperplasia.

Stent diameter is also critical for stent selection. We found that using the Sim&Size ^{TM} simulation software led to a tendency for greater stent diameters. We evidenced these tendencies in our monocentric (4 mm (IQR 3.5–4.3) v.s 3.8 mm (IQR 3.0–4.0)) and multicentric (3.82 mm (IQR 3.69–3.94) v.s 3.81 mm (IQR 3.72–3.92)) evaluation. However, the differences in stent diameters between patients with and without Sim&Size^{TM} simulation lacked statistical support (p-value > 0.050). This lack of statistical support aligns with the findings of other studies (83)(87). In these studies, Piergallini et al. (83)(87) found tendencies toward decreased stent diameters in simulated patients (3.8 mm vs. 4.0 mm), and Ospel et al. (87) towards increased stent diameters (3.94 mm vs. 3.89 mm). The lack of consensus and statistical support in these evaluations suggests that using the Sim&Size^{TM} simulation software does not impact the stent diameter selection. However, we consider the tendency towards greater diameters interesting as they might result from the neuro-intervenionalist trying to achieve a proper stent-vessel wall apposition. The Sim&Size^{TM} simulation software shows a color map illustrating stent contact with the vessel walls. A larger stent diameter could guarantee a better wall apposition as it assures no gaps between the stent and the vessel wall, reducing the possibility of treatment failure.

Personalized medicine aims to achieve better outcomes for patients. Interventional Neuroradiology clinical practices have used virtual simulation software such as the Sim&Size^{TM} simulation software while treating patients with intracranial aneurysms. This software is improving the FD selection. It helps neuro-interventionalists select the proper FD size, reducing stent mispositioning and associated complications. An adequate apposition to the parent artery lowers the risk of device migration, late stent rupture, stroke, and acute thrombus formation (53)(36)(89). Additionally, using a stent with the proper size reduces the probability of stent shortening, lowers the need for a second device, and reduces the risk of covering branches emerging from the parent artery such as the ophthalmic and anterior choroidal arteries.

8.4.3 Balloon angioplasty

Balloon angioplasty allows achieving a straight landing zone by shortening the stent's proximal end. Neuro-interventionalists might be using these devices to accomplish the stent's proximal end recommended by the Sim&Size^{TM} simulation software, helping to explain the higher rates of Balloon angioplasty observed in our multicentric evaluation for patients with the Sim&Size^{TM} simulation (15.3% vs. 4.6%).

8.4.4 Complications

The complication rate was 12.6 % in our monocentric cohort and 6.3% in our multicenter cohort. The complications rate was lower in patients with the Sim&Size^{TM} simulation (4.1% and 4.86% of patients, respectively) than those without simulation (5.5% and 8.26% of patients, respectively). However, the difference was not statistically supported (P-value>0.050). No mortality occurred after 30 days of the procedure in the monocentric and multicentric evaluations.

The complications in patients with the Sim&Size^{TM} simulation did not relate to using the Sim&Size^{TM} simulation software. These complications were associated with the antiplatelet therapy and coiling placement, not stent placement. However, we recommend not disregarding the possibility of the Sim&Size^{TM} simulation increasing the risk of some complications, and further evaluations are necessary (90).

8.5 Limitations

Our monocentric study is limited as it is a retrospective and non-randomized evaluation with a small sample size. It lacked statistical power to support the differences in some of the evaluated variables. Also, more than two-thirds of the patients in the monocentric cohort had the Sim&Size^{TM} simulation in their treatments. This increased number of patients treated using the Sim&Size^{TM} simulation software resulted from the FOSCAL clinic having a low neurointerventional activity before the software acquisition. Finally, the aneurysm sizes in the monocentric cohort were smaller for patients with Sim&Size^{TM} simulation, and their

aneurysms occurred in less tortuous artery segments. These differences between aneurysms might have affected our result interpretations, especially for stent vessel apposition.

The results of our multicentric evaluation are more robust, as we had a more significant sample and a more even ratio of patients with and without the Sim&Size^{TM} simulation. However, this evaluation is still limited as it is retrospective and non-randomized.

8.6 Conclusions

Using Sim&Size^{TM} simulation software for endovascular treatment patients with intracranial aneurysms using PED reduces the stent length. It may also impact the number of devices needed per treatment and decrease the surgical time.

Validation of 3D printed models of intracranial aneurysms
Review

Chapter contents

9.1 Introduction

In August 1984, Charles W Chuck introduced a patent for "Apparatus for production of 3D objects by Stereolithography", which was later accredited with the invention of the world's first 3D printer (US Patent 4,575,330, 1986) (90). 3D printing was primarily used to quickly engineer and design prototypes (91). However, within the last decade, the uses for this technology have expanded in the manufacturing industry due to numerous innovations that have reduced production and technology costs, improved the printed models' accuracy, and expanded the printing materials. These improvements have facilitated the production of various products and made this technology available to consumers for in-home use. 3D printing has also evolved for medical applications as it can produce customized 3D models of devices and implants that can improve patient care (92)(91). Neuroradiology services can benefit from having 3D-printing laboratories, as these laboratories can be used to evaluate devices and train students. These laboratories can also facilitate surgical planning and hemodynamic studies (93).

Several 3D-printing technologies are available. Among these technologies, the Stereolithography (SLA) 3D printers use a low-power ultraviolet laser to solidify a liquid photosensitive polymer. Various printing materials are also available. At least seven materials or material combinations have been described for printing 3D-cerebrovascular models in neurological-clinical practice. These materials include the elastomer Tango Plus, the photo-polymerized resin stereocol, and the acrylonitrile butadiene styrene (ABS) plastic and silicon combination. They also include a photosensitive resin, a polycarbonate-like photoreactive polymer, polylactic acid, and MakerBot Flexible Filament (MakerBot, New York, New York) combination and plaster (zp150 powder and zb6 clear binder)(94).

Despite the 3D printing usefulness, its use is limited in neurological-clinical practice due to its long processing times and the variability of 3D printed models (91). Also, it is challenging to print small structures such as cerebral arteries and remove the support material without breaking the model. Despite these challenges, we have been using an SLA 3D printer in our service to produce 3D models of intracranial aneurysms in an effective and low-time-consuming manner. In this chapter, we aimed to validate the accuracy of these models by

comparing 3D digital subtraction angiography (DSA) of patients' aneurysms and their 3D printed models using the Vascular Modeling Toolkit (VMTK).

9.2 Objective

This chapter aims to validate the geometrical accuracy of the 3D models of intracranial aneurism printed using Stereolithography 3D printing technology.

9.3 Methods

To validate the accuracy of the 3D printed models, we compared the geometry of the aneurysms surface between patients and 3D printed models. Specifically, we used 3D-DSA images taken during the pretreatment planning of five patients with unruptured intracranial aneurysms. Two patients had aneurysms in the anterior communicating artery, two in the middle cerebral artery, and one in the terminus of the intracranial carotid artery (carotid T). The DICOM files of the 3D-DSA were transformed into STL files and used the STL to generate 3D reconstructions of the voxel surface with the Sim&Size^{TM} simulation software (version 1.2). We delimited the aneurysm region, including an expanded part of the proximal and distal vessels. Then, we extended the lumen centerline with the vmtkflowextensions functionality of the VMTK algorithm to allow the plug to the hydraulic circuit.
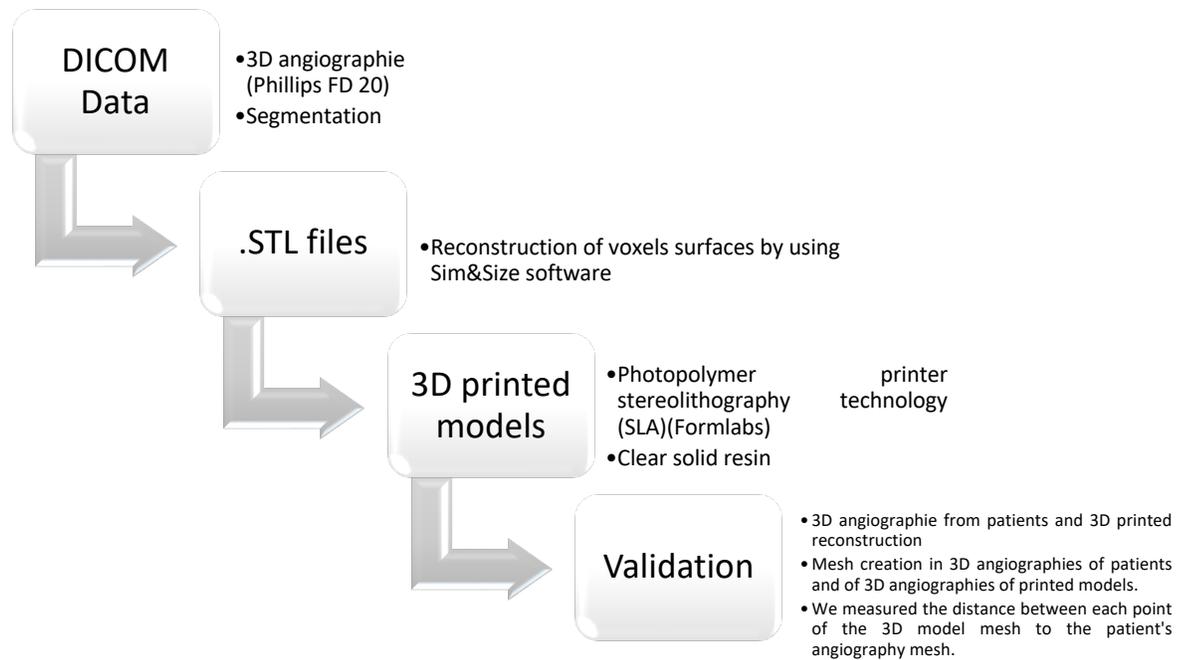
Figure 28: Workflow for manufacturing and validating 3D printed models of intracranial aneurysm.

We used the processed 3D reconstructions to print hollow models of the aneurysms using an SLA 3D printer (Formlabs) with a clear solid resin. Making the 3D printed models took seven hours and required 55 ml of resin on average. We made the 3D-DSA of the 3D printed models and used the DICOM files to generate 3D reconstructions of the voxel surface as before. By the end, we had two 3D reconstructions of the same aneurysm, one from the patient's 3D-DSA and one from the 3D printed model's 3D-DSA (Figure 28).

3D *Digital subtraction angiography* of the patients and 3D printed models

All the 3D-DSA were performed on an Allura Xper FD20 angiography system (Philips Medical Systems, Best, the Netherlands), specifically designed for angiography in interventional radiology. The FD20 system is equipped with a rotational angiography program that facilitates the fast production of data for observing contrast distribution and creating 3D reconstructions of vessels and soft tissue. These evaluations included two 3D-DSA per aneurysms, one from the rotational angiography of the patient's pretreatment and one from the 3D printed model. High contrast object-based reconstructions (contrast agent,

bony structures) were based on a 240 movement range with 120 acquired images. The rotational frames were sent to the XtraVision Workstation, which is integrated with the acquisition system, following their acquisition. The acquisition time was six seconds.

Aneurysm mesh comparison between patients and 3D printed model

ID Size

To compare the aneurysm mesh between the patient and 3D printed model, we opened the DICOM files in the Sim&Size^{TM} simulation software, selected the region of interest, and performed the threshold check. We juxtaposed the 3D reconstructions and manually rotated the images to get the same orientation when needed and measured deviations at different nodes of the patient and 3D printed model meshes.

9.4 Results

We juxtaposed the mesh of the aneurysm's 3D reconstructions obtained with the Sim&Size^{TM} simulation software for five patients and their 3D printed models. Then, we estimated deviations at different nodes of the juxtaposed meshes to validate the 3D printed models' accuracy. The most remarkable differences were observed for one patient having an aneurysm in the anterior communicating artery. The aneurysm's mesh was smaller for the 3D printed model than for the patient, with 80% of the nodes being less than 0.56 mm apart (Figure 29). This patient was also the first to have an aneurysm-3D printed model in our 3D printing laboratory. The greater differences between nodes and the smaller 3D printed model might have come from our inexperience in the printing process and model-drying techniques.
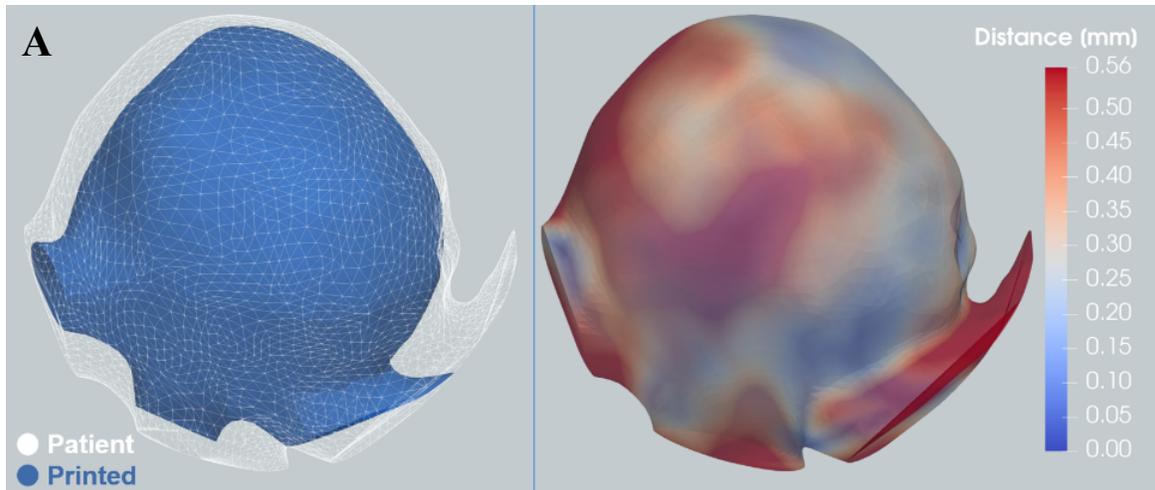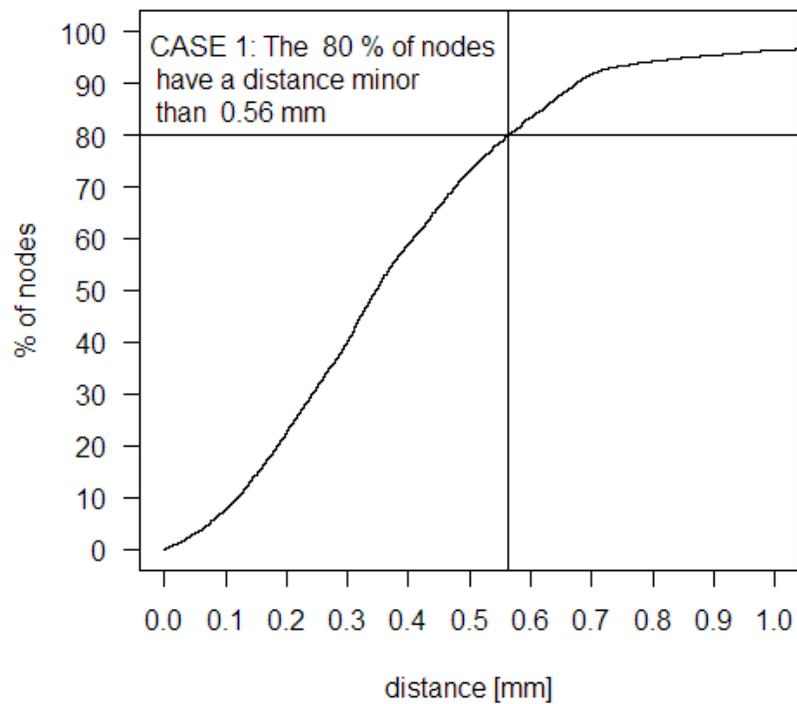
Figure 29: *Differences between the patient and 3D printed model 3D-aneurism reconstructions for an aneurysm in the anterior communicating artery. A) shows the juxtaposed 3D reconstructions (left) and the distance between nodes (right). B) shows the cumulative frequency of the nodes' deviations between juxtaposed 3D reconstructions.*

The second patient had an aneurysm with a small sac in the middle cerebral artery. The aneurysm's mesh of the 3D printed model resembled that of the patient to a greater extent. The deviations were below 0.17 mm for 80% of the meshes' nodes, including those of the small sac, demonstrating a model's increased accuracy (Figure 30).
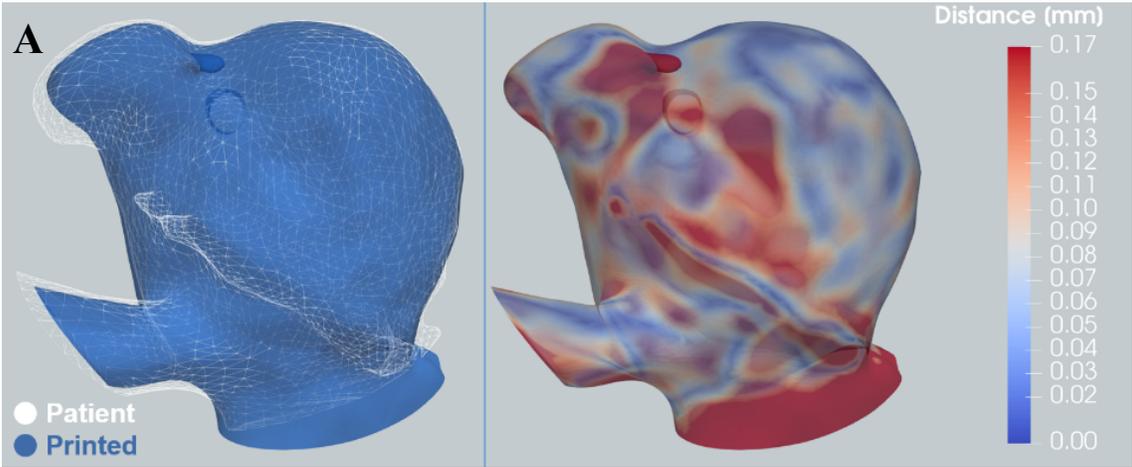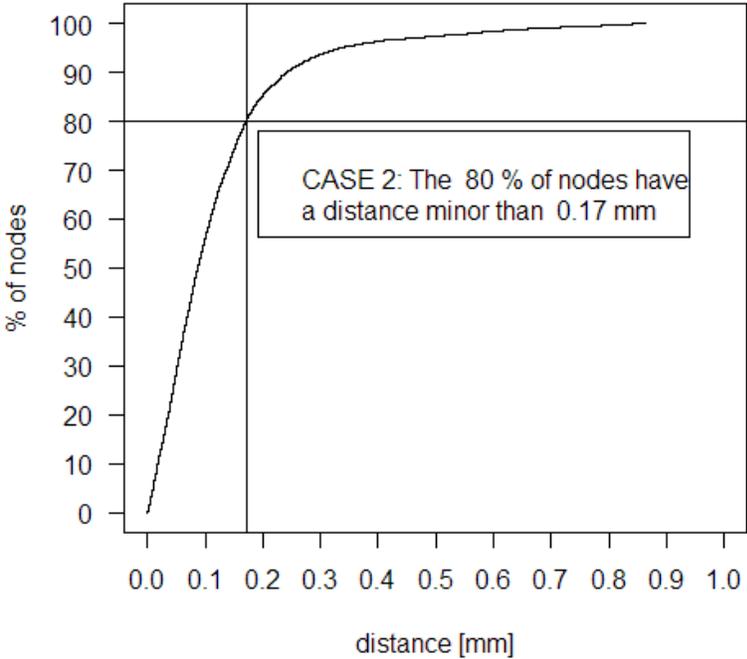
Figure 30: Differences between the patient and 3D printed model 3D-aneurism reconstructions for an aneurysm with a small sac in the middle cerebral artery. A) shows the

juxtaposed 3D reconstructions (left) and the distance between nodes (right). B) shows the cumulative frequency of the nodes' deviations between juxtaposed 3D reconstructions.

The third patient had an aneurysm in the middle cerebral artery but without a small sac. The concordance between the patient and 3D printed model aneurysm's meshes was also good for this patient. However, the concordance was lower than that observed for the second patient. In this case, the deviations were below 0.21 mm for 80% of the meshes' nodes (Figure 31).

A

Distance (mm)
- 0.21
- 0.18
- 0.16
- 0.14
- 0.12
- 0.10
- 0.08
- 0.06
- 0.04
- 0.02
- 0.00

Patient
Printed

B

Cumulated frequency of node distance

CASE 3: The 80 % of nodes have a distance minor than 0.21 mm

% of nodes
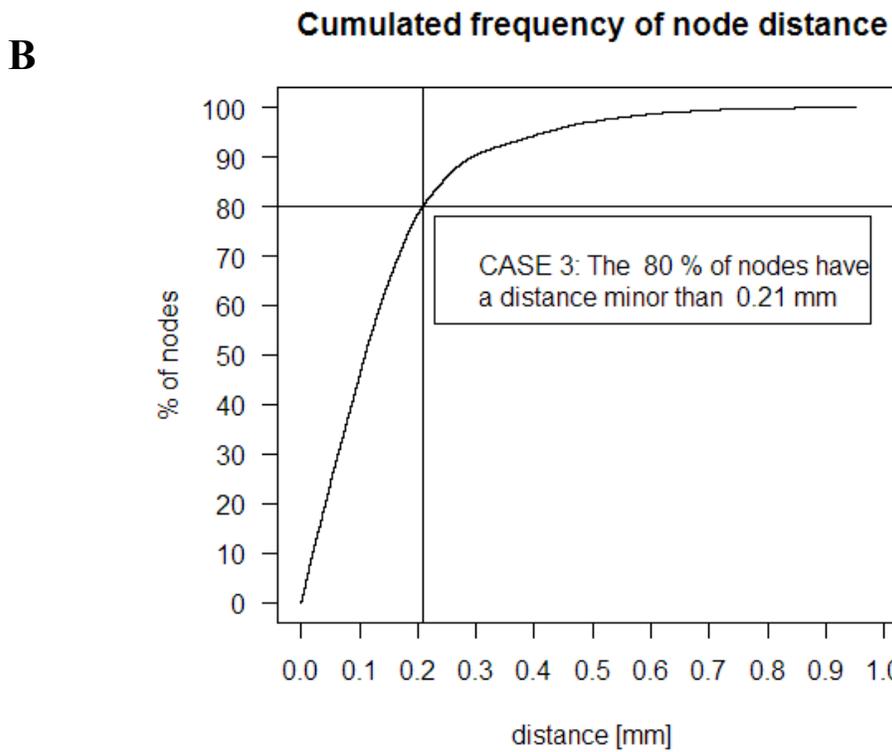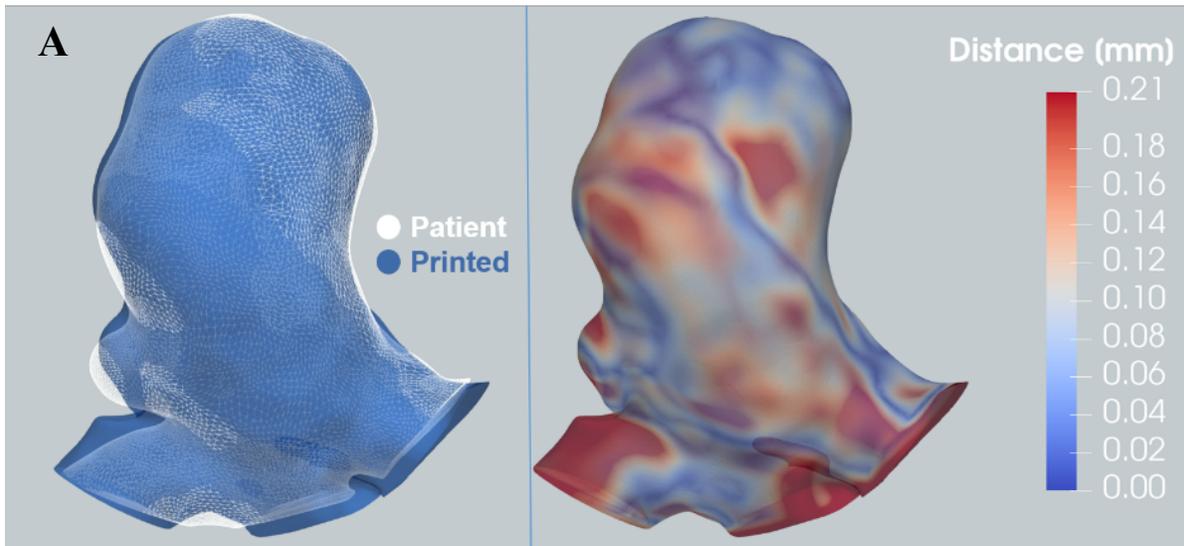
distance [mm]

Figure 31: Differences between the patient and 3D printed model 3D-aneurism reconstructions for an aneurysm in the Middle cerebral artery. A) shows the juxtaposed 3D reconstructions (left) and the distance between nodes (right). B) shows the cumulative frequency of the nodes' deviations between juxtaposed 3D reconstructions.

The fourth patient had an aneurysm in the carotid T. The resemblance between the 3D printed model and the patient aneurysm's meshes was comparable to that of the third patient, with deviations below 0.23 mm for 80% % of the meshes' nodes (Figure 32).
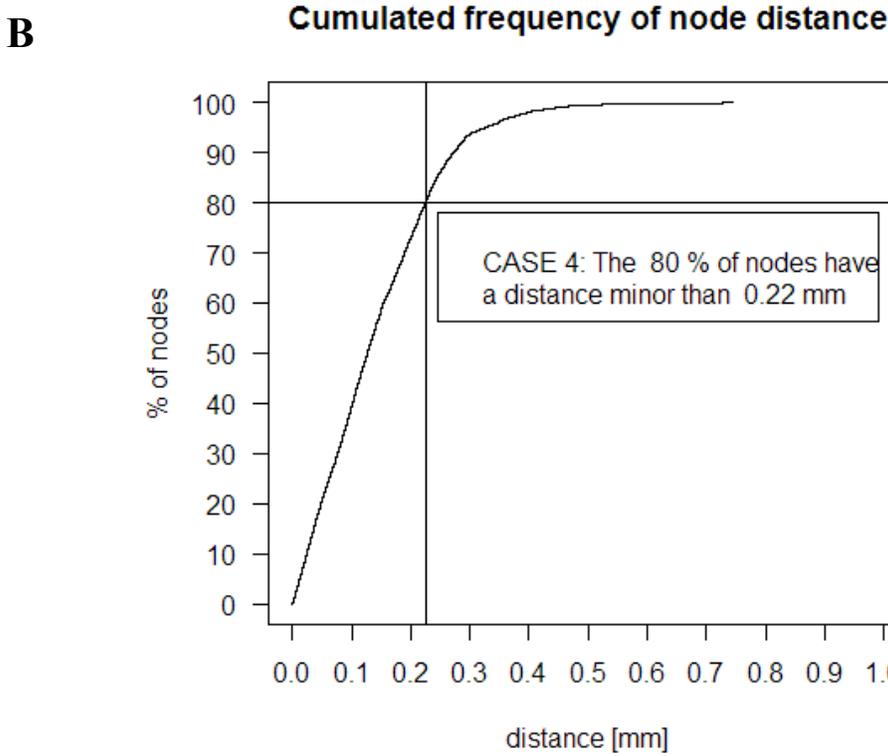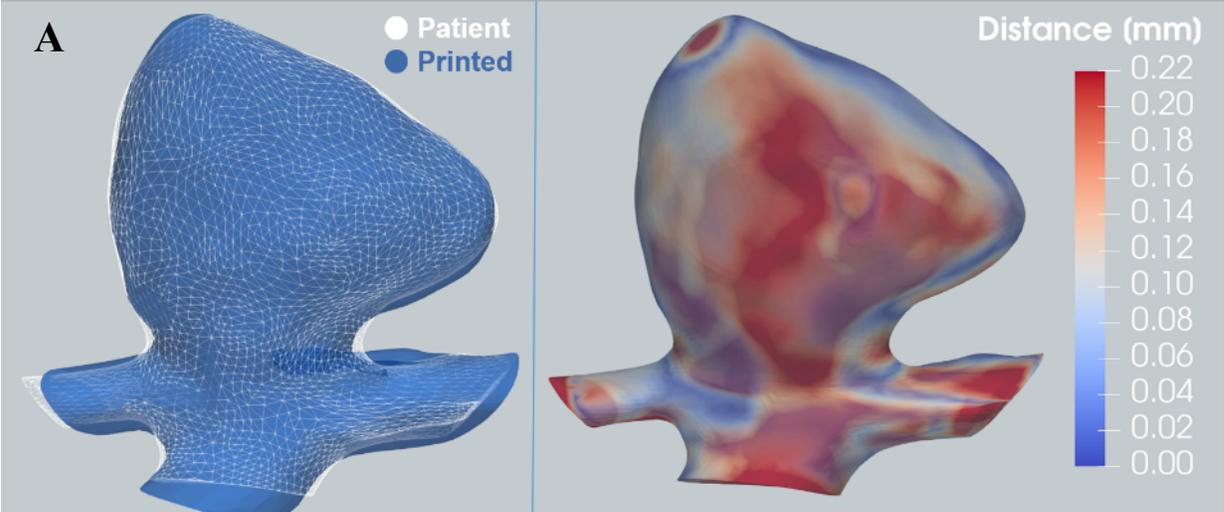
Figure 32: Differences between the patient and 3D printed model 3D-aneurism reconstructions for an aneurysm in the carotid T . A) shows the juxtaposed 3D

reconstructions (left) and the distance between nodes (right). B) shows the cumulative frequency of the nodes' deviations between juxtaposed 3D reconstructions.

The last patient was the other one having an aneurysm in the anterior communicating artery. This patient also had the most accurate 3D printed model, having the highest resemblance between the 3D printed model and the patient aneurysm's meshes. The nodes' deviations were lowest, below 0.11 mm for 80% % of the meshes' nodes (Figure 33).
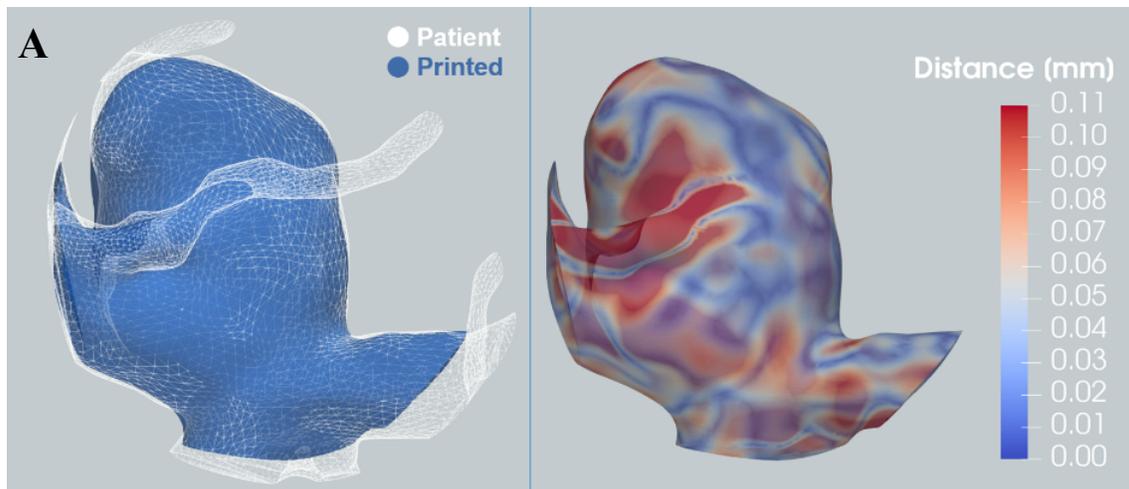
**B**   **Cumulated frequency of node distance**
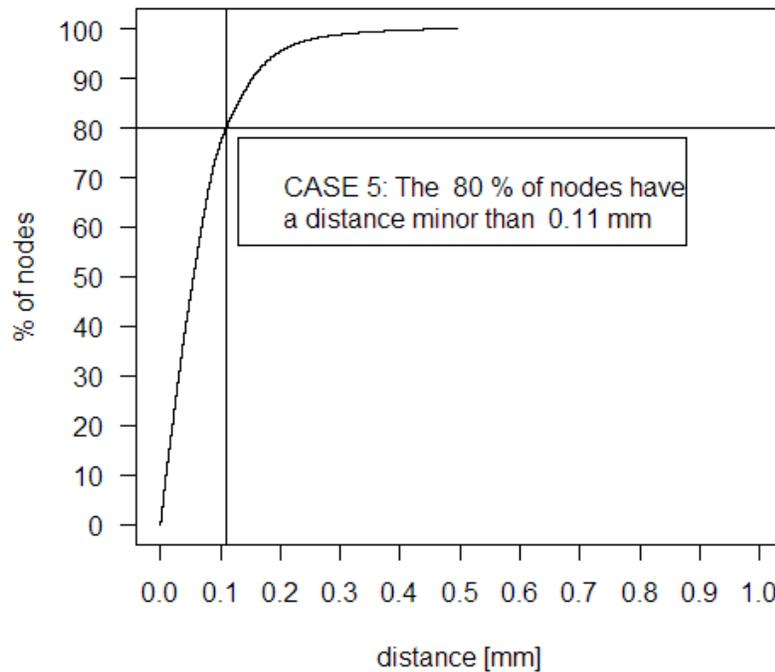
Figure 33: Differences between the patient and 3D printed model 3D-aneurism reconstructions for an aneurysm in the Anterior communicating artery. A) shows the juxtaposed 3D reconstructions (left) and the distance between nodes (right). B) shows the cumulative frequency of the nodes' deviations between juxtaposed 3D reconstructions.

We found an overall deviation below 0.21 mm for 80% of the meshes' nodes when considering the five aneurysms (Figure 34). These overall distance differences show a good resemblance between the 3D printed model and patient 3D reconstructions, indicating that the 3D printed models are accurate

Cumulated frequency of node distance

The 80 % of nodes have
a distance minor than 0.21 mm
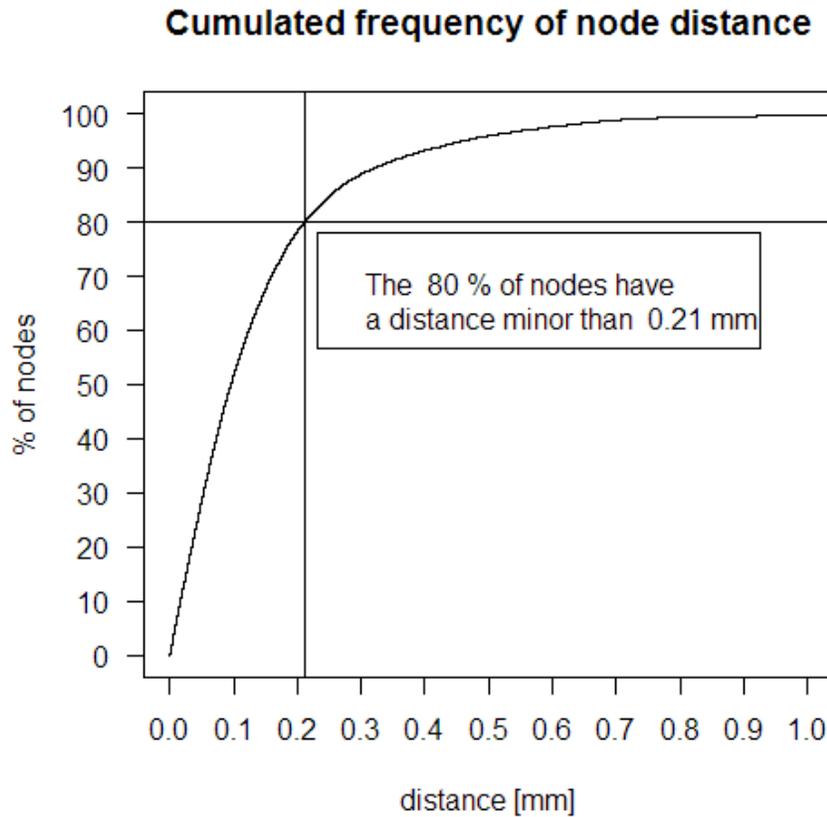
Figure 34: Cumulative frequency of the nodes' deviations between juxtaposed 3D reconstructions showing the differences between the patient and 3D printed model 3D-aneurism reconstructions for the five patients (Global results).

9.5 Discussion

Three-dimensional printing was created in 1984 by Charles W. Hull and later commercialized by 3D Systems Corp. (Rockhill, SC, USA) in 1989 (Horvath, 2014). Since its creation, this technology has been considered a unique and rapidly expanding technology with a wide application variety ranging from in-home use to medical and industrial applications. 3D printing can facilitate medical personnel training, pathology simulation, device testing, and pre-surgical planning in the medical practice. This technology could also be used to educate patients (92)(95)(96)(97)(98).

Several printing methods are available, and they take advantage of unique material properties to selective fix layers on top of other layers (92). The great variability of 3D printers and printing materials has become problematic for this technology as standardized protocols for manufacturing and validating 3D printed models are not available. This lack of standardized protocols is raising questions about the accuracy of 3D printed models (90).

Cumulative errors across the printing process reduce the accuracy and reproducibility of 3D printed models, including those generated from medical images (99). Earlier evaluations have reported discrepancies between 3D printed models and segmented anatomies for models generated using voxel images (<1 mm [typically <0.4 mm] and <3% [typically < 1%]) (91). Also, printing hollow and flexible neurovascular models resembling real tissue is challenging (100). We surpassed these difficulties during our evaluations, as we generated accurate and hollow 3D printed models of intracranial aneurysms from patients' angiography. The differences between the 3D printed models' and patients' aneurism geometries were reasonable for our purposes. These findings are relevant as they suggest that our 3D printed models could be used for simulating endovascular procedures.

Other studies have addressed the validation of neurovascular 3D printed models using dummy surgical interventions carried out by neuro-interventionalist and students (101)(102)(103)(104). However, the conclusions of these evaluations were limited, as they used subjective means in their validations. The accuracy and utility of the 3D printed models were assessed visually or using Likert questionaries filled by participants following the dummy interventions (102). We used a quantitative and objective method during our validations. We used VTMK to compare the geometries of the intracranial aneurism surfaces between patients and their 3D printed models. This quantitative and objective strategy constituted a more rigorous means of validation.

A recent study similar to ours also implemented a quantitative and objective method to validate 3D printed models. These evaluations used fused deposition modeling (FDM) or the PolyJet technology for printing 35 models, including large (aortic) vessels, small (coronary) vessels, aortic aneurysms, and aortic dissections 3D printed models. The authors performed

the surface accuracy analysis using semi-automated "interactive translation" and "global registration" tools that allowed them to compare aneurism meshes generated from STL files of the patients and 3D printed models. In this case, the authors used the part comparison analysis (PCA) tool to estimate deviations on triangles of the juxtaposed meshes. The authors showed, using a color scale and a histogram, that the FDM-3D printed models of the aortic aneurysms were overall accurate (green), despite a minor breakpoint in the visceral part of the aorta (vascular branches) that showed more significant deviations. The PCA of these modes showed a mean deviation value of 0.100 mm. The accuracy of the PolyJet-3D printed models was also overall satisfactory (green) in these evaluations, but the mean deviation was higher for these models (0.15 mm) (105). These evaluations are in agreement with our findings. However, it should be emphasized that obtaining accurate 3D printed models of smaller structures such as intracranial aneurysms comes with an increased challenge.

We used an SLA 3D printer to generate the 3D printed models in our evaluations. The SLA printing technology uses a low-power ultraviolet laser to solidify a liquid photosensitive polymer. We found that the time between the acquisition of the patient's DICOM file and the generation of the STL file of the 3D printed model was reasonable, considering that the printing process is independent of the operator and can be done at any time. Our average printing time was 7 hours, which was in line with the four hours reported by Blaszczyk et al. and shorter than that of other evaluations reporting printing times between 2 days and one week and a half (106)(107)(108).

Establishing laboratories that produce 3D printed models is becoming common in medical practice, and our study showed the utility and feasibility of starting a 3D printing laboratory in a Neurointerventional Radiology Service.

9.6 Conclusion
Our evaluations showed that 3D printed models of intracranial aneurysms are accurate, having surfaces that resemble that of patients' angiographies with 80% cumulative deviation below 0.21 mm.

C h a p t e r

10.

The Woven EndoBridge device, an effective and safe alternative endovascular treatment of intracranial aneurysm
Literature review

Chapter contents

10.1 Introduction

Endovascular treatment has become the primary option for patients with intracranial aneurysms (109). Wide-Necked Bifurcation Aneurysms (WNBAs) represent between 26 % and 36 % of all cerebral aneurysms (110) and include aneurysms located at the internal carotid artery (ICA), middle cerebral artery (MCA), anterior communicating artery (ACA), and basilar artery bifurcations (111). The endovascular treatment of WNBAs is challenging because it should lead to aneurism occlusion while preserving the main bifurcation vessels that usually originate at the aneurysm neck (110)(111). Various techniques have been developed to address these challenges, including embolization with coils, stent- or balloon-assisted coils, and Flow-Diverter Stents (FD). However, some of these techniques have limitations. For example, Some are exclusive for unruptured aneurysms and need long-term dual antiplatelet therapy (109) (111).

The Woven EndoBridge device (WEB; Sequent Medical, Aliso Viejo, CA) was developed as an alternative to treat WNBAs (110). Europa began using this device in 2010 (109), and in January 2019, the Food and Drug Administration (FDA) approved its use in the United States. The FDA approval included the use of the WEB device for treating ruptured and unruptured wide-neck aneurysms of the ACA, MCA, ICA, and basilar artery bifurcations (109) (112). The WEB device consists of a self-expanding, oblong, or spherical-braided mesh of nitinol threads with a platinum core that unfolds inside the aneurysm sac. Blood flow into the aneurysm sac is interrupted after the mesh covers its neck, leading to thrombosis and aneurysm exclusion and providing a solid network for endothelial tissue development (109) (112).

The Initially WEB device design (2010) consisted of a high-profile double layer (WEB-DL) of nitinol delivered through 0.027, 0.033, and 0.038-inch high-profile microcatheters. Within three years (2013), the WEB device evolved into a low-profile single nitinol layer (WEB-SL and WEB-SLS) administered through 0.027-inch microcatheters for WEB device sizes 4 to 7 mm. In 2015, the WEB 21 system (0.021-inch microcatheters for WEB sizes 4 to 7 mm) was released, followed by the WEB 17 system (0.017-inch microcatheters for WEB sizes 3 to 7 mm) in December 2016 (109). Technological advances in the newest WEB device versions (WEB-SL, WEB-SLS, WEB 21 system, and WEB 17 system) allow microcatheters to navigate tortuous vessels. On the contrary, the original design (WEB-DL) only permitted

navigation through straight vessels (109). This chapter is a literature review about the WEB device and addresses the efficacy and safety of this device for the endovascular treatment of ruptured and unruptured intracranial aneurysms.

10.2 Objectives

Review the literature about the WEB device and its efficacy and safety in the endovascular treatment of ruptured and unruptured intracranial aneurysms.

10.3 Methods

This chapter is a systematic literature review on the endovascular treatment of intracranial aneurysms with the WEB device. The literature included was from 2010 and older since the WEB device was introduced this year. We followed the PRISMA-P guidelines (preferred reporting items for systematic review and meta-analysis protocols) and used the PubMed and ScienceDirect databases.

The PubMed search was conducted on the 21 of May 2022 using the algorithm (((((WEB device[Title/Abstract]) OR (WEB[Title/Abstract])) OR (Woven EndoBridge (WEB[Title/Abstract]) device)) OR (Woven EndoBridge[Title/Abstract])) OR (intra saccular flow diverter[Title/Abstract])) AND ((((aneurysm[Title/Abstract]) OR (intracranial aneurysm[MeSH Terms])) OR (ruptured[Title/Abstract])) OR (unruptured[Title/Abstract])). The ScienceDirect search was conducted on the same day with the algorithm Year: 2010-2022 Title, abstract, keywords: (WEB OR WEB device OR Woven EndoBridge) AND (intracranial aneurysm OR aneurysm OR ruptured Or unruptured).

We imported the articles into the Rayyan-Intelligent systematic review (113), where two independent authors (D.M and D.D) reviewed the title and abstract to eliminate irrelevant articles and duplicates. The inclusion criteria for selecting the studies was that they should evaluate the treatment of intracranial aneurysms with the WEB device and report the results and complications associated with embolization. We excluded case reports, commentaries, conference abstracts, reviews, and studies not reporting results.

We focused on the variables: study design, number of patients, number of aneurysms treated, type of aneurysm, number of ruptured and unruptured aneurysms, rate of adequate occlusion according to the Digital Subtraction Angiography, thromboembolic complications, other complications, retreatment at follow-up, ruptured at follow-up and mortality.

10.4 Results

We identified 691 articles about the WEB device, 523 from PubMed, and 168 from ScienceDirect. We excluded 136 duplicated articles and reviewed the title and abstract of the remaining 555. Five hundred twenty-five articles did not pass the inclusion criteria, leaving 30 articles for full content review. Only 22 articles fulfilled all the review inclusion criteria (Figure 35,

Table 10). The studies in these articles involved 1705 patients and 1224 aneurysms, including 475 ruptured aneurysms mostly related to the MCA, the ICA, and the basilar artery.

Identification of studies via databases and registers

Identification

Records identified from PubMed and ScienceDirect:

    PubMed (n = 523)

    ScienceDirect (n = 168)

→

Records removed *before screening*:

    Duplicate records removed (n = 136)

Screening

Title/Abstract screened
(n = 555)

→

Records excluded
(n = 525)

Full-text articles assessed for eligibility
(n = 30)

→

Full-text articles excluded:
(n = 9)

- Duplicate in population (n=4)
- Case report (n=1)

Included

Studies included in review
(n = 22)

Figure 35: Flowchart illustrating the search strategy used for the literature review concerning the use of the WEB device in the endovascular treatment of ruptured and unruptured intracranial aneurysms

Reference	Study design	Patients (n)	Aneurysm treated (n)	Unruptured aneurysms (n)	Aneurysm ruptured (n)	Aneurysm type	Successful WEB placement	WEB DL	WEB SL/S	Additional devices	Antithrombotic therapy	Adequately occlusion immediately	Adequately occlusion follow up	Thromboembolic complications	Other complications	Mortality	Retreatment at follow up	Reruptured
Kewlani B et al. 2022 (114)	RCS	74	74	46	28	Saccular	74	0	74	8	none	48	25	5	1	1	6	0
Pierot L et al. 2018 (115)	PMCS	106	169	155	14	bifurcation	163	78	85	12	various	64	43	9	1	0	NS	0
Spelle L et al. 2021 (116)	PMCS	60	60	0	60	bifurcation	56	0	56	3	various	NS	NS	10	13	2	NS	0
Fiorella D et al. 2016 (117)	PMCS	150	150	141	9	Saccular	148	19	129	7	NS	NS	NS	15	5	0	NS	NS
Khalid C et al. (118)	RCS	16	16	13	3	large wide neck	16	3	13	2	ASA/ heparin	11	9	0	3	0	7	0
Lawson A et al. 2017 (119)	RCS	22	25	21	4	Saccular	22	14	8	3	ASA/ heparin	17	16	3	4	0	NS	1
Gherasim D et al (120)	PMCS	10	10	10	0	wide neck	7	2	5	1	heparin	6	6	1	0	0	0	0
Clajus C et al. 2017 (121)	RCS	108	114	67	47	wide neck	110	49	61	13	ASA/ clopidogrel/hep arin	101	68	11	3	8	15	2
Da Ros et al. 2019 (122)	RMCS	33	33	0	33	wide neck	33	0	33	3	none	23	15	2	7	4	NS	0
Lawson A et al. 2018 (123)	PMCS	109	109	91	18	wide neck	104	57	47	NS	various	NS	NS	4	NS	1	NS	1
Caroff J et al. 2015 (124)	PMCS	90	98	65	33	wide neck bifurcation	93	0	93	12	various	29	45	6	7	2	NS	1
Arthur A et al. 2019 (125)	PMCS	150	148	139	9	wide neck bifurcation	148	0	148	0	various	121	121	7	1	0	8	0
De Beule T et al 2021 (126)	RCS	93	95	95	0	wide neck	92	NS	NS	2	heparin	NS	82	2	1	0	4	0
Van Rooij et al. 2018 (127)	PCS	51	59	59	0	all	59	0	59	4	heparin	53	53	0	1	0	3	0
Raj R et al. 2018 (128)	RMCS	33	33	0	33	wide neck	33	0	33	1	heparin	25	25	3	0	0	2	0
Maurer C et al. 2019 (129)	RMCS	117	127	98	29	wide neck	124	0	124	12	various	27	81	5	1	0	NS	NS
Popielski J et al (130)	RMCS	101	102	65	37	wide neck	98	0	98	15	ASA/ clopidogrel	16	63	4	1	1	10	0
Lubicz B et al. 2013 (131)	RCS	19	20	20	0	wide neck bifurcation	19	NS	NS	4	ASA/ heparin	14	17	2	0	0	0	0
Papagiannaki C et al. 2014 (132)	PMCS	83	85	75	4	all	77	77	0	6	heparin	NS	60	9	2	0	9	0
van Rooij et al. 2017 (133)	PCS	100	100	0	100	all	100	0	100	2	none	NS	71	9	1	1	2	0
Behme B et al. 2015 (134)	RMCS	52	55	41	14	all	51	28	23	NS	ASA/ clopidogrel	NS	29	4	1	0	NS	NS
Lescher S et al. 2016 (135)	RCS	22	23	23	0	wide neck	22	NS	NS	6	ASA/ clopidogrel/ heparin	14	19	0	0	0	1	0

Table 10: Characteristics of the studies included in the literature review concerning the use of the WEB device in the endovascular treatment of ruptured and unruptured intracranial aneurysms. ASA = Acetyl Salicyl Acid. NS = Not Specified. NA = Not Applicable. RMCS = Retrospective Multicenter Cohort Study. PMCS = Prospective Multicenter Cohort Study. RCS = Retrospective Cohort Study. PCS = Prospective Cohort Study. MCA= middle cerebral artery. AComm= anterior communicating artery. Pcomm= Posterior communicating artery. SCA= Superior cerebral artery

10.4.1 Study characteristics

All studies were uncontrolled evaluations, including eight prospective multicenter cohort studies, seven retrospective monocentric cohort studies, five retrospective multicenter cohort studies, and two prospective monocentric cohort studies. In these evaluations, the sample size range between 10 and 150 patients. The proportion of ruptured aneurysms was below 50 % in most evaluations, with four being the exception, only including patients with ruptured aneurysms.

Table 10 summarizes the baseline characteristics of these evaluations.

10.4.2 Technical Success and Adjunctive Device

WEB device placement was successfully in 1649 aneurysms (28,1%). The most common devices were WEB-SL and WEB-SLS, used in 1189 patients, compared with 327 having the WEB-DL. Only 116 procedures (1,9 %) required an additional WEB device, some of which also needed coiling or stenting (Table 11). We could not evaluate the correlations between successful WEB device placement, aneurysm location, and device generation, as most studies did not assess these variables (Table 11).

10.4.3 Adequate Occlusion Rate

The rate of adequated occlusion was 33.3% following the treatment and 49.7% at the follow-up (Table 11). We estimated the rate of adequate occlusion using the BOSS scale, considering complete occlusions or occlusions with opacification in the proximal recess or inside the

WEB device as adequate occlusions. We did not analyze the post-treatment follow-up occlusion rate as most studies did not consider this time point in their evaluations.

10.4.4 Complications

Thromboembolic complications were the most common. Eleven hundred patients (6.5 %) suffered thromboembolic complications, including ischemic strokes, minor ischemic strokes, TIAs, arterial thrombosis, arterial dissection, and thrombus formation during WEB device deployment. Fifty-three patients (3.1%) presented other complications, including those associated with vascular access, hemorrhagic complications, intracranial aneurysm rupture, intraoperative rupture, and cerebral edema. Only 3.9 % of the patients required retreatment at follow-up, and only five aneurysms ruptured (Table 11). Most studies did not consider aneurysm location, the WEB device generation, and complications. Therefore, we could not assess the association between these factors.

10.4.5 Mortality

Twenty deaths occurred during procedure and follow-up. Some deaths occurred in the context of a subarachnoid hemorrhage. These deaths were related to thromboembolic events and the mass effect worsening of a pre-existing aneurysm. At the same time, other deaths were associated with patient comorbidities (Table 11).

Study design	Patients (n)	Aneurysm treated (n)	Unruptured aneurysms (n)	Aneurysm ruptured (n)	Successful WEB placement	WEB DL	WEB SL/S	Addition al devices	Adequately occlusion inmediatly	Adequately occlusion follow up	Thromboembolic complications	Other complications	Mortality	Retreatment at follow up	Reruptured
PCS	151	159	59	100	159	0	159	6	53 (33,33%)	124 (77,98%)	9 (5,66%)	2 (1,25%)	1 (0,62%)	5 (3,14%)	0 (0%)

PMCS	758	829	676	147	796	233	563	41	220 (26,53%)	275 (33,17%)	61 (7,35%)	29 (3,49%)	5 (0,60%)	17 (2,0%)	2 (0,24%)
RCS	354	367	285	82	355	66	156	38	205 (55,85%)	236 (64,30%)	23 (6,26%)	12 (3,26%)	9 (2,45%)	33 (8,99%)	3 (0,81%)
RMCS	336	350	204	146	339	28	311	31	91 (26%)	213 (60,85%)	18 (5,14%)	10 (2,85%)	5 (1,42%)	12 (3,42%)	0 (0%)
Total	1599	1705	1224	475	1649	327	1189	116	569 (33,37%)	848 (49,73%)	111 (6,51%)	53 (3,10%)	20 (1,17%)	67 (3,92%)	5 (0,29%)

Table 11: Outcomes of the studies included in the literature review concerning the use of the WEB device in the endovascular treatment of ruptured and unruptured intracranial aneurysms. RMCS = Retrospective Multicenter Cohort Study. PMCS = Prospective Multicenter Cohort Study. RCS = Retrospective Cohort Study. PCS = Prospective Cohort Study.

10.5 Discussion

The literature reports that nearly one-third of the intracranial aneurysms treated using the WEB device result in adequate occlusion following the treatment and half at the follow-up. About 7 % of treatments caused thromboembolic complications, and nearly 3 % caused other complications. These findings demonstrate the WEB device's high procedural success and safety profile, primarily for treating wide-neck intracranial aneurysms.

Klisch et al. reported the first intracranial aneurysms treated with the WEB device in humans in 2012. The report involved two patients with unruptured wide-neck intracranial bifurcation aneurysms who had successful treatments and showed complete occlusion on their magnetic resonance angiography after eight weeks. In the last decade, the WEB device has evolved from a double-layer to a single-layer design, reducing the need for additional techniques or

devices, morbidity, mortality, and associated complications, especially thromboembolic ones (136).

Overall the literature reports high rates of immediate post-treatment adequated occlusion for intracranial aneurisms treated with the WEB device. Asnafi et al. found a rate of 59%, and Armory et al. reported rates ranging between 65% and 86% in their systematic review, which defined a total occlusion or a neck remnant according to the 3-grade Montreal scale as an adequated occlusion (137). We found a lower immediate post-treatment adequated-occlusion rate (33.3%). This lower rate might come from our literature review included more patients with ruptured aneurysms (n=226). Nearly 8 % of our population were patients with ruptured aneurysms, and we had four studies that only included patients with ruptured aneurysms. The number of such studies was two in other systematic reviews. Our lower rate might also be an estimation artifact resulting from the lack of an adequate-occlusion classification standard. The definition of an adequate occlusion varied depending on the study, making it difficult to extract the information and estimate the immediate post-treatment adequated-occlusion rate. We recommend establishing a standardized classification system for occlusion to evaluate studies and assess their reproducibility objectively.

Asnafi et al. reported an adequate occlusion rate of 85% at the medium-term follow-up in their systematic review, using follow-up times below three months (137). Similarly, in their review and meta-analysis, Tau et al. reported an adequate occlusion rate of 81% at the last angiography follow-up, with a median follow-up of 7 months (138). We also found a lower rate, close to 50%, for this parameter. However, comparing this rate between reviews might not be sensible as the follow-up times in the reviewed studies were not necessarily equal. Our review included studies reporting medium-term follow-ups varying between three and six months.

We found only one study concerning the WEB device learning curve. The authors of these evaluations found that the treatment success rate was 40 % when first implemented but raised to 80 % in time. Such learning curves are relevant and must be considered when introducing new devices. In the case of the WEB device, this learning curve shows the relevance of

implementing simulation laboratories for training neuro-interventionalists in using the device (134).

According to the analyzed studies, nearly 10% of WEB device treatments developed complications, and thromboembolic complications were the most common (6,5 %). These complication rates were below those of other reviews. For example, Asnafi et al. reported a thromboembolic complications rate of 8%, and Tau et al. reported an overall complication rate of 14 % (138). Several factors might influence these complication rates, including the anticoagulation protocol. We found no formal consensus about the anticoagulation protocol in the analyzed studies. The protocol selection seemed arbitrary, depending on the authors' preferences. Future studies evaluating the effect of antiplatelet and anticoagulant therapy on the treatment outcomes and complications are necessary.

Despite the complications, we found that the mortality rate for the WEB device is low (close to 1 %) and positively correlates to the proportion of patients with ruptured aneurysms in the evaluations. However, other authors have found higher mortality rates, including Tau et al., who reported a 5% mortality rate at the seven-month follow-up. The one percent mortality rate is comparable to other endovascular techniques, including stent-assisted coils in complex intracranial aneurysms (137)(138).

Predictive factors for inadequate occlusion

Some studies have evaluated which factors, including patient and aneurysm-associated factors, are predictors of adequate occlusion. Kewlani et al. found that patients' age and gender, aneurysm location, size, neck diameter, and dome-to-neck ratios were poor predictors of aneurysm occlusion success (139). On the contrary, the WEB device size seems to be influential. This finding is relevant as it stresses the need to select a suitable WED device for patient safety and immediate and long-term treatment success. Size selection is currently made using a table proposed by the manufacturer and the average of several 2D height and width measurements of the aneurysm dome. However, these 2D measurements might not be the most appropriate for WEB device size selection since intracranial aneurysms

are 3D structures with multiple influencing factors. Size selection should consider the volumetric features of the aneurysm instead.

Selecting the wrong WEB device size can increase complications. A larger than necessary WEB device could protrude into the main arterial vessel, increasing the risk of thromboembolic complications. On the contrary, a smaller than needed device might lead to poor or incomplete long-term occlusion. In this case, a proper WEB device-aneurism wall apposition will not occur, leading to inadequate aneurysm-ostium coverage. Additionally, the wrong WEB device size might lead to using more than one device per patient, generating higher costs for the health system.

10.6 Conclusion
The WEB device is an effective and safe endovascular treatment for intracranial aneurysms.

Computational fluid dynamics for the understanding of intracranial aneurysms' pathology and treatment outcomes
Narrative review

Chapter contents

11.1 Introduction

The natural history of intracranial aneurysms (IAs) consists of three stages: genesis, growth, and rupture (140). The IA rupture is one of the most feared complications and occurs when the tension on the arterial wall exceeds its resistance. This complication presents a mortality rate between 50 % and 60 % and a dependency rate between 30 % and 40 % among survivors. However, most IAs (between 50% and 80%) do not rupture, especially the small ones (141). Predicting an imminent rupture of a small aneurysm is difficult. Still, a further understanding of their pathology and its association with blood-flow patterns in intracranial vessels and IA might help in these predictions.

Gonzalez et al. published the first article using Computational Fluid Dynamics (CFD) for studying IA in 1992. The authors concluded that "computer modeling can improve our understanding of the factors that determine the origin and progression of intracranial aneurysms" (142). More than ten years later (2013), DA Steinman et al. published the first article about the use of CFD for analyzing IA with patient-specific geometry models. Since these early publications, CFD has become a standard tool for analyzing aneurysm morphological features and hemodynamic factors affecting aneurysm wall, determining factors for IA growth and rupture. This analysis comprises several flow-associated variables, including blood-flow pressure and velocity, wall shear stress (WSS), WSS gradient, oscillatory shear index (OSI), wall tension, intra-aneurysmal flow patterns, and viscous dissipation ratios. CFD is also helpful for evaluating different endovascular-treatment techniques and validating new endovascular devices (140)(141).

IA-CFD models fall into two categories depending on their complexity level, ideal and patient-specific. The former helps the analysis of morphological patterns and neuroendovascular devices' efficacy using geometries of assumed anatomies. While the latter uses patient neuroimaging for recreating a volume mesh of the aneurysm (142). Regardless, both models allow the simulation of the blood-flow patterns within the aneurysm, including the inflow and outflow jets. They also provide a visual representation of the impingement zone (the zone where the inflow jet impacts the aneurysm sac), the areas with increased and decreased WSS, the aneurysm inflow-angle, and the flow complexity and stability (143).

11.2 Intrasaccular flow patterns

Cebral et al. proposed a qualitative classification system for intrasaccular flow patterns, which divided the blood flow into four categories independent of the aneurysm morphology. The authors based the categories on the number of vortices in the aneurysm sac and their stability during the cardiac cycle (Table 12). Their evaluations showed that most ruptured aneurysms were types II to IV, characterized by complex or unstable inflow jets, small impingement regions, and small jet sizes (144).

Classification	Definition
Type I	The parent-artery jet is tangential to the aneurysm sac and does not separate at the neck entry.
Type II	When going through the neck, the jet is separated at an arterial junction with a branching vessel and is further oriented tangentially to the aneurysm sac.
Type III	The incoming jet directly impinges the aneurysm dome and subsequently separates.
Type IV	The blood flow has no clear flow organization inside the aneurysm sac.

Table 12: Classification system for intrasaccular flow patterns according to Cebral et al. (86).

11.3 Intracranial aneurysm growth

The IA pathophysiology is poorly understood. Several factors, including hemodynamic factors, seem responsible for the development of this pathology. Hemodynamic evaluations using CFD have shown that a high WSS and a positive WSS gradient induce aneurysm development. Both conditions increase the endothelial cell mechanoreceptors to levels above the threshold, initiating several biochemical cascades. These processes increase the protease production and activation in the vascular-smooth-muscle cells, leading to internal elastic

lamina damage, apoptosis, and thinning and bulge formation in the vascular wall (Figure 36) (143)(145).
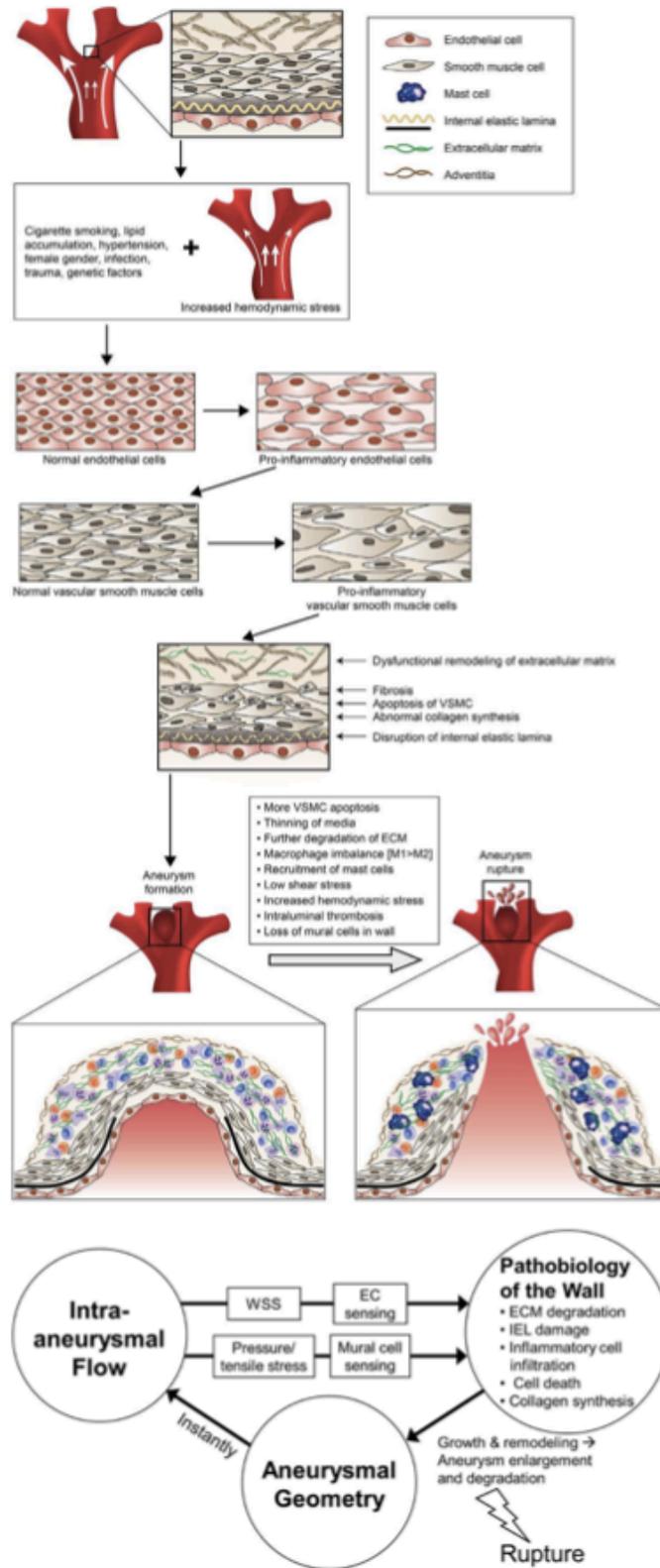
Figure 36: Inflammatory response responsible associated with aneurysm initiation, growth and rupture (Top). The continuous loop between hemodynamics, wall-remodelling and

aneurysm-shape modifications, that ultimately leads to rupture or stabilization (bottom). Taken from "Modélisation in-silico des effets hémodynamiques des prothèses endovasculaires dans le traitement des anévrismes cérébraux: application à l'estimation des chances de succès" by Alain Berod (146).

Regarding the sac-growth morphology, Laplace's law states that cylindrical containers have twice as much wall stress as spherical containers. Therefore, containers will tend towards a spherical shape (Figure 37). However, other aneurysm morphologies may arise due to tension changes within the aneurysm (143)(145). As the aneurysm grows, the WSS decrease in the sac (Figure 38). The oscillatory shear stress provokes an inflammatory response in the endothelium. Then, the endothelial cells generate reactive oxygen species, upregulating surface-adhesion molecules and cytokines in the arterial wall. All these processes lead to increased cell permeability. The endothelium changes and longer blood permanence in the aneurysm sac induce leukocyte migration to the arterial wall as the aneurysm develops, increasing metalloproteinases production. These proteases degrade the extracellular matrix and promote the aneurysm's growth and rupture.

All the above shows that changes in WSS modulate the IA development by destabilizing the aneurysmal wall and the balance between collagen turnover and degradation (143)(145). High WSS areas promote aneurysm-sac development, and low WSS areas aneurismal growth and rupture. Therefore, WSS might be a good marker for IA development (Figure 38).
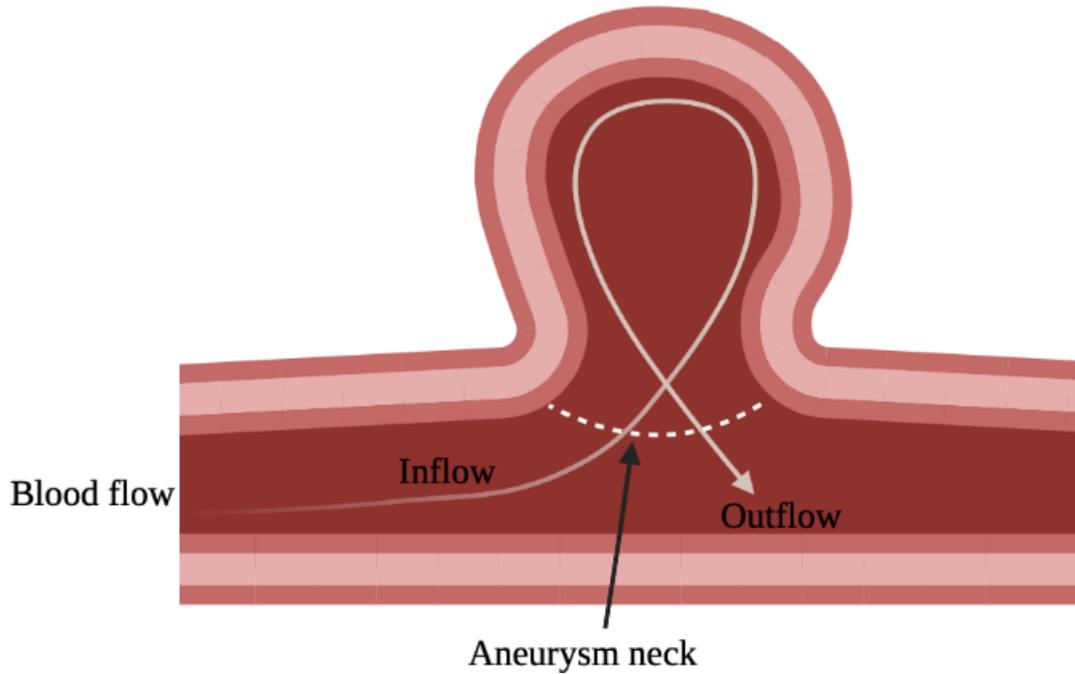
Figure 37: Diagram showing the blood inflow and outflow at the aneurysm neck. Created in Biorender.com by Andrés Felipe Ortiz – Daniela D Vera - Daniel Mantilla.
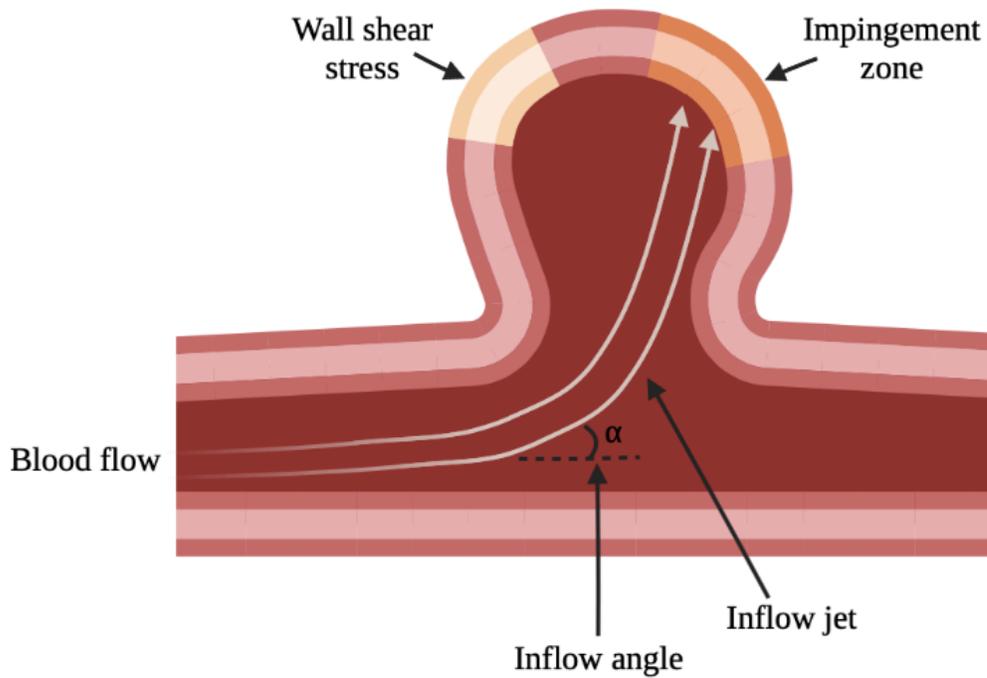
Figure 38: Diagram showing wall shear stress, impingement zone, inflow jet, and inflow angle. Created in Biorender.com by Andrés Felipe Ortiz – Daniela D Vera - Daniel Mantilla.

Few studies have used CFD with patient-specific models to evaluate the IA-growth hemodynamics, as the aneurysm treatment is primarily proactive. Only aneurysms with low rupture risk, generally small aneurysms, are managed conservatively (140). These studies are contradictory regarding their findings about the aneurysm growth-WSS association. For example, Boussel et al. (147) and Miura et al. (148) showed that aneurysm sac growth is related to low WSS, while Cebral et al. (149)(150) showed that aneurysm sac progression was associated with high WSS. Meng et al. argued that high and low WSS influence aneurysm growth and rupture by different means. They claimed that a high WSS and a positive WSSG make the aneurysm area prone to dilatation, while a low WSS and a high OSI drive aneurysm formation (151). The study by Sugiyama et al. followed a patient with six unruptured intracranial aneurysms using catheter angiography every six months. The authors found that the patient had two growing aneurysms adjacent to the right posterior inferior cerebellar artery with different hemodynamic and growth patterns. The proximal multilobular aneurysm had high blood flow and WSS physiological levels, while the distal aneurysm had low blood flow and low WSS in the aneurysm sac (152).

The evaluations give insight into how the aneurysm's hemodynamics affect its growth and rupture. However, their conclusions are limited by the low number of analyzed cases and associated selection bias. More evaluations using a bigger sample size are critical for understanding the aneurysm growth- hemodynamics association.

11.4 Rupture of an intracranial aneurysm

Aneurismal rupture is the most feared IA complication, occurring when the aneurysm-wall tension exceeds the strength. An arterial wall weakening caused by pathological remodeling is responsible for this force imbalance (145). Several studies have addressed the IA rupture, finding that low WSS is the strongest predictor of aneurysm rupture. Looser associations have also been reported for aneurysm rupture and high OSI, low aneurysm formation indicator, prolonged relative residence time, complex flow pattern, irregular flow pattern, and high oscillatory velocity index (153).

Qiu et al. evaluated the correlation between IA morphology and WSS. Their evaluations included 63 patients and 72 aneurysms, including 41 ruptured and 31 unruptured aneurysms. They found an association between IA rupture and the low WSS area proportion (LSAR) (p-value = 0.001), defined as the aneurysm-wall area exposed to WSS below 10% of the parent-artery WSS mean normalized by the dome area. They also found a correlation between IA rupture and increased aneurysms parent WSS ratio (p-value = 0.026). Other findings in these evaluations include the association between narrow-neck aneurysms and increased LSAR (p-value = 0.001) and decreased high spatial mean WSS (p-value = 0.001), mean aneurysm-parent WSS ratio (p-value =0.001), highest WSS (p-value = 0.012), and highest aneurysm-parent WSS ratio (p-value =0.001) (154).

Zhou et al. also addressed the WSS-IA rupture association in their systematic review and meta-analysis, which included 22 studies and 1257 patients. They found that ruptured aneurysms were more likely to have low WSS (0–1.5 Pascal (Pa)) (odds ratio [OR], 2.17; 95% confidence interval (CI), 1.73–2.62). They also showed that patients with ruptured aneurysms had lower mean WSS than patients with un-ruptured aneurysms (0.64 vs. 1.4 Pa) (p-value = 0.037) when pooling 14 studies. Regarding the aneurysm location, posterior communicating artery aneurysms had a lower mean WSS (0.51 Pa) than middle cerebral artery aneurysms (1.1 Pa). Finally, the authors showed that a high OSI was prevalent in ruptured aneurysms when pooling 15 studies (155). These findings should be enough to demonstrate that low WSS is a good predictor of aneurysm rupture.

11.5 Recanalization after embolization

As mentioned above, endovascular management is the most common treatment for patients with IA due to its efficacy and safety. CFD and advances in neuroimaging have permitted adequate modeling of IA hemodynamics. Therefore, they have become a common alternative for assessing parameters affecting the effectiveness of endovascular treatment. The coil packing density, i.e., the coils per aneurysm volume ratio, is among these parameters, with the literature considering it as a good predictor of complete occlusion. Morales et al. made three 3D models for three patients with IA to prove that the coil packing density and configuration impacted the coil embolization. The authors showed that the IA of untreated patients had high-velocity regions in the aneurysm entry zone and distal wall. Then, they

showed that coil embolization reduced the Intra-aneurysmal blood flow velocity and wall WSS decreased, with the first coil decreasing the flow velocity by more than 50%. The authors found that these decrements correlated to the coils' packing density but were not affected by the coils' configuration at high packing densities (close to 30%) (156).

Schirmer and Malek used CFD to assess the coil embolization of a spherical sidewall aneurysm in a curved main vessel. The coils simulation showed a reduction in the intra-aneurysmal blood flow and energy flux into the dome due to coil embolization. The authors also noticed the coil embolization reduced the WSS and its gradient. Partially occluded recurrent IA had higher WSS, and aneurysm recanalization coincided with high WSS areas in the IA residual neck (157)(158). The orientation of the coil was relevant for inducing these alterations, with the parallel orientation being the most effective, followed by the transverse and orthogonal orientations.

A similar study by Li et al. used CFD to evaluate the hemodynamic characteristics of the IA neck of 17 patients with complete occlusion before and after treatment. The evaluation included ten stable and seven recanalized lesions and used patient-specific 3D digital subtraction angiography data. The WSS and spatially averaged WSS at the aneurysm neck during the systolic peak were similar (p-value = 0.914 and p-value = 0.322, respectively) between patients with stable and recanalized lesions before treatment. Nevertheless, the flow pattern changed after embolization, and the WSS at the IA neck differed between the two groups of patients. The maximum WSS and spatially averaged WSS at the aneurysm neck during the systolic peak were higher (p-value = 0.021 and p-value = 0.041, respectively) for patients with recanalized lesions (159). Using CFD, Park et al. also found high WSS at the neck of recurrent aneurysms. This analysis included virtual models of five embolized IA with immediate complete occlusion. These models used the 3D rotational angiography taken after embolization and during follow-up. The results of the Park et al. study align with the Li et al. findings showing that high WSS is associated with lesion recanalization (160).

Some CFD simulations have evaluated the aneurysm treatment with flow-diverter stents (FD). In these evaluations, Larrabide et al. found that the aneurysm morphology, position,

and orientation concerning the main vessel affected the hemodynamics of the aneurysm following FD placement. They found decreased intra-aneurysmal blood flow and increased redirection of blood flow to the main vessel in aneurysms located far from the curvature peak, aneurysms on the bend inner side, aneurysms with no proximal stenosis, and large aneurysms (161). Mut et al. compared the hemodynamics of aneurysms with rapid (complete occlusion at three months) and slow (complete occlusion at six months) occlusion following FD placement. They evaluated 23 aneurysms and found that rapid occlusion occurred in patients with decreased post-treatment mean blood velocity (1.13 cm/s vs. 3.11 cm/s, p-value = 0.020), inflow rate (0.47 mL/s vs. 1.89 mL/s, p-value = 0.004) and shear rate (20.52 1/s vs. 32.37 1/s, p-value = 0.020) (162). Ouared et al. assessed the predicting factors for a successful aneurysms treatment with FD. They found that one-third reductions in blood velocity in the aneurysm following the treatment led to successful outcomes (163).

The above shows that CFD is a valuable tool for studying aneurysm hemodynamics. Understanding how blow-flow patterns in the aneurysm influence the outcome of endovascular treatment is critical for the well-being of patients with IA. Therefore, we conclude that research regarding the aneurysm hemodynamics before and after treatment is of interest for neuro-interventionists since it can provide information relevant for predicting the treatment outcome.

12.

Computational fluid dynamics analysis for the treatment of intracranial aneurysms with Woven EndoBridge devices
Review

Chapter contents

12.1 Introduction

The development of Flow-diverter stents (FD), specifically the Woven EndoBridge device (WEB; Sequent Medical, Aliso Viejo, California), for treating intracranial aneurysms began in 2010. The WEB device disrupts the blood flow at the aneurysm neck, promoting stagnation and gradual thrombosis (136). Neuro-interventionalist primarily use the WEB device for treating complex and high-risk aneurysms such as wide-neck and wide-base bifurcation intracranial aneurysms because other techniques increase the risk for patients (164). Also, the WEB devices do not require long-term antiplatelet therapy and work for ruptured aneurysms (165).

Recent studies have demonstrated that WEB devices are safe and effective. These studies found adequate occlusion rates between 47 % and 85 % for these devices six months following the procedure (166). A meta-analysis also showed that WEB devices have initial adequate and complete occlusion rates of 98 % (95 % coefficient intervale (CI), 95 %–100 %) and 38 % (95 % CI, 25 %–50 %), respectively. Also, It found that they have the latest follow-up adequate and complete occlusion rates of 91 % (95 % CI, 84 % – 98 %) and 61 % (95 % CI, 46 % – 75 %), respectively (167). Some evaluations have shown that inadequate aneurysm occlusion may relate to the aneurysm's location, size, and morphology. Hemodynamic patterns might also be associated with the lack of immediate or adequate occlusion observed for some aneurysms six months after treatment with the WEB device.

Modeling blood-flow dynamics for intracranial aneurysms following the intrasaccular device implantation is essential for understanding the effect of WEB devices on blood-flow dynamics and subsequent outcomes. Knowing before implantation how the device will impact the aneurysm's hemodynamics could help identify which aneurysms will occlude immediately and which will remain patent and would benefit from a different procedure or device (168). Several studies have used Computational Fluid Dynamics (CFD) to assess the association between blood-flow patterns and intracranial aneurysms onset, growth, morphology, and rupture (27)(151)(170). A study including over 210 intracranial aneurysms showed that ruptured aneurysms were associated with increased inflow concentration indices (ratio = 1.52 ± 0.01, p-value < 0.004) (150). Similarly, an evaluation including 22 patients with intracranial aneurysm found that large aneurysms have more complex hemodynamic

patterns than small ones (171). Other evaluations have shown that high or low Wall Shear Stress (WSS) also contributes to aneurysms damage and rupture (151)(154).

Few CFD evaluations regarding intracranial aneurysms treated with FD have focused on the association between hemodynamics and treatment outcomes. Among these evaluations, Chong et al. evaluated the hemodynamic profiles of intracranial aneurysms and found that the jet flow speed decreased within the aneurysm sac in patients with successful treatment. The jet flow speed remained constant for patients with unsuccessful treatments (172). Other evaluations have found that the WSS and the WSS Gradient decrease following the treatment (173). Similarly, other studies have shown that FD placement leads to decreased blood inflow and outflow, contributing to aneurysm thrombosis (174).

Simulating the blood flow in intracranial aneurysms treated with FD comes with several challenges. Blood flow simulations must include device deployment models for patient-specific vascular systems while considering factors related to the FD mesh. For example, the models must assume that the meshes are composed of thin wires and leave gaps when interacting with the vessel walls. All these factors influence the hemodynamics of the treated aneurysm, and simulations must consider them (168). The CFD work addressing the different aspects of treating intracranial aneurysms with WEB devices is limited. However, the number of related studies has been increasing since 2017. We believe a literature review on this topic is pertinent, considering the number of publications available. This chapter aims to review the CFD literature assessing the different aspects of the treatment of intracranial aneurysms with WEB devices.

12.2 Objective

To review the Computational Fluid Dynamics literature regarding the treatment of intracranial aneurysms with Woven EndoBridge devices.

12.3 Methods

This literature review included original studies of patients with intracranial aneurysms treated with WEB devices whose treatments had Computational Fluid Dynamics (CFD) during the evaluation and follow-up. The selected articles were English publications from 2010 and older and came from PubMed, Base, Scielo, Scopus, OVID, and Cochrane and Clinical Trials

databases. Among the excluded articles were those about other types of devices and those not assessing the follow-up hemodynamic.

The PubMed search was on May 9th, 2022, using the algorithm (((((((((((((((((((((((((intracranial aneurysms) OR (Aneurysms, Intracranial)) OR (Aneurysm, Anterior Communicating Artery)) OR (Aneurysm, Basilar Artery)) OR (Artery Aneurysm, Basilar)) OR (Basilar Artery Aneurysms)) OR (Basilar Artery Aneurysm)) OR (Aneurysm, Middle Cerebral Artery)) OR (Middle Cerebral Artery Aneurysm)) OR (Aneurysm, Posterior Cerebral Artery)) OR (Posterior Cerebral Artery Aneurysm)) OR (Berry Aneurysm)) OR (Aneurysm, Berry)) OR (Aneurysms, Berry)) OR (Berry Aneurysms)) OR (Brain Aneurysm)) OR (Aneurysm, Brain)) OR (Aneurysms, Brain)) OR (Brain Aneurysms)) OR (Cerebral Aneurysm)) OR (Aneurysms, Cerebral)) OR (Cerebral Aneurysms)) OR (Aneurysm, Cerebral)) OR (Aneurysm, Anterior Cerebral Artery)) OR (Anterior Cerebral Artery Aneurysm)) OR (Aneurysm, Posterior Communicating Artery)) OR (Posterior Communicating Artery Aneurysm)) AND ((((Computational fluid dynamics) OR (cerebral flow dynamics)) OR (Computational Fluid Dynamics (CFD))) OR (CFD))) AND ((((WEB device) OR (WEB)) OR (Woven EndoBridge (WEB) device)) OR (Woven EndoBridge) OR (intrasaccular flow diverter)).

The search for the remaining database was on May 10th, 2022, using the keywords "intracranial aneurysms," "cerebral flow dynamics," "computational fluid dynamics," "WEB device," or "intrasaccular flow diverter." This search used three different keyword combinations: 1. "intracranial aneurysms," and "cerebral flow dynamics," and "WEB device." 2. "intracranial aneurysms," and "cerebral flow dynamics," and "intrasaccular flow diverter." 3. "intracranial aneurysms," and "computational fluid dynamics," and "intrasaccular flow diverter." Then, we used the title and abstract to verify that the articles filled the selection criteria (
Appendix 1).

12.4 Results

The search started with 143 articles, including 129 from Scopus, eight from PubMed, and six from the BASE. This initial search did not include publications from Scielo, OVID, or

Cochrane and Clinical Trials databases. From the 143 articles, we excluded 42 duplicated articles and 98 that did not meet inclusion criteria, leaving three for further assessments. We coss-checked the reference lists of these three articles and found an additional publication meeting the inclusion criteria for four publications to be reviewed (Figure 39).
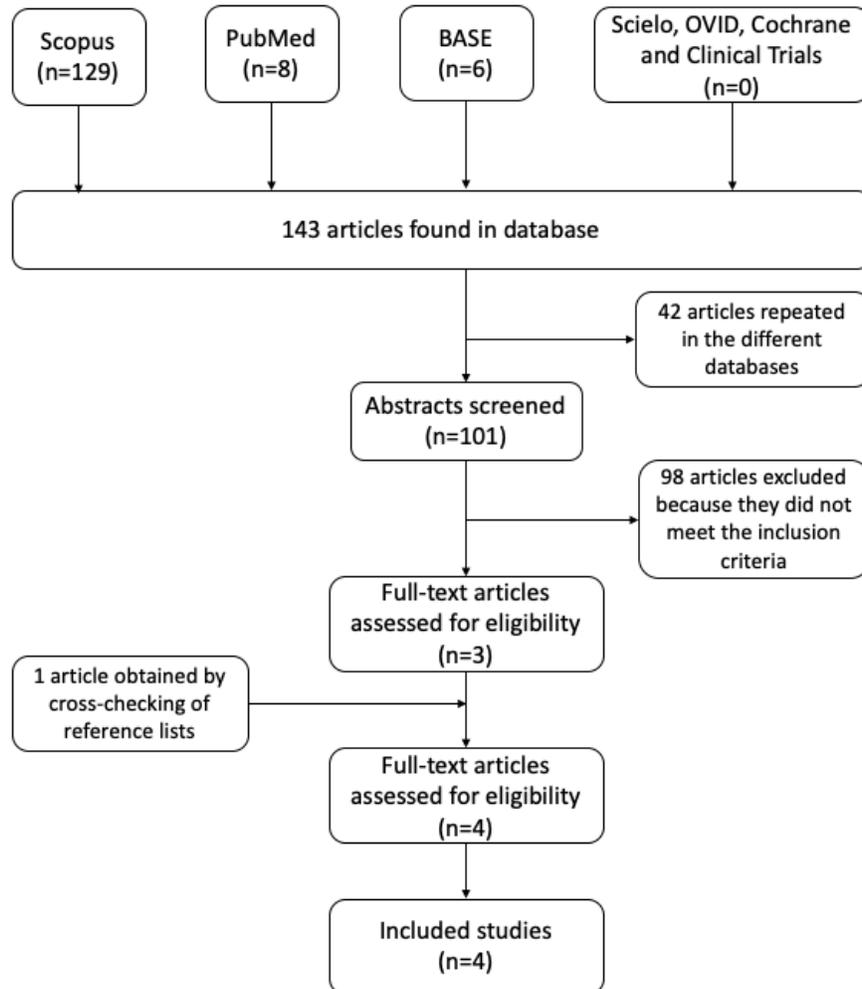
Figure 39. Flow chart showing the article selection process used in the literature review.

Among the four publications, Caroff et al. conducted the first evaluation in 2017. This study included 18 patients (15 women and three men) and 19 basilar tip aneurysms treated with WEB devices. Patients had a first CFD analysis in the pre-operative using their 3D rotational angiography (3DRA) and a second in the follow-up using their digital subtraction angiography (DSA). For the CFD analysis, the authors used a novel CFD package designed for aneurysm research (Hemoscope v1.4, EBM Corp., Japan).

The study evaluated aneurysm morphological variables, including volume, neck size, and aspect ratio, defined as depth to neck ratio. It also assessed blood flow variables, including aneurysmal inflow rate (flow rate entering the aneurysm through a neck) and inflow ratio (flow ratio going inside aneurysm over parent artery flow) (Figure 40) (175).
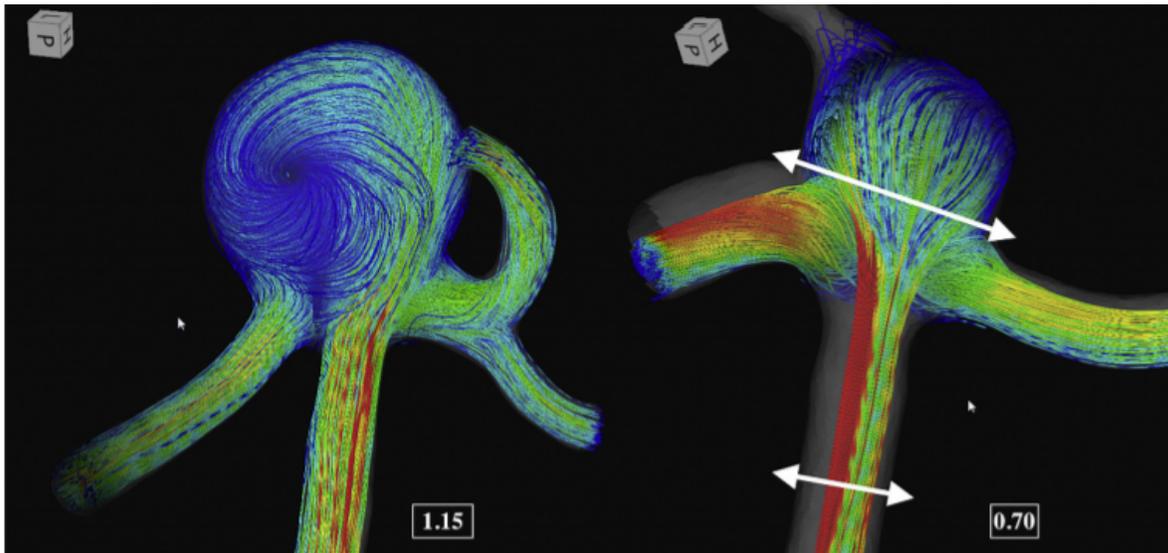
Figure 40. Streamline view showing two aneurysms. White arrows illustrate the cross sections of the parent artery and aneurysm neck used in the Computational Fluid Dynamics (CFD) analysis to calculate the inflow ratio. On the left, the image shows an aneurysm exposed to high flow. Here, the parent artery flow enters the sac through the neck generating an outflow vortex that re-enters the aneurysm (CFD inflow ratio is 1.15). On the right, the image shows an aneurysm exposed to light flow. Here, only ¾ of the parent artery flow enters the sac (CFD inflow ratio is 0.70). Color scales are different between right and left. Image from "A computational fluid dynamics (CFD) study of WEB-treated aneurysms: Can CFD predict WEB "compression" during follow-up?".

The CFD analysis was possible in all patients, and the authors found a mean inflow ratio of 0.8 (range: 0.48 – 1.39) (Figure 41). However, they found no correlation between the CFD absolute-aneurysm-inflow rate and the WEB device compression (p-value = 0.21). Inaccuracies in the estimations of model boundary conditions might be responsible for this lack of correlation. Modeling the blood flow in the intracranial aneurysm requires

information about the model boundary conditions, and the absolute-aneurysm-inflow rates dramatically depend on these estimates' accuracy. Defining the model boundary conditions is challenging, and the literature still argues about the pertinence of using modeled versus measured conditions.

Caroff et al. used the aneurysmal-inflow rate, a parameter described elsewhere, for the practicality of the CFD measurements as using a ratio reduces the variation induced by the boundary conditions. The authors found a correlation between the aneurysmal-inflow rate and the basilar tip aneurysms recanalization. They also found a strong correlation between the intra-aneurysmal and parent artery flows ratio and the WEB device compression (p-value = 0.018) (175).

Caroff et al. also assessed how the device's compression, which has a multifactorial origin, relates to CFD. They found a clear association between the device's compression and the aneurysm flow exposure, as represented by the CFD inflow ratio. The mean inflow ratio was 0.93 ± 0.25 for the devices suffering compression compared with 0.67 ± 0.17 for those not suffering compression (p-value = 0.018), and the optimal operating point was 0.79 (sensitivity 0.73; specificity 0.88) (175).
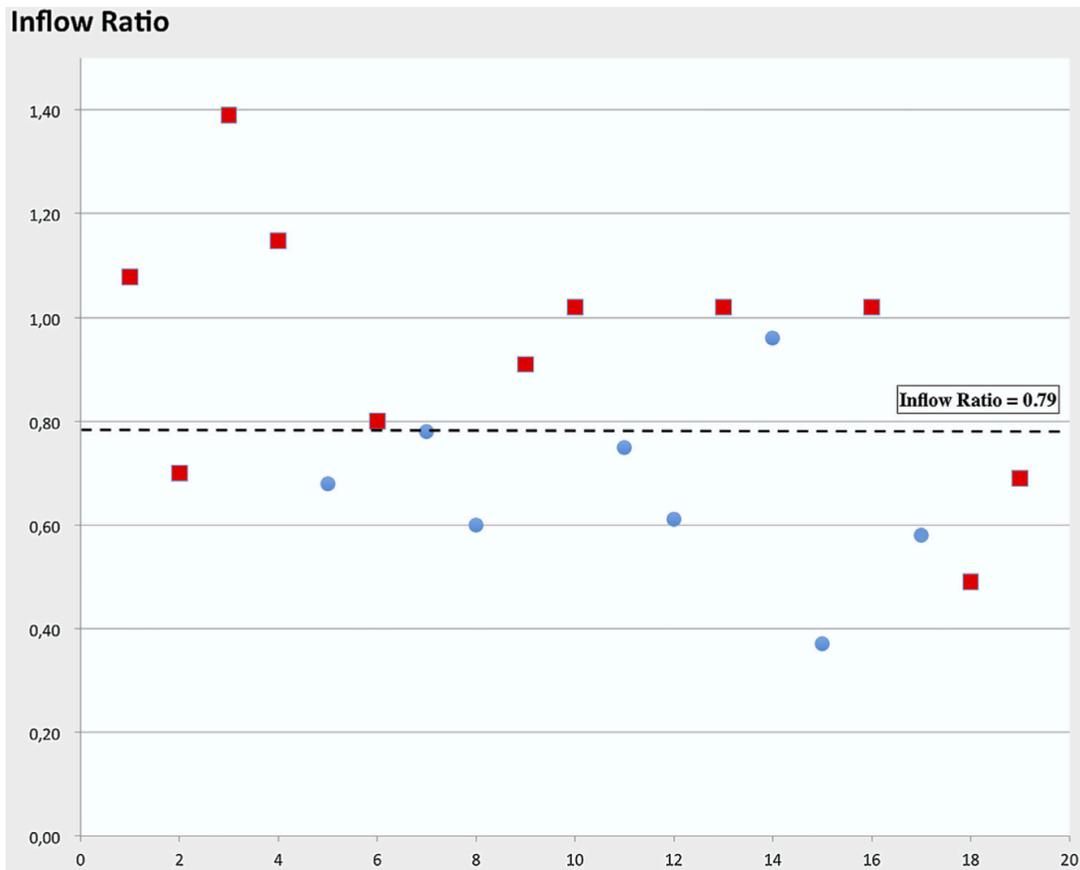
Figure 41: Results of the Computational Fluid Dynamics (CFD) analysis. Each point represents an aneurysm sorted by chronological order. Red squares represent WEB devices suffering compression, and blue circles represent no WEB devices not suffering compression. The ordinate shows the CFD inflow ratios. According to the Receiver Operating Characteristic (ROC) curve analysis, the optimal operating point was 0.79 (sensitivity 0.727; specificity 0.875). A tendency toward fewer WEB device-shape modifications during the follow-up over time, i.e., after November 2013. Image from "A computational fluid dynamics (CFD) study of WEB-treated aneurysms: Can CFD predict WEB "compression" during follow-up?".

Mut et al. published the second study included in this review in 2019. This study aimed to develop a technique for modeling the hemodynamics of intracranial aneurysms treated with intrasaccular devices using the 3D-DSA images from the Deploy tool. The 3D-DSA reconstructions used a 0.25 m voxel size and the entire portion of the parent artery for inflow boundary conditions. Here, the parent artery was typically extended proximally from the

cavernous internal carotid artery in the anterior circulation to the vertebral artery in the posterior circulation. The authors used a nonshrinking algorithm to eliminate noise and smooth surface triangulations. They also used an advancing front method to generate unconstructed isotropic grids. The grids comprised tetrahedral elements with a maximum element size of 0.2 mm and at least 10 points across the vessel diameter. The meshes typically included between 2 million and 5 million elements and represented the vascular domain before being treated. Contact forces were applied when the tetrahedral mesh came in contact (i.e., penetration distance greater than zero) with the vascular wall. Also, radial forces were computed as spring-like forces between the cylinder's centerline and points of the cylindrical surface where the force was zero, and the distance was equal to the specified device dimension (radius) (168).

The authors used the cheDeploy tool for virtual deployment of intravascular devices within reconstructed vascular models, allowing them to manually generate and place the simulated device inside the vascular reconstructions. The simulated devices were a series of wires arranged as a mesh of two-dimensional elements and mapped into an expanded cylindrical surface. The authors discretized the device wire segments as a series of overlapping spheres with a diameter equal to the wire thickness and added virtual markers to the devices. Then, they placed the device according to the 2D angiographic images of the patients, matching the device markers from two images.

The study included the models of four patients with aneurysms in the anterior communicating artery (Figure 42) and three WEB device designs. The first design was a single layer (SL) WEB device with 144 wires, 80 braid angles, and 25 um wire thickness. The second was a dual-layer (DL) WEB device with 2x 144 wires, 80 braid angle, 19um wire thickness outer layer, and 38 um wire thickness inner layer. The device diameters were smaller than 8 mm, and the number of wires in each layer was 108 instead of 144. The third was an SL spherical (SLS) WEB device with 144 wires, 80 braid angles, and 25 um wire thickness (168).

Pulsatile flow conditions were prescribed at the intracranial aneurysm inlet using the Wormersley velocity profile and flow waveforms derived from phase-contrast MRI measurements in normal subjects and scaled with a power of the inflow vessel area (176).

The authors used the unsteady incompressible Navier-stokes equations for blood flow modeling. The equations were solved using finite elements and a fully implicit formulation. The models assumed that the flow was a Newtonian fluid and that the walls were rigid. They also used outflow boundary conditions consistent with Murray's principle of minimum work at the model outlets (168)(177). Simulations included two cardiac cycles using a constant time-step size and 100 time-steps per cycle, and the analysis used the results from the second cycle (168)(178).

The authors used an immersed boundary strategy for post-treatment hemodynamics modeling based on unstructured grids. This approach identifies the mesh elements edges cut by the surface of the endovascular device, introducing new zero-velocity boundary conditions at the intersection points. The main advantage of an immersed boundary approach is that it can deal with complex device geometries that may be in contact with or form minimal gaps with the vascular wall without generating a new body conforming mesh. The authors also used a second refinement strategy over the wires located at the aneurysm hole and not at the dome (168).

Mut et al. computed the mean inflow rate (Q), the mean aneurysm kinetic energy (KE), the mean aneurysm shear rate(SR), the mean aneurysms velocity (VE), the mean aneurysms vorticity (VO), the mean viscous aneurysm dissipation, and WSS by integration over the aneurysm region and averaging over time. Q and VE were the only variables associated with occlusion rates in the treated aneurysms. These findings align with other evaluations associating changes in the mean aneurysm flow amplitude (MAFA) with occlusion after treatment (162). The authors simulated the cases with full and partial refinement, finding less than a 1% difference in inflow rate and mean velocity (168).
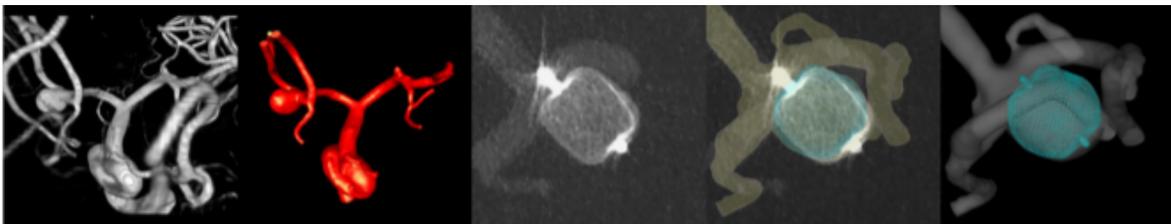
Figure 42: Representative angiography images showing from left to right the 3D images of reconstructed vascular models, the 2D image of the deployed device, the 2D image showing

157

the superposition of the device and vascular model, and the 2D image showing the superposition of the simulated device and the vascular model. Image from: "Image-based modeling of blood flow in cerebral aneurysms treated with intrasaccular flow diverting devices."

Using a partial mesh to optimize computational cost did not compromise the results of the Mut et al. evaluations, as the estimates agreed well with the complete mesh refinement. This finding is essential for future CFD studies, especially those addressing the hemodynamic simulations of large series of intracranial aneurysms treated with intrasaccular devices (168). Out of the four analyzed aneurysms, one was entirely, and two partially occluded six months after treatment. No follow-up data were available for the fourth aneurysm. The aneurysm with complete occlusion was the one with the slowest before and after treatment flows (168). The results from these evaluations indicate that analyzing the likelihood of subsequent total occlusion rather than parameter changes resulting from the treatment is more relevant when assessing the hemodynamic environment created after device implantation.
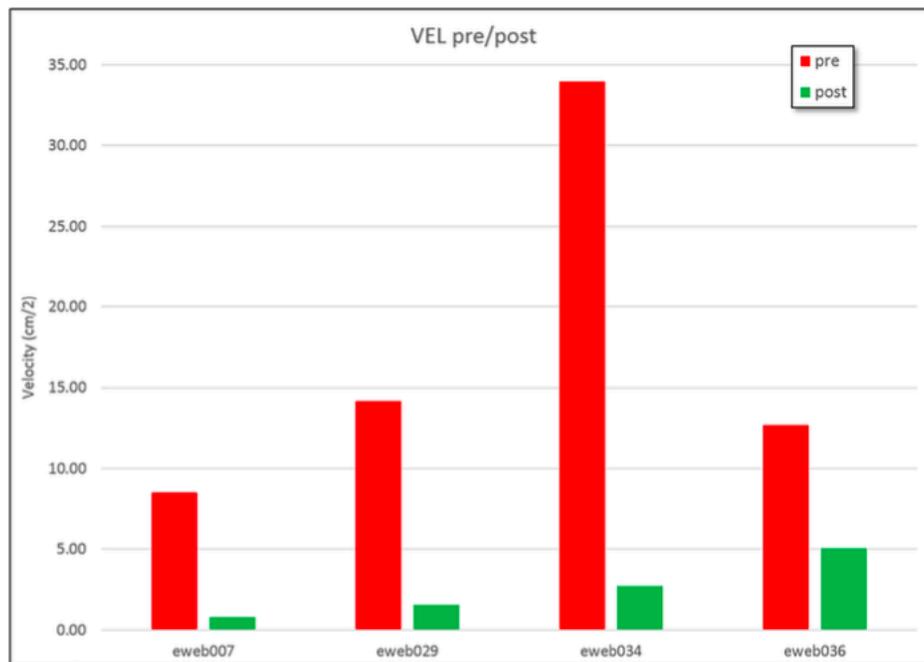
Figure 43: Mean blood flow velocity before (red bars) and after (green bars) implantation of the intrasaccular devices in four intracranial aneurysms.

The third article in this review belonged to Gölitz et al. and was published in 2020. This study comprised 40 patients treated for intracranial aneurysms, including nine ruptured aneurysms, and a 6-month follow-up was available for the patients. The authors performed a time-density curve (TDC) analysis from pre and post-WEB device deployment 2D DSA series. They selected the regions of interest distal to the guiding catheter tip and measured the extent of aneurysm occlusion according to the BOSS classification (179). The variables analyzed included the relative time-to-peak (rTTP) of the filling of the aneurysm (time from the nadir of the curve to maximum peak, measured in seconds) and the aneurysmal inflow velocity/wash-in (average slope of the curve before the peak, measured in density change per s). They also included the outflow velocity/wash-out of the aneurysm (average slope of the curve after the peak, measured in density change per s) and the mean flow velocity ((aneurysmal inflow + outflow velocity)/2) (Figure 44) (179).

These evaluations used the commercially available iFlow software (syngo iFlow, Siemens AG, Healthineers) that converts DSA images into color-coded images and included aneurysms with different locations. The analyzed aneurysms were 15 aneurysms (38 %) at the middle cerebral artery (MCA) bifurcation, 12 (30 %) at the anterior communicating artery, five (13 %) at the carotid terminus, four (10%) at the basilar tip, three (8 %) at M2 segment, and one (3 %) at posterior cerebral artery (179).

Gölitz et al. found that the rTTP of aneurysmal filling suffer a 53 % prolongation (p-value = 0.001) following WEB device placement. They also found a 49 % decrease in the mean flow velocity and a 33 % decrease in the aneurysmal inflow and outflow velocity (p-value < 0.001). Eighteen aneurysms (45%) showed complete occlusion at the six-month follow-up. However, the authors found no association between the evaluated factors and aneurysm occlusion (p-value > 0.05) (179).

Based on their results, Gölitz et al. proposed a post-interventional cutoff of 39 % inflow velocity reduction as a predictor for achieving complete occlusion with an 89 % sensitivity and at the cost of 39 % reductions in specificity. They also claimed that a reduction of the post-interventional outflow velocity below 3% predicted incomplete aneurysm occlusion at follow-up with 100% sensitivity and specificity. However, this statement is based only on two cases (179). No single flow factor was a good predictor of complete aneurysm occlusion (179).
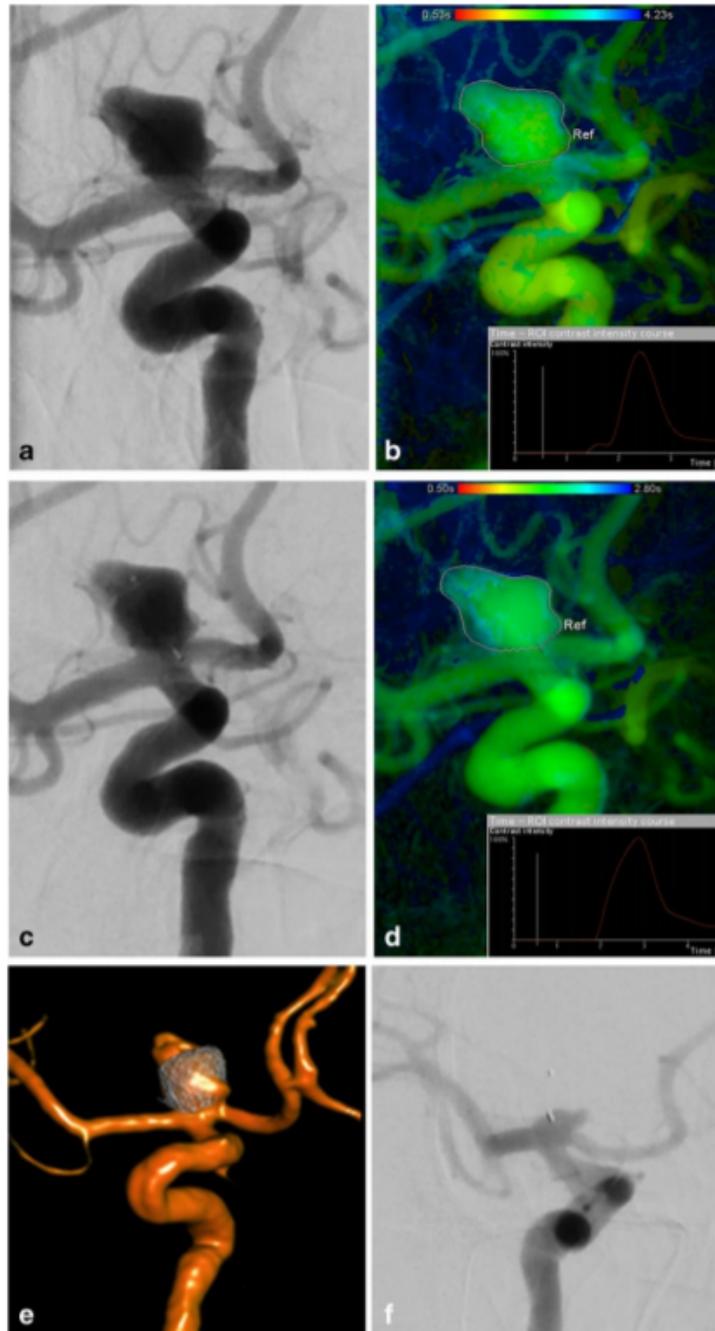
Figure 44: Representing DSA images showing a broad-based aneurysm at the carotid terminus before (a) and after (c) treatment with a WEB device. (b) and (d) The corresponding pre and post-treatment time-density curve (TDC) analysis, reveling that the rTTP of aneurysmal filling was prolonged by 63%, the aneurysmal wash-in/inflow velocity was reduced by 38%, and the aneurysmal wash-out/outflow velocity was decreased by 31% after

160

the WEB device implantation. (e) The 3D rotational run directly after WEB device detachment, confirming the correct device positioning. (f) The six-month follow-up DSA showing an aneurysm remnant (grade 3 according to the BOSS classification) that was re-treated. Imagen from: "What is the hemodynamic effect of the Woven EndoBridge? An in vivo quantification using time-density curve analysis"

The fourth publication addressed in the review included 36 intracranial aneurysms treated with the WEB device representing 39 patients (35 women and four men) with a mean age of 64. The patients had 3D rotational angiography before treatment and 2D DSA before and after WEB device implantation. The authors reconstructed the vascular anatomy using the 3D rotational angiography with previously developed methods (180). They used an advancing front grid generator to construct unstructured grids composed of tetrahedral elements that fill the vascular models' lumen (168). Then, they simulated intrasaccular devices and placed them within the vascular models using DSA image-guidance tools and techniques developed elsewhere. The CFD simulations used an in-house finite-element solver to solve the Navier-Stokes equations, imposing pulsatile flow conditions at the inlet boundary by scaling flow waveforms measured in healthy subjects (176). The authors used an immersed boundary method operating on adaptive unstructured grids to simulate the blood flow after intrasaccular device implantation (181). Here, they used two cardiac cycles and considered the results from the second cycle for computing several flow parameters characterizing the aneurysm hemodynamic environment (182). The flow parameters included mean aneurysm inflow (Q), inflow jet concentration (ICI), mean aneurysm velocity (VE), and mean vorticity (VO, corelen) of the intra-aneurysmal-flow pattern. The authors also assessed several geometric parameters, including aneurysm (Asize) and neck size (Nsize), and aneurysm shape (aspect ratio (VOR)) (183)

The authors classified the aneurysm during the follow-up into four categories, A to C. A and B were complete occlusion, with A having no aneurysm or device remnant or filling and B having a small remnant associated with device proximal compartment filling. D and C were incomplete occlusions, with C having a device proximal compartment filling and D having a

distal device compartment filling (183). These evaluations showed that incomplete occlusion associate with large post-treatment aneurysm inflow rates (Q, p-value = 0.02) and small reductions in inflow (ΔQ, p-value = 0.01) and inflow concentration (ΔICI, p-value = 0.03) following the treatment. The pre-treatment and post-treatment blood flow tended to be more complex (larger vortex corelen length) in aneurysms with incomplete occlusion. Still, the differences with completely occluded aneurysms were not statistically supported when adjusting for multiple testing. Regarding the geometrical features, larger aneurysms and wider necks were more prevalent in aneurysms with incomplete occlusion (182).

12.5 Discussion

Modeling the blood flow dynamics of intracranial aneurysms following endovascular treatment with intrasaccular devices, particularly WEB devices, provides essential information regarding the association between treatment outcomes and the flow conditions created in the aneurysm by the treatment. This information is critical for predicting which treatments could lead to complete immediate occlusion of the aneurysm, which could lead to patent aneurysm, and which could worsen due to compression of the WEB device (175).

All the analyzed publications reported decreased blood flow parameters in the aneurysm following the WEB device placement, including the mean, inflow, and outflow velocities. They also reported reductions in the hemodynamic stress of the aneurysm after treatment. According to the CFD analysis, inflow rates greater than 0.8 were related to WEB device compression, while lower inflow rates were associated with complete aneurysm occlusion. However, the latter association was statistically supported only at a 91 % confidence level (p-value = 0.09). Short follow-up periods and small sample sizes used during the evaluations might be responsible for the lack of statistical power. Regardless, more evaluations are necessary to validate these associations.

Caroff et al. found a trend toward reduced CFD inflow ratio in aneurysms with complete occlusion (mean ratio 0.73) compared to those with incomplete occlusion (mean ratio 0.92). However, these differences also had no statistical support. Despite this lack of statistical support, these inflow reductions align with the findings of other evaluations. For example,

Mut et al. saw a lower mean aneurysm entry rate following the treatment in patients with complete occlusion (mean velocity of 0.8 cm/s) compared to those with incomplete occlusion (mean velocity of 1 cm/s) 56 and 2.75 cm/s) in the four analyzed patients (175). Similarly, Gölitz found that the mean flow velocity decreased from 6.24 to 3.44 following the WEB device placement (p-value = 0.001). They also observed a 33 % inflow (density change/s) and a 49 % outflow reduction, and a 52 % prolongation in the rTTP (relative time-to-peak) of the aneurysmal filling (p-value = 0.001) following the treatment. Nonetheless, this study found no differences between patients with complete and incomplete occlusion or between ruptured and unruptured aneurysms (179).

The knowledge gained from the CFD literature about treating intracranial aneurysms with WEB devices is constrained by the low number of clinical studies addressing this topic and the small sample size used by the available publications. Also, simplifications in the aneurysm hemodynamics and incomplete information regarding the patient's blood flow physiology limit the results of the CFD simulations. The multivariate analysis by Carrof et al. showed that adding aneurysm flow information, particularly the post-treatment inflow rate, improved the occlusion probability estimates (175).

During this study, we used the YALES2BIO platform to evaluate the CFD of intracranial aneurysms treated with the WEB device. We assessed the blood flow before and after the simulated WEB device deployment, making a refinement of the device surface and meshes. The knowledge gained with analysis such as this is relevant as the information about the aneurysm's blood flow before the treatment could facilitate the device and endovascular treatment selection. While the post-treatment blood flow information can help predict treatment outcomes.

Cerebral flow dynamics and WEB device

Chapter contents

13.1 Heterogeneous model application to intrasaccular device

Several fields require generating 3D models of objects, including the medical field. 3D images of the anatomies are more informative to clinicians than 2D images. Several methods based on varying strategies are available for modeling 3D surfaces (184). An early approach used planar contours of triangular shapes to reconstruct the 3D model by mapping consecutive contours pairs to approximate the 3D surface. This approach was limited as it could lead to ambiguities when modeling 3D surfaces with multiple contours per plane (185). Alternative methods included the one proposed by Chen et al., which reconstructed the 3D model by dissecting the space in evenly spaced cuboidal voxels (cuberilles) and the one developed by Farrell, which used ray casting and hue lightness to display the surface model (186)(187). Also, an alternative is a method used at the Mayo Clinic, which renders density volumes rather than 3D surfaces. However, this method is more aligned with conventional shadowgraphs that can be viewed from arbitrary angles (188).

Clinicians can use the methods above for generating 3D images of the anatomies. However, these are limited because they ignore helpful information about the 3D medical data and can introduce artifacts. As an alternative, the marching cubes algorithm was developed as a high-resolution 3D modeling algorithm for medical applications. This algorithm creates triangle models of constant density surfaces by processing the data in scan-line order and calculating triangle vertices using linear interpolation. The resulting polygonal representation of the anatomy's surface can be displayed using conventional graphics-rendering algorithms and display systems. An advantage of this method is that it uses 3D medical data to assure inter-slice connectivity and determine the surface's location and gradient (184).

The marching cubes algorithm consists of two general steps. First, the algorithm locates the surface according to a user-specified value and creates triangles. Then, it calculates the surface normals of the triangles to ensure the quality of the surface render.

Considering the advantages of the marching cubes algorithm, we decided to use a heterogeneous model based on this algorithm to assess how the intra-saccular Woven EndoBridge (WEB) device affects the hemodynamics inside bifurcating aneurysms. Only

one Computational Fluid Dynamics (CFD) study has evaluated the outcomes of WEB-treated aneurysms due to the WEB device's recency and complex shape.

We collaborated with Alain Berod in this chapter as he developed the heterogeneous model used in the evaluations. We used the heterogeneous model to create 3D representations of aneurysms treated with the WEB device and used these 3D representations for the CFD calculations. This chapter describes the model's predictions and angiographic outcomes using aneurysms geometries and devices. Analyzing correlations between occlusion scores and hemodynamic parameters was not the aim of this chapter.

13.2 Methods

13.2.1 Study cohort and analyzed variables

This study is a retrospective analytical evaluation of patients treated with endovascular treatment with WEB devices for intracranial aneurysms. The study cohort included 18 years old patients or older with a diagnosis of ruptured or unruptured intracranial aneurysm and treated with a single WEB device at the Neurointerventional radiology service of CHU Gui-de-Chauliac, Montpellier, between 2014 and 2017. The study only considered patients having high-quality DICOM 3D series and 3D digital subtraction angiography (3D-DSA) follow-up according to the visual inspection. The hospital provided the data as an anonymized database, and we did not collect the patient's informed consent due to the study nature. We did not modify the clinical protocol or the WEB device for our evaluations. These evaluations exclude patients treated with other endovascular devices, including flow-diverter stents, stents, and coils, to avoid bias and focus on the WEB devices' effects on blood-flow patterns. The analyzed data included: (1) DICOM 3D series data before WEB device implantation; (2) 3D-DSA follow-up Beaujon Occlusion Scale Score (BOSS); (3) patient's age and sex; (4) WEB device parameters, including diameter and height; (5) Aneurysm location (internal carotid artery (ICA), middle cerebral artery (MCA), Anterior Communicating Artery (AComA), and basilar artery (BA)); (6) smoking and hypertension comorbidities, when available; and (7) interventional details such as the size of deployed but not detached WEB devices, when available.

13.2.2 Statistical analysis

The demographic and clinical characteristics of patients were analyzed using descriptive statistics. We used Microsoft Excel® (version 16.39) for information extraction.

The evaluations included 27 arterial geometries Table 13, with 60% relating to the MCA, a location prompt for aneurysm development. All interventions used single-layered WEB devices (single-layer (SL); single-layer spherical (SLS)). In the study cohort, most patients were women (70%), and the proportion of aneurysms with incomplete occlusion was 22 %. The lack of homogeneity observed in our patient cohort aligns with other studies (189)(190). However, we must consider these imbalances between groups while analyzing our results.

Case Id	Sex	Age	Hypertension	Smoking	Aneurysm location**	WEB type ***	WEB size	Follow-up delay	Outcome BOSS
2	Masculine	55	No	No	Middle Cerebral Artery	SL	8x4	9	c
3	Femenine	85	Yes	Yes	Middle Cerebral Artery	SL	7x4	3	c
4	Masculine	50	Yes	Yes	Internal Carotid Artery	SL	7x5	4	c
6	Masculine	56	N/A*	N/A	Anterior Communicating Artery	SL	9x4	12	d
10	Masculine	74	Yes	Yes	Internal Carotid Artery	SL	6x4	12	b
12	Femenine	69	Yes	Yes	Middle Cerebral Artery	SLS	10	13	b
14	Femenine	35	Yes	Yes	Middle Cerebral Artery	SL	10x6	15	f
15	Femenine	53	Yes	Yes	Middle Cerebral Artery	SL	11x6	5	c
16	Femenine	72	Yes	Yes	Internal Carotid Artery	SL	9x7	15	b
17	Femenine	69	Yes	Yes	Anterior Communicating Artery	SL	7x4	19	c
18	Femenine	70	Yes	Yes	Middle Cerebral Artery	SL	7x5	5	c
20	Masculine	59	No	Yes	Middle Cerebral Artery	SL	7x5	10	c
21	Femenine	55	No	Yes	Basilar Artery	SLS	7	12	c
23	Femenine	44	N/A	N/A	Basilar Artery	SLS	9	4	f
24	Femenine	83	Yes	Yes	Basilar Artery	SL	7x3	13	b
25	Masculine	59	No	Yes	Internal Carotid Artery	SL	7x5	6	b

26	Femenine	57	Yes	Yes	Middle Cerebral Artery	SL	8x6	26	f
27	Femenine	44	Yes	Yes	Middle Cerebral Artery	SL	10x6	12	f
31	Femenine	62	No	Yes	Middle Cerebral Artery	SL	10x7	8	b
35	Masculine	53	Yes	Yes	Middle Cerebral Artery	SL	7x3	9	b
37	Femenine	62	Yes	Yes	Anterior Communicating Artery	SL	4x3	13	b
38	Masculine	56	Yes	Yes	Middle Cerebral Artery	SL	5x3	13	c
39	Femenine	54	Yes	No	Middle Cerebral Artery	SL	7x3	10	b
41	Femenine	60	Yes	Yes	Middle Cerebral Artery	SL	6x3	14	c
43	Femenine	74	Yes	Yes	Basilar Artery	SL	6x3	26	b
44	Femenine	69	Yes	Yes	Middle Cerebral Artery	SL	4x3	21	b
46	Femenine	51	Yes	Yes	Middle Cerebral Artery	SL	9x4	12	d

Table 13: Patient and device characteristics for the cases used during the 3D modeling of intracranial aneurysms treated with the WEB device with the marching cubes algorithm.

*N/A: Not available

** Internal carotid artery (ICA), middle cerebral artery (MCA), Anterior Communicating Artery (AComA), and basilar artery (BA)

*** single-layer (SL); single-layer spherical (SLS)

13.2.3 Simulation of the WEB device deployment

We simulated the WEB device deployment using the Sim&Size™ simulation software (version 1.2) and following the Workflow specified in Chapter 2 of this thesis. The simulations used patients' 3D DICOM images acquired during the endovascular interventions and the same WEB device reference used for treating the patient. We performed the 3D-arterial reconstruction using the Marching Cubes algorithm implemented in the Sim&Size™ simulation software (191). We manually set the threshold value determining whether a voxel lies inside, across, or outside the artery, assuring a proper visualization in the grey scale (146). Then, we verify the accuracy of the aneurysm limits and 3D-arterial reconstruction.

The Sim&Size™ simulation software used the 3D-arterial reconstructions to specify center lines going from the neck to the dome of the aneurysm. Then, we set the WEB device

positioning along these center lines. The software simulated the WEB device deployment using its internal mechanical solver and resolved the level of apposition between wires and the arterial surface. We validated the simulation results, including the device deformation, and made any changes required for achieving a good apposition. On some occasions, we had to modify the center line to make the position of the simulated WEB device resemble that of the real-life WEB device. We must declare that we made no direct comparison between simulated and real-life device positions as such comparisons are difficult from medical images. However, we mitigated this issue by following the same recommendations used during the interventional procedures, including making the initial release before deployment close to the aneurysm neck.

All our simulations used WEB devices with144 wires, regardless of the device size, to ensure homogeneous comparisons. We chose an arbitrary value because we had no suggestion about the number of wires from the manufacturer. Also, 144 is the minimal number of wires available for the WEB devices. Selecting this minimum value is advantageous because it reduces computational costs and prevents artifacts from simulating devices with more wires than those implanted in patients (146). The resulting 3D-arterial reconstructions showing the simulated WEB devices were used as input for the following CFD analysis.

13.2.4 Arterial Surface preprocessing

We performed the semi-automatic cleaning of the arterial surface mesh using custom python scripts based on the vtmk library for the arterial surface reprocessing (192). We manually removed the small adjacent arteries and surface fusions from imaging artifacts. Then, we filled the holes and extended the inlet and outlet of the parental artery. The surface remeshing consisted of two steps. The first refined the mesh surface using a set value of approximately 0.2 mm. The second used the distance to centerlines as a mesh size constraint to keep a constant number of elements across arterial diameters. Several portions of the aneurysm dome fell far from centerline locations. Therefore, we used a minimum function that used the size values of the first remeshing step to constrain the computation of the mesh size scalar field in the second remeshing step, looking to prevent any mesh coarsening at the aneurysm surface (146). The surface remeshing resulted in meshes of the intracranial aneurysm surface

with set sizes of 0.2 mm, a high enough resolution to generate realistic results using high-order solvers (193).

We visually inspected the intracranial aneurysms meshes to verify their quality, finding that small intracranial aneurysms required additional refinement steps. In these cases, we performed cycles of modifications, surface smoothing, and visual inspections until achieving a satisfactory quality. We present the graphical representations of the cleaned arterial surfaces showing the deployed WEB devices for all the cases included in the study (Cases).

CASE 2:
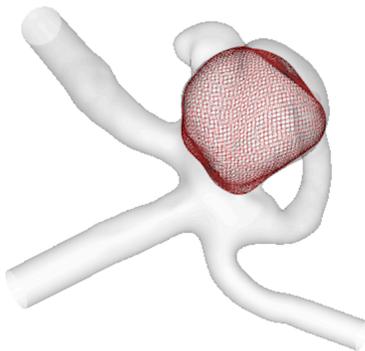
CASE 3:
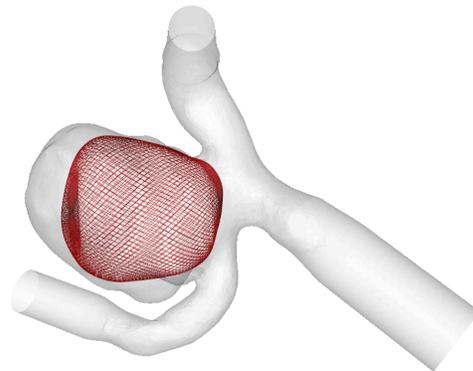
CASE 4:
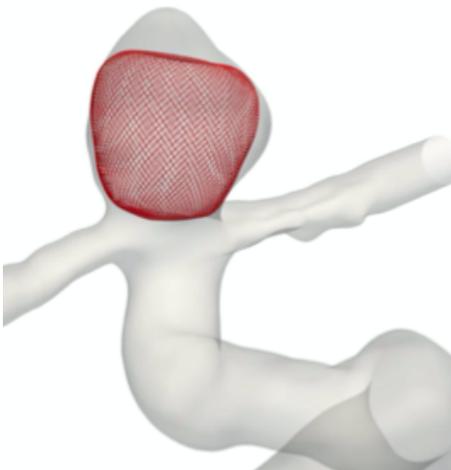
CASE 6:
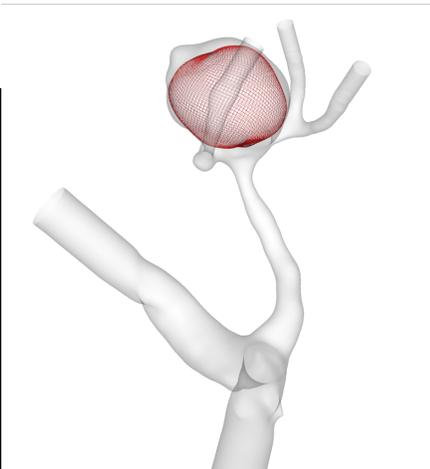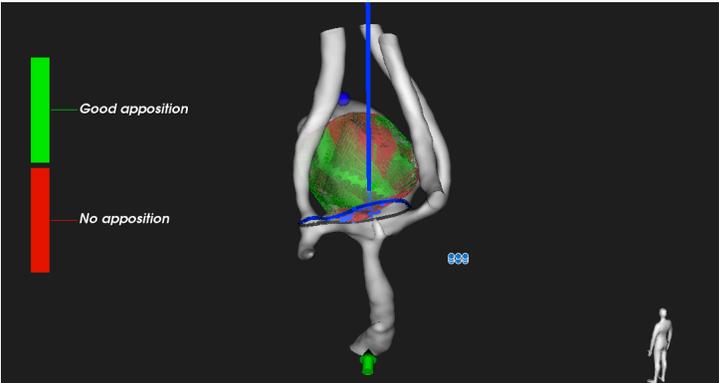
CASE 10:
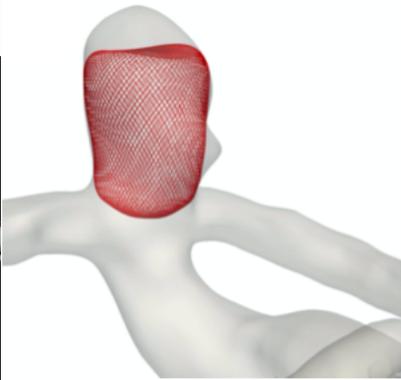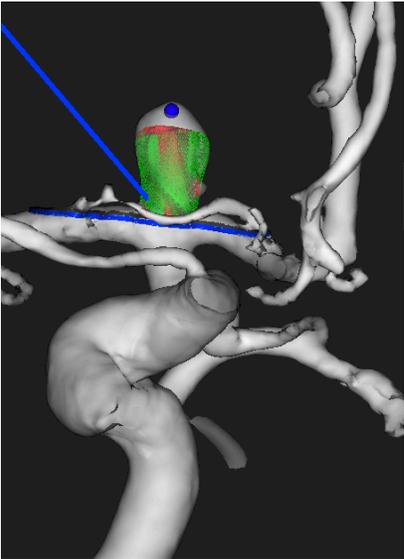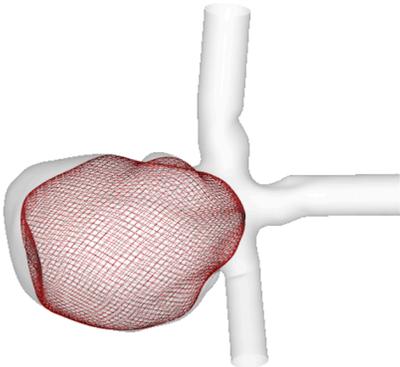
CASE 12:   **CASE 14:**
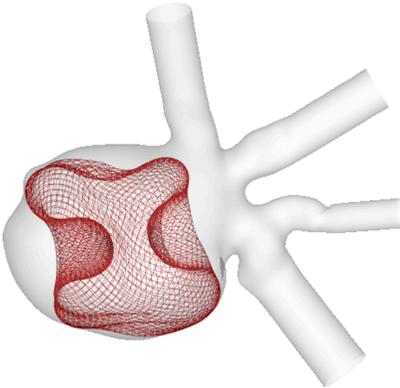
CASE 15:
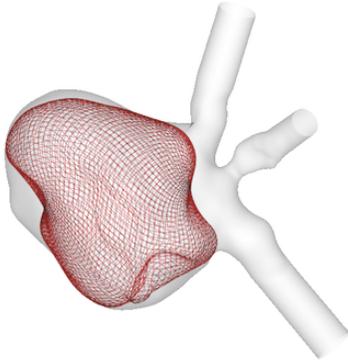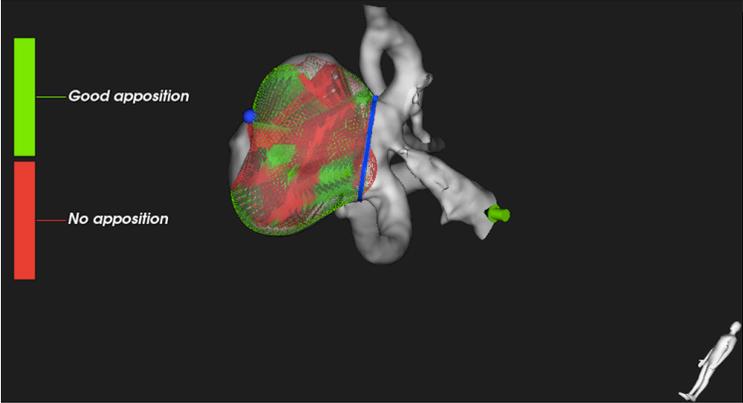
CASE 16:
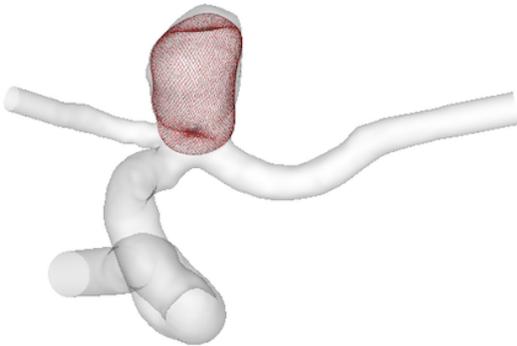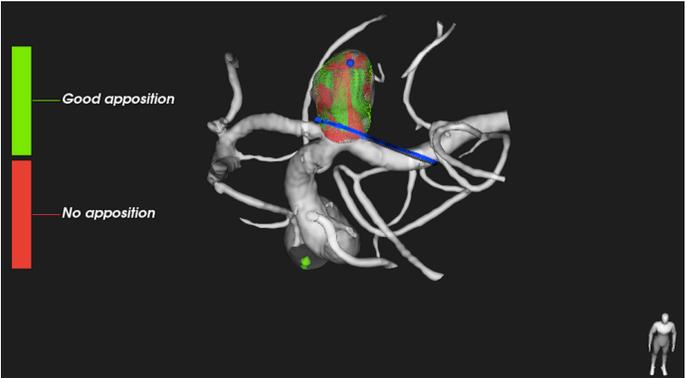
CASE 17:
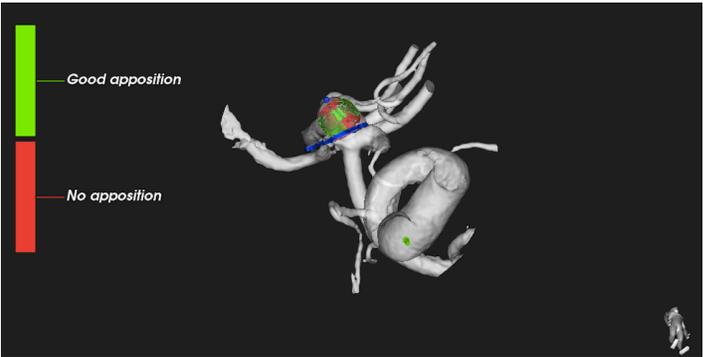
CASE 18:
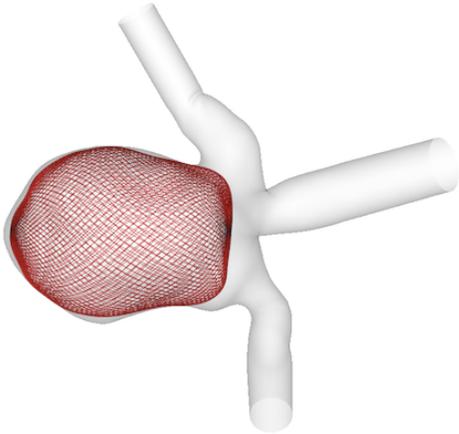
CASE 20:
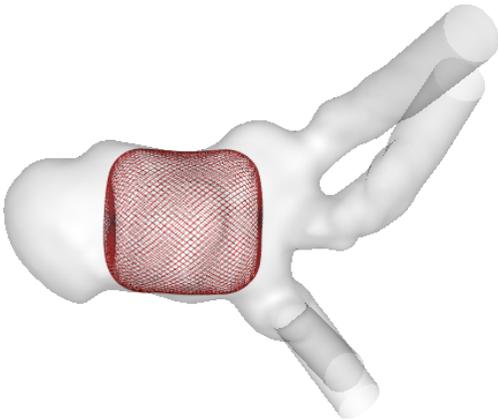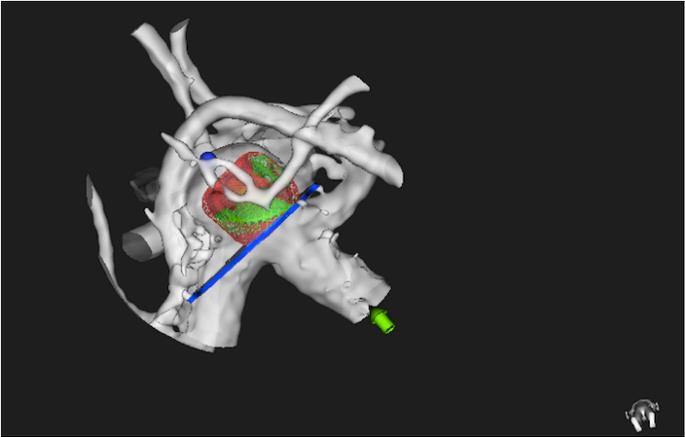
CASE 21:
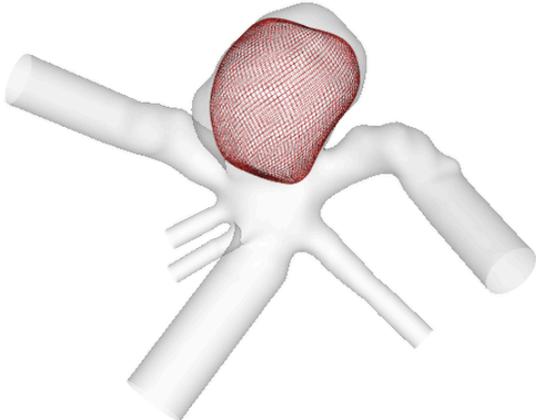
CASE 23:
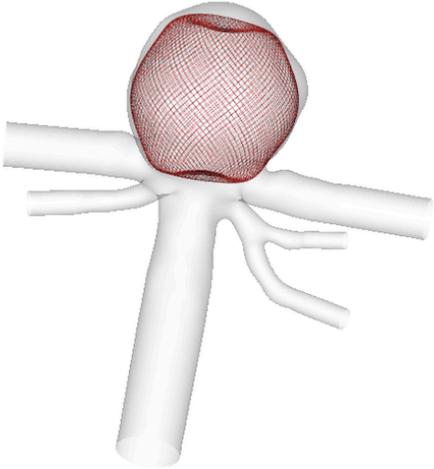
CASE 24:
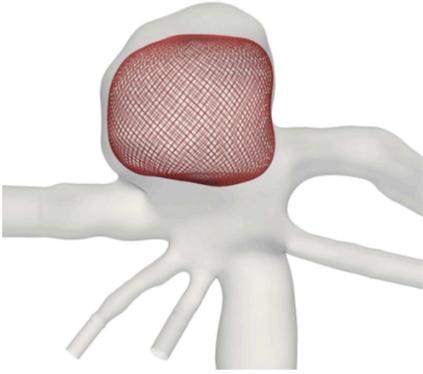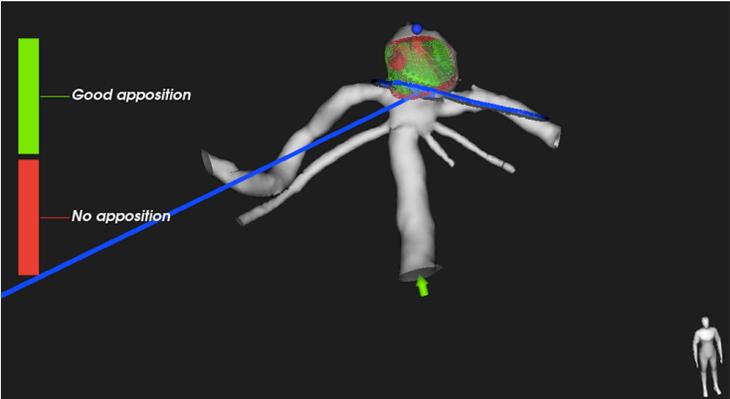
CASE 25:
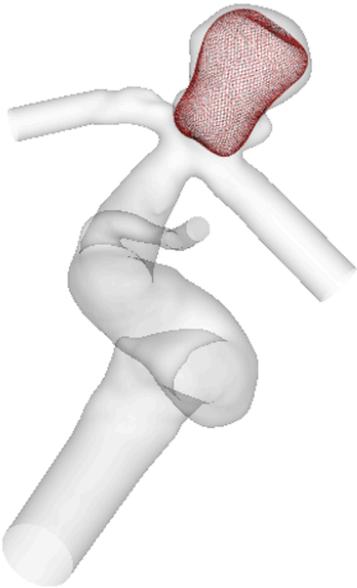
CASE 26:
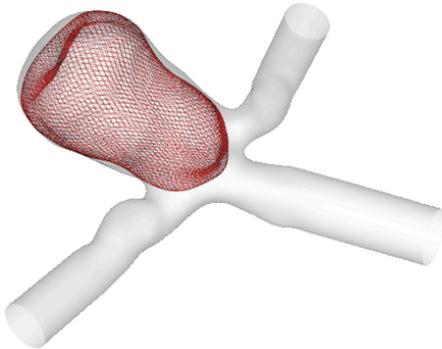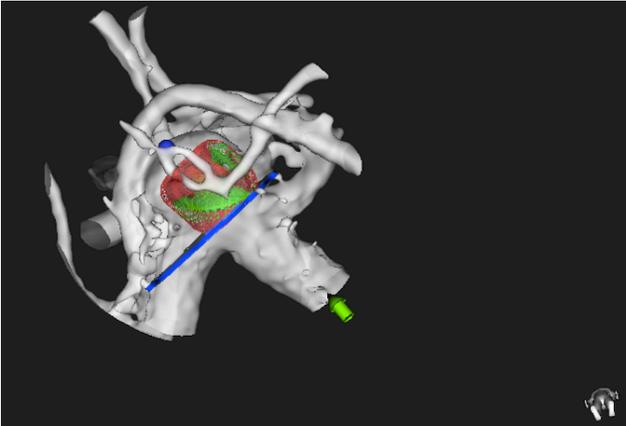
CASE 27:
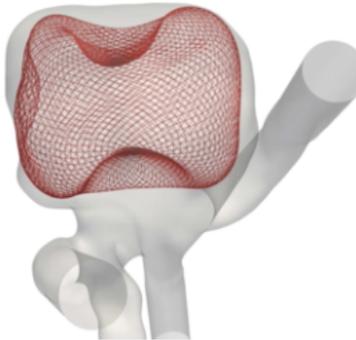
CASE 31:
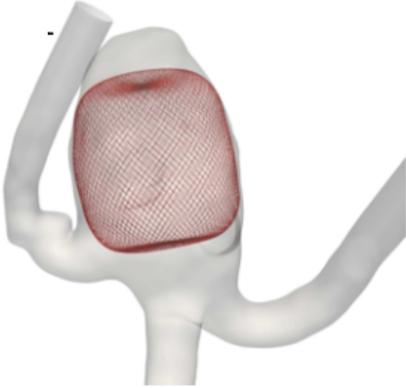
CASE 35:
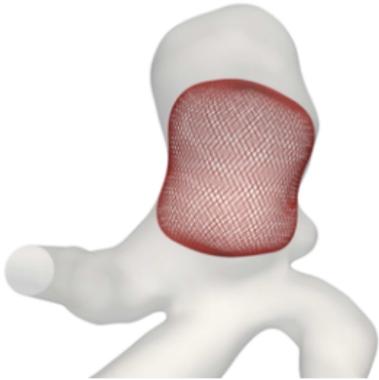
CASE 37:
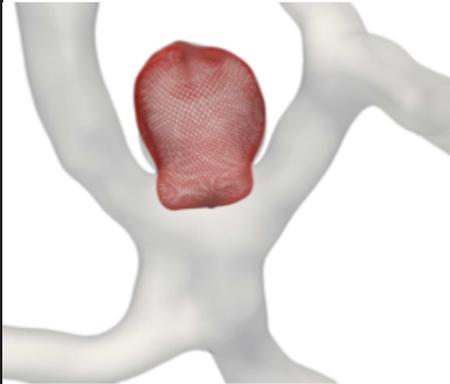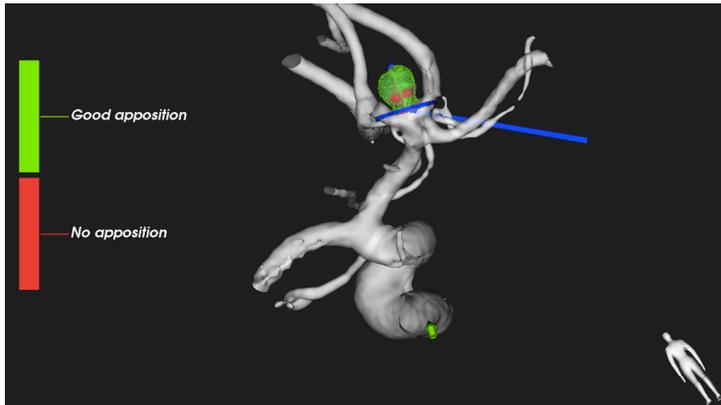
CASE 38:
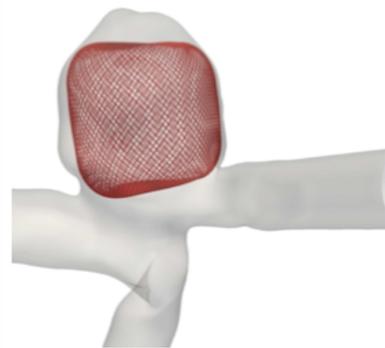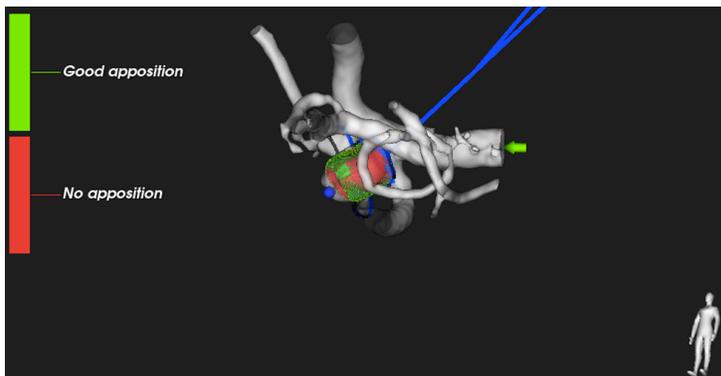
CASE 39:
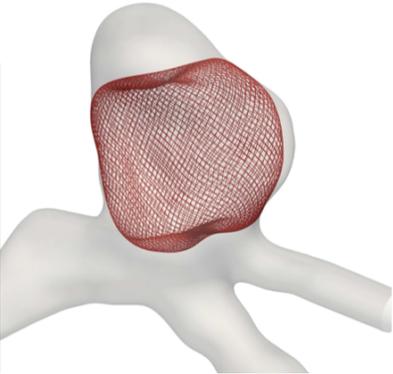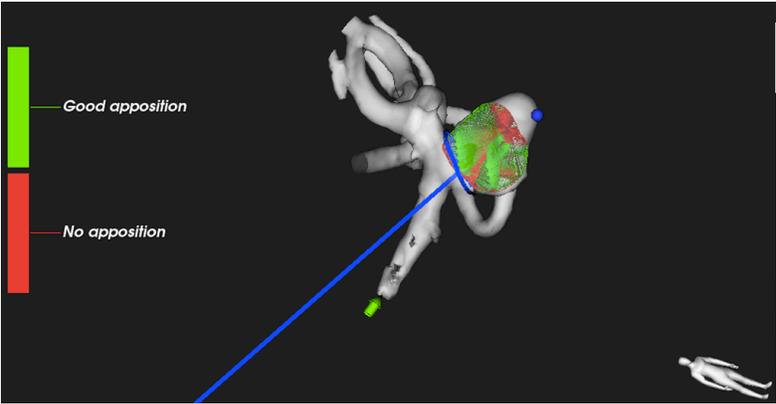
CASE 41:
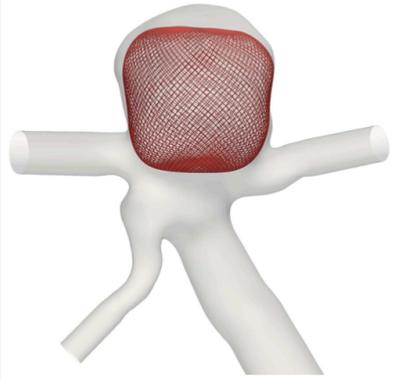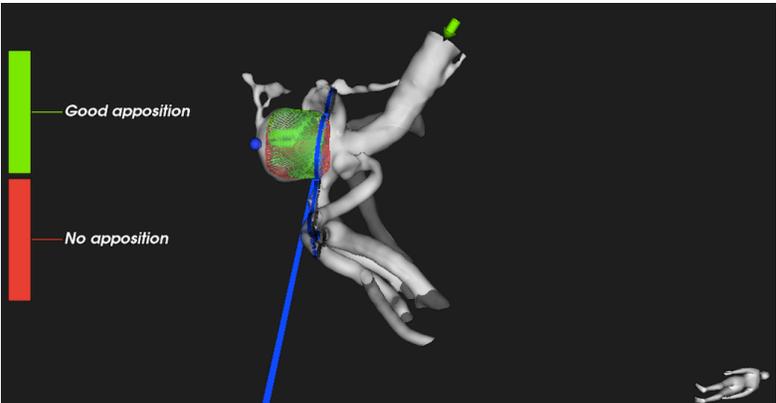
CASE 43:
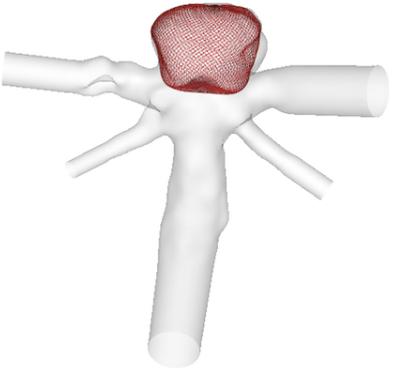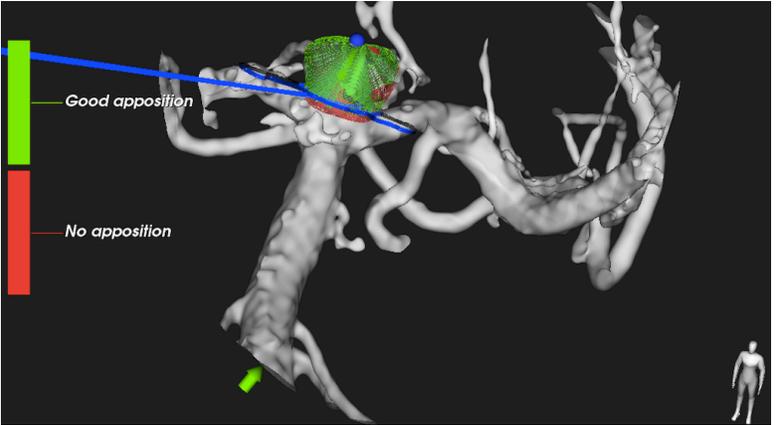
CASE 44:
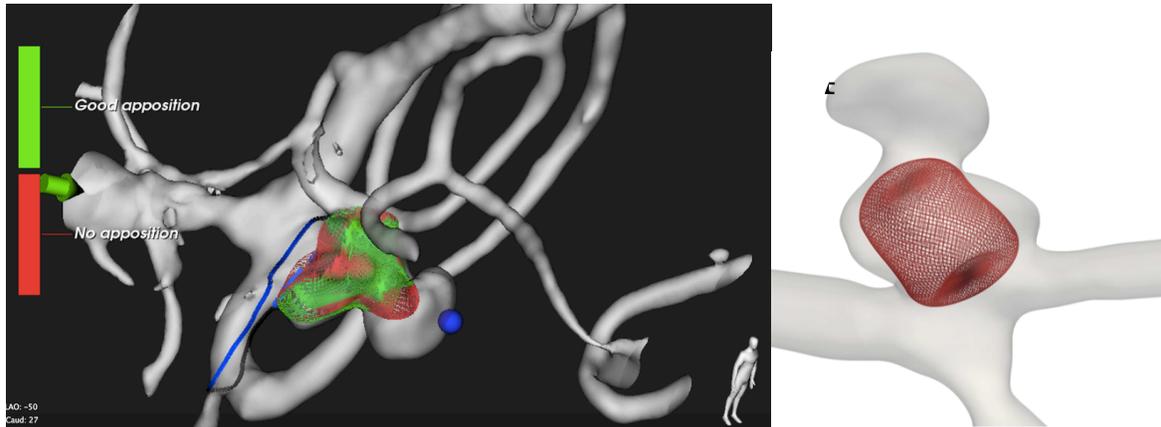
CASE 46:
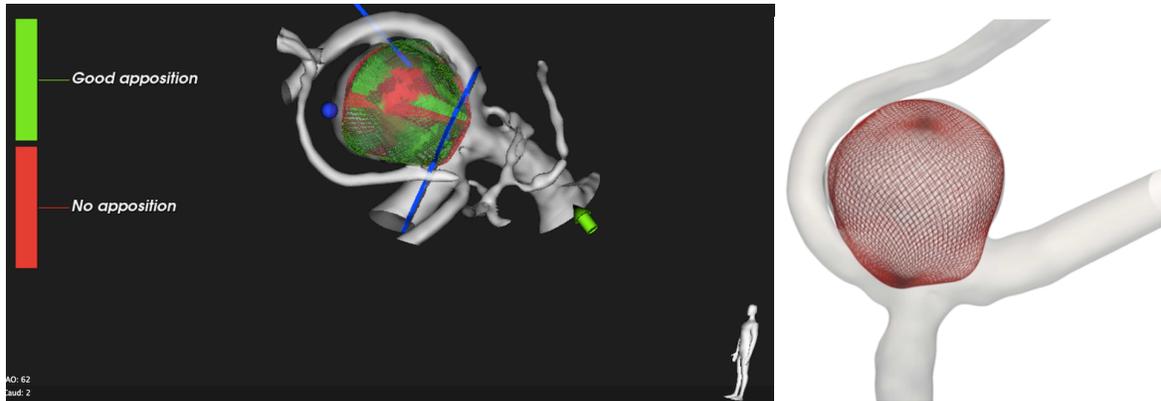
The WEB devices in cases 14, 15, and 17 show compression due to oversizing. On the contrary, WEB devices in cases 20, 35, and 44 fail to cover the aneurysm sac due to their elongated shape (cases 20 and 35) or the aneurysm sac constriction (case 44). Simultaneously, devices in 12, 16, 23, 37, and 46 showed a pronounced proximal protrusion, having irregularities on the intracranial aneurysm sac surface.

13.2.5 Aneurysm trimming and neck surface generation

We developed a semi-automated procedure to trim the aneurysm surface from the parental artery (Figure 45). This procedure consisted in making successive manual clips using a spherical shape on the cleaned arterial surfaces to delimit the aneurysm (red surface on the right of Figure 45). We applied 0.1 mm-length strains along the surface normals surfaces on the previously trimmed aneurysm surface. Then, we closed these surfaces using the VMTK

surface capper, setting the smooth parameter at 0.6 (see the gray surface on the right of Figure 45). The surface deformation resulting from applying strains along the surface normals assured that the volume surrounded by the mesh is within the aneurysm surface, preventing nodule loss, especially at the aneurysm frontier. Some cases (Cases 3 and 46) presented surrounding arteries close to the aneurysm sac, requiring manual adjustment of the warping constant.

We used the aneurysm-trimmed surfaces to estimate anatomic and intrasaccular hemodynamic parameters, including aneurysm volume and neck area. We identified the intra-saccular surface and volume nodes, allowing us to perform spatial averaging. The aneurysm-trimmed surfaces also permitted us to delimit the aneurysm neck surface for further post-processing calculations, including the estimations of positive flow rates (the blue surface on the right of Figure 45). We delimited the aneurysm neck surface by crossing computational volumes (pre and post) with the aneurysm-trimmed surface using a combination of vtkCutter1 and vtkImplicitPolyDataDistance2 filters. Therefore, the resulting discretized surface (blue on the right of Figure 45) differed from the original surface. We used the same procedure for trimming the aneurysm neck surface before and after simulating the WEB device deployment to ensure consistency between comparisons.

We attempted another trimming procedure in this study, which combined spherical and planar shapes for the clipping process. However, we encountered difficulties delimiting the aneurysm neck with this procedure, leading to the development of the approach above. We used the initial approach in six of the cases. However, we expect these differences between protocols not to affect our results as the neck surfaces for these cases were easy to delineate because they matched the arterial geometries.
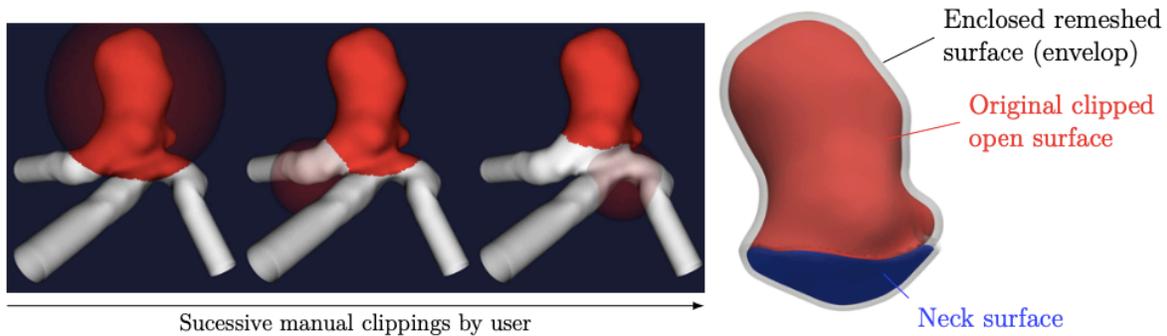
Figure 45: Graphical representation of the semi-automated trimming procedure used for delimiting aneurysm and generating the aneurysm neck surface. The grey surface allows the identification of surface and volume mesh points. The blue surface (aneurysm neck) enables hemodynamic variables estimations.

13.2.6 Device preprocessing

The blood-flow rate calculations must consider the blood passing through the WEB device pores. Therefore, our surface simulations included the surfaces of the neutral fiber cables of the WEB devices in the 3D reconstructions of the Sim&Size^{TM} simulation software. For this purpose, we used wire connectivity to reconstruct the WEB device surface, connecting four points in the rhombus cells by their barycenters. The wires merged at the WEB device corners, resulting in a different data structure. Therefore, we took additional care when reconstructing the mesh of WEB device corners.
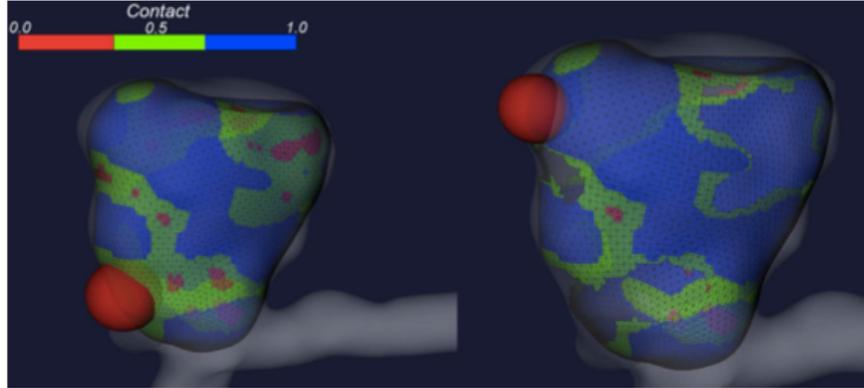
a: Initial surface   b: Final trimmed surface

Figure 46: Graphical user interface showing the WEB device trimming for case 26. The color scale shows the contact apposition with 0 (red) indicating nodes falling outside of the surface, 0.5 (green) indicating nodes falling inside the surface within a distance below 5D, and 1 (red) indicating nodes falling inside the surface at a distance above 5D. D represents the wire diameter.

Subsequently, we created a graphical user interface (GUI) that included a clipping sphere for manually removing portions of the WEB device (Figure 46, red color). We used a 5D threshold for defining the apposition accuracy, with D being the diameter of the WEB device wires (20 μm). We consider appositions having distances below 5D as correct appositions. We based this threshold on the results obtained in "Modélisation in-silico des effets hémodynamiques des prothèses endovasculaires dans le traitement des anévrismes cérébraux: application à l'estimation des chances de succès, Chapter 3, by Alain Berod." In this work, Berod showed that the 5D clipping threshold led to results resembling the GMU calculations (146).

The wires surface and GUI representations used custom python-vtk scripts. We established a penalty source parameter for gaps while modeling high wire densities, considering a 3h-wide region around the WEB device surface to guarantee zero fluid velocity. Figure 46 exemplifies the device trimming process for case 26.

13.2.7 Volume meshing

We used the preprocessed arterial surfaces to simulate two volumes, i. e., pre-treatment (without WEB device) and post-treatment (with WED device) with the VMTK library in the Tetgen tetrahedral mesh generator (194). We used the surface triangulations to interpolate volume grid sizes within the intracranial aneurysm for the pre-treatment volumes, ensuring homogeneous grid sizes. The arterial branches contained a constant number of elements throughout their diameter due to the mesh size constraints used in the second remeshing step of the arterial surface preprocessing. The minimum, maximum, and mean number of cells were 1.0 M, 5.6 M, and 2.2 M in the pre-treatment meshes, respectively, which are within the ranges described in the literature (163)(193)(195)(196).

We create an initial volume mesh for the post-treatment volume by refining the surface regions close to the WEB device sections not previously considered. Here, the surface size interpolations of portions juxtaposed in the previous step led to drastic reductions in the volume grid sizes. We found that this refining strategy disregarded internal parts of the device. Therefore, we performed an additional volume refinement to ensure a grid size of h = w/8 in an 8D area surrounding the device surface, where w represented the mean distance between wires. This size constraint made the number of cells depend on the device's size since the distance between wires increases with the device's size. Finally, we used the MMG3D library to clean and improve the mesh quality of the mesh (197). The mesh sizes in these evaluations were sufficient to produce good quantitative comparisons acording to the "Modélisation in-silico des effets hémodynamiques des prothèses endovasculaires dans le traitement des anévrismes cérébraux: application à l' estimation des chances of succès, Chapter 3, by Alain Berod" (146).

The minimum, maximum, and mean number of cells were 14.0 M, 33.0 M, and 21.0 M in the pos-treatment meshes, respectively. These values were lower than those in the literature. However, we must analyze these higher values with care since they come from an evaluation using duel-layered WEB devices (WEB-DL). These devices have higher cable density than the WEB-SL used in these evaluations (183).

Figure 47 exemplifies the volume mesh sizes for case 35. Here, the asterisk shows how the device trimming affects the mesh size and how the smoothness increases in the areas close to the device's wires. The figure also shows that the resolution of the mesh size is not enough

to resolve the wires' diameter. However, it can still capture potential jet flows within the diamond cells, which was the aim of developing the heterogeneous model.
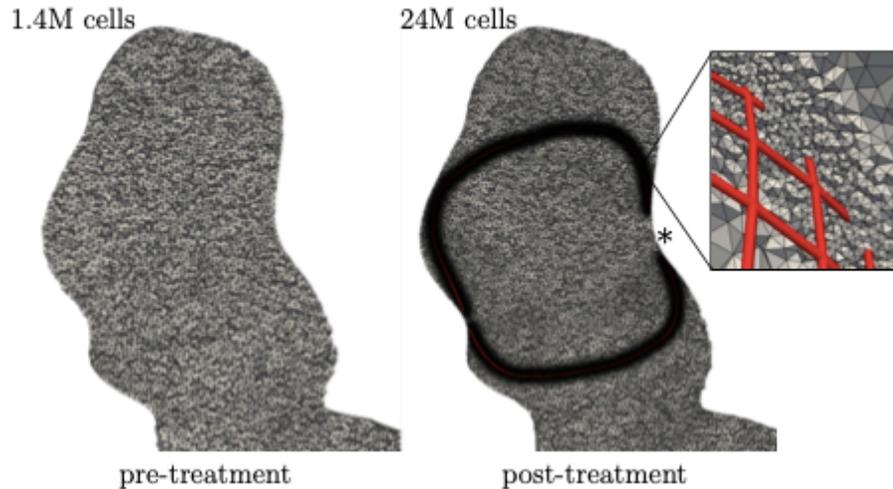
Figure 47: Representative images of volume slices showing pre and post-treatment mesh sizes for case n35. The close-up view shows the number of cells between rhombus cells and the smooth mesh coarsening. The wires diameter (in red) is at the same scale as the real-life WEB device, i.e., 20 μm.

13.2.8 Fluid and boundary conditions

For the FCD analysis, we assumed that the blood was an incompressible and Newtonian fluid, with a density ρ = 1060 kg.m−3 and a kinematic viscosity ν = 3.5 × 10−6 m.s−2 (198). A zero slip boundary condition was applied to the arterial wall and convective outflows were specified for the outflow sections using equation 3.3.1 from "Modélisation in-silico des effets hémodynamiques des prothèses endovasculaires dans le traitement des anévrismes cérébraux: application à l' estimation des chances of succès, Chapter 3, by Alain Berod" (146). Blood-flow rates were not available for all the patients. Therefore, we used the pulsatile waveform in Figure 5 in conjunction with a fully developed Poiseuille velocity profile. We considered a 30 % reduction in the Fourier coefficients to account for the decreased pulsatility in MCA inputs (196).
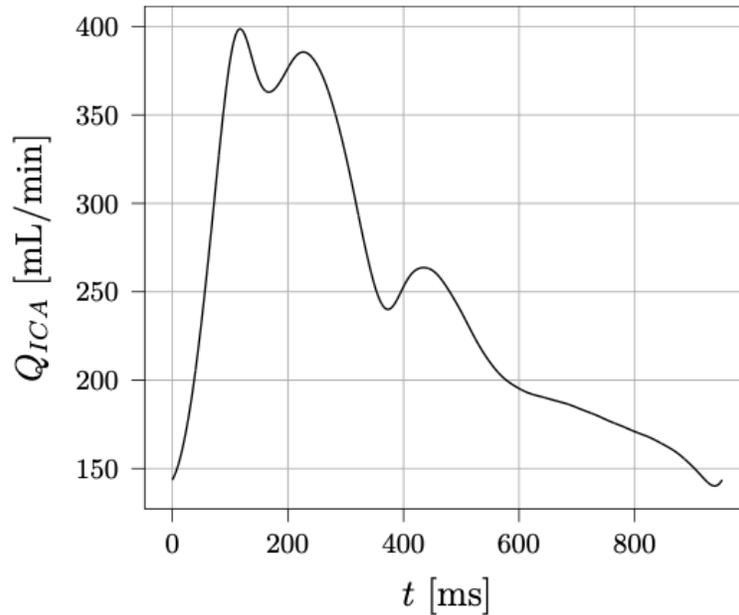
Figure 48: Representative blood-flow rate for the intracranial carotid artery of an elder adult, with a cardiac cycle period of Tp = 0.951 s (199)

We used different strategies to scale the mean value of the waveform to account for the various input locations (ICA, MCA, and BA). As the literature recommended for the ICA inputs, we used a mean speed of 0.27 m.s−1 (200). For the MCA inputs, we estimated a mean velocity of 0.37 m.s−1 (196). We escalated the MCA, and ICA average inlet flows estimations according to the square law using the inlet diameter.

The literature has shown that the cube law of mean flow rate is appropriate for the vertebral arteries that feed the BA (176)(196). Therefore, we computed a mean flow rate (Q) for the BA inlets producing a mean wall share stress of 1.5 Pa using the equation $Q = (WSS\pi/32\mu)$ x D3, where D is the inlet diameter, WSS is wall shear stress, and μ is the dynamic viscosity. The simulations included three and four cardiac cycles for the pre and post-treatment, respectively, to ensure the washing out of the initial zero-velocity condition. We considered only the last simulated cardiac cycle for the qualitative and quantitative analyses.

13.2.9 Quantities of interest

We divided the patient's cohort into two groups, patients with complete and incomplete aneurysm occlusion, for the quantitative analysis of the hemodynamic (Table 14), anatomical, and device-related (Table 15) characteristics of the deployed WEB device. The hemodynamic analysis included the pre and post-treatment values and the post-treatment to pre-treatments ratios (post/pre).

Quantity	Definition	Unit	Description
ICI	$< \dfrac{Q_i/Q_p}{A_i/A_{neck}} >$	[−]	The Inflow Concentration Index (ICI) measures how much the flow entering the aneurysm through the neck is concentrated, but also compares to which extent the aneurysm is fed by its parent artery [101]. Q_i is the positive flow rate at the neck with its associated area A_i. Q_p and A_{neck} are parent artery flow rate and neck area, respectively. The neck normal was orientated towards the aneurysm sac to compute Q_i.
Q^+	$< Q_i >$	[$m^3.s^{-1}$]	Positive flow-rate Q^+ is the time-averaged inflow Q_i trough the neck surface [101].
FN	$\dfrac{T_p Q^+}{V_a}$	[−]	The flushing Number (FN) compares the total blood volume that entered through the neck during one cardiac cycle of period T_p with the aneurysm volume V_a. It is a measure of blood exchange amount between the parent artery and the aneurysm and is introduced in this study.
U_a	$\dfrac{1}{V_a} \displaystyle\int_{\Omega_a} \|< \mathbf{U} >\| dV$	[$m.s^{-1}$]	U_a, which was already defined in Equation 3.3.2, is the spatial and time-averaged velocity inside the aneurysm sac [110].
SR_a	$\dfrac{1}{V_a} \displaystyle\int_{\Omega_a} 2\sqrt{< S_{ij} >< S_{ij} >} dV$	[s^{-1}]	The shear rate spatially averaged inside the aneurysm (SR_a) [101], with S_{ij} the symmetrical part of the velocity gradient tensor $G_{ij} = \dfrac{\partial u_i}{\partial x_j}$ such that $\bar{\bar{\mathbf{S}}} = \dfrac{1}{2}(\bar{\bar{\mathbf{G}}} + \bar{\bar{\mathbf{G}}}^T)$. G_{ij} components are computed via the high-order numerical gradient reconstruction available in the yales2bio code and time-averaged component-wise.
VO_a	$\dfrac{1}{V_a} \displaystyle\int_{\Omega_a} \|< \nabla \times \mathbf{U} >\| dV$	[s^{-1}]	The vorticity spatially averaged inside the aneurysm (VO_a) [101]. The same numerical gradient reconstruction as SR_a was used, as well as component-wise time integration.
MATT	$\dfrac{V_a}{U_a A_{neck}}$	[s]	Mean Aneurysm Transient Time (MATT) is representative of a convective time inside the aneurysm [102], and can be termed as an averaged intra-saccular residence time.
TAWSS	$\dfrac{1}{S_a} \displaystyle\int_{\Gamma_a} \|< \boldsymbol{\tau}_\mathbf{w} >\| dS$	[Pa]	Time-Averaged Wall Shear Stress (TAWSS) spatially averaged on the aneurysm surface Γ_a [101]. $\boldsymbol{\tau}_\mathbf{w}$ is the wall shear stress vector computed such as $\boldsymbol{\tau}_\mathbf{w} = 2\mu\bar{\bar{\mathbf{S}}} \cdot \mathbf{n_w}$ with $\mathbf{n_w}$ the wall outward normal vector.

Table 14: Hemodynamic variables analyzed in the study. $< \bullet >$ represents the last cardiac cycle time-averaging operator such that $< \bullet > = \dfrac{\frac{1}{T_p} \int_{T_p} \bullet\, dt}{}$. Time-averaging was performed at each time step for aneurysm-related parameters, while quantities that needed the neck surface, such as Q^+, were estimated posteriorly using 30 regularly outputted solutions during the last cardiac cycle.

Quantity	Definition	Unit	Description
Anatomical			
V_a	$\int_{\Omega_a} \mathrm{d}V$	[mL]	The total aneurysm volume. In practice, all volume points lying inside the previously described surface Figure 4.6 are first extracted using the vtkSelectEnclosedPoints filter [3]. Then, nodal volume scalar field is computed and further numerical integration is performed.
S_{neck}	$\int_{\Gamma_n} \mathrm{d}S$	[mm²]	The total neck surface (see the blue surface in Figure 4.6).
R_a	$\dfrac{\sqrt[3]{V_a}}{\sqrt{S_{\text{neck}}}}$	[−]	The volume to neck surface ratio, which measures the aneurysm elongation.
Device-related			
R_d	$\dfrac{V_{\text{device}}}{V_a}$	[−]	The ratio between the aneurysm volume V_a and the device one V_{device}. Measures how well the device fills the aneurysm cavity. In practice, the device trimming step depicted in Figure 4.7 also outputs the entire unclipped surface, from which V_{device} was computed using the vtkMassProperties filter [4]. Since vtkMassProperties makes uses of the divergence theorem, device cell normals must be oriented outwards and consistently across the surface, which was ensured with the vtkPolyDataNormals[5] filter.
D_{neck}	$\dfrac{1}{S_{\text{neck}}} \int_{\Gamma_n} \lVert \mathbf{X}_{\text{neck}}^{\text{device}} \rVert \mathrm{d}S$	[mm]	D_{neck} measures the averaged distance between neck and device. In practice, for each point on the neck surface Γ_n, its closest neighbour on the device is obtained via the vtkCellLocator[6] filter, $\mathbf{X}_{\text{neck}}^{\text{device}}$ being the vector between these two points.
ApR	$\dfrac{S_{\text{apposed}}}{S_{\text{device}}}$	[−]	The Apposition Ratio (ApR) measures to which extent the device is apposed to the arterial surface. Threshold distance for apposition was fixed to $5D$ in accordance with previous sections. Proximal and distal apposition of FDs was proved to be associated to aneurysm occlusion by Rouchaud et al. [128], but no similar studies have been conducted for WEBs to date.

Table 15: Anatomic and device-related variables analyzed in the study.

13.3 Results

13.3.1 Hemodynamics

a. *Pre-treatment flow characteristics inside bifurcation aneurysms*

Bifurcation aneurysms have jet-like flow structures that disperse and divide inside the sac, unlike most sidewall aneurysms for which a large primary

vortex fills the sac. Cebral et al. (144) observed that the geometries and hemodynamics vary from one aneurysm to another. However, they defined four intrasaccular flow patterns according to the number of vortices within the sac and their stability during the cardiac cycle. In a follow-up study using a more extensive patient cohort (n = 120), Cebral et al. showed that aneurysm rupture was associated with unstable flow characteristics, such as small jets through the aneurysm neck and concentrated impingement zones. Also, It was related to complex flows having flow separations or multiple vortices within the sac (201). These findings agreed with other evaluations addressing the occlusion of AComA aneurysms. According to our database, most AComA aneurysms occur in bifurcations (202). We also found four flow patterns while visually inspecting the velocity fields averaged over time for all cases.

Type I	The parent-artery jet is tangential to the aneurysm sac and does not separate at the neck entry
Type II	When going through the neck, the jet is separated at an arterial junction with a branching vessel and is further oriented tangentially to the aneurysm sac
Type III	The incoming jet directly impinges the aneurysm dome and subsequently separates
Type IV	No clear flow organization inside the sac.

Table 16: Characteristics of the most prominent flow patterns found in the analyzed aneurysms.

Type flow	Case
Type I	4, 15, 16*,20, 31, 38, 41, 43, 46
Type II	2, 3, 12, 21, 24, 26, 27, 35*, 39, 44
Type III	6*, 14, 17, 18, 23
Type IV	10, 25, 37*

*Table 17: The aneurysms distribution in the flow patterns for the analyzed aneurysm before being treated with the WEB device. * denotes the cases used for illustrating the aneurysm flow patterns in Figure 49.*

Most aneurysms had types I and II flow patterns (37% each) (Table 16 and Table 17). Both flow patterns had evenly distributed parietal stresses in the aneurysm sac, blebs, and irregularities. However, Type II flows also had a zone of high parietal friction at the neck bifurcation due to the flow jet separation. The distinction between these flow patterns was challenging since they share some features. Therefore, the classification of flow patterns into these two groups depended to some extent on the observer.

Type III flows represented 19 % of the aneurysms. The flow jet in these aneurysms impacted the aneurysm dome in this flow pattern creating high time-averaged WSS (TAWSS) regions (~ 25 Pa) on the sac that disperses rapidly. Lastly, the flow of three aneurysms had no distinctive organization falling in the type IV flow pattern. The relative location of the aneurysm sac to the main artery might be responsible for this lack of organization. The bifurcation angle in cases 25 and 27 directs most of the proximal flow towards one or both downstream arteries, leaving the aneurysm sac without an inflow jet. In case 10, the upstream elongation and curvature of the main artery produced an indeterminate flow jet within the aneurysm sac, directing the blood towards distal arteries.
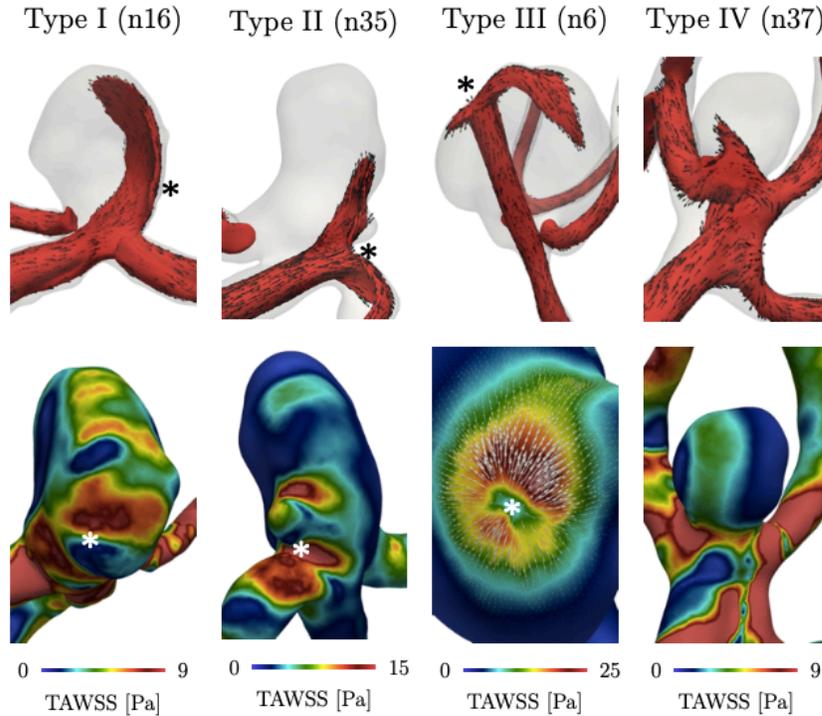
*Figure 49: Representative velocity contour (top panel) and the time-average wall shear stress maps (TAWSS) (low panel) for the most prominent flow patterns found in the analyzed aneurysms before being treated with the WEB device. Since views are different between the top and bottom rows, * symbols were placed to show the 3D correspondence between views. TAWSS vectors for Type III were oriented negatively to illustrate the flow separation. The color maps in the TAWSS have different scales.*

b. <u>*Effect of WEB device treatment on the flow characteristics inside bifurcation aneurysms.*</u>

We used a median value (30.2%) of the apposition ratio (ApR) index to differentiate between good and improper wall appositions while analyzing the impact of the WEB device on the aneurysm hemodynamics. We also used time-averaged velocity fields for visually assessing the presence of a flow jet between the aneurysm sac and the device frontier (referred to as "5") (Table 18). Most cases with a proper wall apposition lacked near-wall flow jets close

to the wall (Table 18, group 3), with case 4 being the exception (Table 18 and Figure 50, group 1).

In case 4, the device was placed correctly at one side of the aneurysm sac. However, the main artery curvature created a flow jet impacting the side of the neck where the device placement was faulty, leading to a near-wall flow jet appearance. The post-treatment flow, in this case, remained unchanged until meeting the WEB device top, where it deflected and reduced its magnitude. Interestingly, a recirculating cell formed near the bottom of the aneurysm, similar to a cavity flow driven by a cap (Figure 50, n4, ∗ symbol). Case 4 was peculiarity since the ApR index was 30.4 %, close to the 30.2 % threshold used for defining a correct wall apposition. Whether this case belongs to the group having aneurysm with a good wall apposition is debatable.

		Degree of apposition	
		Good (ApR > 0.3)	**Bad (ApR < 0.3)**
Near wall jet presence	**Yes**	$1^{(1)}$ (case 4)	$6^{(2)}$ (case 3,15,16,20, 35,44)
	No	$12^{(3)}$ (case 6,10,12, 18,21,26,37,38,39, 41,43,46)	$8^{(4)}$ (case 2,14,17,23, 24,25,27,31)

Table 18: Contingency table showing the cases divided according to the degree of apposition (good (ApR > 0.3) and improper (ApR < 0.3)) and the presence of near-wall flow jets. The superscript numbers inside the parenthesis divide the cases into four groups referenced in the text.

Poor device apposition did not necessarily lead to a near-wall flow jet. We found that 30 % of the cases showed no near-wall flow jet despite poor wall apposition (Table 18, group 4). In Case 2, the inflow jet impacted a device region with low wires density and correct wall apposition, preventing the flow from passing into the near-wall areas. The flow jet stayed inside the device despite encountering non-apposed device portions when recirculating the aneurysm sac (Figure 50, n2). Case 24 resembled case 2, but in this case, the

device protrusion deviated the jet flow towards downstream arteries. The flow jet failed to pass across the device due to the high wire density encountered near the impact site (Figure 50, n24). Case 25 resembles case 4 since the device had proper apposition in the region where the inflow jet impacted. However, I had poor apposition in other areas (Figure 50, n25). In case 14, device over-sizing caused severe compressions and reorientation areas, leading to low ApRs ($\sim 21\%$). However, the inflow jets tangentially impacted re-oriented and compressed device portions and diverted towards the downstream arteries without reaching regions close to the artery wall (Figure 50, n14). The inflow jet in case 23 was blocked as it impacted a device protrusion with a high wire density and diverted towards downstream branches (Figure 50, n23).

On the other hand, poor wall apposition coincided with near-wall flow jets in 26% of cases. In particular, cases 20 and 44 had the WEB devices deployed near the aneurysm neck. Still, the wall apposition was faulty, or the device was disoriented at the sac area where the inflow jet impacted, allowing blood flow between the device and the aneurysm wall (Figure 50, n20 and n44).

These cases above show the utility of pre-treatment CFD analysis for the endovascular treatment of intracranial aneurysms, as they can provide treatment guidelines. During the deployment of intra-saccular devices, neuro-interventionalists seek to fill the aneurysm while placing the device near the neck to prevent recanalization. However, predicting the device positioning within the aneurysm sac and wall apposition is challenging during the deployment, and VasoCT images only provide rough estimates after device deployment. Tools such as the Sim&Size^{TM} simulation software can help with these predictions. Neuro-interventionalists can use these tools to know where to place the device for blocking the inflow jet. Clinical routines could use these simulations in combination with other deployment recommendations, i.e., filling and minimal neck distance, during treatment planning to increase the efficacy. However, this planning method is probably only feasible for

elective cases. In our evaluations, the numerical computations used during the pre-treatment simulations required a couple of hours, and these estimations do not include the surface cleaning and preprocessing times. The utility of introducing a planning strategy for the endovascular treatment of intracranial aneurysms, including pre-treatment CFD analysis, to clinical practice is apparent. However, retrospective and prospective studies must validate their utility.
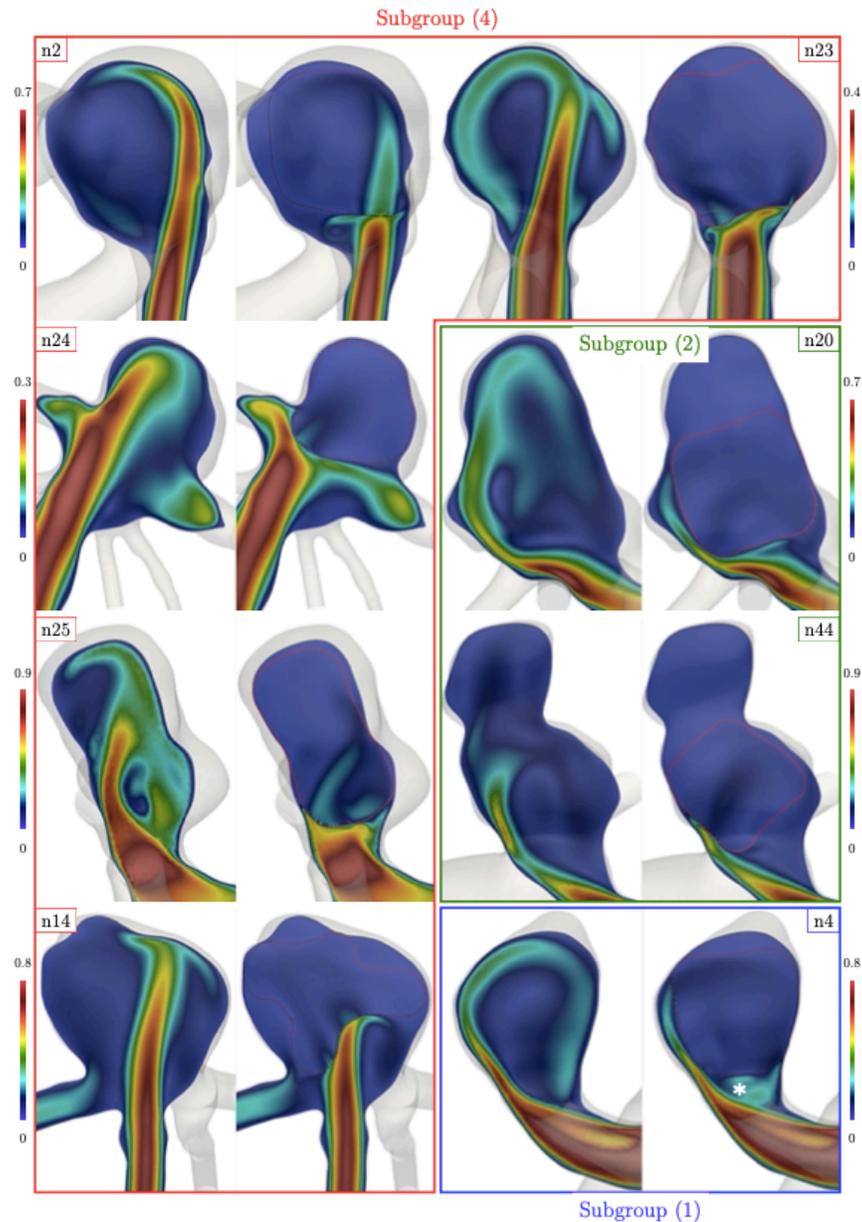
Figure 50: Representative images showing the effect of WEB device deployment on the blood flow patterns. The subgroups relate to the groups

defined in table 5. Pre- (left) and post-treatment (right) time-averaged <U> velocity fields for are represented for selected cases.

c. _Impact of WEB device protrusion on the blood flow patterns_

We visually assessed portions of the devices crossing the surface of the intracranial aneurysm neck. Then, we used this information to divide the cases into aneurysms presenting and not presenting device protrusion. We also split the aneurysms according to the neck inflow Q+ post- to pre-treatment ratio (post/pre ratio) by visual inspection, using an arbitrary cut-off of 0.5 to separate the groups into high al low Q+ post/pre ratios.

In our cohort, 44 % of cases presented device protrusion. The literature reports protrusion percentages up to 47% (124). However, these percentages might not be comparable since they come from evaluations using protocols different from ours. Also, other clinical center-related factors might have influenced these estimations, including the neuro-interventionalists experience with WEB devices, device sizing, and mechanical manipulation during device deployment. An example of the disagreement between evaluations comes from the studies by Caroff et al. (124) and by Cagnazzo et al.(189), reporting protrusion percentages of 47% in 2015, and 0 % in 2019, respectively. The drop in protrusion percentages might come from Cagnazzo's team gaining experience in WEB devices. Also, Cagnazzo et al. cohort included patients treated using the Sim&Size^{TM} simulation software after 2017 (64 % of patients) (189). The software predicts the device's final unfolded shape, meaning that device protrusion could have been anticipated.

Device protrusion is associated with low Q+ post/pre ratios due to effective flow jet blockage by the device. We confirmed this association in our patient's cohort, with most cases presenting device protrusion showing low Q+ post/pre ratios (Table 19). Cases 16 and 44 were the exception, possibly due to the device positioning concerning the aneurysm neck and the area impacted by the inflow jet.

Device protrusion in case 16 (represented by the area between the green and red lines in Figure 51) did not affect the inflow jet since it had an orientation towards the left side of the device. Here, the device is tilted and is not juxtaposed to the aneurysm sac, leaving a space for the blood to flow tangentially to the device (Figure 51, black symbol ∗). In case 44, the device protrusion locally redirects the flow creating a region with higher neck-oriented velocities, increasing the neck mean flow rate after the treatment (Figure 51, white symbol ∗).

| | | Q^+ ratio group | |
		High	Low
	Yes	2 (case 16,44)	10 (case 10,12,21,23,24,24, 26,37,43,46)
Device protrusion	No	15 (case 2,3,4,6,14,15 17,18,20,27,31,35,38,39 41)	0

Table 19: Contingency table showing the cases divided according to high (Q+ post/pre ratio > 0.5) and low (Q+ post/pre ratio < 0.5) and the presence of device protrusion.
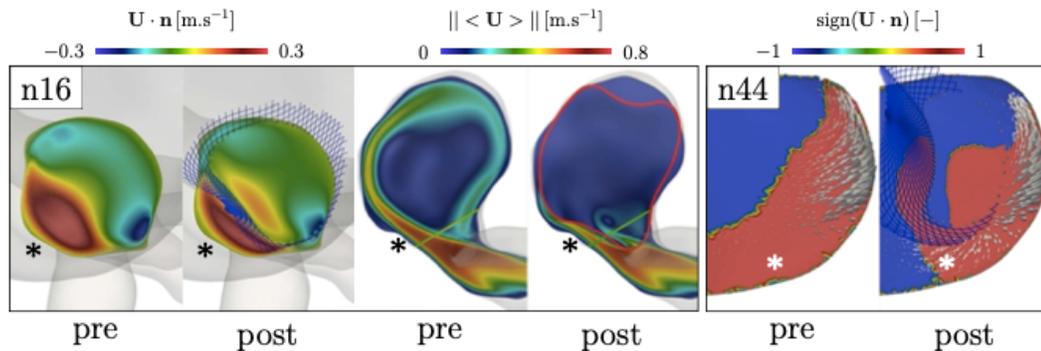
Figure 51: Representative images showing the effect of the non-protruding WEB device on the inflow Q+ post/pre ratio. Pre and post refer to pre and post-treatment images, and the color scales resemble the inflow Q+ post/pre ratio. In case 16 (n16), the left view represents pre and post-treatment projected velocity at the aneurysm neck surface for the last instant of the

cardiac cycle. The device (in blue) has been clipped to enhance flow visualization. On the right, green and red lines correspond to neck and device surfaces. In case 44 (n44), the sign of the projected velocity at the neck is represented, along with velocity vectors in white, showing how the device protrusion modifies the local hemodynamics environment.

Cases with pronounced device protrusion presented a significant flow redirection towards the downstream arteries. For example, in case 12, the high wire density in the lead area impacted by the inflow jet prevented blood circulation within the aneurysm (Figure 52, n12). Case 26 had a similar flow jet pattern, but in this case, the inflow jet impacted an area of the device with low wire density allowing the formation of a residual flow jet (Figure 52, n26). The redirection is not limited to cases where the device protrudes. For example, in case 38, the upstream arterial constriction focuses the flow jet toward the device recess section, causing a clear flow jet redirection towards downstream arteries (Figure 52, n38). However, due to the absence of device protrusion and subsequent flow constriction, the inflow Q+ ratios of separated jets are not as low as those of protruding cases 12 and 26 (Figure 52, white ∗ symbols).
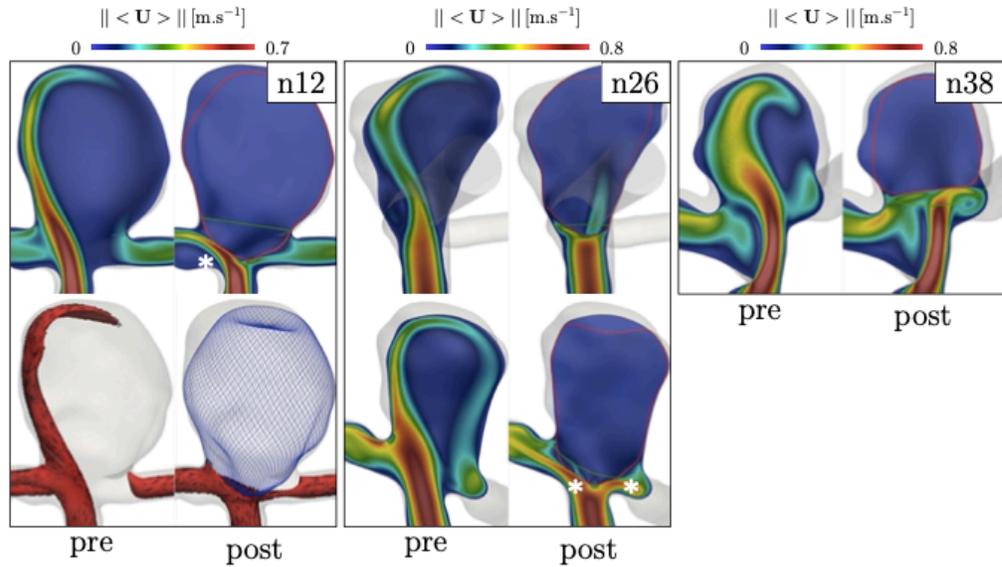
Figure 52: Representative images showing the effect of WEB device protrusion on the inflow Q+ post/pre ratio. Pre and post refer to pre and post-treatment images, and the color scales resemble the inflow Q+ post/pre ratio. Cases 12 (n12) and 26 (n26), showing device protrusion, exhibited a major flow redirection due to device presence beyond the aneurysm neck. Case 38 (n38), having no device protrusion, also presented flow redirection to a lesser extent than cases 12 and 26.

d. <u>*Counterintuitive Conclusions Provided by Hemodynamic Indices*</u>

We expected the post/pre ratios to be below one for all hemodynamic variables analyzed since the WEB device blocked or reduced the blood flow into the aneurysm sac. The post/pre ratios were below one for Ua, SRa, VOa, MATT, and TAWSS for all the cases. However, we found three cases having ICI, Q+, or FN post/pre ratios above one. For example, case 6 had Q+ and FN post/pre ratios of 1.17 and 1.13. In this case, the pre-treatment velocity field showed a constriction in the aneurysm neck, creating a localized inflow jet with high velocities (1.1 m.s−1) (Figure 53, n6, pre-treatment). The WEB device blocked most of this jet. However, it left a small persistent intrasaccular jet that separated upstream of the device. Consequently, we

197

evidenced areas having flow jets with high normal velocities, Q+, and FNl in the aneurysm neck following device placement (Figure 53, n6, post-treatment).

The ICI post/pre ratio was 1.3 for cases 15 and 31. In case 31, the pre-treatment flow jet created two distinct areas with positive normal components. The first was common among the evaluated cases and occurred at the jet entrance near the parent artery bifurcation. The second was close to the downstream artery, resulting from the blood recirculation within the sac and the aneurysm neck size, which was the largest in the study (45 mm2) and induced blood reentering through the neck before exiting the aneurysm (Figure 53, n31, pre-treatment). The WEB device organized the intrasaccular flow, dissipating the blood recirculation in the aneurysm sac and the second area with positive normal components. It

also prevented the flow from reentering through the neck, increasing the Ai and, consequently, the ICI (Table 14). A Qi decrease failed to compensate for the ICI increase in this case since the device landed far from the inflow jet at the bifurcation.
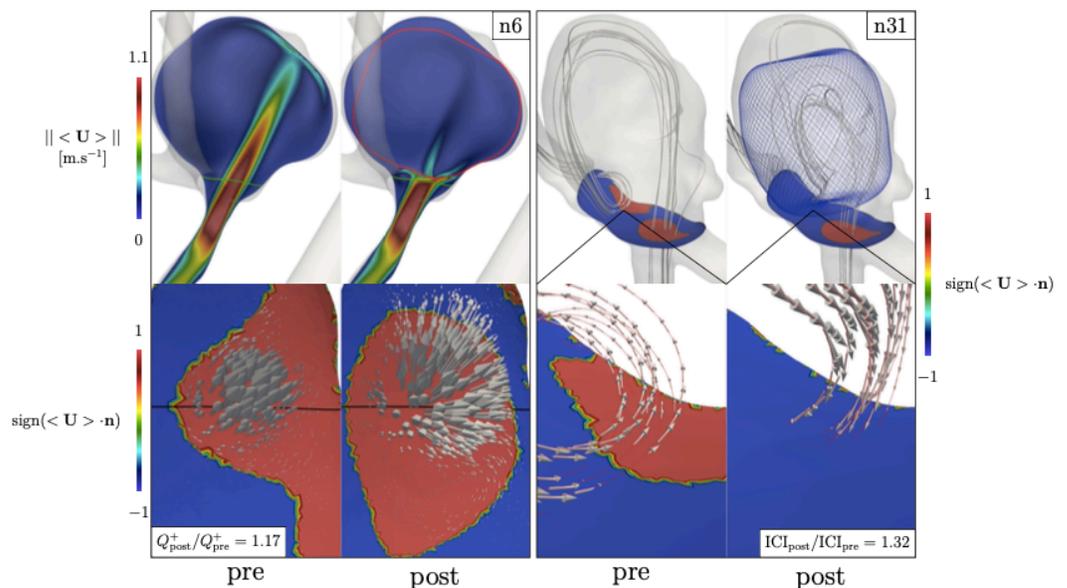
Figure 53: Representative images showing the cases with Q+ and ICI post/pre ratios above one. In case 6 (n6), the arterial constriction and the WEB device

located close to the aneurysm neck entail a flow jet separation that creates higher normal velocity components absent before device placement (see white velocity vectors at the neck). In case 31 (n31), the WEB device reorganizes the blood flow inside the aneurysm neck, removing one of the positive flow rate areas and increasing the post-treatment ICI. On the top row, red, green, and black lines represent the device, neck, and plane used for blood flow visualization. The streamlines' computations employed temporally averaged velocities using the same baseline points at the aneurysm neck. Velocity vectors are overlaid on streamlines for flow visualization.

13.3.2 <u>Association between hemodynamic, anatomic, and device-related factors and medical outcome</u>

This section is a preliminary evaluation assessing the association between several parameters, including patients' hemodynamic, anatomic, and device-related factors, and retrospective medical outcomes, aiming to identify underlying mechanisms leading to occlusion success. We used the univariate two-sided Mann-Whitney rank-sum test with the python library scipy (version 1.9.0) for this evaluation. The reasons for choosing this test are as follows.

a. The occlusion groups (Success and Failure) were internally and externally independent, meaning that the occlusion status of one case does not impact another.

b. The analyzed variables were continuous and non-parametric, verified using the Shapiro-Wilk test, and visually inspecting the raw data histograms.

c. Our sample sizes were small, and the Mann-Whitney rank-sum test performs better than other tests when dealing with small sample sizes.

To establish the occlusion status, we visually evaluated the follow-up DSA images using the Beaujon Occlusion Scale score (BOSS) (124). This scale divides occlusion into six classes (a, b, c, d, e, and f) depending on the occlusion grade (Figure 54A). Class a refers to intracranial aneurysms laking of the device. On the contrary, class b

represents intracranial aneurysms with properly placed devices leading to complete neck coverage and the absence of contrast material circulation inside the aneurysm. Class c includes treated intracranial aneurysms with proximal recess opacification and class d with a non-negligible amount of contrast material inside the device, despite the proper placement of the device. Class e has aneurysms with devices placed distally from the neck. These aneurysms have regions between the neck and the proximal recess where the contrast material circulates freely. Finally, class f includes aneurysms with poor device appositions or proximal placement, which results in free spaces between the aneurysm wall and the device allowing contrast material flow. We considered classes b and c as successful occlusions (Success) and d, e, and f as falling occlusions (Failure) (Figure 54).

13.3.3 Association between occlusion status, patient's age, and follow-up times

The aneurysm healing takes time due to thrombotic reactions, making the follow-up time relevant. Our patient's cohort varied widely in the follow-up times, going from 3 to 26 months following the procedure (Figure 54B). However, we found no association between the follow-up times and occlusion status (p-value = 0.600). In long-term studies, analyzing occlusion status at different times along the study might introduce biases to the analysis due to protocol changes or a better pathology understanding. For example, we found that cases treated before 2014 (Figure 54B blue dots) had shorter follow-up times than more recent cases (p-value = 0.001). These changes in the interventional follow-up protocols came from a better understanding of the long-term treatment efficacy following the WEB-SL device

(A)

Mann-Whitney follow-up time:

- Failure and sucess groups: $p = 0.6$
- Treatment year groups: $\mathbf{p = 0.0009^{**}}$

(B)
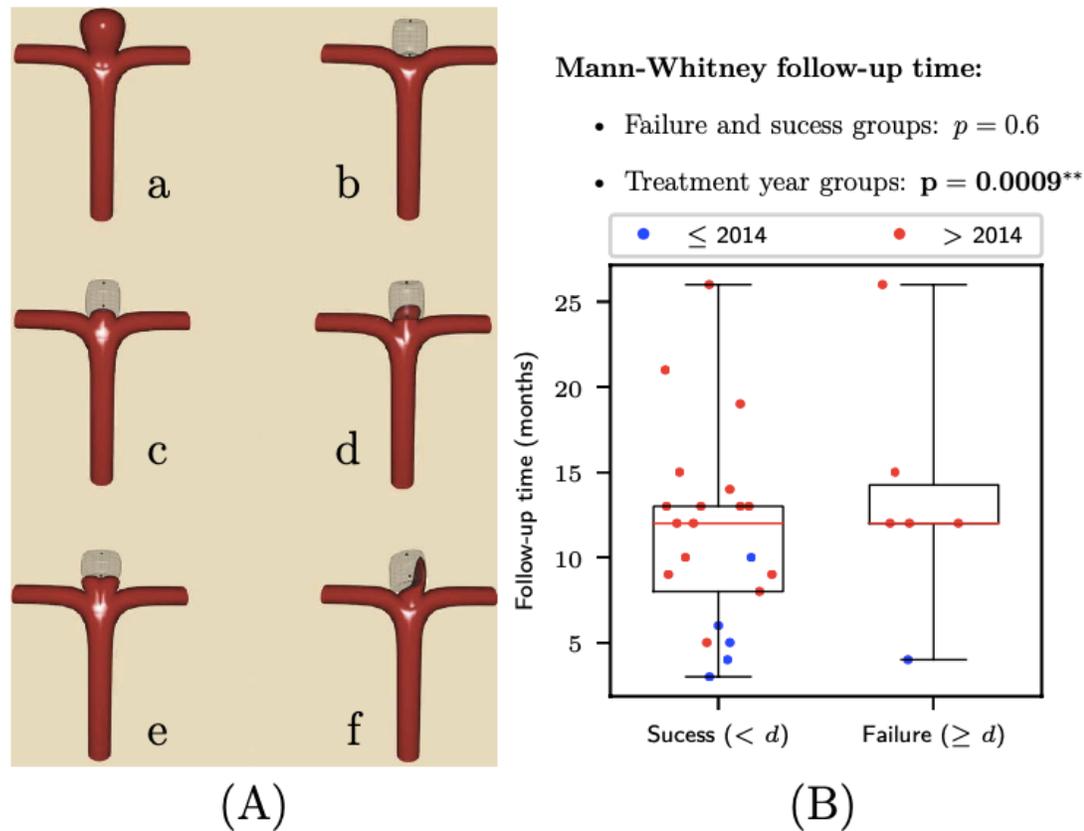
Figure 54: Effect of the follow-up times on the occlusion success of intracranial aneurysms treated with WEB devices. (A) The Beaujon Occlusion Scale Score used for assessing occlusion success (124). The letters represent the different classes of occlusion where a means no device implanted; b, complete occlusion; c, proximal recess opacification; d, intra-device opacification; e, neck remnant; f, aneurysm remnant with contrast agent presence inside the device and in the gaps between the device and the arterial walls. Classes a and b were considered complete occlusions (Success). Classes c, d, e, and f were considered incomplete occlusions (Failure). (B) Box-plot showing the association between follow-up time and occlusion status (Success and Failure). Red and black lines show the median, first, and third quartiles of the follow-up times, and the error bars the minimum and maximum values. The dots' colors resemble the year the occlusion was evaluated, with blue points measured before 2014 and red after.

Regarding patients' age, we found that younger patients were more likely to present occlusion failure than older patients (p-value = 0.005). However, these findings are opposed to the Cagnazzo et al. study, evaluating the in vivo performance of the WEB device in a larger patient cohort (189). Our evaluations did not include the history of tobacco use and hypertension, as this information was missing for some patients.

13.3.4 <u>Association between occlusion status, device-related, and anatomic parameters</u>

We found that large aneurysm volumes (Va) were associated with occlusion failure (Table 20). The literature regarding this association is contradictory. For example, our findings agree with the study of Cebral et al. but not with the in vivo study of Cagnazzo et al., which found no association between occlusion failure and Va (183)(189). However, Cagnazzo et al. (189) demonstrated that tall aneurysm domes modified the WEB device shape. We must be careful when comparing our results with these other evaluations since they used different methods. Cebral et al. used their aneurysm size index Asize, which is different from our Va index as it measures the maximum sac diameter (183). Cagnazzo et al. (189) used an index based on the aneurysm dome resembling ours. However, they used a different measurement method due to the in vivo nature of their evaluations. Their estimates rely on points manually placed while ours on automatic measures. These methodological differences might be responsible for the contradictory results between studies.

Regarding the aneurysm neck, Cebral et al. found that the maximum diameter was systematically wider in patients with occlusion failure (183). We did not observe a similar trend when analyzing the analogous index S_{neck} (p-value = 0.502). Nevertheless, the aneurysm volume to neck surface ratio (R_a), measuring aneurysm elongation, was higher for patients with occlusion failure (Table 20). This finding agrees with the Cebral et al. evaluations but only before adjustments for multiple testing (183).

We found no association between device-related parameters (R_d, D_{neck}, and ApR) and occlusion status (Success and Failure) (p-value > 0.05) (Table 20). However, we could not compare these findings with the literature since we found no similar evaluations. These findings show a need to create more informative device-related

parameters or modify those currently available to gain information about the probability of occlusion success. For example, we could normalize D_{neck} by aneurysm size or parent-artery diameter. Also, we could modify the ApR since this index does not discriminate between the device portions that should come in contact with the aneurysm (lateral side and distal recess) and those that do not (the proximal recess), introducing a bias proportional to the device size.

Index	Success	Failure	p-value
V_a	0.25 ± 0.18	0.39 ± 0.09	$0.025**$
S_{neck}	21.12 ± 8.43	22.72 ± 4.65	0.502
R_a	1.32 ± 0.17	1.54 ± 0.14	$0.021**$
R_d	0.75 ± 0.15	0.76 ± 0.13	0.884
D_{neck}	0.61 ± 0.39	0.88 ± 0.71	0.705
ApR	0.34 ± 0.15	0.29 ± 0.11	0.466

*Table 20: Association between the occlusion status (Success and Failure) and the anatomic and devices-related parameters. Shown are the mean and standard deviations. * denotes differences between the occlusion-status groups at a 95 % confidence level according to the two-sided Mann-Whitney rank-sum test.*

13.3.5 Association between occlusion status and hemodynamic parameters

Regarding the pure hemodynamic index (Q+ and ICI), meaning those not involving anatomic parameters, we saw lower treatment inflow concentration indexes (ICI) before the placement of the WEB device (pre-treatment) for cases with successful occlusions (p-value = 0.029) (Table 21). The CFD study by Caroff et al. analyzed an index similar to ICI (i.e., inflow ratio defined as aneurysm neck inflow divided by parent-artery flow rate) during the pre-treatment of 19 patients. They also found that patients with complete occlusion tended toward lower inflow ratios. However, their results were not statistically supported (203).

The remaining pure hemodynamic index, Q+ (pre-treatment, post-treatment, and ratio), and ICI (post-treatment and ratio) did not differ between cases with successful and unsuccessful occlusions. These results do not agree with the Cebral et al. evaluations finding differences between occlusion groups for both indexes. Several

factors might be responsible for these differences between studies. For example, 80% of the devices assessed by Cebral et al. were WEB-DL devices. These devices have higher lead densities in the proximal recess, resulting in increased flow blockage and decreased input values. Also, Cebral et al. evaluations used an evenly distributed patient cohort with 18 patients presenting complete occlusion and 18 non-occlusion, giving their result greater statistical reliability than ours. Finally, 44% of Cebral et al. patients had devices protruding the aneurysm neck, resulting in patients with distinct inflow ratios (high and low). These differing inflow ratios could have generated a bias when analyzing post-treatment neck-related parameters since measurements highly depend on the device positioning in the aneurysm neck. The authors could not assess the association between hemodynamic index and occlusion status within the patients with different inflow ratios. The study lost three patients in each inflow ratio group leading to insufficient statistical power for obtaining reliable results (183). On the other hand, Cebral et al. did not report the device protrusion rate, so we could not make a comparison.

Index	Success	Failure	p-value
Q^+			
Pre	1.55 ± 1.31	1.28 ± 0.45	0.930
Post	1.24 ± 1.46	0.81 ± 0.33	0.793
Ratio	0.70 ± 0.32	0.73 ± 0.35	0.620
U_a			
Pre	0.13 ± 0.08	0.09 ± 0.03	0.232
Post	0.05 ± 0.05	0.02 ± 0.01	0.096*
Ratio	0.31 ± 0.14	0.25 ± 0.11	0.540
ICI			
Pre	2.12 ± 1.31	3.14 ± 0.93	0.029**
Post	1.80 ± 2.03	2.27 ± 1.68	0.398
Ratio	0.72 ± 0.40	0.63 ± 0.36	0.838
SR_a			
Pre	409.86 ± 228.40	258.14 ± 101.04	0.122
Post	197.81 ± 221.29	80.02 ± 45.25	0.044**
Ratio	0.41 ± 0.20	0.33 ± 0.15	0.466
VO_a			
Pre	297.17 ± 167.71	187.06 ± 73.55	0.109
Post	131.58 ± 151.28	52.64 ± 32.04	0.051*

Ratio	0.38 ± 0.19	0.30 ± 0.15	0.431
TAWSS			
Pre	2.69 ± 2.29	1.66 ± 0.77	0.307
Post	0.90 ± 1.15	0.27 ± 0.16	0.058*
Ratio	0.30 ± 0.15	0.18 ± 0.07	0.051*
MATT			
Pre	0.11 ± 0.07	0.25 ± 0.19	0.011**
Post	0.69 ± 1.23	1.02 ± 0.46	0.006**
Ratio	4.92 ± 4.64	5.13 ± 3.00	0.540
FN			
Pre	7.56 ± 5.92	3.35 ± 1.51	0.018**
Post	5.34 ± 5.89	1.99 ± 0.83	0.021**
Ratio	0.69 ± 0.32	0.71 ± 0.33	0.540

*Table 21: Association between the occlusion status (Success and Failure), pre and post-treatment hemodynamic parameters, and their post to pre-treatment ratios (ratio). Shown are the mean and standard deviations. * and ** denotes differences between the occlusion-status groups at a 90 % and 95% confidence level according to the two-sided Mann-Whitney rank-sum test.*

Another important finding was that non-occluded cases had lower post-treatment shear rates (SR_a) than cases with successful occlusions (p-value = 0.044) (Table 21). These cases also had lower post-treatment U_a, VO_a, and TAWSS but at a lower confidence level (p-value < 0.010) (Table 21). These results contradict the literature about FDs. For example, a study by Mut et al. (162) demonstrated increased mean velocities and shear rates related to slow occlusion since a poor proximal device apposition allowed flow passage towards the aneurysm. Similarly, Ouared et al. (163) found higher mean velocity ratios in non-occluded patients. They proposed a mean velocity ratio threshold of 0.65 for predicting occlusion with 99 % and 67 % sensitivity and specificity, respectively. However, the sample size for this study was small, including 12 patients with only three non-occluded patients.

Brina et al. (204) found lower systolic velocity reduction ratios (PVRR) in cases presenting late or no aneurysm thrombosis 12 months following the treatment with FDs while assessing in vivo 3D-PCMRI. PVRR is defined as $1 - (U_a^{post}Q_{ICA,pre})/(U_a^{pre}Q_{ICA,post})$ with U_a being aneurysm velocity spatially averaged and QICA the parent artery flow rate. Therefore, the lower PVRR implied a higher U_a^{post}/U_a pre ratio

for patients with late thrombosis. However, these results were not statistically supported. The in silico Cerebral et al. study supported the Brina et al. findings regarding the U_a reduction (183). However, as previously declared, we must be cautious when comparing studies due to differences in methodologies.

Regarding the other hemodynamic metrics, we found that cases with occlusion failures had higher pre-treatment and post-treatment MATT (Table 21), suggesting that the blood flowing into non-occluded aneurysms had longer residence times. These results were unexpected since longer residence times stabilize the aneurysm sac and promote healing, increasing the chances of getting a good treatment outcome. Also surprising, we found lower pre-treatment and post-treatment FN in non-occluded cases, indicating that these cases had less blood flowing through the aneurysm neck before and after WEB device placement. However, we must consider that MATT and FN are compound indexes. Therefore, we do not know whether the differences between successful and unsuccessful-occlusions cases resulted from hemodynamic (Q+ and Ua) or anatomic (Va) features.

We found it difficult to cross-validate our unexpected results since we found only one evaluation assessing the effect of WEB devices on aneurysm hemodynamics in silico (183). Also, only one in vivo study used hemodynamic parameters similar to ours and found no difference between patients with successful and unsuccessful occlusions (179). However, we know that FD and WEB devices differentially affect the aneurysm hemodynamics. These differences might partly be responsible for our unexpected results and the differences we found in the literature. For example, FD implantation results in large recirculation regions within the aneurysm sac due to its lateral position concerning the parent artery and likely remanent flow jets due to proximal device malapposition. Also, the device's proximity to the neck surface and parent artery facilitates the endothelialization of the DF surface. The endothelialization starts from apposed device regions and continues looking to isolate the aneurysm (205)(206). Since WEB devices center on bifurcating aneurysms, they encounter stronger inflow jets. Also, WEB devices and FDs have a different porosity distribution across the aneurysm neck, which leads to different flow topologies.

Therefore, comparing these devices' occlusion rates using different metrics might not be relevant.

Furthermore, the thrombosis mechanisms leading to occlusion vary between these devices. In WEB devices, Intrasaccular thrombosis relates to conformational changes, evidenced by device compression within the intracranial aneurysm sac (207). Therefore, the occlusion rates may change over time due to the WEB device positioning within the sac affecting the hemodynamic parameters. FD remains unvaried in the aneurysm neck. Then, they lack this device positioning effect.

A plausible explanation for the higher MATT and lower SRa in cases with unsuccessful occlusions is that thrombotic reactions occur faster due to the lower velocities and higher residence time. These faster thrombotic reactions result in thrombus formation inside the device and the aneurysm sac, which could modify the WEB device shape. These conformational changes might affect the aneurysm neck-device apposition, leading to intra-device opacification (class d), neck remanent (class e), or aneurysm remanet (class f) (Figure 54). On the contrary, higher velocities and lower residence times might result in delayed thrombus formation in cases with successful occlusion. Therefore, the device conformational changes associated with thrombosis are less likely.

We base the hypothesis above on our previous knowledge regarding the effect of WEB device positioning on intra-saccular hemodynamics. Therefore, we expect major WEB device-shape modifications to induce important hemodynamic changes. However, we must emphasize that further evaluations must validate this hypothesis since no evidence is available supporting the association between WEB devices' conformational changes and treatment outcomes (189) (207). Also, we found only three cases having WEB device-shape modifications in our patient cohort, two with successful and one with unsuccessful occlusions.

Understanding the mechanisms behind intrasaccular thrombus initiation and evolution and their association with the prognosis of patients treated with the WEB device for intracranial aneurysms might confirm our hypothesis. A in silico evaluation using FD silicone models showed that deploying two FD with different sizes in the same anatomy resulted in similar thrombus initiation. However, the thrombus evolved

depending on the device. In one device, the thrombus was organized and stable thrombus with a robust proportion of fibrin-rich regions. Conversely, the thrombus was unstable in the other device and had increased erythrocyte-rich areas and reduced platelet- and fibrin-rich regions. This thrombus collapsed upon the silicon-device removal (208). . Similar evaluations using WEB devices would be useful to validate our arguments. However, further studies should attempt these evaluations since we could not find such a study while searching the literature.

13.4 Limitations

This section lists the limitations of our work according to their relevance:

1. The follow-up time from which we determined the treatment outcome and based our CFD calculations were between three and 26 months following the WEB device placement. Therefore, our CFD analysis can not account for short-term blood flow changes, including hemodynamic changes resulting from intrasaccular thrombus formation or device-shape modifications following device detachment. Ding et al. showed that five-minute angiograms differed from three-month angiograms in endovascular treated patients (207)(209). We must be careful while analyzing the angiographs and extrapolating our results to ensure that they adequately reflect features such as intra-saccular flow jets and recirculations. Since we do not know whether our CFD models can accurately simulate thrombus formation, further evaluations focusing on these short-term outcomes can be useful to validate our CFD models and increase their confidence.

2. We did not compare the in vivo device positioning inside the aneurysm sac with the simulation result since such comparisons were difficult to make using the control images. Although, we followed the recommendations used by the doctors in the procedure to simulate the WEB device deployment to mitigate this lack of comparison. In particular, we minimized the distance between the device and the aneurysm neck while preventing protrusion and assuring a proper intrasaccular filling to match our cohort's high and low medians Rd and Dneck (0.8 mm and 0.5 mm, respectively). We ignore whether small device-position changes lead to different

CFD results. To overcome this uncertainty, we could simulate the WEB device deployment multiple times, varying parameters such as neck-to-dome centerlines (Figure 47B) and perform the CFD analysis for each placement. These simulations would show how robust our simulations are regarding the WEB device position. We expect such a study would be more relevant for cases with non-apposed devices since those with apposed devices have no room for maneuvering inside the sac.

3. Our successful and unsuccessful occlusion groups are uneven, meaning they have different sample sizes. These differences could affect the reliability of our statistical methods. Also, we could not perform a multivariate analysis to assess interactions between the evaluated parameter due to our small sample size.

4. We did not use inter and intra-observer agreements while assessing the occlusion status with the BOSS scale. Having independent assessments of an aneurysm occlusion would assure an objective estimate, increasing the confidence of our results. Moreover, we could use multiple occlusion gradation scales to improve our understanding of occlusion patterns. This deeper understanding could allow us to initiate a discussion about how aneurysm hemodynamics relates to occlusion.

5. We set the number of wires per device to 144 regardless of the WEB device size since we have no manufacturer's recommendation for this parameter. We recommend performing evaluations using the same anatomies and device sizes but setting the number of wires to values recommended by the manufacturer to assess the effect of this parameter.

6. We have no patient-specific flow rates. Therefore, we used idealized boundary conditions. Additionally, we assume that the blood behaves as a Newtonian fluid and that the artery walls are rigid, which are common intracranial aneurysms CFD studies assumptions.

13.5 Conclusion

Using reduced computational resources and basic CFD knowledge, we constructed a database of intracranial aneurysms treated with WEB devices, including hemodynamic information. We identified different pre-treatment blood flow patterns resulting from the varying parent-artery anatomies. Also, our post-treatment CFD analysis allowed us to simulate hemodynamic conditions depending on device apposition and protrusion.

Regarding the occlusion mechanism, we found several anatomic and hemodynamic parameters related to the occlusion state of the aneurysm. However, some of these parameters had unexpected associations with the occlusion state. We could not validate these unforeseen associations with the literature since the work regarding the hemodynamics of intracranial aneurysms treated with WEB devices is scarce.

We encounter various limitations while developing this work. Therefore, these evaluations must be considered as an initial step toward understanding the association between hemodynamic conditions and occlusion in the intracranial aneurysm treatment with WEB devices. We recommend that further studies must address our study limitations. We believe it is necessary to continue researching the hemodynamics of intracranial aneurysms treated with WEB devices. We recommend further evaluations addressing our study limitations, including evaluations using a more robust sample size to validate our results and proposed mechanisms.

Nomenclature

2D-DSA : 2D digital subtraction angiography

3D-DSA : 3D digital subtraction angiography

ABS: Acrylonitrile butadiene styrene

ACA : Anterior cerebral artery

AComA : Anterior communicating artery

AI : Artificial intelligence

ApR : Apposition Ratio

ASA : Acetylsalicylic acid

Asize : Aneurysm size

BasA : Basilar artery

BOSS: Beaujon Occlusion Scale Score

BP : Blood pressure

CE Marking : European Commission

CFD : Computational Fluid Dynamics

CI : Confidence interval

CTA : Computed tomography angiography

DED : Derivo embolization device

DQ : Design qualification

FD : Flow Diverter Stent

FDA : Food and Drug Administration

FDM : Fused deposition modeling

FN: Flushing number

HPC : Hydrophilic polymer coating

HR : Hazard ratio

IA : Intracranial aneurysm

ICA : Internal carotid artery

ICI : Inflow concentration Index

IQ : Installation Qualification

IQR : Interquartile ranges

ISUIA : Unruptured Intracranial Aneurysms

KE : Kinetic energy

LSAR : low wall shear stress area proportion

MAFA : Aneurysm flow amplitude

MATT : Mean aneurysm transient time

MCA : Middle cerebral artery

MRI : Magnetic resonance imaging

MSC : Surface Metal Coverage

Multiple : Multiple selection category

NA : Not applicable

NS : Not specified

Nsize : Neck size

OQ : Operational Qualification

OR : Odds ratio

OSI : oscillatory shear index

PCA : Posterior cerebral artery

PCAS : Part comparison analysis

PComA : Posterior communicating artery

PcomP: Posterior communicating artery

PCS : Prospective Cohort Study

PD : Pore Density

PED : Pipeline Embolisation Device

PHASES : Population, Hypertension, Age, Size, Earlier subarachnoid hemorrhage, and Site

PMCS : Prospective Multicenter Cohort Study

PQ : Performance Qualification

PRC : Pressure Reduction Coefficient

Q : Aneurysms Inflow rate

RCS : Retrospective Cohort Study

RMCS : Retrospective multicenter cohort study

ROC : Receiver operating characteristic

RR : Relative risk

rTTP : Relative time-to-peak

SAH : Subarachnoid hemorrhage

SCA : Superior cerebral artery

SDF 1 : cellular stromal-derived factor

Single : Single selection category

SLA : Stereolithography

Sneck : Total neck surface

SPED : Pipeline Flex with Shield

SR : Shear rate

TAWSS : Time-Averaged Wall Shear Stress

TDC : Time-density curve

UIA: Unruptured intracranial aneurysm

UIATS : Unruptured intracranial aneurysm treatment score

VE : Aneurysms velocity

VMTK : Vascular Modeling Toolkit

VO : Aneurysms vorticity

WEB : Woven EndoBridge

WEB-DL : Woven EndoBridge dual layer

WEB-SL : Woven EndoBridge single layer

WEB-SLS : Woven EndoBridge single layer spherical

WNBA : Wide-Necked Bifurcation Aneurysm

WSS : Wall shear stress

Bibliography

1. Hollnagel Erik WDD. Joint Cognitive Systems, Foundations of Cognitive Systems Engineering. 1st Editio. 2005.
2. Schmettow M, Schnittker R, Schraagen JM. An extended protocol for usability validation of medical devices: Research design and reference model. J Biomed Inform [Internet]. 2017;69:99–114. Available from: http://dx.doi.org/10.1016/j.jbi.2017.03.010
3. Lin L, Vicente KJ, Doyle DJ. Patient safety, potential adverse drug events, and medical device design: A human factors engineering approach. J Biomed Inform. 2001;34(4):274–84.
4. Texakalidis P, Bekelis K, Atallah E, Tjoumakaris S, Rosenwasser RH, Jabbour P. Flow diversion with the pipeline embolization device for patients with intracranial aneurysms and antiplatelet therapy: A systematic literature review. Clin Neurol Neurosurg [Internet]. 2017;161(August):78–87. Available from: http://dx.doi.org/10.1016/j.clineuro.2017.08.003
5. Pierot L, Wakhloo AK. Endovascular treatment of intracranial aneurysms: Current status. Stroke. 2013;44(7):2046–54.
6. Brown RD, Broderick JP. Unruptured intracranial aneurysms: Epidemiology, natural history, management options, and familial screening. Lancet Neurol [Internet]. 2014;13(4):393–404. Available from: http://dx.doi.org/10.1016/S1474-4422(14)70015-8
7. Wiebers DO. Unruptured intracranial aneurysms: Natural history, clinical outcome, and risks of surgical and endovascular treatment. Lancet. 2003;362(9378):103–10.
8. Vlak MHM, Algra A, Brandenburg R, Rinkel GJE. Prevalence of unruptured intracranial aneurysms, with emphasis on sex, age, comorbidity, country, and time period: a systematic review and meta-analysis. Lancet Neurol [Internet]. 2011;10(7):626–36. Available from: https://www.sciencedirect.com/science/article/pii/S1474442211701090
9. Singer Robert J OgilvyChristopher S RG. Unruptured intracranial aneurysms [Internet]. 2022. Available from: https://www.uptodate.com/contents/unruptured-intracranial-aneurysms?search=intracranial aneurysm&source=search_result&selectedTitle=1~150&usage_type=default&display_rank=1
10. Liu H, Zhang T, Jiao S, Li B, Guan J, Wang YXJ. Epidemiological investigation of 264 sporadic cases of ruptured cerebral aneurysm at a single institution in southwest China. Neuropsychiatr Dis Treat. 2015;11(2):1609–14.
11. Feigin VL, Lawes CM, Bennett DA, Barker-Collo SL, Parag V. Worldwide stroke incidence and early case fatality reported in 56 population-based studies: a systematic review. Lancet Neurol [Internet]. 2009;8(4):355–69. Available from: http://dx.doi.org/10.1016/S1474-4422(09)70025-0
12. Lori C. Jordan, Claiborne Johnston, Yvonne W. Wu, Stephen Sidney HJF. The

Importance of Cerebral Aneurysms in Childhood Hemorrhagic Stroke: A Population-based Study. Stroke [Internet]. 2009;23(1):1–7. Available from: https://www.ncbi.nlm.nih.gov/pmc/articles/PMC3624763/pdf/nihms412728.pdf

13. Hyodo A. Eddleman, and Alan S, Boulos, (Eds): handbook of neuroendovascular surgery. Acta Neurochir (Wien). 2012;154(8):1537–8.

14. Etminan N, Dörfler A, Steinmetz H. Unruptured intracranial aneurysms—pathogenesis and individualized management. Dtsch Arztebl Int. 2020;117(14):235–42.

15. Greving JP, Wermer MJH, Brown RD, Morita A, Juvela S, Yonekura M, et al. Development of the PHASES score for prediction of risk of rupture of intracranial aneurysms: A pooled analysis of six prospective cohort studies. Lancet Neurol. 2014;13(1):59–66.

16. Backes D, Rinkel GJE, Laban KG, Algra A, Vergouwen MDI. Patient-and aneurysm-specific risk factors for intracranial aneurysm growth: A systematic review and meta-analysis. Stroke. 2016;47(4):951–7.

17. Kundra S, Mahendru V, Gupta V, Choudhary AK. Principles of neuroanesthesia in aneurysmal subarachnoid hemorrhage. J Anaesthesiol Clin Pharmacol. 2014;30(3):328–37.

18. Petridis AK, Kamp MA, Cornelius JF, Beez T, Beseoglu K, Turowski B, et al. Aneurysmal subarachnoid hemorrhage-diagnosis and treatment. Dtsch Arztebl Int. 2017;114(13):226–35.

19. Hanel RA, Kallmes DF, Lopes DK, Nelson PK, Siddiqui A, Jabbour P, et al. Prospective study on embolization of intracranial aneurysms with the pipeline device: The PREMIER study 1 year results. J Neurointerv Surg. 2020;12(1):62–6.

20. Merenzon MA, Ignacio J, Escalante G, Prost D, Seoane E, Mazzon A. Preoperative imaging features : Are they useful tools for predicting IDH1 mutation status in gliomas Grades II – IV ? 2022;13(332):1–6.

21. Urasyanandana K, Songsang D, Aurboonyawat T, Chankaew E, Withayasuk P, Churojana A. Treatment outcomes in cerebral artery dissection and literature review. Interv Neuroradiol. 2018;24(3):254–62.

22. Smith W.S., Johnston S.C., Skalabrin E.J., Weaver M., Azari P., Albers G.W. et al. Spinal manipulative therapy is an independent risk factor for vertebral artery dissection. Neurology. 2003;61(9):1314–5.

23. Friedman JA, Piepgras DG, Pichelmann MA, Hansen KK, Brown RD, Wiebers DO. Small cerebral aneurysms presenting with symptoms other than rupture. Neurology. 2001;57(7):1212–6.

24. Fujiwara S., Fujii K., Nishio S., Matsushima T. FM. Oculomotor nerve palsy in patients with cerebral aneurysms Shigeru Fujiwara, Kiyotaka Fujii, Shunji Nishio, Toshio Matsushima, and Masashi Fukui. Neurosurg Rev. 1989;12:123–32.

25. Matsuda M, Watanabe K, Saito A, Matsumura K ichi, Ichikawa M. Circumstances, Activities, and Events Precipitating Aneurysmal Subarachnoid Hemorrhage. J Stroke Cerebrovasc Dis. 2007;16(1):25–9.

26. Perry JJ, Sivilotti MLA, Sutherland J, Hohl CM, Émond M, Calder LA, et al. Validation of the Ottawa Subarachnoid Hemorrhage Rule in patients with acute headache.

Cmaj. 2017;189(45):E1379–85.

27. Butzkueven H. Onset seizures independently predict poor outcome after subarachnoid hemorrhage. Neurology. 2001;56(10):1423–4.

28. WI. S. Intracranial Aneurysms. N Engl J Med. 1997;10(4):739–49.

29. Singer Robert J, Ogilvy Christopher S RG. Aneurysmal subarachnoid hemorrhage: Clinical manifestations and diagnosis [Internet]. 2022. Available from: https://www.uptodate.com/contents/aneurysmal-subarachnoid-hemorrhage-clinical-manifestations-and-diagnosis?search=intracranial aneurysm&topicRef=1132&source=see_link

30. Tawk RG, Hasan TF, D'Souza CE, Peel JB FW. Diagnosis and Treatment of Unruptured Intracranial Aneurysms and Aneurysmal Subarachnoid Hemorrhage. Mayo Clin Proc [Internet]. 2021;96(7):1970–2000. Available from: https://doi.org/10.1016/j.mayocp.2021.01.005

31. Bijlenga P, Gondar R, Schilling S, Morel S, Hirsch S, Cuony J, et al. PHASES Score for the Management of Intracranial Aneurysm: A Cross-Sectional Population-Based Retrospective Study. Stroke. 2017;48(8):2105–12.

32. Szikora I, Turányi E, Marosfoi M. Evolution of flow-diverter endothelialization and thrombus organization in giant fusiform aneurysms after flow diversion: A histopathologic study. Am J Neuroradiol. 2015;36(9):1716–20.

33. Lylyk P, Miranda C, Ceratto R, Ferrario A, Scrivano E, Luna HR, et al. Curative endovascular reconstruction of cerebral aneurysms with the pipeline embolization device: The Buenos Aires experience. Neurosurgery. 2009;64(4):632–42.

34. Atasoy D, Kandasamy N, Hart J, Lynch J, Yang SH, Walsh D, et al. Outcome study of the pipeline embolization device with shield technology in unruptured aneurysms (PEDSU). Am J Neuroradiol. 2019;40(12):2094–101.

35. Li YL, Roalfe A, Chu EYL, Lee R, Tsang ACO. Outcome of flow diverters with surface modifications in treatment of cerebral aneurysms: systematic review and meta-analysis. Am J Neuroradiol. 2021;42(2):327–33.

36. Park SH, Choi J, Byeon JS. Key principles of clinical validation, device approval, and insurance coverage decisions of artificial intelligence. Korean J Radiol. 2021;22(3):442–53.

37. U.S. Food and Drug Administration. General Principles of Software Validation; Final Guidance for Industry and FDA Staff (Document issued on: January 11, 2002). FDA Guid [Internet]. 2002;47. Available from: http://www.fda.gov/downloads/RegulatoryInformation/Guidances/ucm126955.pdf

38. Refaeilzadeh P, Tang L, Liu H, Angeles L, Scientist CD. Cross-Validation. Encycl Database Syst. 2020;

39. Faes L, Liu X, Wagner SK, Fu DJ, Balaskas K, Sim D, et al. A clinician's guide to artificial intelligence: How to critically appraise machine learning studies. Transl Vis Sci Technol. 2020;9(2):3–5.

40. Augsburger L, Reymond P, Rufenacht DA, Stergiopulos N. Intracranial Stents Being Modeled as a Porous Medium: Flow Simulation in Stented Cerebral Aneurysms. Ann Biomed Eng. 2011 Feb;39(2):850–63.

41. Jou L-D, Chintalapani G, Mawad ME. Metal coverage ratio of pipeline embolization

device for treatment of unruptured aneurysms: Reality check. Interv Neuroradiol. 2016 Feb;22(1):42–8.

42.   Augsburger L, Farhat M, Reymond P, Fonck E, Kulcsar Z, Stergiopulos N, et al. Effect of Flow Diverter Porosity on Intraaneurysmal Blood Flow. Clin Neuroradiol. 2009 Aug;19(3):204–14.

43.   Park MS, Kilburg C, Taussky P, Albuquerque FC, Kallmes DF, Levy EI, et al. Pipeline Embolization Device with or without Adjunctive Coil Embolization: Analysis of Complications from the IntrePED Registry. Am J Neuroradiol. 2016 Jun;37(6):1127–31.

44.   Zhang M, Anzai H, Chopard B, Ohta M. Towards the patient - specific design of flow diverters made from helix - like wires : an optimization study. Biomed Eng Online. 2016;15(s2):371–82.

45.   Narata AP, Blasco J, Roman LS, Macho JM, Fernandez H, Moyano RK, et al. Early Results in Flow Diverter Sizing by Computational Simulation: Quantification of Size Change and Simulation Error Assessment. Oper Neurosurg. 2018 Jan;

46.   ISO 9241-11. Ergonomic requirements for office work with visual display terminals (VDTs) - Part 11: Guidance on usability. 1998;1998.

47.   Evaluation USD of H and HSF and DAC for D and RHO of D. Applying Human Factors and Usability Engineering to Medical Devices. Guid Ind Food Drug Adm Staff. 2016;(301):1601–5.

48.   Schraagen JM, Verhoeven F. Methods for studying medical device technology and practitioner cognition: The case of user-interface issues with infusion pumps. J Biomed Inform [Internet]. 2013;46(1):181–95. Available from: http://dx.doi.org/10.1016/j.jbi.2012.10.005

49.   Nunnally M, Nemeth CP, Brunetti V, Cook RI. Lost in menuspace: User interactions with complex medical devices. IEEE Trans Syst Man, Cybern Part ASystems Humans. 2004;34(6):736–42.

50.   Turjman F, Levrier O, Combaz X, Bonafé A, Biondi A, Desal H, et al. EVIDENCE Trial: design of a phase 2, randomized, controlled, multicenter study comparing flow diversion and traditional endovascular strategy in unruptured saccular wide-necked intracranial aneurysms. Neuroradiology. 2015;57(1):49–54.

51.   Brinjikji W, Murad MH, Lanzino G, Cloft HJ, Kallmes DF. Endovascular treatment of intracranial aneurysms with flow diverters: A meta-analysis. Stroke. 2013;44(2):442–7.

52.   Dornbos D, Powers CJ. Acute distal migration of a flow diverting stent. J Clin Neurosci. 2017;44:223–5.

53.   Kühn AL, Rodrigues K de M, Wakhloo AK, Puri AS. Endovascular techniques for achievement of better flow diverter wall apposition. Interv Neuroradiol. 2019;25(3):344–7.

54.   Cohen JE, Gomori JM, Moscovici S, Leker RR, Itshayek E. Delayed complications after flow-diverter stenting: Reactive in-stent stenosis and creeping stents. J Clin Neurosci. 2014;21(7):1116–22.

55.   Chalouhi N, Satti SR, Tjoumakaris S, Dumont AS, Gonzalez LF, Rosenwasser R, et al. Delayed migration of a pipeline embolization device. Neurosurgery.

2013;72(June):229–34.

56. Shapiro M, Raz E, Becske T, Nelson PK. Building multidevice pipeline constructs of favorable metal coverage: A practical guide. Am J Neuroradiol. 2014;35(8):1556–61.

57. Shapiro M, Raz E, Becske T, Nelson PK. Variable porosity of the pipeline embolization device in straight and curved vessels: A guide for optimal deployment strategy. Am J Neuroradiol. 2014;35(4):727–33.

58. Cagnazzo F, Lefevre P-H, Mantilla D, Rouchaud A, Morganti R, Perrini P, et al. Patency of the supraclinoid internal carotid artery branches after flow diversion treatment. A meta-analysis. J Neuroradiol. 2018 Aug;

59. Rangel-Castilla L, Munich SA, Jaleel N, Cress MC, Krishna C, Sonig A, et al. Patency of anterior circulation branch vessels after Pipeline embolization: longer-term results from 82 aneurysm cases. J Neurosurg. 2017 Apr;126(4):1064–9.

60. Kulcsár Z, Ernemann U, Wetzel SG, Bock A, Goericke S, Panagiotopoulos V, et al. High-Profile Flow Diverter (Silk) Implantation in the Basilar Artery. Stroke. 2010 Aug;41(8):1690–6.

61. Marosfoi M, Langan ET, Strittmatter L, van der Marel K, Vedantham S, Arends J, et al. In situ tissue engineering: endothelial growth patterns as a function of flow diverter design. J Neurointerv Surg. 2017 Oct;9(10):994–8.

62. Dandapat S, Mendez-Ruiz A, Martínez-Galdámez M, Macho J, Derakhshani S, Foa Torres G, et al. Review of current intracranial aneurysm flow diversion technology and clinical use. J Neurointerv Surg. 2020;neurintsurg-2020-015877.

63. Bonney PA, Connor M, Fujii T, Singh P, Koch MJ, Stapleton CJ, et al. Failure of Flow Diverter Therapy: Predictors and Management Strategies. Neurosurgery. 2020;86(1):S64–73.

64. Ma D, Dargush GF, Natarajan SK, Levy EI, Siddiqui AH, Meng H. Computer modeling of deployment and mechanical expansion of neurovascular flow diverter in patient-specific intracranial aneurysms. J Biomech [Internet]. 2012;45(13):2256–63. Available from: http://dx.doi.org/10.1016/j.jbiomech.2012.06.013

65. Bouillot P, Brina O, Yilmaz H, Farhat M, Erceg G, Lovblad KO, et al. Virtual-versus-real implantation of flow diverters: Clinical potential and influence of vascular geometry. Am J Neuroradiol. 2016;37(11):2079–86.

66. Seshadhri S, Janiga G, Beuing O, Skalej M, Thévenin D. Impact of stents and flow diverters on hemodynamics in idealized aneurysm models. J Biomech Eng. 2011;133(7):1–10.

67. Augsburger L, Reymond P, Rufenacht DA, Stergiopulos N. Intracranial stents being modeled as a porous medium: Flow simulation in stented cerebral aneurysms. Ann Biomed Eng. 2011;39(2):850–63.

68. Hauck EF, Natarajan SK, Langer DJ, Hopkins LN, Siddiqui AH, Levy EI. Retrograde trans-posterior communicating artery snare-assisted rescue of lost access to a foreshortened pipeline embolization device: Complication management. Neurosurgery. 2010;67(SUPPL. 2):495–502.

69. Wong GKC, Kwan MCL, Ng RYT, Yu SCH, Poon WS. Flow diverters for treatment of intracranial aneurysms: Current status and ongoing clinical trials. J Clin Neurosci [Internet]. 2011;18(6):737–40. Available from:

http://dx.doi.org/10.1016/j.jocn.2010.10.011

70. Gascou G, Ferrara R, Ambard D, Sanchez M, Lobotesis K, Jourdan F, et al. The pressure reduction coefficient: A new parameter to assess aneurysmal blood stasis induced by flow diverters/disruptors. Interv Neuroradiol. 2017;23(1):41–6.

71. Liou TM, Li YC. Effects of stent porosity on hemodynamics in a sidewall aneurysm model. J Biomech. 2008;41(6):1174–83.

72. Guglielmi G. The beginning and the evolution of the endovascular treatment of intracranial aneurysms: From the first catheterization of brain arteries to the new stents. J Neurointerv Surg. 2009;1(1):53–5.

73. Kulcsár Z, Houdart E, Bonafé A, Parker G, Millar J, Goddard AJP, et al. Intra-aneurysmal thrombosis as a possible cause of delayed aneurysm rupture after flow-diversion treatment. Am J Neuroradiol. 2011;32(1):20–5.

74. Giordan E, Sorenson TJ, Brinjikji W, Vine R, Lanzino G. Risk factors for growth of conservatively managed unruptured intracranial aneurysms. Acta Neurochir (Wien). 2018;160(12):2419–23.

75. David Altschul TV and SU. Endovascular treatment of brain aneurysms. Neurovascular Imaging From Basics to Adv Concepts. 2016;551–81.

76. Hackenberg KAM, Hänggi D, Etminan N. Unruptured Intracranial Aneurysms: Contemporary Data and Management. Stroke. 2018;49(9):2268–75.

77. Caroff J, Neki H, Mihalea C, D'Argento F, Abdel Khalek H, Ikka L, et al. Flow-diverter stents for the treatment of saccular middle cerebral artery bifurcation aneurysms. Am J Neuroradiol. 2016;37(2):279–84.

78. Nishimura K, Otani K, Mohamed A, Dahmani C, Ishibashi T, Yuki I, et al. Accuracy of Length of Virtual Stents in Treatment of Intracranial Wide-Necked Aneurysms. Cardiovasc Intervent Radiol [Internet]. 2019;42(8):1168–74. Available from: https://doi.org/10.1007/s00270-019-02230-9

79. Kühn AL, Wakhloo AK, Gounis MJ, Kan P, De Macedo Rodrigues K, Lozano JD, et al. Use of self-expanding stents for better intracranial flow diverter wall apposition. Interv Neuroradiol. 2017;23(2):129–36.

80. Oldford RW. Statistics and Computing: Editorial. Stat Comput. 2002;12(1):7.

81. Wickham H. Ggplot2, Elegant Graphics for Data Analysis. Applied Spatial Data Analysis with R. New York: Springer-Verlag; 2016. 21–54 p.

82. Guzzardi G, Stanca C, Cerini P, Del Sette B, Divenuto I, Malatesta E, et al. Long-term follow-up in the endovascular treatment of intracranial aneurysms with flow-diverter stents: update of a single-centre experience. Radiol Medica [Internet]. 2018;123(6):449–55. Available from: https://doi.org/10.1007/s11547-018-0857-8

83. Piergallini L, Cagnazzo F, Conte G, Dargazanli C, Derraz I, Lefevre PH, et al. Virtual simulation with Sim&Size software for Pipeline Flex Embolization: Evaluation of the technical and clinical impact. J Neurointerv Surg. 2020;12(10):968–73.

84. Hahnemann ML, Ringelstein A, Sandalcioglu IE, Goericke S, Moenninghoff C, Wanke I, et al. Silent embolism after stent-assisted coiling of cerebral aneurysms: Diffusion-weighted MRI study of 75 cases. J Neurointerv Surg. 2014;6(6):461–5.

85. Cheung NK, Boutchard M, Carr MW, Froelich JJ. Radiation exposure, and procedure and fluoroscopy times in endovascular treatment of intracranial aneurysms: A

methodological comparison. J Neurointerv Surg. 2018;10(9):902–6.

86. Griessenauer CJ, Gupta R, Shi S, Alturki A, Motiei-Langroudi R, Adeeb N, et al. Collar sign in incompletely occluded aneurysms after pipeline embolization: Evaluation with angiography and optical coherence tomography. Am J Neuroradiol. 2017;38(2):323–6.

87. Ospel JM, Gascou G, Costalat V, Piergallini L, Blackham KA, Zumofen DW. Comparison of pipeline embolization device sizing based on conventional 2D measurements and virtual simulation using the Sim&Size software: An agreement study. Am J Neuroradiol. 2019;40(3):524–30.

88. Zhang H, Gao X, Liang H, Ren Y. Incomplete stent apposition of low-profile visualized intraluminal support stents in the treatment of cerebral aneurysms. J Neurointerv Surg. 2020;12(6):591–7.

89. Van Der Marel K, Gounis MJ, Weaver JP, De Korte AM, King RM, Arends JM, et al. Grading of Regional Apposition after Flow-Diverter Treatment (GRAFT): A comparative evaluation of VasoCT and intravascular OCT. J Neurointerv Surg. 2016;8(8):847–52.

90. Faraj MK, Hoz SS, Mohammad AJ. The use of three-dimensional anatomical patient-specific printed models in surgical clipping of intracranial aneurysm: A pilot study. Surg Neurol Int. 2020;11(381):1–5.

91. Mitsouras D, Liacouras P, Imanzadeh A, Giannopoulos AA, Cai T, Kumamaru KK, et al. Medical 3D printing for the radiologist. Radiographics. 2015;35(7):1965–88.

92. Randazzo M, Pisapia J, Singh N, Thawani J. 3D printing in neurosurgery: A systematic review. Surg Neurol Int. 2016;7(34):S801–9.

93. Kono K, Shintani A, Okada H, Terada T. Preoperative simulations of endovascular treatment for a cerebral aneurysm using a patient-specific vascular silicone model. Neurol Med Chir (Tokyo). 2013;53(5):347–51.

94. Waqas M, Mokin M, Lim J, Vakharia K, Springer ME, Meess KM, et al. Design and physical properties of 3-dimensional printed models used for neurointervention: A systematic review of the literature. Neurosurgery. 2020;87(4):E445–53.

95. Ozbolat IT, Yu Y. Bioprinting Toward Organ Fabrication : Challenges and Future Trends Bioprinting Toward Organ Fabrication : Challenges and Future Trends. IEEE Trans Biomed Eng. 2015;60(November):691–9.

96. Krebs FC, Tromholt T, Jørgensen M. Upscaling of polymer solar cell fabrication using full roll-to-roll processing. Nanoscale. 2010;2(6):873–86.

97. Ferris CJ, Gilmore KG, Wallace GG, In Het Panhuis M. Biofabrication: An overview of the approaches used for printing of living cells. Appl Microbiol Biotechnol. 2013;97(10):4243–58.

98. Rengier F, Mehndiratta A, Von Tengg-Kobligk H, Zechmann CM, Unterhinninghofen R, Kauczor HU, et al. 3D printing based on imaging data: Review of medical applications. Int J Comput Assist Radiol Surg. 2010;5(4):335–41.

99. George E, Liacouras P, Rybicki FJ, Mitsouras D. Measuring and establishing the accuracy and reproducibility of 3D printed medical models. Radiographics. 2017;37(5):1424–50.

100. Nagassa RG, McMenamin PG, Adams JW, Quayle MR, Rosenfeld J V. Advanced 3D

printed model of middle cerebral artery aneurysms for neurosurgery simulation. 3D Print Med. 2019;5(1).

101. Wang L, Ye X, Hao Q, Ma L, Chen X, Wang H, et al. Three-dimensional intracranial middle cerebral artery aneurysm models for aneurysm surgery and training. J Clin Neurosci. 2018;50(September 2013):77–82.

102. Ryan JR, Almefty KK, Nakaji P, Frakes DH. Cerebral Aneurysm Clipping Surgery Simulation Using Patient-Specific 3D Printing and Silicone Casting. World Neurosurg [Internet]. 2016;88:175–81. Available from: http://dx.doi.org/10.1016/j.wneu.2015.12.102

103. Popli S, Daugirdas JT, Neubauer JA, Hockenberry B, Hano JE, Ing TS. Transdermal Clonidine in Mild Hypertension A Randomized, Double-blind, Placebo-Controlled Trial. Arch Intern Med. 1986;146(11):2140–4.

104. Liu Y, Gao Q, Du S, Chen ZC, Fu JZ, Chen B, et al. Fabrication of cerebral aneurysm simulator with a desktop 3D printer. Sci Rep [Internet]. 2017;7(September 2016):1–13. Available from: http://dx.doi.org/10.1038/srep44301

105. Dorweiler B, Baqué PE, Chaban R, Ghazy A, Salem O. Quality control in 3D printing: Accuracy analysis of 3D-printed models of patient-specific anatomy. Materials (Basel). 2021;14(4):1–13.

106. Błaszczyk M, Jabbar R, Szmyd B, Radek M. 3D printing of rapid, low-cost and patient-specific models of brain vasculature for use in preoperative planning in clipping of intracranial aneurysms. J Clin Med. 2021;10(6):1–12.

107. Wurm G, Tomancok B, Pogady P, Holl K, Trenkler J. Cerebrovascular stereolithographic biomodeling for aneurysm surgery: Technical note. J Neurosurg. 2004;100(1):139–45.

108. Chueh JY, Wakhloo AK, Gounis MJ. Neurovascular modeling: Small-batch manufacturing of silicone vascular replicas. Am J Neuroradiol. 2009;30(6):1159–64.

109. van Rooij SBT, Sprengers ME, Peluso JP, Daams J, Verbaan D, van Rooij WJ, et al. A systematic review and meta-analysis of Woven EndoBridge single layer for treatment of intracranial aneurysms. Interv Neuroradiol. 2020;26(4):455–60.

110. Goyal N, Hoit D, Dinitto J, Elijovich L, Fiorella D, Pierot L, et al. How to WEB: A practical review of methodology for the use of the Woven EndoBridge. J Neurointerv Surg. 2020;12(5):512–20.

111. Lv X, Zhang Y, Jiang W. Systematic Review of Woven EndoBridge for Wide-Necked Bifurcation Aneurysms: Complications, Adequate Occlusion Rate, Morbidity, and Mortality. World Neurosurg [Internet]. 2018;110:20–5. Available from: https://doi.org/10.1016/j.wneu.2017.10.113

112. Muskens IS, Senders JT, Dasenbrock HH, Smith TRS, Broekman MLD. The Woven Endobridge Device for Treatment of Intracranial Aneurysms: A Systematic Review. World Neurosurg [Internet]. 2017;98:809-817.e1. Available from: http://dx.doi.org/10.1016/j.wneu.2016.11.020

113. Mourad Ouzzani, Hossam Hammady, Zbys Fedorowicz and AE. Rayyan — a web and mobile app for systematic reviews. Systematic Reviews (2016) 5:210.

114. Kewlani B, DJ R, Henry J, Wyse G, Fanning N. A single centre retrospective analysis of short- and medium-term outcomes using the Woven EndoBridge (WEB) device and

identification of the device-to-aneurysm volume ratio as a potential predictor of aneurysm occlusion status. Interv Neuroradiol J peritherapeutic Neuroradiol Surg Proced Relat Neurosci [Internet]. 2022;15910199221092578. Available from: https://pubmed.ncbi.nlm.nih.gov/35404152/

115. Pierot L, Moret J, Barreau X, Szikora I, Herbreteau D, Turjman F, et al. Safety and efficacy of aneurysm treatment with WEB in the cumulative population of three prospective, multicenter series. [Internet]. Vol. 10, Journal of neurointerventional surgery. 2018. p. 553–9. Available from: https://pubmed.ncbi.nlm.nih.gov/28965106/

116. Spelle L, Herbreteau D, Caroff J, Barreau X, JC F, Fiehler J, et al. CLinical Assessment of WEB device in Ruptured aneurYSms (CLARYS): results of 1-month and 1-year assessment of rebleeding protection and clinical safety in a multicenter study. J Neurointerv Surg [Internet]. 2021; Available from: https://pubmed.ncbi.nlm.nih.gov/34493578/

117. Fiorella D, Molyneux A, Coon A, Szikora I, Saatci I, Baltacioglu F, et al. Demographic, procedural and 30-day safety results from the WEB Intra-saccular Therapy Study (WEB-IT). J Neurointerv Surg [Internet]. 2017;9(12):1191–6. Available from: https://pubmed.ncbi.nlm.nih.gov/28096478/

118. Khalid Z, Sorteberg W, Nedregaard B, Sorteberg A. Efficiency and complications of Woven EndoBridge (WEB) devices for treatment of larger, complex intracranial aneurysms-a single-center experience. [Internet]. Vol. 161, Acta neurochirurgica. Austria; 2019. p. 393–401. Available from: https://pubmed.ncbi.nlm.nih.gov/30547246/

119. Lawson A, Goddard T, Ross S, Tyagi A, Deniz K, Patankar T. Endovascular treatment of cerebral aneurysms using the Woven EndoBridge technique in a single center: preliminary results. J Neurosurg [Internet]. 2017;126(1):17–28. Available from: https://pubmed.ncbi.nlm.nih.gov/27081907/

120. DN G, Gory B, Sivan-Hoffmann R, Pierot L, Raoult H, JY G, et al. Endovascular treatment of wide-neck anterior communicating artery aneurysms using WEB-DL and WEB-SL: short-term results in a multicenter study. [Internet]. Vol. 36, AJNR. American journal of neuroradiology. 2015. p. 1150–4. Available from: https://pubmed.ncbi.nlm.nih.gov/25792534/

121. Clajus C, Strasilla C, Fiebig T, Sychra V, Fiorella D, Klisch J. Initial and mid-term results from 108 consecutive patients with cerebral aneurysms treated with the WEB device. J Neurointerv Surg [Internet]. 2017;9(4):411–7. Available from: https://pubmed.ncbi.nlm.nih.gov/27075486/

122. Da Ros V, Bozzi A, Comelli C, Semeraro V, Comelli S, Lucarelli N, et al. Ruptured Intracranial Aneurysms Treated with Woven Endobridge Intrasaccular Flow Disruptor: A Multicenter Experience. World Neurosurg [Internet]. 2019;122:e498–505. Available from: https://www.sciencedirect.com/science/article/pii/S1878875018323866

123. Lawson A, Molyneux A, Sellar R, Lamin S, Thomas A, Gholkar A, et al. Safety results from the treatment of 109 cerebral aneurysms using the Woven EndoBridge technique: preliminary results in the United Kingdom. J Neurosurg [Internet].

2018;128(1):144–53. Available from: https://pubmed.ncbi.nlm.nih.gov/28156251/

124. Caroff J, Mihalea C, Klisch J, Strasilla C, Berlis A, Patankar T, et al. Single-Layer WEBs: Intrasaccular Flow Disrupters for Aneurysm Treatment—Feasibility Results from a European Study. [Internet]. Vol. 36, AJNR. American journal of neuroradiology. 2015. p. 1942–6. Available from: https://pubmed.ncbi.nlm.nih.gov/26159516/

125. AS A, Molyneux A, AL C, Saatci I, Szikora I, Baltacioglu F, et al. The safety and effectiveness of the Woven EndoBridge (WEB) system for the treatment of wide-necked bifurcation aneurysms: final 12-month results of the pivotal WEB Intrasaccular Therapy (WEB-IT) Study. J Neurointerv Surg [Internet]. 2019;11(9):924–30. Available from: https://pubmed.ncbi.nlm.nih.gov/30992395/

126. T DB, Boulanger T, Heye S, WJ van R, W van Z, Stockx L. The Woven EndoBridge for unruptured intracranial aneurysms: Results in 95 aneurysms from a single center. Interv Neuroradiol J peritherapeutic Neuroradiol   Surg Proced Relat Neurosci [Internet].   2021;27(5):594–601.   Available   from: https://pubmed.ncbi.nlm.nih.gov/33745363/

127. SB van R, WJ van R, JP P, Sluzewski M. The Woven EndoBridge (WEB) as primary treatment for unruptured intracranial aneurysms. Interv Neuroradiol J peritherapeutic Neuroradiol   Surg Proced Relat Neurosci [Internet]. 2018;24(5):475–81. Available from: https://pubmed.ncbi.nlm.nih.gov/29768963/

128. Raj R, Rautio R, Pekkola J, Rahi M, Sillanpää M, Numminen J. Treatment of Ruptured Intracranial Aneurysms Using the Woven EndoBridge Device: A Two-Center Experience. World Neurosurg [Internet]. 2019;123:e709–16. Available from: https://www.sciencedirect.com/science/article/pii/S1878875018328328

129. Maurer C, König I, Berlis A, Weber W, Fischer S. Two-Center Experience in the Endovascular Treatment of Intracranial Aneurysms Using the Woven EndoBridge 17 Device Including Midterm Follow-Up Results: A Retrospective Analysis. AJNR Am J Neuroradiol   [Internet].   2019;40(9):1517–22.   Available   from: https://pubmed.ncbi.nlm.nih.gov/31467237/

130. Popielski J, Berlis A, Weber W, Fischer S. Two-Center Experience in the Endovascular Treatment of Ruptured and Unruptured Intracranial Aneurysms Using the WEB Device: A Retrospective Analysis. AJNR Am J Neuroradiol [Internet]. 2018;39(1):111–7. Available from: https://pubmed.ncbi.nlm.nih.gov/29051205/

131. Lubicz B, Mine B, Collignon L, Brisbois D, Duckwiler G, Strother C. WEB device for endovascular treatment of wide-neck bifurcation aneurysms. [Internet]. Vol. 34, AJNR. American journal of neuroradiology. 2013. p. 1209–14. Available from: https://pubmed.ncbi.nlm.nih.gov/23292529/

132. Papagiannaki C, Spelle L, AC J, Benaissa A, JY G, Costalat V, et al. WEB intrasaccular flow disruptor-prospective, multicenter experience in 83 patients with 85 aneurysms. AJNR Am J Neuroradiol [Internet]. 2014;35(11):2106–11. Available from: https://pubmed.ncbi.nlm.nih.gov/24994823/

133. SBT van R, WJ van R, JP P, Sluzewski M, RS B, HG K, et al. WEB Treatment of Ruptured Intracranial Aneurysms: A Single-Center Cohort of 100 Patients. AJNR Am J Neuroradiol   [Internet].   2017;38(12):2282–7.   Available   from: https://pubmed.ncbi.nlm.nih.gov/28882858/

134. Behme D, Berlis A, Weber W. Woven EndoBridge Intrasaccular Flow Disrupter for the Treatment of Ruptured and Unruptured Wide-Neck Cerebral Aneurysms: Report of 55 Cases. AJNR Am J Neuroradiol [Internet]. 2015;36(8):1501–6. Available from: https://pubmed.ncbi.nlm.nih.gov/25953761/

135. Lescher S, R du M de R, Berkefeld J. Woven Endobridge (WEB) device for endovascular treatment of complex unruptured aneurysms-a single center experience. Neuroradiology [Internet]. 2016;58(4):383–90. Available from: https://pubmed.ncbi.nlm.nih.gov/26767527/

136. Klisch J, Sychra V, Strasilla C, Liebig T, Fiorella D. The woven endobridge cerebral aneurysm embolization device (WEB II): Initial clinical experience. Neuroradiology. 2011;53(8):599–607.

137. Asnafi S, Rouchaud A, Pierot L, Brinjikji W, Murad MH, Kallmes DF. Efficacy and safety of the woven endobridge (web) device for the treatment of intracranial aneurysms: A systematic review and meta-Analysis. Am J Neuroradiol. 2016;37(12):2287–92.

138. Tau N, Sadeh-Gonik U, Aulagner G, Turjman F, Gory B, Armoiry X. The Woven EndoBridge (WEB) for endovascular therapy of intracranial aneurysms: Update of a systematic review with meta-analysis. Clin Neurol Neurosurg [Internet]. 2018;166(2010):110–5. Available from: http://dx.doi.org/10.1016/j.clineuro.2018.01.025

139. Kewlani B, Ryan DJ, Henry J, Wyse G, Fanning N. A single centre retrospective analysis of short- and medium-term outcomes using the Woven EndoBridge (WEB) device and identification of the device-to-aneurysm volume ratio as a potential predictor of aneurysm occlusion status. Interv Neuroradiol. 2022;

140. Sforza DM, Putman CM, Cebral JR. Computational fluid dynamics in brain aneurysms. Int j numer method biomed eng. 2012;28(6–7):801–8.

141. Saqr KM, Rashad S, Tupin S, Niizuma K, Hassan T, Tominaga T, et al. What does computational fluid dynamics tell us about intracranial aneurysms? A meta-analysis and critical review. J Cereb Blood Flow Metab. 2020;40(5):1021–39.

142. Gonzalez CF, Cho YI, Ortega H V., Moret J. Intracranial aneurysms: Flow analysis of their origin and progression. Am J Neuroradiol. 1992;13(1):181–8.

143. Etminan N, Macdonald RL. Computational Fluid Dynamics and Intracranial Aneurysms: Higher Mathematics Meets Complex Biology. World Neurosurg [Internet]. 2015;83(6):1017–9. Available from: http://dx.doi.org/10.1016/j.wneu.2015.02.015

144. Cebral JR, Castro MA, Burgess JE, Pergolizzi RS, Sheridan MJ, Putman CM. Characterization of cerebral aneurysms for assessing risk of rupture by using patient-specific computational hemodynamics models. Am J Neuroradiol. 2005;26(10):2550–9.

145. Ansari A. Computational Fluid Dynamics in Cerebral Aneurysms—Explaining the Aneurysm's Shape and the Timing of Rupture with Theoretical Physics. World Neurosurg [Internet]. 2019;126:591–2. Available from: https://doi.org/10.1016/j.wneu.2019.03.214

146. Berod A, Nicoud F, Mendez S. Modélisation in-silico des effets hémodynamiques des prothèses endovasculaires dans le traitement des anévrismes cérébraux : application

à l'estimation des chances de succès. 2021.

147. Boussel L, Rayz V, Mcculloch C, Martin A, Acevedo-bolton G, Lawton M, et al. Aneurysm growth occurs at region of low wall shear stress: Patient-specific correlation of hemodynamics and growth in a longitudinal study. Stroke. 2009;39(11):2997–3002.

148. Miura Y, Ishida F, Umeda Y, Tanemura H, Suzuki H, Matsushima S, et al. Low wall shear stress is independently associated with the rupture status of middle cerebral artery aneurysms. Stroke. 2013;44(2):519–21.

149. Cebral JR, Hendrickson S, Putman CM. Hemodynamics in a lethal basilar artery aneurysm just before its rupture. Am J Neuroradiol. 2009;30(1):95–8.

150. Cebral JR, Mut F, Weir J, Putman C. Quantitative characterization of the hemodynamic environment in ruptured and unruptured brain aneurysms. Am J Neuroradiol. 2011;32(1):145–51.

151. Meng H, Tutino VM, Xiang J, Siddiqui A. High WSS or Low WSS? Complex interactions of hemodynamics with intracranial aneurysm initiation, growth, and rupture: Toward a unifying hypothesis. Am J Neuroradiol. 2014;35(7):1254–62.

152. Sugiyama SI, Meng H, Funamoto K, Inoue T, Fujimura M, Nakayama T, et al. Hemodynamic analysis of growing intracranial aneurysms arising from a posterior inferior cerebellar artery. World Neurosurg [Internet]. 2012;78(5):462–8. Available from: http://dx.doi.org/10.1016/j.wneu.2011.09.023

153. Ishida Fujimaro, Tsuji Masanori, Tanioka Satoru, Tanaka Katsuhiro YS& HS. Computational Fluid Dynamics for Cerebral Aneurysms in Clinical Settings. In: Trends in Cerebrovascular Surgery and Interventions [Internet]. 2021. p. 27–32. Available from: https://library.oapen.org/bitstream/20.500.12657/48720/1/9783030634537.pdf

154. Qiu T, Jin G, Xing H, Lu H. Association between hemodynamics, morphology, and rupture risk of intracranial aneurysms: a computational fluid modeling study. Neurol Sci. 2017;38(6):1009–18.

155. Zhou G, Zhu Y, Yin Y, Su M, Li M. Association of wall shear stress with intracranial aneurysm rupture: Systematic review and meta-analysis. Sci Rep. 2017;7(1):1–8.

156. Morales H. G, Kim M, Vivas EE, Villa-Uriol M-CC, Larrabide I, Sola T, et al. How Do Coil Configuration and Packing Density. Ajnr. 2011;1935–41.

157. Schirmer CM, Malek AM. Critical influence of framing coil orientation on intra-aneurysmal and neck region hemodynamics in a sidewall aneurysm model. Neurosurgery. 2010;67(6):1692–702.

158. Luo B, Yang X, Wang S, Li H, Chen J, Yu H, et al. High shear stress and flow velocity in partially occluded aneurysms prone to recanalization. Stroke. 2011;42(3):745–53.

159. Li C, Wang S, Chen J, Yu H, Zhang Y, Jiang F, et al. Influence of hemodynamics on recanalization of totally occluded intracranial aneurysms: A patient-specific computational fluid dynamic simulation study. Laboratory investigation. J Neurosurg. 2012;117(2):276–83.

160. Park W, Song Y, Park KJ, Koo H-W, Yang K, Suh DC. Hemodynamic Characteristics Regarding Recanalization of Completely Coiled Aneurysms: Computational Fluid Dynamic Analysis Using Virtual Models Comparison. Neurointervention.

2016;11(1):30.

161. Larrabide I, Geers AJ, Morales HG, Aguilar ML, Rüfenacht DA. Effect of aneurysm and ICA morphology on hemodynamics before and after flow diverter treatment. J Neurointerv Surg. 2015;7(4):272–80.

162. Mut F, Raschi M, Scrivano E, Bleise C, Chudyk J, Ceratto R, et al. Association between hemodynamic conditions and occlusion times after flow diversion in cerebral aneurysms. J Neurointerv Surg. 2015;7(4):286–90.

163. Ouared R, Larrabide I, Brina O, Bouillot P, Erceg G, Yilmaz H, et al. Computational fluid dynamics analysis of flow reduction induced by flow-diverting stents in intracranial aneurysms: A patient-unspecific hemodynamics change perspective. J Neurointerv Surg. 2016;8(12):1288–93.

164. Pierot L, Biondi A. Endovascular techniques for the management of wide-neck intracranial bifurcation aneurysms: A critical review of the literature. J Neuroradiol [Internet]. 2016;43(3):167–75. Available from: http://dx.doi.org/10.1016/j.neurad.2016.02.001

165. Ding YH, Lewis DA, Kadirvel R, Dai D, Kallmes DF. The woven endobridge: A new aneurysm occlusion device. Am J Neuroradiol. 2011;32(3):607–11.

166. Pierot L, Costalat V, Moret J, Szikora I, Klisch J, Herbreteau D, et al. Safety and efficacy of aneurysm treatment with WEB: Results of the WEBCAST study. J Neurosurg. 2016;124(5):1250–6.

167. Xie Y, Tian H, Xiang B, Liu J, Xiang H. Woven EndoBridge device for the treatment of ruptured intracranial aneurysms: A systematic review of clinical and angiographic results. Interv Neuroradiol

168. Mut F, Chung BJ, Chudyk J, Lylyk P, Kadirvel R, Kallmes DF, et al. Image-based modeling of blood flow in cerebral aneurysms treated with intrasaccular flow diverting devices. Int j numer method biomed eng. 2019;35(6):1–14.

169. Castro MA, Putman CM, Cebral JR. Computational fluid dynamics modeling of intracranial aneurysms: Effects of parent artery segmentation on intra-aneurysmal hemodynamics. Am J Neuroradiol. 2006;27(8):1703–9.

170. Schnell S, Ansari SA, Vakil P, Wasielewski M, Carr ML, Hurley MC, et al. Three-dimensional hemodynamics in intracranial aneurysms: Influence of size and morphology. J Magn Reson Imaging. 2014;39(1):120–31.

171. Lee UY, Chung GH, Jung J, Kwak HS. Size-dependent distribution of patient-specific hemodynamic factors in unruptured cerebral aneurysms using computational fluid dynamics. Diagnostics. 2020;10(2):1–13.

172. Chong W, Zhang Y, Qian Y, Lai L, Parker G, Mitchell K. Computational hemodynamics analysis of intracranial aneurysms treated with flow diverters: Correlation with clinical outcomes. Am J Neuroradiol. 2014;35(1):136–42.

173. Levitt MR, McGah PM, Aliseda A, Mourad PD, Nerva JD, Vaidya SS, et al. Cerebral aneurysms treated with flow-diverting stents: Computational models with intravascular blood flow measurements. Am J Neuroradiol. 2014;35(1):143–8.

174. Alkhalili K, Hannallah J, Cobb M, Chalouhi N, Philips J, Echeverria A, et al. The effect of stents in cerebral aneurysms: A review. Asian J Neurosurg. 2018;13(2):201.

175. Caroff J, Mihalea C, Da Ros V, Yagi T, Iacobucci M, Ikka L, et al. A computational fluid

dynamics (CFD) study of WEB-treated aneurysms: Can CFD predict WEB "compression" during follow-up? J Neuroradiol [Internet]. 2017;44(4):262–8. Available from: http://dx.doi.org/10.1016/j.neurad.2017.03.005

176. Cebral JR, Castro MA, Putman CM, Alperin N. Flow-area relationship in internal carotid and vertebral arteries. Physiol Meas. 2008;29(5):585–94.

177. Painter PR, Edén P, Bengtsson HU. Pulsatile blood flow, shear force, energy dissipation and Murray's Law. Theor Biol Med Model. 2006;3.

178. Cebral JR, Duan X, Gade PS, Chung BJ, Mut F, Aziz K, et al. Regional Mapping of Flow and Wall Characteristics of Intracranial Aneurysms. Ann Biomed Eng. 2016;44(12):3553–67.

179. Gölitz P, Luecking H, Hoelter P, Knossalla F, Doerfler A. What is the hemodynamic effect of the Woven EndoBridge? An in vivo quantification using time-density curve analysis. Neuroradiology. 2020;62(8):1043–50.

180. Cebral JR, Castro MA, Appanaboyina S, Putman CM, Millan D, Frangi AF. 感度血球 .Pdf. 2005;24(4):457–67.

181. Appanaboyina S, Mut F, Löhner R Lo, Cebral, Putman CM, R. J. Computational fluid dynamics of stented intracranial aneurysms using adaptive embedded unstructured grids. Int J Numer Methods Fluids. 2011;65(October 2010):236–53.

182. Mut F, Löhner R, Chien A, Tateshima S, Viñuela F, Putman C, et al. Computational hemodynamics framework for the analysis of cerebral aneurysms. Int j numer method biomed eng. 2011;27(6):822–39.

183. Cebral JR, Chung BJ, Mut F, Chudyk J, Bleise C, Scrivano E, et al. Analysis of flow dynamics and outcomes of cerebral aneurysms treated with intrasaccular flow-diverting devices. Am J Neuroradiol. 2019;40(9):1511–6.

184. Fuchs H, Kedem ZM, Uselton SP. Optimal surface reconstruction from planar contours. Commun ACM. 1977;20(10):693–702.

185. Keppel E. Approximating Complex Surfaces By Triangulation of Contour Lines. IBM J Res Dev. 1975;19(1):2–11.

186. Chen LS, Herman GT, Reynolds RA, Udupa JK. Surface Shading in the Cuberille Environment. IEEE Comput Graph Appl. 1985;5(12):33–43.

187. Farrell EJ. Color Display and Interactive Intepretation of Three-Dimensional Data. IBM J Res Dev. 1983;27(4):356–66.

188. Robb RA, Hoffman EA, Sinak LJ, Harris LD, Ritman EL. High-Speed Three-Dimensional X-Ray Computed Tomography: The Dynamic Spatial Reconstructor. Proc IEEE. 1983;71(3):308–19.

189. Cagnazzo F, Ahmed R, Zannoni R, Dargazanli C, Lefevre P-H, Gascou G, et al. Predicting factors of angiographic aneurysm occlusion after treatment with WEB (Woven EndoBridge) device: A single-center experience with mid-term follow-up. J Neuroradiol [Internet]. 2020;47(2):104–5. Available from: https://www.sciencedirect.com/science/article/pii/S0150986120300237

190. Zhang XJ, Hao WL, Zhang DH, Gao BL. Asymmetrical middle cerebral artery bifurcations are more vulnerable to aneurysm formation. Sci Rep [Internet]. 2019;9(1):1–10. Available from: http://dx.doi.org/10.1038/s41598-019-51734-4

191. Pierot L, Klisch J, Liebig T, JY G, Leonardi M, NP N, et al. WEB-DL Endovascular

Treatment of Wide-Neck Bifurcation Aneurysms: Long-Term Results in a European Series. AJNR Am J Neuroradiol [Internet]. 2015;36(12):2314–9. Available from: https://pubmed.ncbi.nlm.nih.gov/26228882/

192. Antiga L, Piccinelli M, Botti L, Ene-Iordache B, Remuzzi A, Steinman DA. An image-based modeling framework for patient-specific computational hemodynamics. Med Biol Eng Comput. 2008;46(11):1097–112.

193. Khan MO, Valen-Sendstad K, Steinman DA. Narrowing the expertise gap for predicting intracranial aneurysm hemodynamics: Impact of solver numerics versus mesh and time-step resolution. Am J Neuroradiol. 2015;36(7):1310–6.

194. Si H. TetGen, a Delaunay-based quality tetrahedral mesh generator. ACM Trans Math Softw. 2015;41(2).

195. Cebral JR, Raschi M, Mut F, Ding Y-H, Dai D, Kadirvel R, et al. Analysis of flow changes in side branches jailed by flow diverters in rabbit models. Int j numer method biomed eng [Internet]. 2014;4179(April):53. Available from: http://knowledgebase.terrafrica.org/fileadmin/user_upload/terrafrica/docs/Final_Rockefeller_Report4April08.pdf

196. Valen-Sendstad K, Steinman DA. Mind the gap: Impact of computational fluid dynamics solution strategy on prediction of intracranial aneurysm hemodynamics and rupture status indicators. Am J Neuroradiol. 2014;35(3):536–43.

197. Dapogny C, Dobrzynski C, Frey P. Three-dimensional adaptive domain remeshing, implicit domain meshing, and applications to free and moving boundary problems. J Comput Phys [Internet]. 2014;262:358–78. Available from: http://dx.doi.org/10.1016/j.jcp.2014.01.005

198. Chnafa C, Bouillot P, Brina O, Najafi M, Delattre BMA, Vargas MI, et al. Errors in power-law estimations of inflow rates for intracranial aneurysm CFD. J Biomech [Internet]. 2018;80:159–65. Available from: https://doi.org/10.1016/j.jbiomech.2018.09.006

199. Hoi Y, Wasserman BA, Xie YJ, Najjar SS, Ferruci L, Lakatta EG, et al. Characterization of volumetric flow rate waveforms at the carotid bifurcations of older adults. Physiol Meas. 2010;31(3):291–302.

200. Valen-Sendstad K, Piccinelli M, KrishnankuttyRema R, Steinman DA. Estimation of Inlet Flow Rates for Image-Based Aneurysm CFD Models: Where and How to Begin? Ann Biomed Eng. 2015;43(6):1422–31.

201. Cebral JR, Mut F, Weir J, Putman CM. Association of hemodynamic characteristics and cerebral aneurysm rupture. Am J Neuroradiol. 2011;32(2):264–70.

202. Castro MA, Putman CM, Sheridan MJ, Cebral JR. Hemodynamic patterns of anterior communicating artery aneurysms: A possible association with rupture. Am J Neuroradiol. 2009;30(2):297–302.

203. Caroff J, Mihalea C, Da Ros V, Yagi T, Iacobucci M, Ikka L, et al. A computational fluid dynamics (CFD) study of WEB-treated aneurysms: Can CFD predict WEB "compression" during follow-up? J Neuroradiol [Internet]. 2017;44(4):262–8. Available from: https://www.sciencedirect.com/science/article/pii/S0150986116301778

204. Brina O, Bouillot P, Reymond P, Luthman AS, Santarosa C, Fahrat M, et al. How flow

reduction influences the intracranial aneurysm occlusion: A prospective 4D phase-contrast MRI study. Am J Neuroradiol. 2019;40(12):2117–23.

205. Kadirvel R, Ding YH, Dai D, Rezek I, Lewis DA, Kallmes DF. Cellular mechanisms of aneurysm occlusion after treatment with a flow diverter. Radiology. 2014;270(2):394–9.

206. Rouchaud A, Ramana C, Brinjikji W, Ding YH, Dai D, Gunderson T, et al. Wall apposition is a key factor for aneurysm occlusion after flow diversion: A histologic evaluation in 41 rabbits. Am J Neuroradiol. 2016;37(11):2087–91.

207. Ding Y, Dai D, Rouchaud A, Janot K, Asnafi S, Kallmes DF, et al. WEB device shape changes in elastase-induced aneurysms in rabbits. Am J Neuroradiol. 2021;42(2):334–9.

208. Gester K, Luchtefeld I, Busen M, Sonntag SJ, Linde T, Steinseifer U, et al. In vitro evaluation of intra-aneurysmal, flow-diverter-induced thrombus formation: A feasibility study. Am J Neuroradiol. 2016;37(3):490–6.

209. Ding YH, Dai D, Schroeder D, Kadirvel R, Kallmes DF. Experimental testing of the dual-layer Woven EndoBridge device using an elastase-induced aneurysm model in rabbits. Interv Neuroradiol. 2016;22(3):299–303.

Appendix 1: STROBE Statement—checklist of items that should be included in reports of observational studies

	Item No	Recommendation	Caroff et al	Mut et al	Gölitz et al	Cebral et al
Title and abstract	1	(*a*) Indicate the study's design with a commonly used term in the title or the abstract	No	No	No	No
		(*b*) Provide in the abstract an informative and balanced summary of what was done and what was found	Yes	Yes	Yes	Yes
Introduction						
Background/rationale	2	Explain the scientific background and rationale for the investigation being reported	Yes	Yes	Yes	Yes
Objectives	3	State specific objectives, including any prespecified hypotheses	Yes	Yes	Yes	Yes
Methods						
Study design	4	Present key elements of study design early in the paper	Yes	Yes	Yes	Yes
Setting	5	Describe the setting, locations, and relevant dates, including periods of recruitment, exposure, follow-up, and data collection	Yes	Yes	Yes	Yes

Participants	6	(*a*) *Cohort study*—Give the eligibility criteria, and the sources and methods of selection of participants. Describe methods of follow-up *Case-control study*—Give the eligibility criteria, and the sources and methods of case ascertainment and control selection. Give the rationale for the choice of cases and controls *Cross-sectional study*—Give the eligibility criteria, and the sources and methods of selection of participants	Yes	Yes	Yes	Yes
Variables	7	Clearly define all outcomes, exposures, predictors, potential confounders, and effect modifiers. Give diagnostic criteria, if applicable	Yes	Yes	Yes	Yes
Data sources/ measurement	8*	For each variable of interest, give sources of data and details of methods of assessment (measurement). Describe comparability of assessment methods if there is more than one group	Yes	Yes	Yes	Yes
Bias	9	Describe any efforts to address potential sources of bias	No	No	No	No
Study size	10	Explain how the study size was arrived at	Yes	Yes	Yes	Yes
Quantitative variables	11	Explain how quantitative variables were handled in the analyses. If applicable, describe which groupings were chosen and why	Yes	Yes	Yes	Yes

Statistical methods	12	(*a*) Describe all statistical methods, including those used to control for confounding	Yes	Yes	Yes	Yes
		(*b*) Describe any methods used to examine subgroups and interactions	Yes	Yes	Yes	Yes
		(*c*) Explain how missing data were addressed	Yes	Yes	Yes	Yes
		(*d*) *Cohort study*—If applicable, explain how loss to follow-up was addressed *Case-control study*—If applicable, explain how matching of cases and controls was addressed *Cross-sectional study*—If applicable, describe analytical methods taking account of sampling strategy				
		(*e*) Describe any sensitivity analyses				

Results

Participants	13*	(a) Report numbers of individuals at each stage of study—eg numbers potentially eligible, examined for eligibility, confirmed eligible, included in the study, completing follow-up, and analysed	Yes	Yes	Yes	Yes
		(b) Give reasons for non-participation at each stage	Yes	Yes	Yes	Yes
		(c) Consider use of a flow diagram	No	No	No	No
Descriptive data	14*	(a) Give characteristics of study participants (eg demographic, clinical, social) and information	Yes	Yes	Yes	Yes

		on exposures and potential confounders				
		(b) Indicate number of participants with missing data for each variable of interest	Yes	Yes	Yes	Yes
		(c) *Cohort study*—Summarise follow-up time (eg, average and total amount)	Yes	Yes	Yes	Yes
Outcome data	15*	*Cohort study*—Report numbers of outcome events or summary measures over time	No	No	No	No
Main results	16	(*a*) Give unadjusted estimates and, if applicable, confounder-adjusted estimates and their precision (eg, 95% confidence interval). Make clear which confounders were adjusted for and why they were included	Yes	Yes	Yes	Yes
		(*b*) Report category boundaries when continuous variables were categorized				
		(*c*) If relevant, consider translating estimates of relative risk into absolute risk for a meaningful time period				
Other analyses	17	Report other analyses done—eg analyses of subgroups and interactions, and sensitivity analyses	Yes	Yes	Yes	Yes
Discussion						
Key results	18	Summarise key results with reference to study objectives	Yes	Yes	Yes	Yes
Limitations	19	Discuss limitations of the study, taking into account sources of potential bias or imprecision. Discuss both direction and magnitude of any potential bias	Yes	Yes	Yes	Yes

Interpretation	20	Give a cautious overall interpretation of results considering objectives, limitations, multiplicity of analyses, results from similar studies, and other relevant evidence	Yes	Yes	Yes	Yes
Generalisability	21	Discuss the generalisability (external validity) of the study results	Yes	Yes	Yes	Yes
Other information							
Funding	22	Give the source of funding and the role of the funders for the present study and, if applicable, for the original study on which the present article is based	Yes	Yes	Yes	Yes